NON-CONTACT ULTRASONIC STUDY ON THIXOTROPIC ALLOYS

by

AZMI IDRIS

A Thesis Submitted for the Degree of Doctor of Philosophy

University of Warwick

Department of Physics

January 1995

CONTENTS

LIST OF ILLUSTRATIONS

ACKNOWLEDGEMENTS

I would like to convey my special thanks to Professor Stuart B. Palmer for his close supervision and guidance throughout my studies. My special thanks also goes to Dr. Chris Edwards for his untiring assistance, guidance and expert advice. I would like to thank the management of the Standard and Industrial Research Institute of Malaysia (SIRIM) for providing me the opportunity to continue my study, the Malaysian Government for making my study possible, Lucas (Advanced Engineering Centre) in particular, Dr. Chris Benson for their financial support and in supplying samples for the work, and Dr. Pluto Kapranos from the Department of Engineering Materials, The University of Sheffield for his cooperation. I would also like to express my thanks to Dr. Duncan Billson, the group technician Mr. John Reed, and the workshop technicians, in particular Mr. Pat Beecraft for their willingness to provide assistance whenever needed. Also not to forget I would like to thank the solid-state boys for making my life in the department enjoyable.

Lastly, I would like to convey my special thanks to my wife Nor Akasah Zainudin, and my children, Muhammad Ikhwan, Muhammad Safwan, Muhammad Nazim, Nurul Ameera and Ahmad Azfar for their patience and courage during my studies.

DECLARATION

The material presented in this thesis is my own work except where specified otherwise. The work was carried out in the Department of Physics, University of Warwick, in the period from October 1991 to January 1995. No part of this thesis has been submitted previously to the University of Warwick, nor any other academic institution for admission to a higher degree. Some of the work has already appeared in the form of publications which are listed in the bibliography.

SUMMARY

Thixotropic metals have better fluid flow behaviour in the semi-solid state when compared to conventional metals and have been increasingly used commercially for the production of high quality engineering components using the technique of thixoforming. However in industrial production, there is no proper quality control system available at present to monitor the softness or to estimate the percentage of solid/liquid fractions of the metal before it is forged into the required shapes. Due to the existence of a temperature gradient within the sample when heated in the R.F furnace a bulk measurement is needed.

This thesis examines the capability of non-contact ultrasound to make acoustic wave measurements into the semi-solid state. In particular we have identified pulsed laser generation and EMAT reception as being the most appropriate approach. The Nd:YAG laser has proved capable of generating broadband ultrasound and a water-cooled spiral coil permanent magnet EMAT an efficient detector of both shear and longitudinal waves. The system enables both the longitudinal and shear waves to be detected simultaneously. Investigations have been conducted on various thixotropic metals ranging from lower melting temperature Al-Si alloys (≈ 570 °C) to the higher melting point M2 tool steel (≈1200 °C). A Cu-Sn alloy that has a melting temperature of around 830 °C was also used for the investigation. Due to the high price and difficulty in obtaining the thixotropic materials preliminary measurements were carried out on non-thixotropic Al-Si alloys and a commercial mild steel. A water-cooled shear EMAT, furnace systems and an ultrasonic cell have been designed and constructed for the thesis. The experiment was carried out in a through transmission arrangement with the laser and the EMAT on epicentre. The experimental work is presented in chapters 4 to 6. Chapter 4 covers the investigation on the Al-Si alloys, chapter 5 covers investigations on the higher melting point materials, and chapter 6 presents investigations into the efficiency of the chosen laser-EMAT system and analyses systematic errors.

The laser-EMAT system has proved capable of making measurements not only in the partially molten state but also in the fully molten state with sample temperatures up to 1140 °C. The sudden drop in the longitudinal wave to shear wave transit time ratio indicates that the onset of melting could be detected. Since the ratio depends only on the temperature and the percentage of solid and liquid present in the sample and is independent of the sample dimensions it could be a suitable parameter for monitoring the percentage of liquid/solid fractions necessary for thixoforging. However work has yet to be carried out in the industrial environment to prove the capability of the system in monitoring the softness of the metal during thixoforming.

CHAPTER 1

CHAPTER 1

INTRODUCTION

1.0 Introduction

The production of components for the automotive, aerospace, military, and other industries by forming from thixotropic (semi-solid) metals is now a rapidly expanding commercial process [Kenney et. al., 1988]. In thixoforming, the cast billet (slug) is normally heated to a semi-solid region of around 30 to 50 % liquid before it is forced into the mould. In this state the thixotropic microstructure changes its rheological behaviour and the material can be deformed to very large strains at very low loads without cracking or the separation of liquid and solid phases on a macroscopic scale. Materials formed using this process will have good quality finish with improved surface smoothness and reduced formation of shrinkage cavities. However, it is essential that the material be in the right condition or softness prior to thixoforming to ensure that the optimum required microstructure has been obtained and the material will behave thixotropically during forging. Therefore a suitable material control system must be made available to monitor the solid/liquid volume fractions of the material. Lucas Industries plc is a company that produces a wide range of products for the automotive, aerospace and light engineering industrial sectors and are interested in the development of a control system capable of handling a range of materials typically in the high strength/high melting point range including copper based alloys and tool steel. The present thesis specifically describes the development of an ultrasonic monitoring system for the measurement of the solid/liquid fraction and has been carried out in collaboration with Lucas.

An experimental method to monitor the degree of partial melting of the thixotropic metal before forging has been reported by Fleming et. al., [1976] and Mc Lelland et. al., [1991]. Both groups used an alumina probe or "penetrometer" which determined the penetration rate which can then be related to the volume of the solid/liquid fraction for the material. The probe was initially set resting on the surface of the slug being heated. Once the material starts to soften, the penetrometer will start sinking into the material and when the rate of penetration indicating the right condition is reached (by referring to the calibration curves for the particular material and probe), the penetrometer is moved out of the path of the material and the forming step is initiated. The method used is only suitable for lower temperature alloys, because for higher temperature alloys the probe could not be accommodated as the material has to be heated in a controlled atmosphere chamber to prevent or reduce oxidation. Moshinin, [1992] in his experiment to manufacture automotive components from an Al 7 % Si thixotropic alloy refers to the solidification curve of the solid fraction versus temperature of the particular alloy. The temperature is then used to determine the correct condition before the semi-solid metal is transferred to the die-casting machine to be forced into the required shapes.

In industrial production, the slug is normally heated by induction or R.F methods to the required solid/liquid fraction before thixoforming. The sample surface can be hot but the interior is cool, therefore a quality control system that could provide bulk information on the characteristic of the material is needed. It is understood that at present, there is no quality control system available for the above purpose. The industry must therefore rely on a pre-determined heating routine by controlling the appropriate parameters which results in the necessary liquid fraction

depending on the individual application. Ultrasonic methods can be used for this type of measurement, as the acoustic waves propagate through the bulk of the material and the measurements obtained could be representative of the state of the material under examination. Due to the high temperature involved, conventional contact ultrasonic techniques using piezoelectric transducers are not suitable for this application, hence a non-contact ultrasonic technique has to be applied. A feasibility study using a non-contact ultrasound system to measure the degree of partial melting in Al-Si alloys had been reported by Edwards and Palmer, [1990]. A Q-switched Nd:YAG (Neodymium:Yttrium Aluminium Garnet) pulsed laser and a stabilised He-Ne Michelson interferometer were used as the ultrasound generator and detector respectively. This approach demonstrated that the onset of partial melting can be detected ultrasonically, however results could only be obtained when the sample detection surface was polished to a mirror finish to provide maximum reflectivity. In addition the system had to operate in a low vibration environment. Heterodyne Fabry-Perot interferometer could be used to detect ultrasound on rough surfaces but the system would be bulky and expensive.

In the present thesis the combination of laser generation and an ElectroMagnetic Acoustic Transducer (EMAT) detection system was chosen to monitor the state of the partially molten thixotropic material. The aim was to avoid the use of an expensive interferometer detector that is environment sensitive. With an EMAT detector the sample need not be specially prepared as it can operate on rough surfaces, the EMAT is insensitive to the industrial environment and is comparatively cheap and easy to operate. EMATs can have a reasonable detection sensitivity and can be designed to have the required detection bandwidth (1-10 MHz). With the

water-cooled EMAT, measurements could be made at a very high temperature. In the evaluation made in chapter 3 of this thesis, we mention that from the comparison work reported by Hutchins et. al., [1986] the laser-EMAT system has proved capable of detecting sharp and sufficiently high amplitude longitudinal and shear wave pulses. Both acoustic waves are generated simultaneously (as required in this work) when a laser pulse, of sufficiently high power density to cause a weak ablation, is incident on the sample surface. Furthermore both modes can be detected by a spiral coil EMAT. In addition the laser-EMAT system is less bulky compared to the laser-laser system.

Thixotropic material can be considered as a new material and is still not well known in many industries. This chapter will provide a detailed description of this special material including the production processes available for the raw material, and their advantages and disadvantages. The work covered by the thesis will also be described.

1.1 Thixotropic Material

Thixotropic or semi-solid material, when in the semi-solid state, behaves as a solid under very small applied stresses but, under greater stresses, behaves as a liquid. When the stresses are removed, the material settles back into its original consistency, though not its original size and shape. This material when heated to the semi-solid condition will exhibit a structure which comprises solid particles in the form of globules or spheroids suspended in the matrix of a lower melting point liquid. The resulting "composite" can have a viscosity as low as an olive oil at sufficiently high stresses.

Thixotropic metals were first discovered in the early 1970s by Spencer, [1971] from Massachusetts Institute of Technology (MIT). In a review paper by Flemings, [1991] it is mentioned that the discovery was made while Spencer was carrying out a hot tearing experiment on a Sn 15 weight percent Pb alloy for his PhD thesis. Rather than partially solidifying the alloy before beginning the shear, he began above the liquidus and then slowly cooled the alloy into the solidification range while it was being sheared. He found that the shear stress increased very slowly as the temperature was decreased below the liquidus. The stress measured at a particular temperature below the liquidus was orders of magnitude less than that measured for samples cooled to the same temperature before shear. The viscosity of the material is time dependent and decreases with increasing shear rates. Since then, extensive studies have been carried out in this field, by researchers from the United States, United Kingdom, West Germany, Japan and elsewhere, to produce thixotropic raw material from different alloys by either using similar methods or by introducing new production processes. They have also studied the material rheological behaviour and properties and their ability to be used for manufacturing engineering components for various industrial applications.

1.1.1 Raw Material Production Process

There are various methods available to produce this special material namely, rheocasting [Flemings et. al., 1976], spray deposition [Leatham et. al., 1989], an extrusion process which is known as the strain-induced, melt-activated process or SIMA process [Young et. al., 1983], and the shearing/cooling roll or SCR process that was proposed recently [Kiuchi and Sugiyama, 1992]. A simpler method,

consisting of reheating standard cast billets to the semi-solid state and waiting for globulization of the grains, has also been tested but is of limited value because the grain size is too large for the thixotropic process. In rheocasting, the shear stresses are applied continuously by either vigorous mechanical stirring (figure 1.1) or electrohydrodynamic (MHD) stirring (figure 1.2) during the solidification of the molten metal. Dendritic structures, that initially grow at the inner surface of the crucible due to cooling, are crushed into small solid particles by the stirrer and dispersed in the remaining molten metal, thus a mixture of solid particles and molten metal is formed. The average solid particle diameters are primarily controlled by the solidification rate, while the optimisation of the spheroidal shape is controlled by the shear rate. High solidification rates can produce finer particle diameters and high shear rate may result in more rounded particle shapes with less clustering of particles. To show optimal thixotropic properties in the semi-solid state, the metallic alloys must have very fine and isotropic grains. Typically, solid particle diameters range from 100 to 400 μm for normal solidification. Several mechanical agitation approaches have been used, such as the batch rheocaster, the continuous rheocaster [Fleming et. al., 1976] or the Gircast process [Collot, 1985 & 1986] but these processes have problems with regard to metal quality, contamination, process control and economics, hence are not suitable to be applied for commercial production processes.

In the MHD casting system, there is no physical contact between the liquid metal and stirrer. The molten metal, held near the freezing point in the mould, is vigorously stirred by a dynamic electromagnetic field, which creates the necessary shearing action. At the same time and location, controlled conductive heat transfer through the mould wall to a surrounding water jacket induces freezing. The MHD

casting process has the ability to control precisely the shearing action and the rate of heat removal and thus deliver the desired solidification microstructure with a grain size that is normally about 30 μm. This process has been used commercially to produce large billets from 38 to 152 mm diameter and the billets produced have a fine grain, non-dendritic microstructure and freedom from oxides, non-metallic inclusions and gas.

Thixotropic material formed by the spray deposition method can be produced by the Osprey process [Leatham, et. al., 1989]. By this process an alloy is first melted in an induction heating furnace and poured directly into the atomiser and subjected to gas atomisation under inert conditions (usually nitrogen or argon is used). The gas overpressure is used to control the metal dispensing rate. The atomised droplets are collected in a mould in which final solidification occurs. A range of droplets (e.g. 10 - 300 μm) at different temperatures and states of solidification arrive at the collector surface. The condition of deposition is ideally controlled in such a manner that a layer of semi-solid metal of controlled thickness is maintained at the surface of the preform throughout the deposition operation (figure 1.3). For a given alloy and atomising gas, the cooling rate of the particles in flight is determined mainly by their individual sizes. Under optimum conditions, the coarse particles are deposited in the fully molten state, the fine particles will be fully solidified at a temperature close to that of the atomising gas and intermediate size particles will be deposited in the semi-solid/semi-liquid condition. Thus, the preform surface consists of a mixture of dendrite fragments, pre-solidified particles and liquid metal. The fine, pre-solidified particles and the dendrite fragments appear to re-melt in the liquid metal, aided partly by the release of latent heat. Rapid solidification occurs by convective cooling to the relatively cold

atomising gas as it flows over the surface of the preform. Solidification probably originates from either the remains of the dendrite fragments or solid particles, and occurs in a non-dendritic mode. This may occur as a result of turbulence at the surface of the preform arising from the momentum transfer of the gas stream and the impacting droplets. Initially, this turbulence will cause bending, fracture and remelting of dendrite arms. The turbulence also ensures local homogeneity of both temperature and composition, making dendrite growth difficult. This results in the rapid, non-dendritic growth of a spherical primary phase which forms in a subsurface zone of the preform. The liquid metal surrounding the spherical primary phase becomes enriched with solute to form a molten network of low melting point material.

The time-temperature profile of the SIMA process [Young et. al., 1983] is shown in figure 1.4. The normal billet with dendritic microstructure that was initially produced by the continuous casting process is heated between the recrystallisation and the solidus temperature of the material and is hot extruded into round bars before it is quenched in water, oil or brine. The extruded bars will then exhibit a directional grain microstructure. In order to improve the thixotropic properties of the extruded bar in the semi-solid state, the bar is further subjected to additional cold work until sufficient strain is induced. When heated to the semi-solid condition the bar will have a fine spheroidal microstructure within the low melting liquid matrix which is necessary for thixoforming. This process is cost effective and suitable for production of small diameter (< 38 mm) raw material bars.

The mechanics of the SRC process [Kiuchi and Sugiyama, 1992] consists of a rotating shearing/cooling roll, a shoe fixed to the supporting block and a stripper (figure 1.5). The roll and the shoe are set so that the necessary gap is maintained

between them. The molten metal, which is heated to the required temperature is introduced into the roll-shoe gap through the flow guide attached to the top of the gap. The molten metal is drawn into the gap by frictional force provided by the rotating roll. In the gap, it is cooled and at the same time stirred by the rotating roll and shoe. Due to the cooling, dendritic structures start to grow on the surfaces of both the roll and the shoe but are crushed into small solid particles by the shearing force provided by the rotating roll and the fixed shoe. The solid particles are dispersed into the molten metal to form a semisolid metal. The semi-solid metal is drawn downward by the rotating roll and extruded out through the exit gap where it is stripped off by the stripper.

1.1.2 Advantages and Disadvantages of Thixotropic Material

Thixotropic materials offer several advantages over conventional casting material for forming into shapes. If we consider the die-casting process, the small billets cut from the continuous thixotropic bar need to be heated only to the semi-solid condition, not to the fully molten state, before being forced into the die. Hence, only 65 % [Kenney et. al., 1988] of the heating energy is required which offers significant reduction in the energy consumption. The lower temperature will speed up the casting velocity due to less heat of fusion to be extracted and also cause less thermally induced die erosion and contribute to the increase in the production rate. In thixoforming much lower pressures are involved than with conventional forging so the mould can be made much more cheaply. In the semi-solid condition, the material produces less liquid/solid shrinkage and less microporosity, therefore higher quality finished product can be produced. The improved fluid flow behaviour enables the

filling of thinner sections and the forming of lighter parts. Thixotropic materials allow a certain degree of automation to be incorporated into the material handling system with no need to handle liquid metal which is a hazard to the workers. A more nearly net-shape component can be achieved by precision control of the process during thixoforming and results in less machining. The viscous behaviour of semi-solid alloys also allows for substantial benefits in particle-incorporated processes to produce metal matrix composite (MMC) materials and thixoforming can be a viable process for shaping the difficult-to-cast and machine MMC materials. The main disadvantage of thixotropic material is that it needs to be specially prepared using expensive capital equipment making it more expensive than the conventional casting material.

1.3 Work Covered by the Thesis

The initial part of this chapter explained the reason why a quality control system is needed to monitor the softness or the percentage of solid/liquid volume fractions of thixotropic metals prior to forming to the required shapes, and why ultrasonic methods and in particular the non-contacting laser-EMAT system may be a suitable system for the above purpose. The major part of the chapter described in some detail the background to thixotropic metals including the production processes available to produce the raw material, and the advantages and disadvantages of using the material for making industrial components. The final part of the first chapter is this section outlining the contents of the remainder of the thesis.

Chapter 2 provides briefly the theory of acoustic wave propagation in isotropic solids, liquids, and in the semi-solid state. This is followed by a review of the attenuation that can occur in the three media which is useful for the later discussions

in the experimental chapters. A comparison of the theoretical and experimental longitudinal wave velocity, as a function of increasing temperatures, in Al 4.86 % Si alloy is also presented. Chapter 3 basically reviews the applications of the non-contacting ultrasonic systems, in particular laser and electromagnetic based techniques at elevated temperature. The principles of laser ultrasound generation mechanisms and operation of EMATs are provided to allow a better understanding of the experimental procedures used to obtain the results described in chapters 4, 5 and 6. An evaluation on the advantages and disadvantages of each individual technique and the reason why a combination of a Nd:YAG pulsed laser as the ultrasound generator and a spiral coil EMAT as the detector was selected for the thesis is also presented. Chapter 4 demonstrates the capability of the combination of a Nd:YAG laser as the ultrasound generator and a spiral coiled EMAT as the receiver for making acoustic wave measurements not only in the semi-solid state but also up to the fully molten state. For the purpose of the thesis, water-cooled shear EMATs, furnace systems and an ultrasonic cell were designed and constructed as described in chapter 4. The split electric furnace used is capable of heating samples up to 1100 °C, sufficient for heating the Al-Si and other higher melting temperature alloys such as the Cu-Sn alloy, thixotropic or non-thixotropic, into the fully molten state (660 °C for pure aluminium). The chapter also covers descriptions of the samples used including their chemical compositions and method of analysis, and the processes involved in making them.

In chapter 5 the capability of the laser-EMAT system is extended, this time for making measurements on materials with much higher melting temperatures. Measurements were made on thixotropic copper alloy with 10.2 % tin, a commercial

mild steel, and thixotropic M2 tool steel using the experimental set-up similar to that described in chapter 4. Since the electric furnace used has a maximum operating temperature of only 1200 °C, the M2 tool steel could only be heated up to 1100 °C. Measurements on the M2 tool steel were then extended using an induction furnace in a new experimental set-up that was specifically designed and constructed to enable the tool steel to be heated into the partially molten state. The description of the experimental procedure is provided in section 5.4. Chapter 6 is divided into three sections, the first section describes the experiment carried out to examine the causes of the unusual behaviour of the shear wave velocity observed between 350 and 400 °C as described in chapter 4. The second section investigates the extent of the effect of the water-cooled EMAT on the temperature of the sample, and therefore the accuracy of the acoustic wave transit time measurement. The final section describes experiments carried at elevated temperature on an aluminium alloy and M2 tool steel using a pulsed CO_2 laser as the ultrasound generator. The results obtained are then compared with that obtained in chapter 4 for the aluminium alloy and chapter 5 for the M2 tool steel using a pulsed Nd:YAG laser.

Finally, chapter 7 concludes the outcome of the thesis by describing the peformance of the laser-EMAT system on both the lower melting temperature Al-Si alloys, and the higher melting temperature Cu 10.2 % Sn alloy, mild steel and the M2 tool steel, and problems encountered in the work. A few suggestions for future work are also presented.

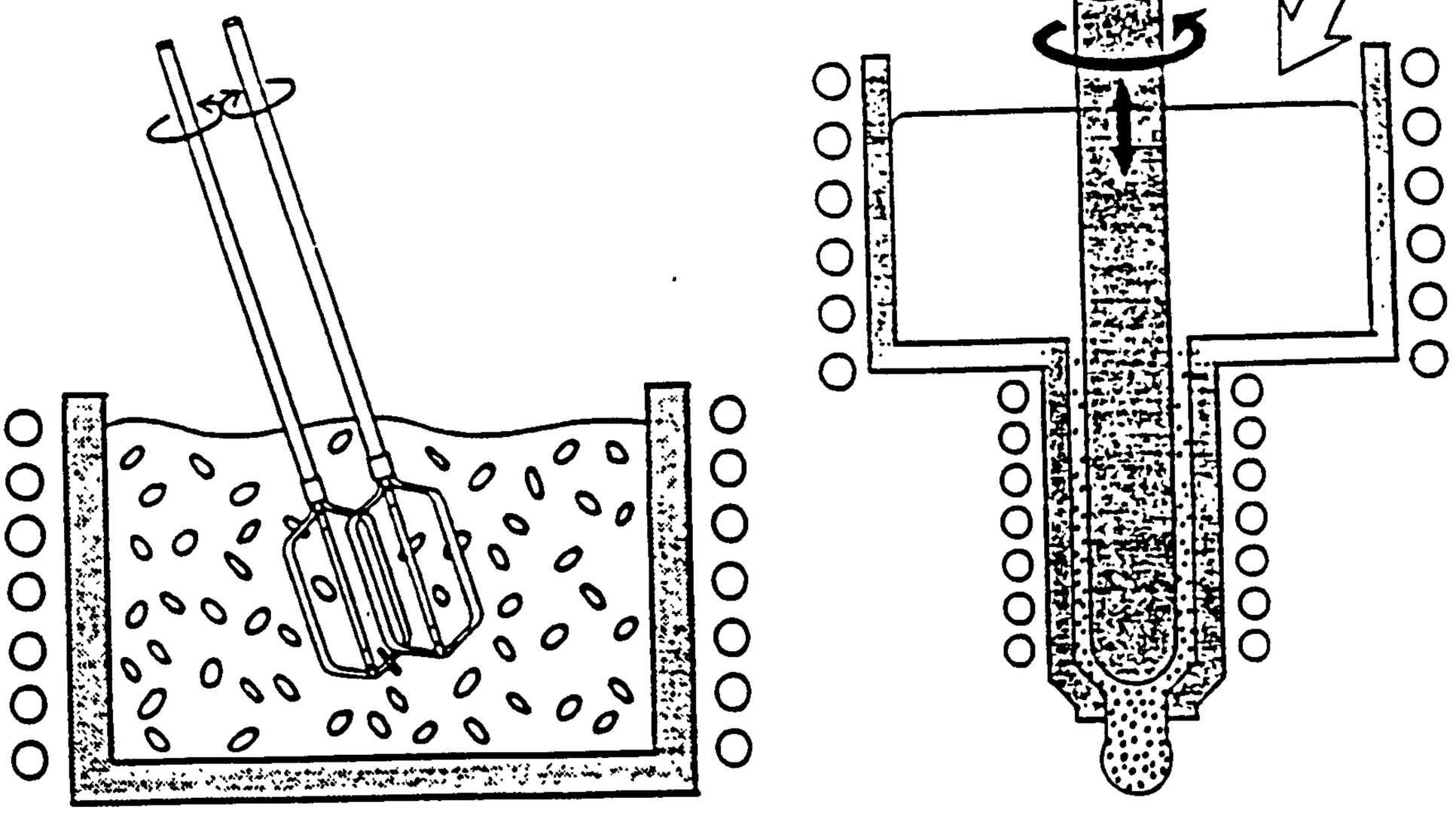

Fig. 1.1 Mechanical stirring [after Fleming, 1991].

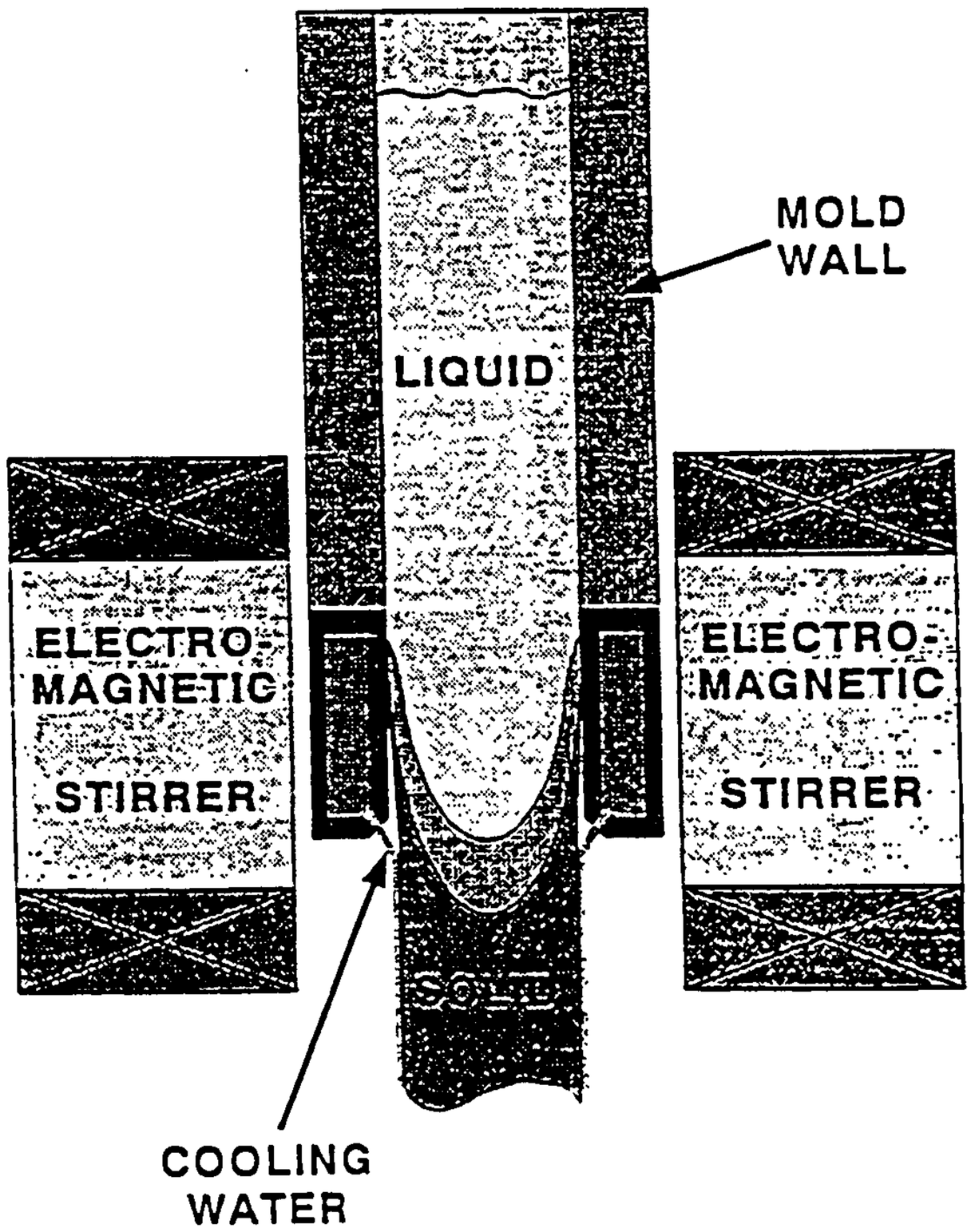

Fig. 1.2 Electrohydrodynamic stirring [after Gabathuler et. al., 1992].

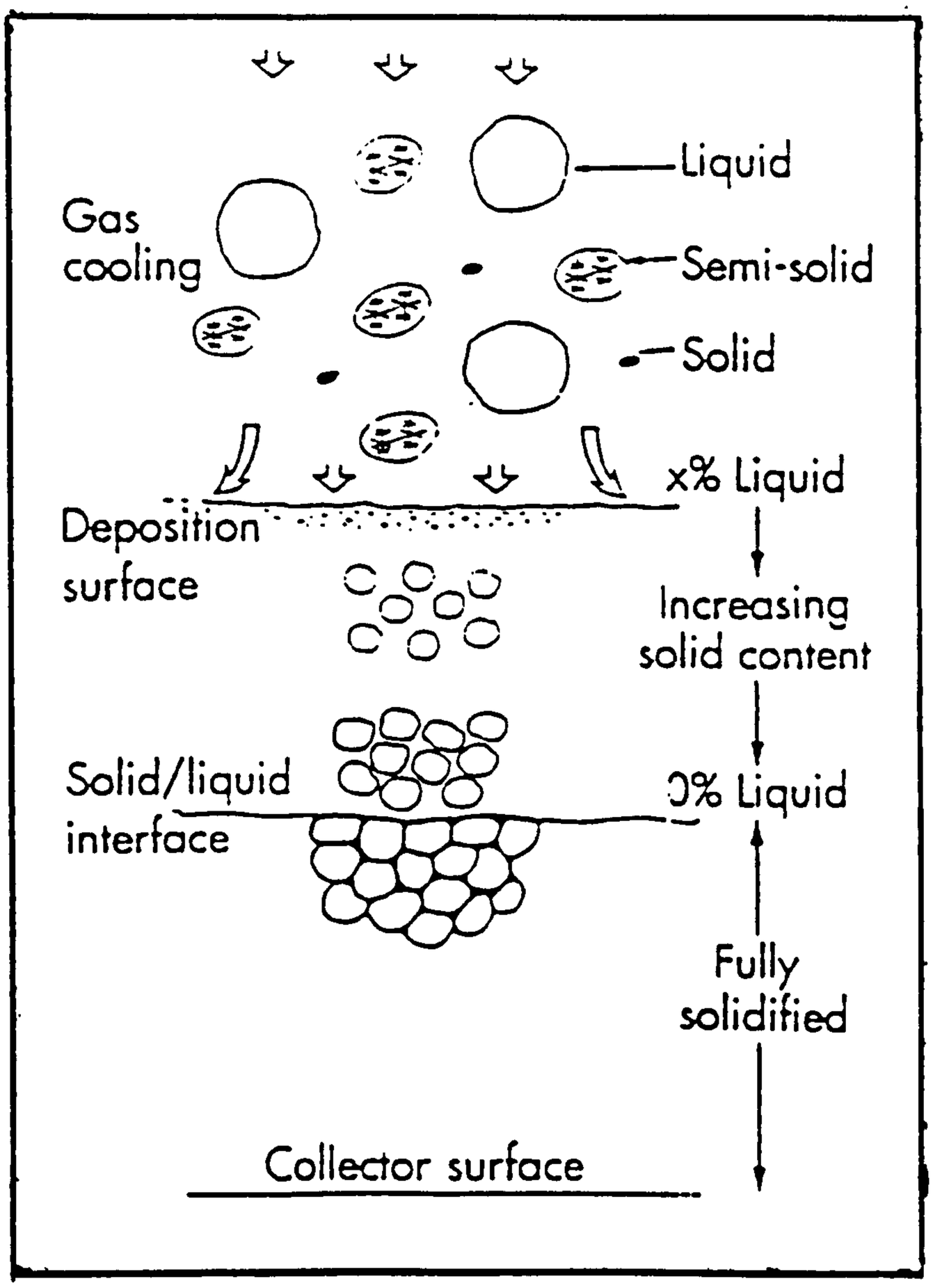

Fig. 1.3 Condition of deposition of the Osprey process [after Leatham et. al., 1989].

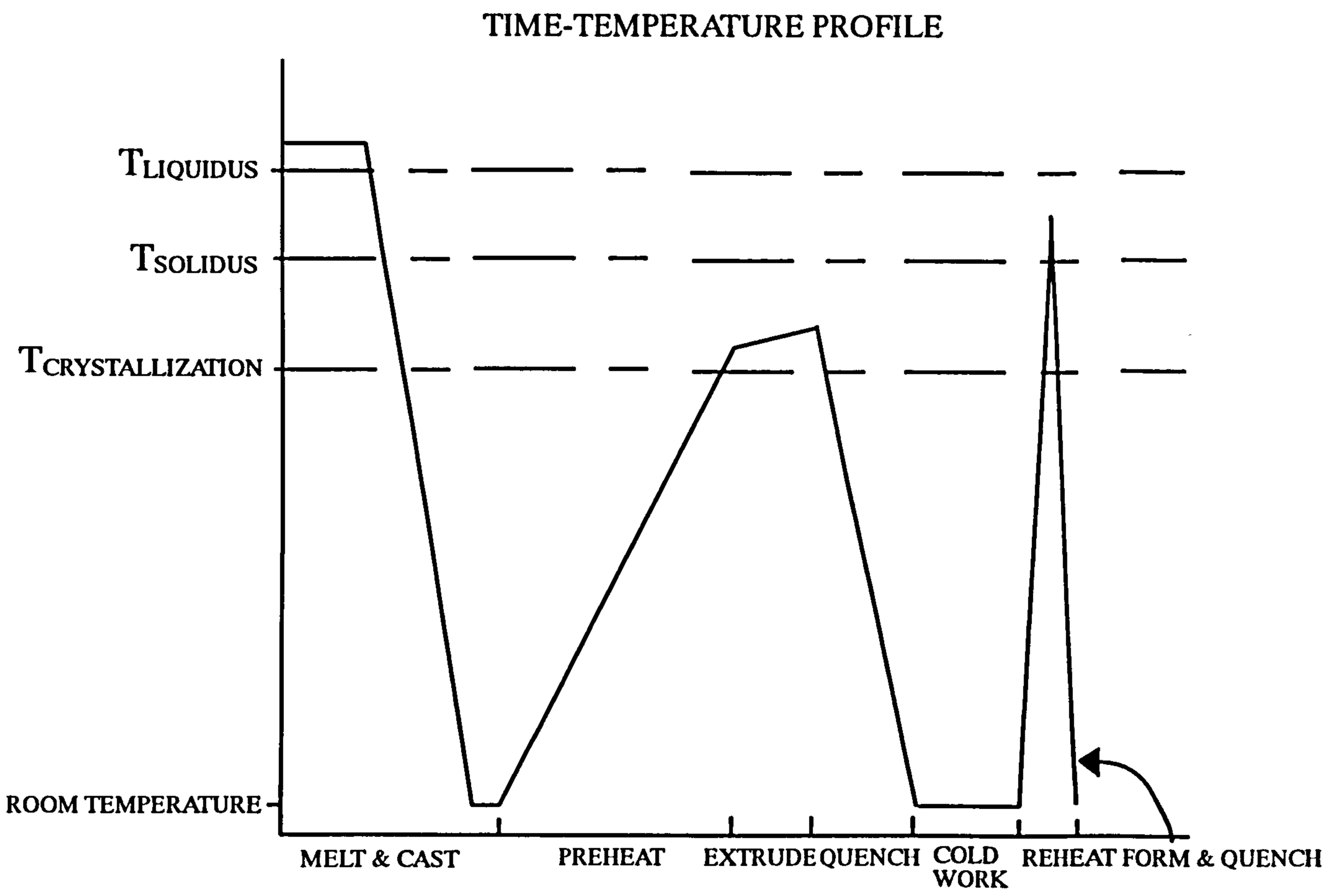

Fig. 1.4 Time-Temperature Profile of the SIMA process [after Young et. al., 1983].

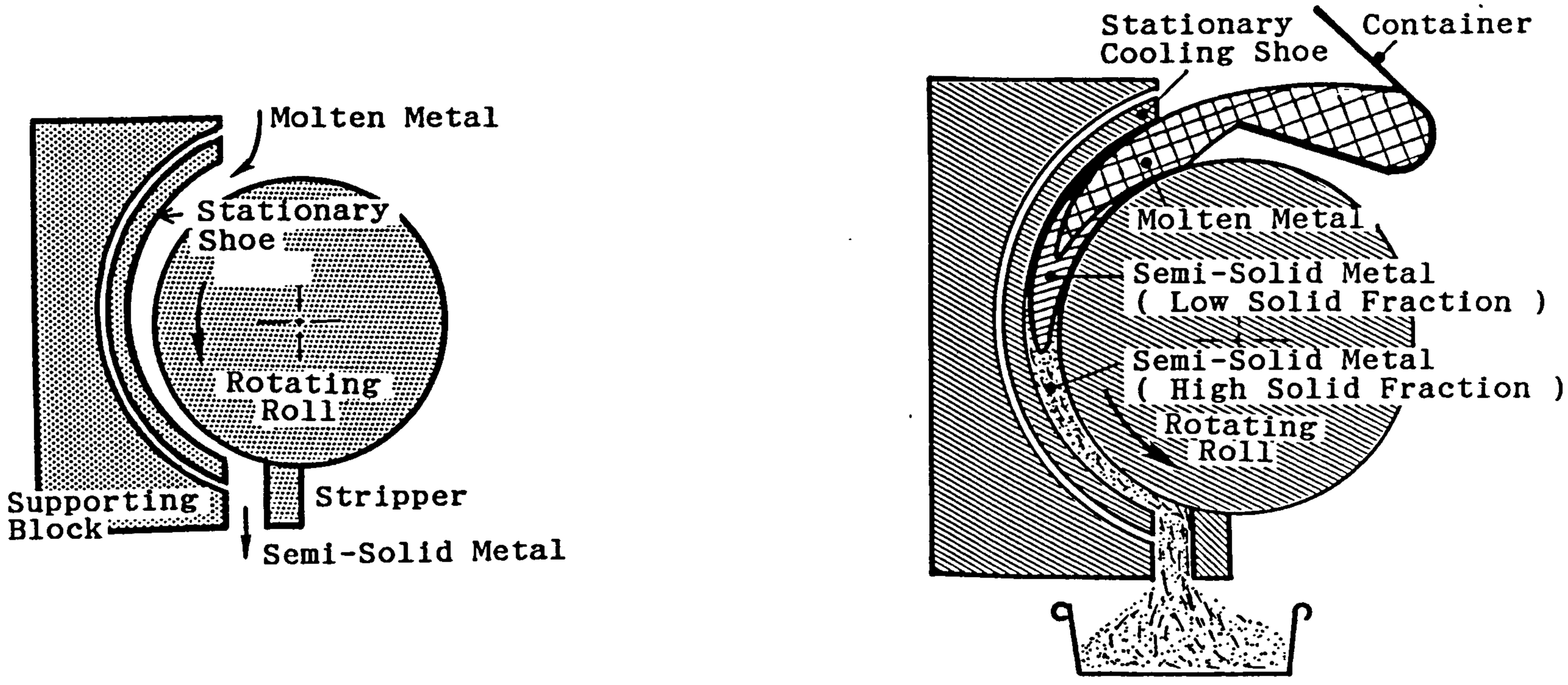

Fig. 1.5 Mechanics of shearing/cooling roll (SCR) process [after Kiuchi and Sugiyama, 1992].

CHAPTER 2

CHAPTER 2

WAVE PROPAGATION THEORY

2.0 Introduction

An alloy when heated at elevated temperature will first undergo a phase transition from a solid to a mixed solid/liquid phase before it becomes 100 per cent molten. Above the solidus temperature the percentage of liquid fraction will increase and the solid particles will gradually dissolve as the temperature rises. The process of transformation from a total solid to total liquid phase will affect the type of ultrasonic wave modes that can propagate through the medium due to the changes in the elastic properties.

This chapter will provide a brief theory of ultrasonic wave propagation in isotropic elastic solids, liquids and the mixed solid/liquid phase, which will be useful for the understanding of the results described in the experimental chapters. Mechanisms of ultrasonic attenuation that could occur in solids, liquids and the mixed state will also be discussed.

2.1 Ultrasonic Wave Propagation in Elastic Solids

The theory of ultrasonic wave propagation in elastic solids had been explained in many publications [Kolsky, 1953, Mason, 1958, Gooberman, 1964, Blitz, 1964, Achenbach, 1980, Cracknell, 1980 and Shutilov, 1988]. An elastic solid exhibits both bulk and shear elasticity, which enables it to support the various wave modes. If the solid is unbounded only bulk (longitudinal and shear) waves can propagate through it. A longitudinal wave occurs when the particle motion is along the direction of wave

propagation, and transverse or shear waves occur when the particle motion is perpendicular to the direction of wave propagation. If the solid has a free boundary, a Rayleigh surface wave may also propagate. The longitudinal velocity of sound in solid can be expressed as a function of the bulk modulus K and modulus of rigidity or shear modulus G and is written as:-

$$c_l = \sqrt{\frac{K+\frac{4}{3}G}{\rho}}\,, \tag{2.1}$$

where ρ is the density of the solid.

The shear velocity is expressed as:-

$$c_s = \sqrt{\frac{G}{\rho}}\,. \tag{2.2}$$

The longitudinal and shear wave velocities can also be expressed in terms of the Lame' constants μ and λ, and can be written :-

$$c_l = \sqrt{\frac{\lambda+2\mu}{\rho}}\,, \text{ and} \tag{2.3}$$

$$c_s = \sqrt{\frac{\mu}{\rho}}\,. \tag{2.4}$$

Silber and Ganglbauer, [1970] give the relationship between the density variation of the solid with temperature ρ_t as :-

$$\rho_t = \frac{\rho_{20^oC}}{1+3\alpha\Delta t} \tag{2.5}$$

where α is the linear coefficient of thermal expansion, and Δt is the difference in temperature referred to 20 °C. As temperature rises, there is usually an increase in the average atomic separation (thermal expansion) producing a reduction in the elastic constants of the material. It is reported by Brammer and Percival, [1970] that in the case of polycrystalline 2024 aluminium alloy at temperatures between 22 °C and 500 °C the bulk modulus K decreases by 13 per cent, the Young's modulus E by 30 per cent and the shear modulus decreases by 42 per cent. From equations (2.1) and (2.2) the acoustic wave velocities are directly proportional to the square root of K and G, and therefore the velocities are expected to decrease with increasing temperature.

2.1.1 Stress-Strain Relationship

A solid body is said to be in a state of stress and simultaneously be deformed when it is subjected to external forces. The strain (ratio of the increase in length to the initial length) components introduced can be either tensile or shear depending on the direction in which the strain occurs. Similarly, the stress acting on a body can be resolved into components parallel to the principal axes (fig. 2.1). For a body with symmetry, the stress and strain can be represented by only six independent components, three tensile and three shear. Within the elastic limit, the linear relation between the components of the stress tensor (σ_i) and the components of strain tensor (ε_j) can be expressed by the generalised Hooke's law:-

$$\sigma_i = C_{ij}\varepsilon_j \qquad (i,j = 1,2,3,4,5,6) \tag{2.6}$$

where the coefficients of form C_{ij} are the elastic constants of the material.

For an elastically isotropic solid there are no preferred directions in the material, only two independent elastic constants are required to describe the behaviour of the medium. The two coefficients are known as the Lame' constants and are denoted by λ and μ. We therefore have:-

$$\begin{aligned} C_{12} &= C_{13} = C_{21} = C_{23} = C_{31} = C_{32} = \lambda \\ C_{44} &= C_{55} = C_{66} = \mu \\ C_{11} &= C_{22} = C_{33} = \lambda + 2\mu \end{aligned} \tag{2.7}$$

Thus the final stress-strain relationship for an isotropic medium becomes:-

$$\begin{aligned} \sigma_1 &= (\lambda + 2\mu)\varepsilon_1 + \lambda\,\varepsilon_2 + \lambda\varepsilon_3 \\ \sigma_2 &= \lambda\,\varepsilon_1 + (\lambda + 2\mu)\varepsilon_2 + \lambda\,\varepsilon_3 \\ \sigma_3 &= \lambda\,\varepsilon_1 + \lambda\,\varepsilon_2 + (\lambda + 2\mu)\varepsilon_3 \\ \sigma_4 &= \lambda\,\varepsilon_4 \\ \sigma_5 &= \lambda\,\varepsilon_5 \\ \sigma_6 &= \lambda\,\varepsilon_6 \end{aligned} \tag{2.8}$$

2.1.2 The Equation of Wave Motion for an Isotropic Elastic Solid.

The type of acoustic wavefront propagating into a medium depends on the shape of the acoustic source. If the source is in the form of a pulsating sphere, the particle vibrations are directed radially and acoustic waves are propagated uniformly in all directions, resulting in spherical waves. If the source is vibrating in such a way that all the points on the surface are in phase, the wavefronts are plane, resulting in plane waves being generated. However, when the spherical waves are sufficiently far away from the source, the curvature of the wave fronts is so small that it can be regarded as a plane wave. The radius of the laser source is generally less than 1 mm and therefore can be considered as a 'point' source generating spherical waves.

However after travelling into the sample for a certain distance the waves progressively approximate to plane waves.

The general one dimensional wave equation for a plane source vibrating with simple harmonic motion is given by:-

$$\frac{\partial^2 u}{\partial t^2} = c^2 \frac{\partial^2 u}{\partial x^2} \tag{2.9}$$

where u is the displacement at a distance x from the source at a time t, and c is the propagation velocity.

In the case of a spherical source pulsating in a uniform isotropic medium the surface expands and contracts radially about its mean position. The acoustic intensity will fall off with distance from the source in accordance with the inverse square law. The general wave equation for a spherical wave can be written as:-

$$\frac{\partial^2 (rp)}{\partial t^2} = c^2 \frac{\partial^2 (rp)}{\partial r^2} \tag{2.10}$$

where r is the distance from the source and p is the acoustic pressure.

2.1.3 Reflection and Transmission of Elastic Waves at the Boundary

When an acoustic wave encounters an interface between two media, both reflection and transmission can take place. The energy of the wave is partitioned depending upon the type of incident wave (longitudinal or shear), how the wave approaches the interface (either at normal or oblique incidence to the interface), and the acoustic properties such as the characteristic impedance of the two media. The acoustic impedance Z is defined as the product of the density of the medium and the

acoustic wave velocity in the medium. At the boundary, in order to preserve continuity and for the media to be always in contact to each other, certain boundary conditions have to be satisfied. The normal displacements, tangential displacements, normal stresses and the tangential stresses must be equal on both sides of the interface.

2.1.3.1 At Normal Incidence

We will consider a plane boundary separating two half spaces which consist of homogeneous isotropic media 1 and 2 with characteristic impedance Z_1 and Z_2 (Fig. 2.2). For an acoustic plane wave incident normal to the boundary, part of the incident energy in medium 1 will be reflected back along its original path and the remainder will be transmitted into medium 2. The amount of the energy reflected and transmitted is determined by the intensity coefficient of reflection r and the intensity coefficient of transmission t respectively. The intensity coefficient of reflection which is defined as the ratio of the reflected to the incident acoustic wave intensity can be written as:-

$$r = \left(\frac{Z_1 - Z_2}{Z_1 + Z_2}\right)^2 \tag{2.11}$$

The intensity coefficient of transmission which is defined as the ratio of the transmitted to incident acoustic wave intensity is written as:-

$$t = \frac{4Z_1Z_2}{(Z_1+Z_2)^2} \tag{2.12}$$

These equations show that, when Z_1 and Z_2 are equal, t reaches its maximum value of unity and r becomes equal to zero. If Z_2 is much less than Z_1 then almost 100 per cent of the acoustic wave will be reflected (at for example a metal to air interface).

2.1.3.2 At Oblique Incidence

If the longitudinal wave C_1 is directed obliquely to the boundary (see fig.2.3), the type of waves that can be produced may be determined by resolving the stress and displacement components of the incident wave perpendicular and parallel with it. Since solids can sustain both shear and dilatational stresses, mode conversion can occur in the medium. Mode conversion that occurs in order to satisfy the boundary conditions results in partitioning of the energy into two or more modes each travelling at their own velocity. If both medium 1 and medium 2 shown in figure 2.3 are solids and medium 2 has a lower characteristic impedance than medium 1, then the layers of the media in the vicinity of the boundary will suffer both compressional and shear stresses. Hence both shear and longitudinal waves may be reflected and transmitted. The longitudinal and shear waves (C_2 and C_3, respectively) are reflected at angles θ_2 and θ_3 to the interface normal. The transmitted longitudinal and shear waves C_4 and C_5, are refracted at angles θ_4 and θ_5 respectively. Since C_1 and C_3 travel in the same medium velocity C_1 must be equal to C_3 and angle θ_1 must be equal to θ_2. The velocity and direction of the waves are given in accordance with Snell's law by the expression:-

$$\frac{C_1}{\sin\theta_1} = \frac{C_2}{\sin\theta_2} = \frac{C_3}{\sin\theta_3} = \frac{C_4}{\sin\theta_4} = \frac{C_5}{\sin\theta_5} \qquad (2.13)$$

Some of the samples supplied for the work were relatively small (approximately 33 mm) in diameter (only twice the size of the approximately 15 mm diameter EMAT detection coil), and the acoustic waves generated by the pulsed laser are travelling at certain angles to the normal of the sample surfaces. It is therefore possible that, in addition to the direct acoustic wave pulses and the multi-reflection echoes, mode converted signals from the end and side faces are also detected. Hence Snell's law has to be applied in deciding the optimum dimensions of the sample so that the side wall reflection signals would not superimpose and interfere with the direct pulses.

2.2 Acoustic Wave Propagation in Liquids

Liquids normally exhibit only volume elasticity where deformation due to hydrostatic compression are possible whereas the modulus of rigidity (G) is zero. Therefore only longitudinal waves can propagate in liquids. Even though the formation of shear waves is also possible in some viscous liquids, such waves are attenuated over negligibly small distances from the source, so can be neglected. Molten metals are often in this category The velocity of sound in liquid can be written as:-

$$c = \sqrt{\frac{K_l}{\rho}} = \sqrt{\frac{1}{\kappa_l \rho}} \qquad (2.14)$$

where K_l is the adiabatic bulk modulus, κ_l is the adiabatic compressibility, and ρ is density of the liquid. It is reported by Shutilov, [1988] that the velocity of ultrasound in almost all liquids decreases monotonically and quite considerably (2-6 ms^{-1} per °C)

with temperature. However Kamioka and Sumino, [1984] reported that there is hardly any change in the ultrasound velocity in the eutectic Bi-Sn composition but they observed a steady decrease of less than 1 ms^{-1} per °C in the case of hyper-eutectic alloys.

2.3 Acoustic Wave Propagation in Solid-Liquid Mixtures

In the semi-solid state a solid-liquid mixture can be assumed to be equivalent to that of a suspension where the solid particles are suspended in the liquid. The acoustic wave speed in the solid-liquid mixture can be therefore said to be dependent on the material properties of the two constituents as well as their relative concentrations [Atkinson and Kytomaa, 1992]. To obtain the stress-strain relationship of the mixed medium, we can consider following Biot, [1954], where a volume of the solid-liquid mixture is represented by a cube of unit size. The stress tensor in the medium can be separated into two parts, one for the solid and one for the liquid.

As written by Atkinson and Kytomaa, [1992] the wave speed c is given by:-

$$c = \sqrt{\frac{K}{\rho}} \tag{2.15}$$

where the effective bulk modulus of the system is given by:-

$$\frac{1}{K} = \frac{\upsilon}{K_s} + \frac{(1-\upsilon)}{K_l} \tag{2.16}$$

where K_s and K_l are the bulk moduli of the solid and liquid respectively, and υ is the solid volume fraction. Equation (2.16) is applicable when the particle size is much less then the wavelength. The density of the solid-liquid mixture is given by:-

$$\rho = \nu\rho_s + (1-\nu)\rho_l \qquad (2.17)$$

where ρ_l and ρ_s are the densities of the solid and liquid respectively. In a mixed solid/liquid phase there is a substantial decrease in the acoustic wave velocities as the percentage of liquid increases. This phenomenon was observed in Bi-Sn alloys having eutectic and hyper-eutectic compositions [Kamioka, 1983]. Similar behaviour was also observed by Atkinson and Kytomaa, [1992] when they modelled the acoustic wave propagation in a monodispersed suspension of varying solid concentrations for wavelengths much larger than the particle size (for frequency range of 100 kHz to 1 MHz which corresponded to ka ~ 0.2-0.6, where ka is the ratio of the particle radius (a) to wavelength (λ) since the wave number $k = 2\pi/\lambda$). They also observed that the sound speed is insensitive to frequency and all other factors except the fluid and particles densities and compressibilities. However Hampton, [1967] reported that for a frequency range of 4-200 KHz corresponding to ka ~ 6.66×10^{-5}, the velocity of sound in sendiment is close to the velocity of water at low concentrations but reaches a minimum at about 25 % concentration and than increases with increasing concentrations. He also reported that the measured velocity increases with frequency with a dispersion of approximately 2 % over the above mentioned frequency range. Ahuja and Hendee, [1978] observed that for large differences in density between suspension components, there are substantial effects of particle shape, orientation, and ultrasonic frequency on the velocity of ultrasound through the suspension.

Figure 2.4 shows the theoretical and experimental (data obtained from chapter 4 of this thesis) variations of the longitudinal wave velocities as a function of temperature in the Al 4.86 % Si alloy. The theoretical values appear to be lower then

the measured values obtained in the semi-solid state. The theoretical values in the semi-solid state were determined based on the model by Atkinson and Kytomaa, [1992] on monodisperse suspensions of varying solid concentration, for wavelengths much larger than the particle size, including unsteady motion of particles in a viscous fluid, for the situation where particle interactions are predominantly inviscid. They assumed that the particles as well as the liquid phase constitute a continuum. The above models attempt to calculate the acoustic velocity in suspensions of solid particles in a liquid at fixed temperature. The theoretical graphs plotted in fig. 2.4, from a total solid to a total liquid phase, were based on this approach but as the solid to liquid ratio was varied the elastic constants and densities of the two phases were varied. The velocities in the solid and liquid phases were represented by straight line fits to the experimental data, these lines were extrapolated to estimate the elastic constants in the two phase region as a function of temperature. At the eutectic temperature the alloy has to melt to 40 % liquid before any further increase in temperature is possible. The densities of the two phases were estimated from equation (2.5) using the linear coefficient of thermal expansion of pure aluminium, Kaye and Laby, [1986], the density of the liquid was assumed to be 5 % less than the solid at each temperature. A compressional wave will propagate through a liquid at a velocity determined by the bulk modulus, however the elastic constant that determines the velocity through solid particles suspended in the liquid will depend on the particle size, the acoustic wavelength and interconnections between particles. If the particle size is much smaller than the wavelength and the particles are isolated equation (2.16) applies as shown by curve b. If the particle size is larger than the wavelength and the particles are interconnected to form a solid framework, it might be more appropriate

to replace K_s in equation (2.16) with the longitudinal modulus (curve a). From figure 2.4 it appears that curve a is closer to the experimental data compared to curve b.

2.4 Attenuation of Ultrasonic Waves

Attenuation refers to the diminishing of intensity of the wavefront as it progresses through the medium. For infinite plane wavefronts, attenuation is mainly caused by absorption and scattering, and practically occurs in all solids and fluids as the ultrasonic beam propagates. Absorption can be caused by several factors such as internal friction (viscosity), elastic hysteresis, heat conduction and relaxation phenomena. Scattering takes place whenever there exists regions of varying density or elasticity such as grain boundaries, inclusions, and other forms of discontinuities.

2.4.1 Attenuation in Solids

The attenuation of acoustic energy in polycrystalline metals is generally due to elastic hysteresis, thermoelastic relaxation and scattering [Mason, 1958, and Darbari et. al., 1968]. The elastic hysteresis is caused by the time-independent nonlinear stress-strain relationship. Loss due to thermoelastic relaxation is caused by the fluctuations in the stress distribution which results in irreversible heat currents. Scattering due to the polycrystalline grains contributed a large part of the ultrasonic attenuation in polycrystalline metals [Papadakis, 1965]. Even though a polycrystalline solid may be isotropic because of the random orientation of its grains, the grains themselves are usually anisotropic. This leads to differences in characteristic impedances on either side of a grain boundary. Reflection can thus occur and the acoustic beam will be defracted or scattered, depending on the grain size and acoustic

frequency. There are three types of scattering, firstly the one that occurs when the acoustic wavelength is much greater than the average grain diameter and is known as Rayleigh scattering, secondly stochastic scattering occurs when the acoustic wavelength is approximately equal to the average grain diameter, and finally diffusion scattering occurs when the acoustic wavelength is lesser than or equal to the average grain diameter. Attenuation due to scattering is most noticeable at frequencies greater than 1 MHz. Rayleigh scattering is proportional to the third power of the average grain diameter (D) and to the fourth power of the frequency (f) of the acoustic waves ($\alpha \propto D^3 f^4$), [Mason, 1958]. Stochastic scattering is proportional to the average grain diameter and to the second power of the frequency [Papadakis, 1965]. However, diffusion scattering is inversely proportional to the grain diameter and independent of the frequency [Mason and McSkimin, 1948]. Since mode conversion occurs at the interface, so the scattered energy is carried away by both the longitudinal and shear waves. An expression for Rayleigh scattering of the longitudinal and shear acoustic waves by cubic crystallites has been given by Bhatia, [1967] and written as:-

$$\alpha_l = \frac{8\pi^3 \mu^2 D' f^4}{375 \rho^2 V_l^3}\left(\frac{2}{V_l^5} + \frac{3}{V_s^5}\right) \tag{2.18}$$

$$\alpha_s = \frac{2\pi^3 \mu^2 D' f^4}{125 \rho^2 V_s^3}\left(\frac{3}{V_s^5} + \frac{2}{V_l^5}\right) \tag{2.19}$$

where $\mu = c_{11} - c_{12} - 2c_{44}$ and c_{11}, c_{12} and c_{44} are the single crystal elastic constants of the cubic material, V_l and V_s are the longitudinal and shear wave velocities respectively, ρ is the density of the material, f is the frequency of the acoustic wave and D' is the average grain size volume. The above expressions

indicate that both attenuation coefficients are proportional to the average grain size volume and inversely proportional to the acoustic wave velocities. For most solids, the longitudinal wave velocity is approximately equal to twice the shear wave velocity, therefore it appears that the shear wave velocity should contribute more to both attenuation coefficients. Furthermore since the acoustic wave velocities in general decrease with increasing temperature the attenuations are therefore expected to increase as the temperature rises as expressed by equations (2.18) and (2.19). The grain size of the material is expected to grow when it is heated for a certain period of time, and according to Papadakis, [1965] the average grain volume D' is given by:-

$$D' = \frac{4\pi\langle R^6\rangle}{3\langle R^3\rangle} \tag{2.20}$$

where R is the radius of the spherical grain. Therefore, the average grain size volume increases as the grain size grows. Since the longitudinal and shear attenuation coefficients are proportional to the average grain size volume, both coefficients are expected to increase greatly as the grain size grows with increasing temperature.

2.4.2 Attenuation in Liquids

Absorption in liquids generally varies with the square of the frequency. In liquids absorption can be due to the viscosity, thermal conductivity and relaxation mechanisms. Viscous losses arise in a liquid when compression waves pass through it and the medium is subjected to shear stresses. The resultant viscosity absorption coefficient given by Blitz [1964] is expressed as:-

$$\alpha_{vis.} = \left(\frac{8\pi^2}{3}\right)\left(\frac{\eta}{\rho c^3}\right) f^2 \qquad (2.21)$$

where is ρ the density, η is the viscosity, and c the acoustic velocity for the medium; f is the frequency of the acoustic wave.

Thermal conduction losses occur because of the sinusoidal distribution of acoustic pressure with distance where certain layers in the liquid are compressed and others expanded. The compressed layers that have higher temperatures compared to the expanded layers create a temperature gradient within the liquid and cause a small overall increase in temperature of the medium and hence absorption of ultrasound occurs. The thermal absorption coefficient α_{th} is expressed as:-

$$\alpha_{th} = \left(\frac{2\pi^2 K}{\rho c^3 c_v}\right) f^2 \frac{(\gamma-1)}{\gamma} \qquad (2.22)$$

where K is the coefficient of thermal conductivity, c_v the specific heat at constant volume, and γ is the ratio of c_v to the specific heat at constant pressure (c_p) for the medium. Both expressions (2.21) and (2.22) indicate that the absorption coefficient increases as the acoustic wave velocity decreases.

Thermal or structural relaxation losses in liquids are due to molecular internal energy exchanges. Thermal relaxation arises from exchanges of energy between different thermal states of the molecules, and absorption occurs because of phase differences between the alternating exchanges of energy and the acoustic waves. Structural relaxation losses occur when the displacement of the molecules from one position in a lattice to another becomes out of phase with the sound wave. According to Webber and Stephens, [1970] molten metals are monatomic in character and attenuation due to thermal conduction is the principal loss mechanism which is about

5 to 12 times greater than that due to shear viscosity. It is mentioned by Kaye and Laby, [1986] that the attenuation in liquids generally decreases with increasing temperature. However in a study by [Kamioka and Sumino, 1984] on eutectic and hyper-eutectic Bi-Sn alloys, it was observed that the attenuation is almost constant at temperatures between 140 °C and 160 °C but shows a marked increase at higher temperatures. Scattering could also occur in liquids and may dominate the attenuation coefficient when there are gas bubbles present in the medium.

2.4.3 Attenuation in Solid-Liquid Mixtures

Similar to solids and liquids, the attenuation in the mixed solid/liquid phase can also occur by both absorption and scattering processes. Allergra and Hawley, [1972] reported that the absorption of ultrasound in emulsions and suspensions is due to viscous and thermal transport processes occuring at the interface of the non-homogeneities, as well as to the intrinsic absorption in the materials comprising the system. Since in the mixed phase solid particles are suspending in the liquid, attenuation due to scattering could be the dominating factor, in particular Rayleigh scattering, when the wavelength of the acoustic wave is much greater than the average particle size. Hampton, [1967] reported that the acoustic attenuation of high frequency sound (50-600 KHz) in suspensions of small particles (corresponding to low value of ka) is non-monotonic with respect to the concentration of solids in suspension, and there is a distinct maximum in attenuation between 15 % and 20 % concentration. This is in agreement with the results obtained by Atkinson and Kytomaa, [1992] who observed that for frequencies between 0.1 MHz and 1 MHz the attenuation seems to have non-monotonic behaviour with respect to solids fraction at

low frequencies and it becomes monotonic at high frequencies. In a study on Bi-Sn alloys Kamioka, [1984] observed that the attenuation of ultrasound in a liquid is less than that in the corresponding solid. He also observed that the attenuation is a maximum from 20 to 30 % liquid fractions and decreases at higher temperatures as the percentage of solid fraction decreases. Blue and McLeroy, [1968] have shown that the attenuation in suspension depends upon the shape of the particles, where over the frequency range of 0.15 to 1.5 MHz, the measured absorption coefficients for disk-like and needle-shaped particles are less than those for equivalent spheres by 5 % to 27 % and 24 % to 41 %, respectively.

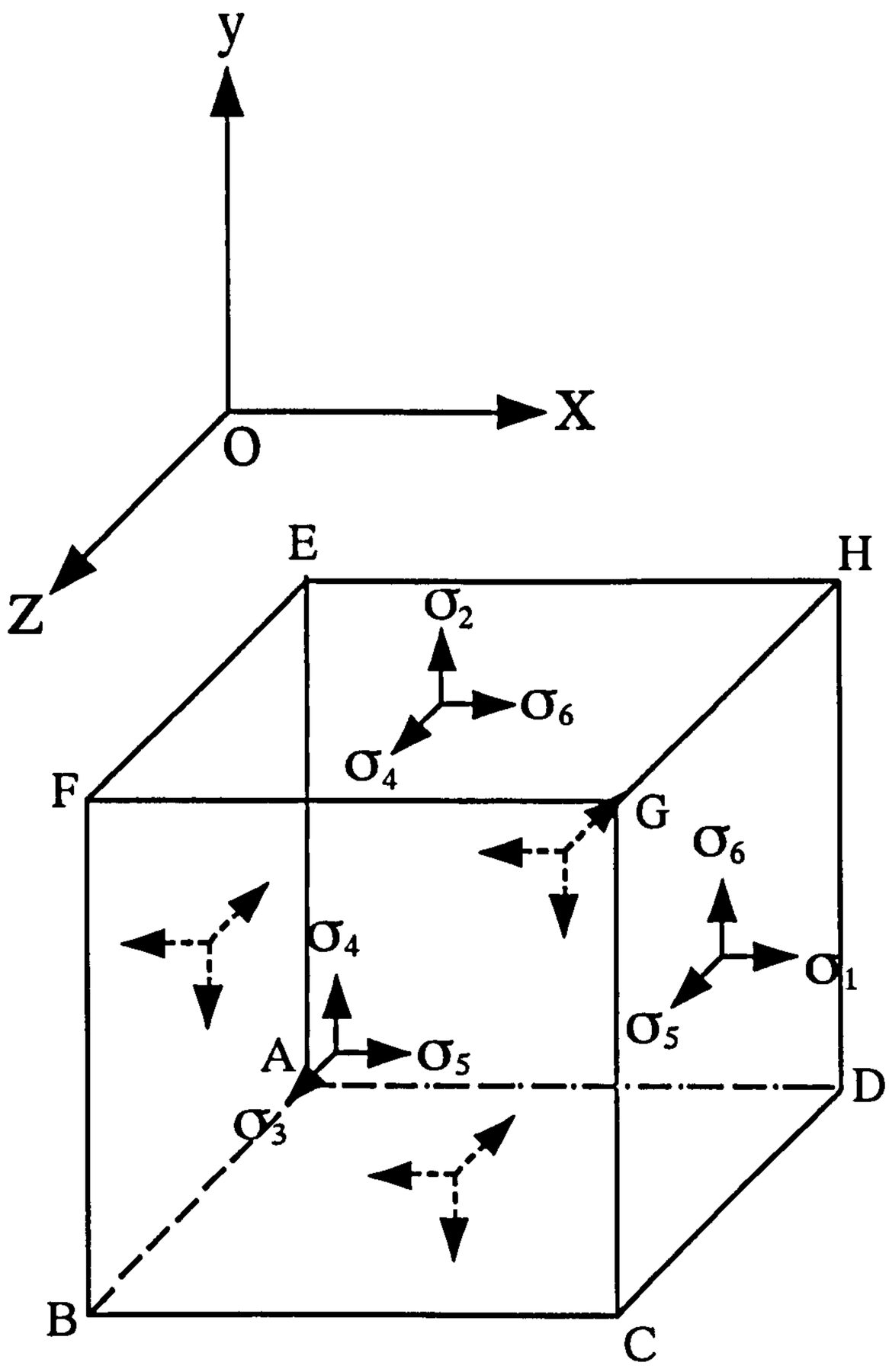

Fig. 2.1 The six components of stress.

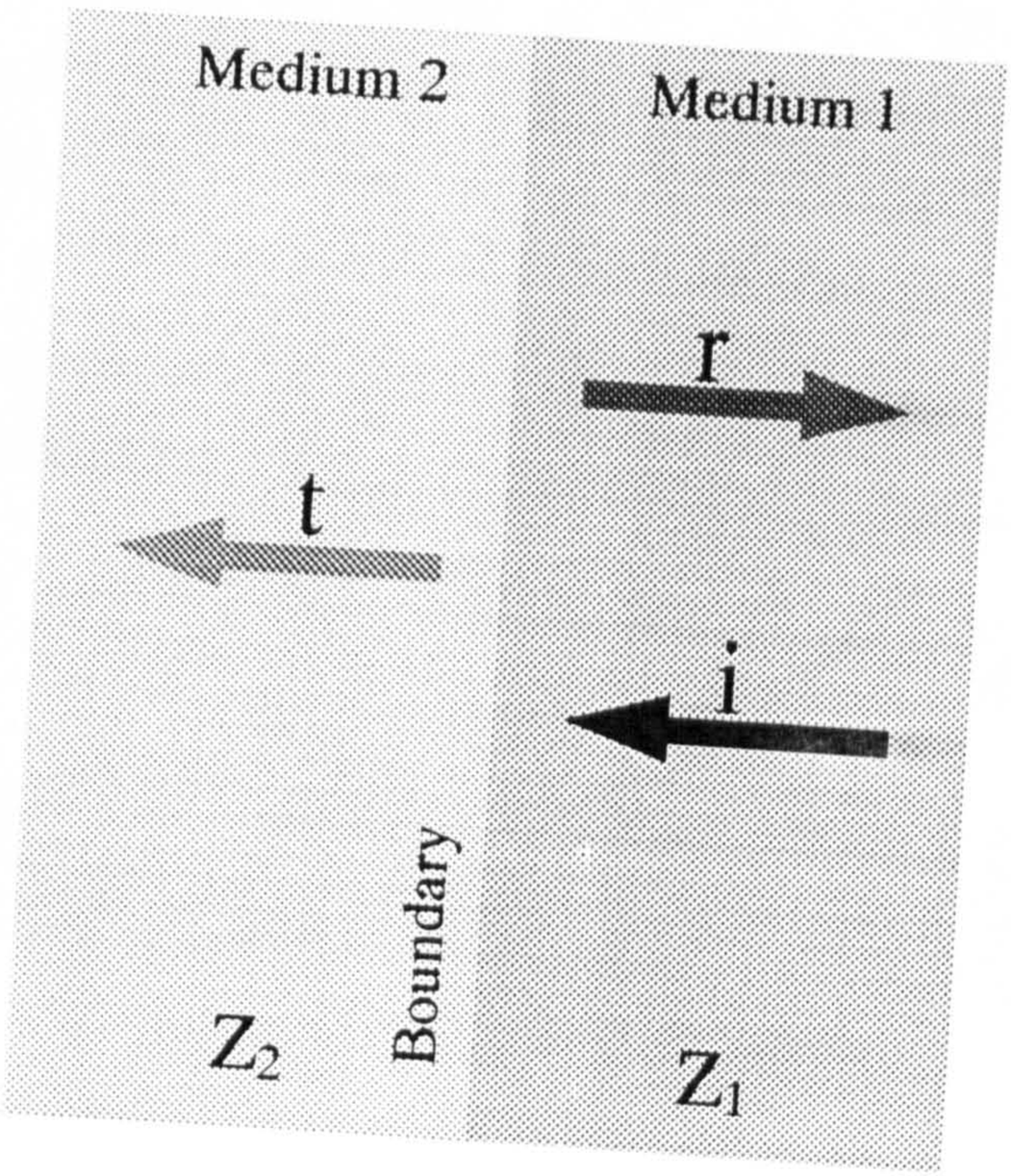

Fig. 2.2 Reflection and transmission of plane waves at normal incidence to a plane boundary; i is the incident wave, r is the reflected wave and t is the transmitted wave.

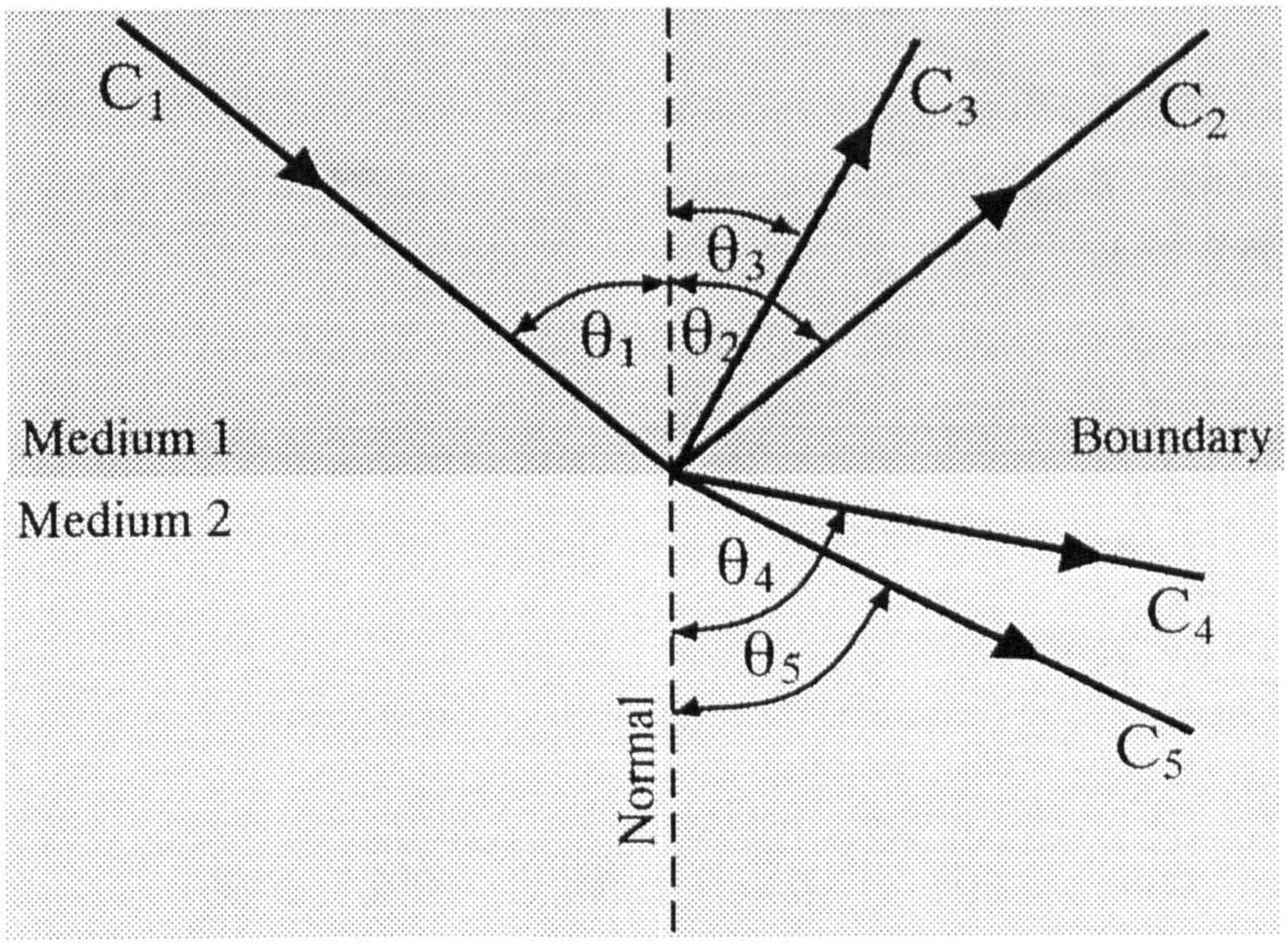

Fig. 2.3 Reflection and refraction of longitudinal wave incident to a plane boundary separating two media.

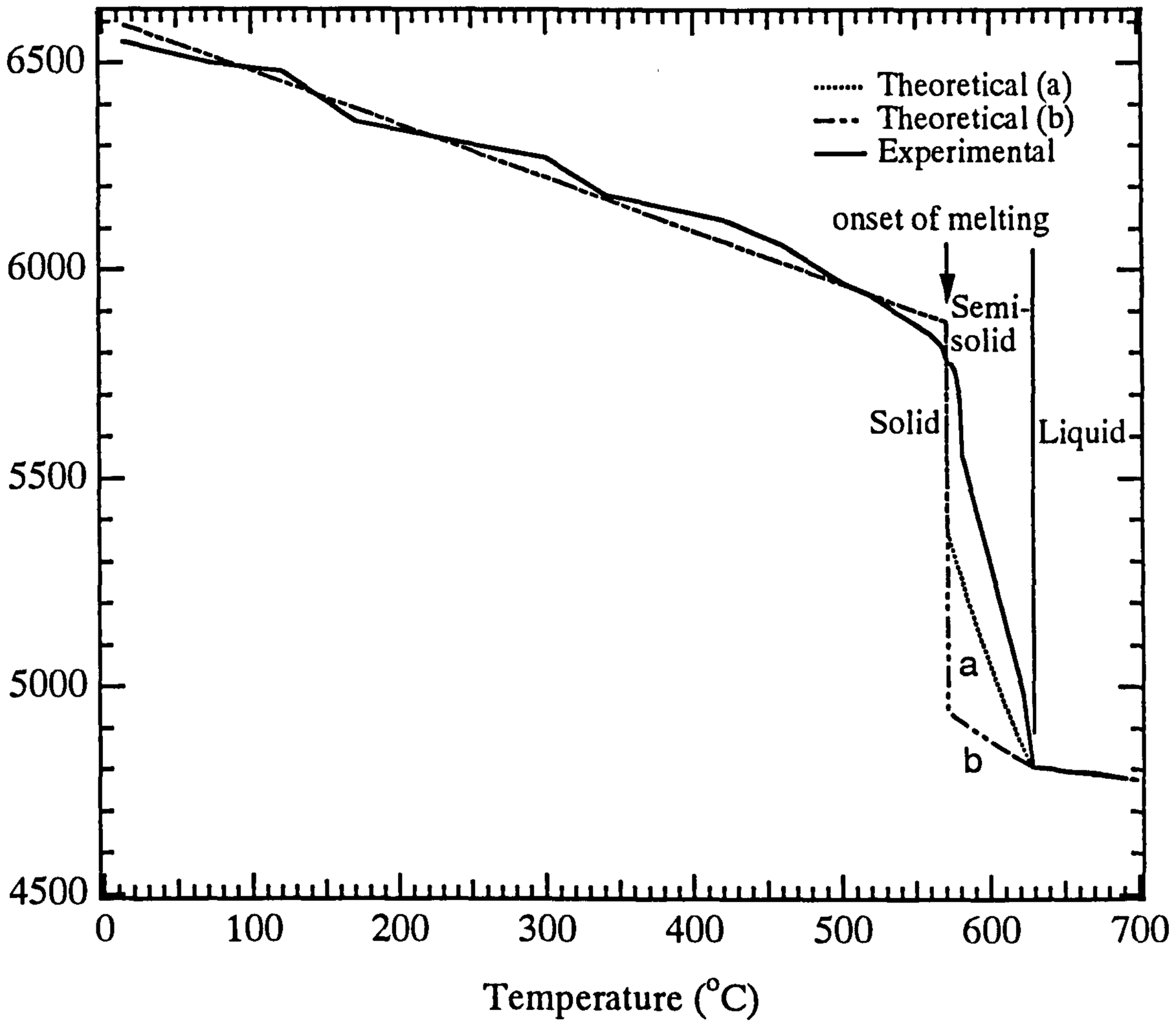

Fig. 2.4 The theoretical and experimental variations of longitudinal wave velocities as a function of temperature in Al 4.86 % Si alloy.

CHAPTER 3

CHAPTER 3

LITERATURE REVIEW-APPLICATIONS OF NON-CONTACTING ULTRASOUND AT ELEVATED TEMPERATURE

3.0 Introduction

Ultrasonic methods have been widely used as a means for quality control in various industries such as the energy power plant, the oil and gas industries, chemical industries, and the aerospace industries. The inspection is normally carried out at or near ambient temperature by qualified non-destructive testing (NDT) personnel using conventional contact ultrasonic techniques. With these techniques, the piezoelectric transducer is usually coupled to the test piece with the aid of a liquid couplant, to allow maximum transmission of ultrasonic waves into the test piece. The same transducer is used to detect the reflected acoustic waves. However in the production plant such as the steel making industry, it has been identified that in the production of billets, it would be more economical to carry out inspection at an early stage of the processing sequence when the material is still hot. The procedure will prevent processing defective materials and reduce the material losses which will then result in substantial reduction in the plant production cost and time. Realising the need to carry out ultrasonic inspections at high temperature, extensive studies have been carried out since the early 1960s to develop high temperature ultrasonic probes for various industrial applications. A wide range of high temperature transducer systems, either contacting or non-contacting, have been designed to study the temperature dependence of elastic constants [Brammer and Percival, 1970], attenuation [Darbari et. al., 1971] and phase transformations [Lavender, 1971]. The use of high

temperature ultrasonics for flaw detection [Kubota et. al., 1986], thickness measurement [Wilkinson, 1964] and internal temperature measurement [Wadley et. al., 1986] has also been investigated.

Measurements at elevated temperature using conventional contact ultrasonic techniques are problematic and need extra considerations, a temperature gradient must be created between the transducer and the hot sample surface, and a viscous fluid with high evaporating temperature is required as the couplant. Andrews [1982], reviews the various methods designed to meet the first requirement, such as the water column or water flow system and the use of buffer rods on which the transducer is mounted at one end and coupled under pressure to the sample by dry contact. However, such methods can result in sample cooling and deformation over the area of contact. With respect to the second requirement, most ultrasonic couplants are not suitable to be used for temperatures above 300 °C as they tend to lose their viscosity, evaporate, and undergo chemical degradation. Therefore in order to overcome these problems, true non-contacting ultrasonic systems have been seriously considered.

In this chapter previous applications of non-contacting ultrasound at elevated temperature, in particular the laser and electromagnetic based techniques are reviewed and evaluated.

3.1 Non-Contacting Ultrasonic Techniques

In non-contacting ultrasound the transducers are physically not in contact with the sample surface. No coupling fluid is needed between the transducer and the hot sample surface since the acoustic source is located in or near the surface of the sample under examination. True non-contact techniques do not disturb the elastic wave

propagation into the material by loading the sample surface. The earliest usage of the pulsed laser technique to generate ultrasound at elevated temperature was reported by Brammer and Percival, [1970], however the system was not totally non-contact because a conventional piezoelectric transducer was used as the detector. Other non-contact methods available include the capacitance transducer [Hutchins and Macphail, 1985] which can only be used as a detector, and the spark discharge method [Cooper, 1985] which is only able to be used as an ultrasound generator. However these methods are not widely used because of the fact that the transducer must be operated within a few micrometers from the sample surface in the case of capacitance measurements, and the spark discharge is hazardous.

3.1.1 Laser Generation of Ultrasound

A pulsed laser such as Ruby, Nd:YAG or CO_2 is capable of producing sufficiently high energy pulses in the 1-100 ns range and can generate wide bandwidth ultrasound in both electrically conducting and non-conducting materials including those with rough or coated surfaces. In a solid, both the bulk (longitudinal and shear) waves and surface waves can be generated simultaneously with only a single laser pulse. The dominant wave mode generated is greatly dependent on the type of ultrasound generation mechanism selected. However, in a liquid only the longitudinal wave is generated as the medium cannot support the induced shear stresses. There are several reviews of laser ultrasound generation mechanisms available [Scruby et. al., 1989, Scruby and Drain, 1990 and Davies et. al., 1993], however since the understanding of the generation mechanisms is essential for the thesis, they will be briefly described in the next sub-sections.

3.1.1.1 Thermoelastic Source

The generation mechanism may be selected by varying either the incident optical power density or the conditions of the irradiated surface. When a clean metal surface is irradiated by a laser pulse of sufficiently low power density (less than 2.0 x 10^7 Wcm^{-2}), the rapid local temperature rise results in transient thermoelastic stresses and strains at the surface. In this case, the acoustic generation occurs by thermal expansion of a thin surface disc. The stresses and strains in the source are primarily dipolar and parallel to the surface, the stress free boundary conditions almost totally relieve the normal component (Fig. 3.1). Thus this type of source results in predominantly shear wave generation. The source also has a wide bandwidth and does not damage the irradiated metal surface. In the thermoelastic regime, the longitudinal and shear wave directivity patterns are mainly confined to lobes centred around directions of 55 ° and 30 ° normal to the sample surface respectively.

3.1.1.2 Ablation Source

If higher power densities are used, so that the threshold for ablation (i.e. the melting point of the metal) is exceeded, removal of solid from the metal leads to a normal recoil force over the irradiated surface. The normal force leads to efficient longitudinal mode generation which propagates normal to the surface (Fig. 3.2). Hence, there will be an increase in longitudinal wave signal amplitude on epicentre (on the opposite side directly behind the source) and a relative decrease in the shear wave amplitude as the optical power density is increased to create a more vigorous ablation. At elevated temperature, if the laser power density is kept constant there will be a

tendency for the normal component to increase relative to the in-plane component as progressively less energy is required to raise the hot material to the ablation threshold. As a result enhanced longitudinal wave generation occurs as the temperature increases. In the ablation regime, the longitudinal wave energy is concentrated about a normal to the surface and the shear wave pattern is less directional compared to that in the thermoelastic case.

3.1.1.3 Source Due to Constrained Surfaces

Longitudinal wave generation can also be enhanced at low power densities by altering the surface conditions, that is, by coating the sample surface with a suitable liquid such as water, oil, or acetone. Under such conditions the laser energy tends to be absorbed within the liquid, causing it to evaporate. The recoil force from this process causes the resultant acoustic source to be dominated by forces normal to the surface. These forces will have a pulse like time dependence and although thermoelastic stresses will still exist they will tend to be negligible in comparison. A different approach is to constrain the metal surface with a well bonded transparent solid as shown in figure 3.3. In this case, there will be changes in the elastic boundary conditions at the surface of the metal. The surface is no longer free. Hence, in addition to the dipolar stresses parallel to the surface, there are also dipolar stresses normal to the surface.

3.1.1.4 Breakdown Source

The breakdown source is normally obtained using a pulsed CO_2 laser [Taylor, 1992]. It is caused by the localised addition of the incoming and reflected laser beams just above the surface of the sample by arranging the metal surface to be close to the focal point of the lens. The initial electron concentration required to seed the breakdown process comes from vaporisation of a small amount of the target material by absorption of the incident beam. The shock wave propagating to the sample surface from the air breakdown provides the source of ultrasound in the sample. The generation of ultrasound by this mechanism produces no damage to the metal surface even after repeated shots. The waveform is characteristic of a normal force with Heaviside time dependence due to the relatively long persistence of the expanding plasma.

3.1.2 Laser Detection of Ultrasound

The ultrasonic waves can be detected by laser interferometery. There are many types of laser interferometers and the ones commonly used for ultrasonics are the stabilised Michelson [McKie, 1987], optical heterodyning [Monchalin and Heon, 1986] and Fabry-Perot [Aussel and Monchalin, 1989, and Telchow et. al., 1990] interferometers. In the Michelson interferometer the light scattered or reflected from the sample surface is made to interfere with a reference beam, thus giving a measure of optical phase and hence instantaneous surface displacement. Stabilisation is achieved by changing the effective optical path length of the reference beam to compensate for the low frequency component of the movement of the surface. This

can be done by feeding back the output from the balanced detectors to control an electro-mechanical, piezoelectric or electro-optic phase shifting device in the reference beam. The arrangement of the stabilised Michelson interferometer used by McKie, [1987] is shown in figure 3.4.

An optical heterodyning interferometer relies on beating the wave scattered by the surface with a frequency-shifted reference wave. An acousto-optic Bragg cell is generally used to shift the optical frequency. The output signal of the technique is centred on the shift frequency but phase modulated in proportion to the displacement of the surface. The technique is sensitive to optical speckle and the best sensitivity is obtained when one speckle is effectively detected. An example of the heterodyning interferometer is shown in figure 3.5. A Fabry-Perot interferometer is designed to detect changes in the frequency of the scattered or reflected light, thus, giving an output dependent on the velocity of the surface. The interferometer is insensitive to the low frequency vibration motion of the surface, and for rough surfaces the sensitivity is not fundamentally limited by the speckle effect. Heterodyne confocal Fabry-Perot interferometers are normally used for ultrasound measurements as they have a large light gathering aperture and can be stabilised. The interference is produced by two waves issuing from different points on the surface or from one single point illuminated by two distinct beams, one frequency shifted by an opto-acoustic modulator. The signal detected is proportional to the differential particle displacement and is insensitive to uniform sample motion from ambient disturbances. Since both the signal and reference beams are reflected from the same sample surface, they will remain parallel regardless of any sample tilt and are therefore not very sensitive to the

surface orientation. A schematic diagram of the Fabry-Perot interferometer used by Telschow et. al., [1990] is shown in figure 3.6

Michelson interferometers are suited to laboratory work concerning ultrasonics but they are unsuitable for routine inspection tasks because of their reliance on high reflectivity at the detection surface. When the surface of the specimen is rough and optically scattering, the optical heterodyning or Fabry-Perot interferometer can be considered. With the combinations of a pulsed laser as the ultrasound generator and an interferometer as the detector, the system can be remote and suitable for making measurements in materials at elevated temperature, in corrosive and other hostile environments. The system can also be applied in geometrically difficult to reach locations.

Various combinations of the totally remote laser systems have been used to study different types of materials for different purposes at elevated temperature. The applications had been reported by many researchers, and will be reviewed in the next section.

3.1.3 Applications of Laser-Laser Systems

Some of the earlier applications of the laser-laser systems at elevated temperature had been reviewed by McKie, [1987], and Scruby and Drain, [1990]. It should be noted that the earliest study, using the totally remote laser system to detect the elastic waves generated in materials at elevated temperature, was reported by Calder and Wilcox, [1978]. Elastic waves were generated by Q-switched Nd:Glass laser pulses of up to 15 Joules in energy and 30 ns duration, incident at one end of the sample and detected on the opposite side by a Michelson interferometer. A single

frequency argon laser, operated at 514.5 nm with power levels of the order of 0.1 W, was used to provide the light source for the Michelson interferometer. The sample detection surface was polished to a mirror finished to provide maximum reflectivity and became one mirror of the interferometer. Measurements were made on 6061-T6 aluminium, AISI-304 stainless steel, copper, brass, tantalum, and molybdenum. The samples were heated in a clamshell oven that was opened at both ends to give convenient optical access for both generating and detecting the acoustic waves, and also for sample loading. The degradation of the polished sample surface at high temperatures prevented them from making measurements to the expected temperatures except for stainless steel. In anticipation of potential oxidation problems at high temperature, they also gold plated the polished end of one sample of every material, however they still failed to obtain high temperature data since, although gold is corrosion resistant at high temperatures, it did not adhere well to the sample surface. In another related experiment Calder et. al., [1981] used a similar system to measure the elastic constants of pure plutonium and Pu-1 wt % Ga delta-stabilised alloy at elevated temperatures. However, in this case they used a single frequency 50 mW He-Ne laser to provide the light for the Michelson interferometer. To minimise the possibility of radiation reaching the laboratory environment, the test chamber was fabricated from stainless steel, and had two containment barriers. As an additional safety feature, inert gas was circulated between the primary and secondary containment barriers and filtered with a high efficiency particulate filter. Two sapphire windows located at each end of the chamber were used as seals and also provided laser access. The specimen was heated by a clamshell oven located inside the test chamber, and the system evacuated to reduce the oxidation rate of the polished end of

the plutonium rod. They intended to test the pure Pu through all its phases to temperatures approaching the melting point (640 °C), however the sudden degradation of the specimen mirror at 119 °C, the α to β phase change temperature, prevented data at higher temperatures being obtained. In the case of plutonium alloy, there were no phase changes until the δ to ε phase and the mirror degradation was reported to be gradual with increasing temperature. They concluded that the results obtained using this technique were in good agreement with the limited published data available, and showed linearly decreasing values of the Young's and shear moduli with increasing temperature.

The determination of both shear and longitudinal wave velocities in ceramics and metal/ceramic composites at temperature up to 1000 °C have been described by Monchalin and Heon, [1986]. To prevent oxidation, the samples were located inside a continuously pumped tubular oven with vacuums of below 10^{-5} torr. The experiment was carried out on epicentre (detection and generation at opposite locations). A Q-switched Nd:YAG laser providing 8 ns pulses with a maximum energy of 750 mJ was used as ultrasound generator and a heterodyne interferometer using a 1.0 W single mode argon ion laser, was used as the detector. The use of the argon ion laser gives a better sensitivity and permitted samples with optically rough surfaces to be probed.

McKie, [1987] studied the possibility of making precise ultrasonic velocity measurements using a modified Michelson interferometer as the detector. A 5 mW power He-Ne laser was used to provide light for the interferometer. The variation of longitudinal velocity with increasing sample temperature had been examined in five polycrystalline materials, namely iron, Dural, aluminium, AISI-310 stainless steel and

graphite. A Q-switched Nd:YAG laser, of 25 ns duration and 65 mJ energy was used as the acoustic source. A 50 cm focal length lens partially focused the incident pulse onto one face of the test sample, producing a weak plasma that generated brief longitudinal ultrasonic pulses. The other face of the sample was polished allowing it to form a mirror of a modified Michelson interferometer. The samples, which were in the form of discs 19 mm in diameter and 8 mm thick, were located in the centre of a temperature controlled furnace, after the interferometer and Nd:YAG beams had been aligned. This ensured that the measurements were carried out through the true thickness of the sample. It was claimed that the system was capable of making measurements up to 1000 °C, with an absolute accuracy in velocity of $\pm$ 1 % and relative accuracies of better than 0.1 %. Parts of the work have also been reported by Dewhurst et. al., [1988].

More recently Telschow et. al., [1990] described the capability of a Nd:YAG pulsed laser with a 10 ns duration and energies up to 300 mJ as the ultrasound source and a confocal Fabry-Perot interferometer as a detector to monitor the sintering of zinc oxide at temperatures from 850 to 950 °C. The confocal Fabry-Perot interferometer used is insensitive to the speckle nature of the scattered light from the sample surface and allows measurements to be made on rough and diffusely reflecting surfaces. In order to compensate for much of the lack of specular reflection due to the rough sample surfaces, an argon ion continuous laser with maximum output of about 1.0 W was used to illuminate the sample surface.

3.1.4 Principles of Ultrasound Generation and Detection by EMATs

EMATs can be used to generate and detect ultrasonic waves at the surface of conducting materials without any contact. The principles of ultrasound generation and detection by EMATs are contained in several articles [Frost, 1979, Maxfield et. al., 1987 and Dobbs, 1973]. To produce ultrasonic waves, a generating coil is fed with a burst of radio frequency (R.F) drive current (I_T) which induces an eddy current density (J) approximately within the skin depth of the metal. The skin depth δ can be expressed as :-

$$\delta^2 = 2/\mu\mu_o\sigma\omega \qquad (3.1)$$

where σ is the electrical conductivity of the metal, μ is its relative permeability, μ_o is the permeability of free space, and ω is the angular frequency of the incident flux. The distribution of the eddy current induced is similar to the distribution of the current in the coil and the frequency of the ultrasound generated equals the frequency of the current flowing in the coil. Hence, the wavelength of ultrasound can be readily varied by varying the R.F oscillator frequency. The induced eddy current (I) is smaller than the drive current because of the air gap between the coil and the sample surface and can be measured by an exponential factor related to the dimensions D of the wire loop (for example, in the case of a spiral pancake coil, D is the outside diameter of the coil) and the size of the air gap G. This is expressed by Alers and Burns, [1987] as :-

$$I = I_T \exp(-2\pi G/D) \qquad (3.2)$$

Hence it is advantageous to keep the air gap as small as possible to induce the maximum eddy current.

To provide a substantial force on the sample, an external steady magnetic field of flux density (**Bo**) is applied to the sample. The field interacts with the eddy currents resulting in Lorentz forces (**F = J x Bo**) which set the sample surface into vibration. Thus, a burst of ultrasound is propagated into the bulk of the material. The external magnetic field can be applied by means of either a permanent magnet or electromagnet. The polarisation of bulk waves (longitudinal or shear) depends upon the coil geometry and the direction of external magnetic field. If the field is normal to the sample surface, the resultant force will be in the plane of the surface leading to efficient shear wave generation. Conversely, with the field parallel to the surface and perpendicular to the eddy current density, a normal force will result in the longitudinal mode being favoured.

The ultrasound reception occurs via the reciprocal process (Fig. 3.7), sample surface movements (**M**), caused by the arriving ultrasonic wave, interact with the external magnetic field (**Bo**) to give rise to currents (**C**) which in turn induce a current to flow in the receiving coil (R). The pulse voltage induced in the coil is given by Kawashima, [1984] :-

$$V(t) = -2\,NA\mathbf{Bo}\,d(S(t,0))/dt \qquad (3.3)$$

where S(t,0) is the displacement amplitude of ultrasound pulse at the surface of the conductor, **Bo** is the applied field strength, N is the number of turns of the coil and A is the coil area. When an EMAT is used on ferromagnetic material, in addition to the

Lorentz force mechanism described above, a magnetostriction mode is also possible and might dominate the acoustic signal, there is also a mechanism due to the discontinuity in magnetic properties at the surface.

3.1.5 Applications of EMAT-EMAT Systems

EMATs have been successfully applied for material characterization in metals and for measurement of metallic properties such as material anisotropy (texture) and internal stress (strain) state, even though its sensitivity is much lower (by 40 to 100 dB) than sensitivities achieved by conventional contact probe. At elevated temperature EMAT-EMAT systems have been used for on-line inspection of hot semi-finished products such as steel blooms, slabs and bars, where temperatures of up to 1200 °C were encountered, and in the measurement of hot tube wall thickness. The systems are also able to be scanned at high speed and generate ultrasound in metals covered by a protective coating. However, the efficiency of ultrasound generation and reception decrease rapidly with increase in lift-off distance between the EMAT face and the surface of the test object. The other drawback is that it can only be applied on electrically conducting materials or non-conductive material with a well bonded conductive coating.

Parkinson and Wilson, [1977] described experimental work using shear wave EMATs as both the generator and detector of ultrasound to measure and evaluate the amplitude, attenuation and velocity of non-contact shear wave generation in steel with temperature over the range of 20 to 900 °C. It was observed that when the temperature of steel exceeds 750 °C, the ferromagnetic properties of the steel disappear, and a large drop (24 dB) in shear wave signal strength occurs. It was also

observed that very strong longitudinal waves were generated in the temperature range of 760 to 800 °C. The paper also mentioned the development of the first practical application of EMAT-EMAT systems, which was made at the Round Oak Steel Works by The Tube Investment Research Laboratories for the internal on-line inspection of steel bars with surface temperature up to 500 °C. Details of the application were explained by Whittington, [1978], where a direct current shear wave electromagnetic EMAT system was used for both generation and reception. The electromagnet was housed in a pot-type casing and the two spirally wound eddy current coils, one for transmitting and the other for receiving were mounted on separate removable pole-pieces inserted through the central limb of the electromagnet. Initially water was used to cool the system but later it was changed to oil.

Cole, [1978] carried out tests on mild steel at temperatures up to 1200 °C, using a surface wave EMAT to study the variations of signal amplitude and shape with temperature and magnetic field. The transducer comprised an E-core electromagnet, with identical transmitting and receiving grids arranged between the pole pieces. The EMAT was water cooled, allowing the test to be carried out continuously for 6 hours or more without overheating problems. It was observed that the signal amplitude increased with magnetic field drive and did not exhibit saturation characteristics. The results obtained demonstrated that a surface wave could be generated and received in mild steel at surface temperatures up to 1000 °C.

Kubota et. al., [1986] presented an improved electromagnetic ultrasonic testing technique for more sensitive detection of internal flaws in hot steel slabs and billets at temperatures up to 1000 °C. Improvements were made on the electromagnet, the transmitter and the detector circuits. For the purpose of efficient generation and

detection of ultrasonic longitudinal waves, a tunnel-type electromagnet that is capable of generating a high magnetic field of more than 1 Tesla was developed. The magnet had a large tunnel formed by surrounding the exciting coil and magnetic poles, through which the test object pass. The gap between the object surface and the magnet pole can be adjusted by means of a movable magnet core. In order to generate a high-power pulse and to improve flaw detection sensitivity, the slight variations caused by flaws in an object were magnified. This was achieved by developing a voltage-multiplying pulser circuit with multistage thyristors and a peak-differential detector, respectively. The system was able to detect side drilled holes (4 mm dia.) in a hot steel billet (865 °C, 18 mm thick) and another (10 mm dia.) in a hot steel slab (930 °C, 250 mm thick).

Lee and Ahn, [1992] studied the variation of velocity and signal amplitude of ultrasonic waves generated by both the longitudinal and shear wave EMATs as a function of temperature in non-magnetic aluminium and stainless steel, and in ferromagnetic mild steel. Measurements were made up to only 800 °C. As was expected, the longitudinal and shear wave velocities decreased linearly with increasing temperature in aluminium and stainless steel. In the case of mild steel there was a change in slope around 550 °C for the shear wave velocity, and they could only observe the longitudinal wave waveforms over a narrow range of temperature where the velocities decrease only slightly as a function of temperature. They also observed that the signal amplitude generated by EMATs was very different between ferrous and non-ferrous materials. In stainless steel, the amplitudes generally decrease as a function of temperature but for mild steel, there was an increase of amplitudes in the

temperature range between 600 °C and 800 °C in the shear wave and between 715 °C and 735 °C in the longitudinal wave.

3.1.6 Applications of Laser-EMAT Systems

The combination of laser generation and EMAT detection has been applied to measure the internal temperature of hot steel objects. A laser-EMAT system used for the above mentioned purpose has been described by Boyd and Sperline, [1988]. They developed a system using a liquid dye Q-switched pulsed ruby laser for the generation of acoustic waves and a longitudinal pulsed EMAT as the receiver in a through transmission technique. The system was capable of making acoustic wave measurements up to 1100 °C or greater and the average sample temperature was determined using a calibrated relationship between velocity and temperature. In another study, Wadley et. al., [1986] applied the system to determine the internal temperature distributions in 304 austenitic stainless steel of both cylindrical and square cross section. The samples were heated to approximately 700 °C in an induction heating unit before being removed to the testing apparatus. In these experiments a Q-switched Nd:YAG laser was used to generate ultrasound pulses of approximately 25 ns duration and up to 850 mJ in energy. A water-cooled EMAT with a sensing coil of 4 mm x 4 mm was placed at a stand-off distance of 1 mm from the surface of the sample. Thermocouples were mounted at various positions in the sample to provide a continuous record of the internal temperature profile. The reconstructed temperature and the thermocouple temperature values agreed to within $\pm$ 20 K for the cylindrical geometry and were within $\pm$ 10 K for the square geometry.

Billson and Hutchins, [1993] described the shear wave measurements of phase transitions in Zircalloy using the laser-EMAT system arranged in the through transmission set-up. Measurements were taken on hydrided and unhydrided samples during cooling. The graphs of shear wave arrival times against sample temperatures show that there is a change in gradient on the hydrided sample indicating the occurrence of a phase transition, which is not present on the unhydrided sample.

The most recent work indicating the capability of the laser-EMAT system to make measurements at elevated temperature have been reported by Edwards, [1994]. The experiment was carried out on 20 mm thick low carbon steel disc mounted rigidly on two stainless steel tubes, and heated in a large cylindrical bore electric furnace. A 100 mJ Nd:YAG laser, and a concentric water cooled EMAT having a 3.5 mm diameter hole, was used as the ultrasound generator and detector respectively. Measurements were made using the pulse echo method with the laser source and the EMAT detection surface on the same side of the sample. The sample was heated up to 605 °C and measurements made both during heating and cooling.

3.1.7 Evaluation of Non-contacting Ultrasound Technique

Every non-contacting ultrasound technique has its own advantages and disadvantages for non-destructive evaluation. In this particular case, we must consider the need to monitor the degree of partially molten metal. The laser beam technique has several advantages as an ultrasound generator, besides being able to generate several wave modes simultaneously. It can operate at a totally remote distance, which eliminates the problem of coupling to the sample, and the effect of cooling the transducer from the heat of the hot sample under inspection. Hence, the technique is

very suitable for application at elevated temperature. On rough or coated surfaces, most of the incident laser energy will be absorbed and enhance the ultrasound generation process. In practice, the technique is easier to apply as it does not need careful alignment relative to the sample. A Q-switched pulsed laser can deposit enough energy in a sufficiently short time to set up the stresses required to generate ultrasonic signals of comparable magnitude and bandwidth. The power density of the laser beam reaching the sample can be adjusted simply by using an optical lens or by placing a high density filter between the source and the sample. Its main disadvantages are in terms of safety, since it has to operate in a controlled area with complete safety and warning devices, and the relatively high prices and bulky equipment.

An EMAT source has a narrow bandwidth if it is operated at resonance and is a relatively inefficient ultrasound generator. It can generally generate only one type of wave mode at a time as it depends greatly on the direction of the static magnetic field and the configuration of the EMAT coil. It is difficult to design an EMAT that can generate both the longitudinal and shear waves simultaneously. Furthermore, in order to generate high intensity acoustic waves into the sample, the EMAT must be placed very close to the sample surface as both the static and dynamic magnetic field strengths decrease with increase in lift-off.

The detection of ultrasound by laser interferometers offer several advantages, firstly, the surface of the sample being inspected is only in contact with the laser beam which enables the contact pressure to be neglected and thus the sample surface will not be loaded. Secondly, no mechanical contact is required for the interferometer to detect the displacement of the material surface, hence avoiding the need for the use of a coupling medium and eliminating all the problems associated with it. The wide

bandwidth interferometer enables a wide range of acoustic waves to be detected simultaneously, and finally, the interferometer can be placed at a considerable distance from the sample to be tested since only optical access is required; thus, the interferometer may be shielded from the hostile environment at elevated temperature. However, the sensitivity of the interferometer is strongly dependent on the amount of light that comes back from the sample surface. The sample surface must, therefore, be reflective and fairly smooth in order to allow the interferometer to approach its maximum sensitivity. Nevertheless, laser interferometers can also be applied for detection of ultrasound on rough surfaces by selecting a suitable interferometric technique. To be used in the industrial environment where the surfaces are rough and absorbing, where vibrations and turbulence levels are high, the interferometer must have a proper sensitivity and immunity to environment disturbances which can be achieved with a laser source of adequate stability and sufficient power.

EMATs have a reasonable detection sensitivity and can be designed to have a reasonable detection bandwidth. The efficiency of an EMAT as a receiver can be improved by increasing the number of coil turns so as to maximise the coupling between the coil and eddy currents generated in the sample surface. EMATs have proved to have enough sensitivity to be used for on-line inspection of hot semi-finished products and measurement of hot tube wall thickness. In addition, an EMAT detector is relatively cheap and easy to make.

3.2 Discussion

A comparison of laser and EMAT techniques for non-contact ultrasonics has been described by Hutchins et. al., [1986]. The results show that the combination of a

laser generator and interferometric detection system can lead to waveforms exhibiting reasonable sensitivity and wide bandwidth. However, such results could be obtained only on a polished metal surface, where the reflectivity was sufficiently high for interferometry. This is unusual in the plant environment especially at elevated temperature, where there is difficulty in maintaining the maximum reflectivity, as the sample tends to oxidise and tarnish the surface. In the study carried out by McKie, [1987] and Edwards et. al., [1992] using the laser-laser system, it was noted that the shear wave transit time could not be determined accurately at higher temperatures because of its weak and broad features. With the EMAT-EMAT system it is difficult to obtain both the longitudinal and shear wave transit time simultaneously, at the particular temperature. A reasonable sensitivity could be achieved using the combination of laser generation and EMAT detection [Hutchins et. al., 1986]. Sufficiently high and sharp longitudinal and shear wave signals could be obtained when a laser pulse of sufficiently high power density was incident on the sample causing a weak ablation, enabling the transit time of both waves to be measured more accurately. Even though the study was carried out at room temperature, it can still be applicable at elevated temperatures since the laser power density can be altered to control the degree of ablation.

3.3 Conclusions

The purpose of the thesis is to develop a control system that is less bulky, and comparatively cheaper than the laser-laser system, and able to be used for industrial applications. Thus it was concluded that the most practical non-contacting ultrasonic technique for this work is to use a laser capable of producing intense ultrasonic pulses

(longitudinal and shear waves) and an EMAT that is sensitive to both bulk waves, able to be applied on rough surfaces, and also requires no sample preparation. Hence, a Nd:YAG pulsed laser was selected as the ultrasound generator and a spiral coil EMAT as the detector. Even though a Nd:YAG laser was mainly used for the thesis, experiments were also conducted to evaluate and compare the efficiency between a Nd:YAG and CO_2 laser as the ultrasound generator, and are reported in chapter 6 of this thesis.

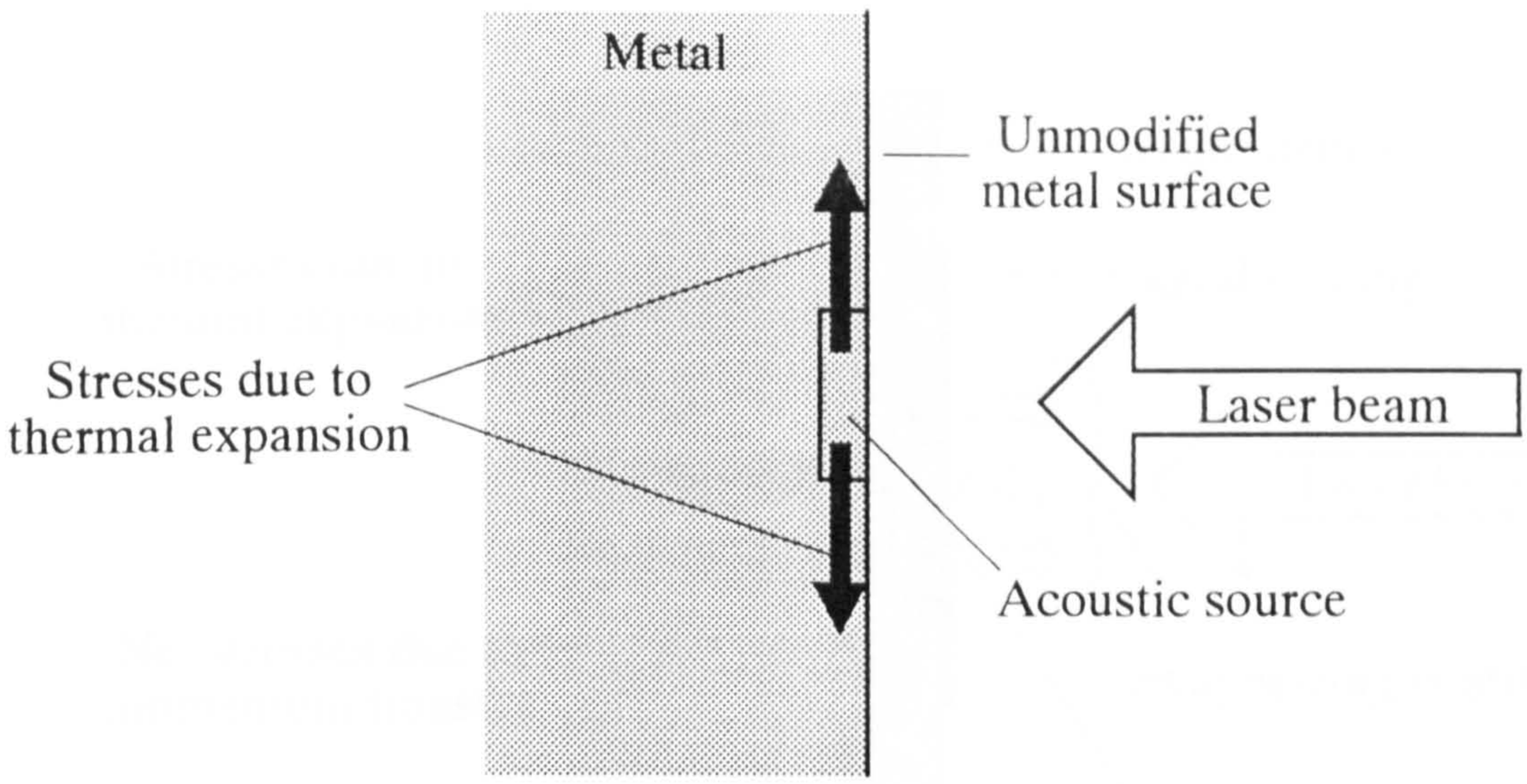

Fig. 3.1 Thermoelastic source formed by pulsed laser irradiation

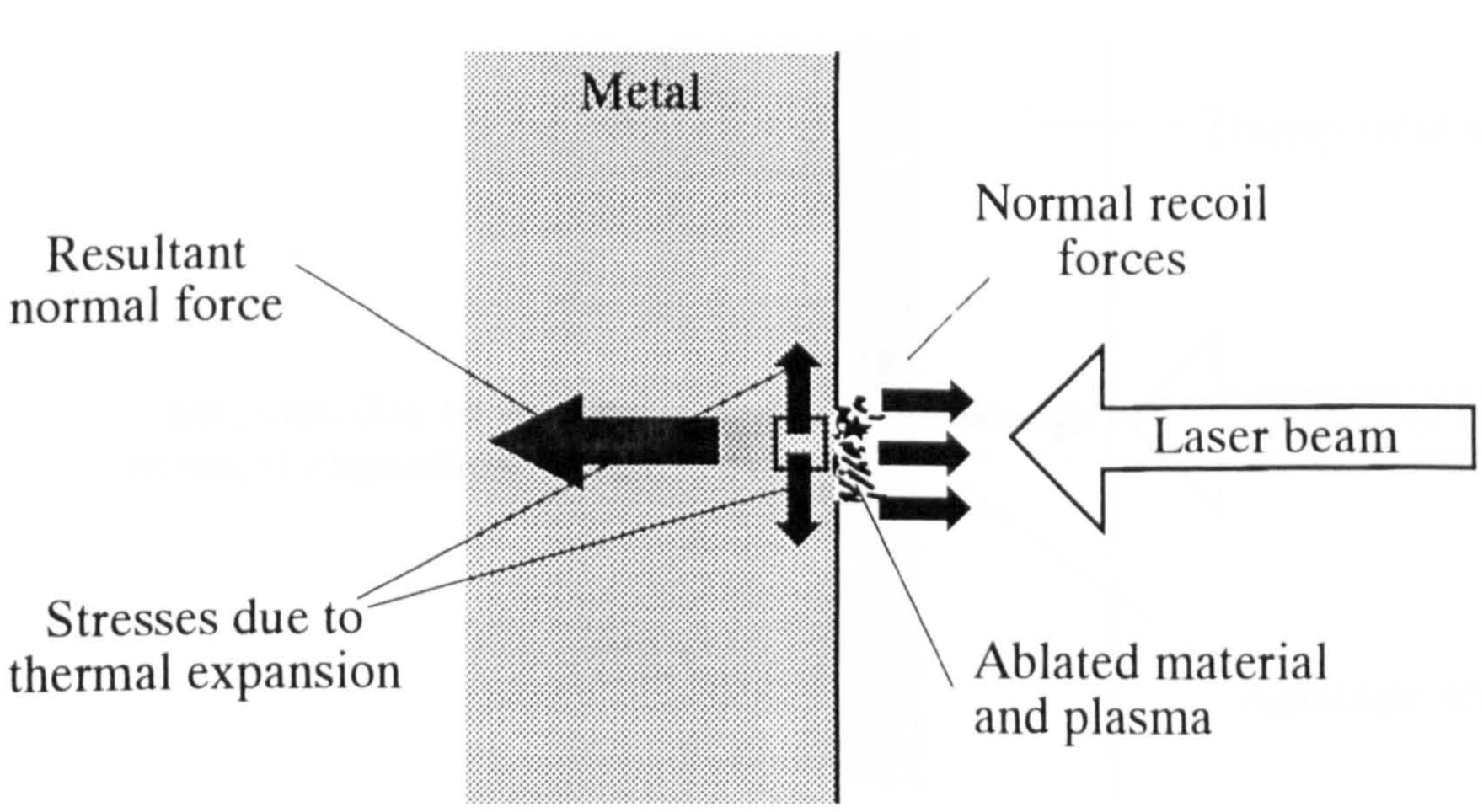

Fig. 3.2 Ablation source formed by pulsed laser irradiation.

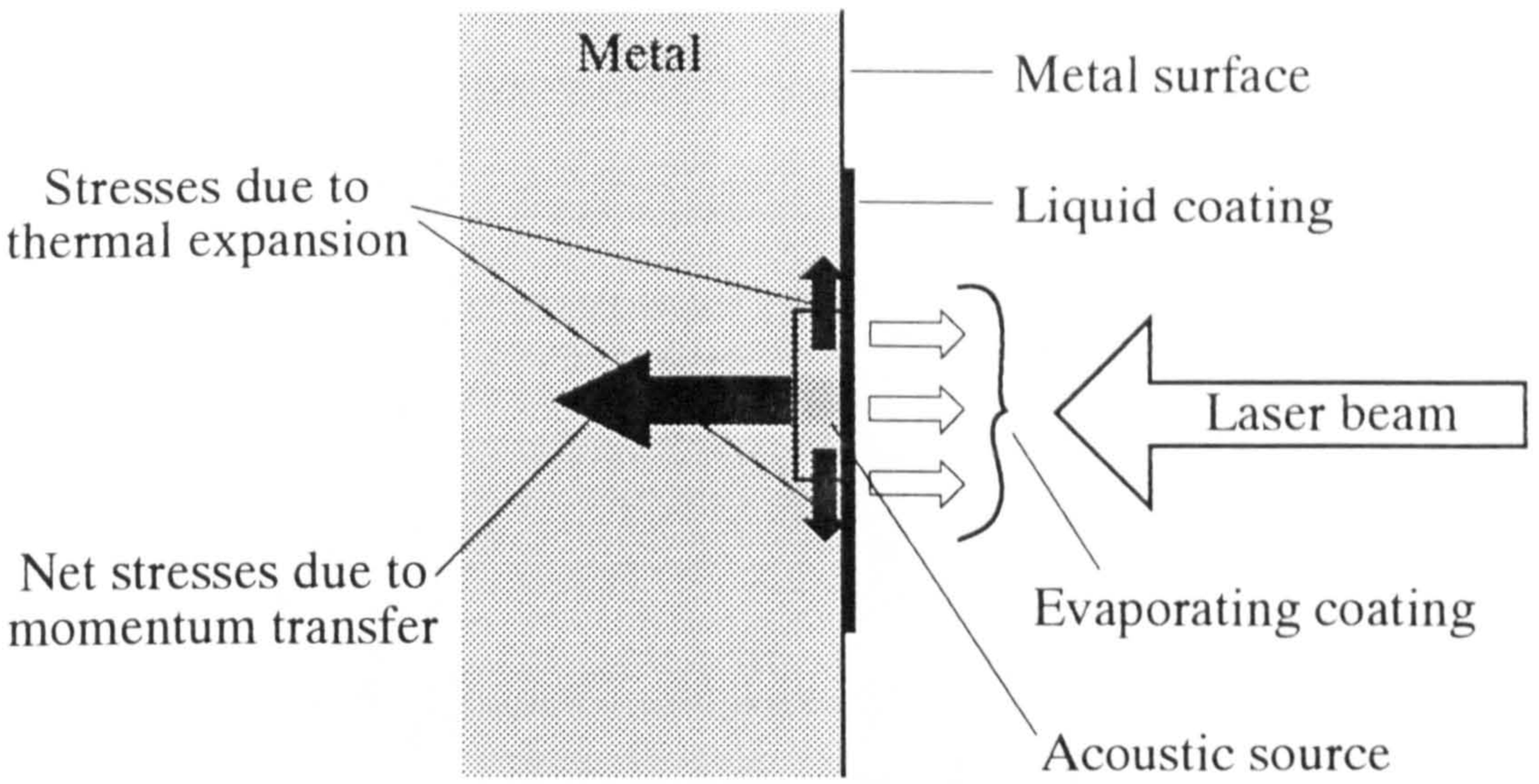

a) Liquid coating

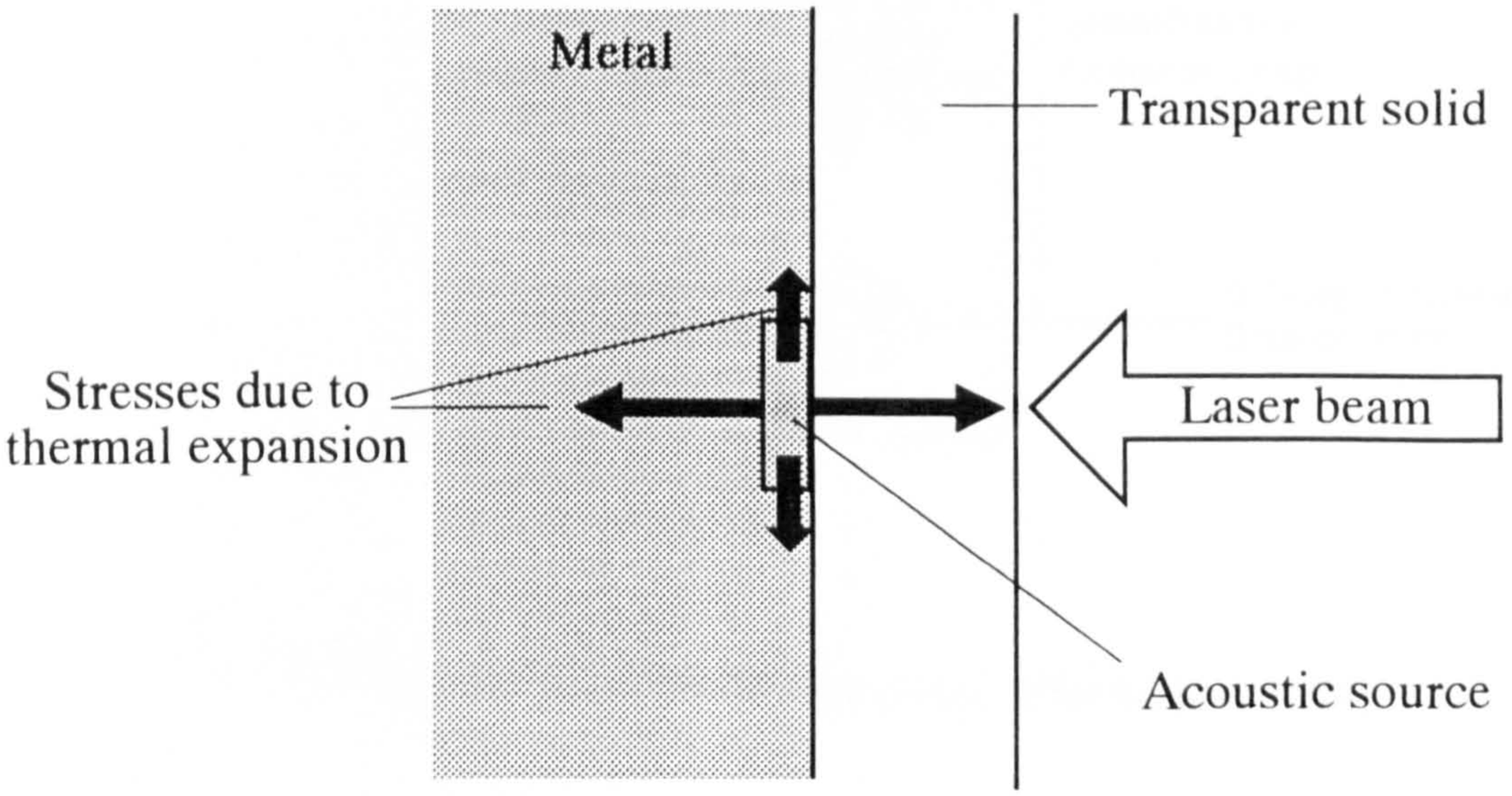

b) Transparent solid

Fig. 3.3 Acoustic source formed by laser irradiation on constrained surfaces

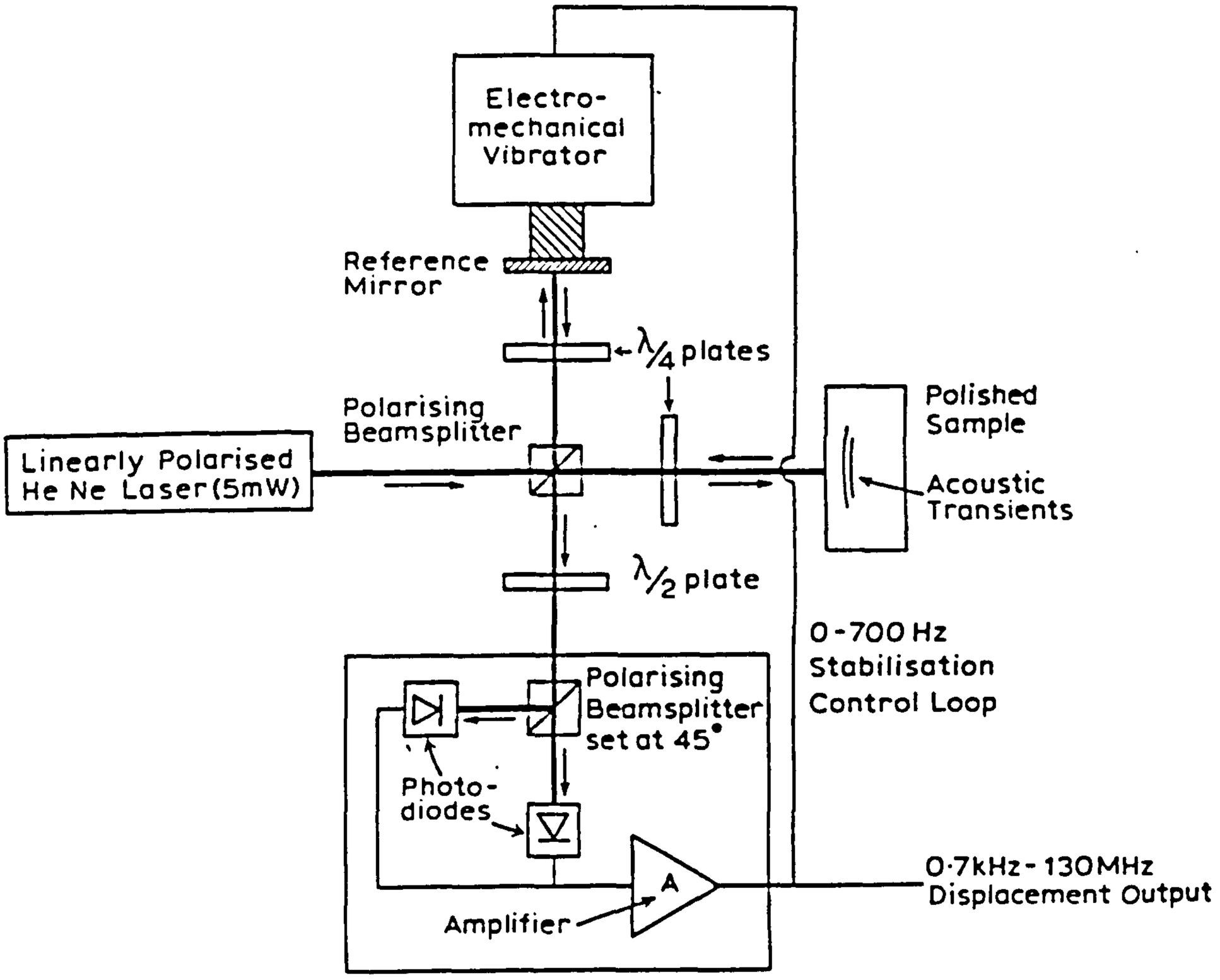

Fig. 3.4 Stabilised Michelson interferometer [after McKie, 1987].

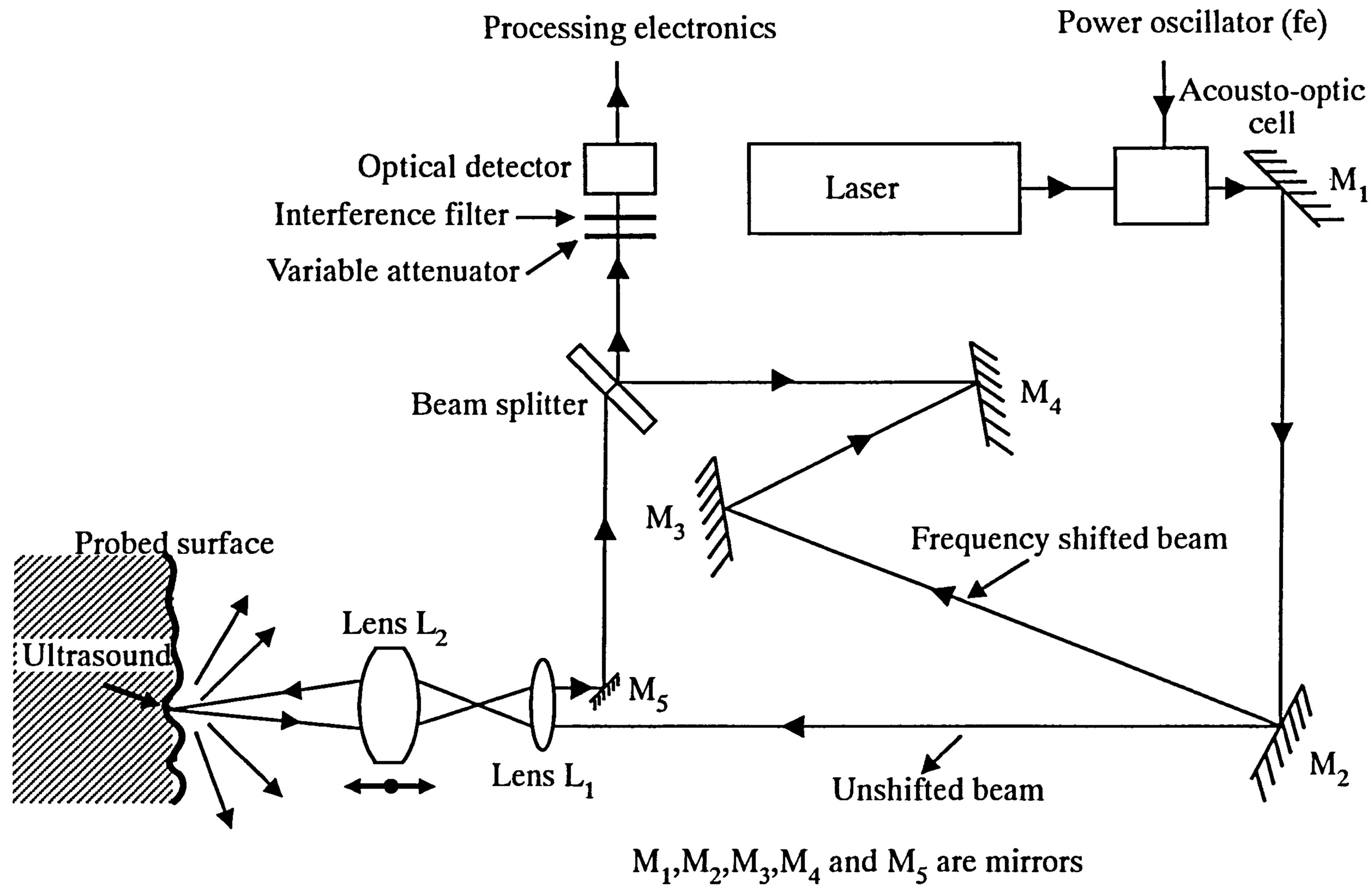

Fig. 3.5 Schematic diagram of a heterodyne Michelson interferometer for the detection of ultrasonic displacements [after Monchalin, 1986].

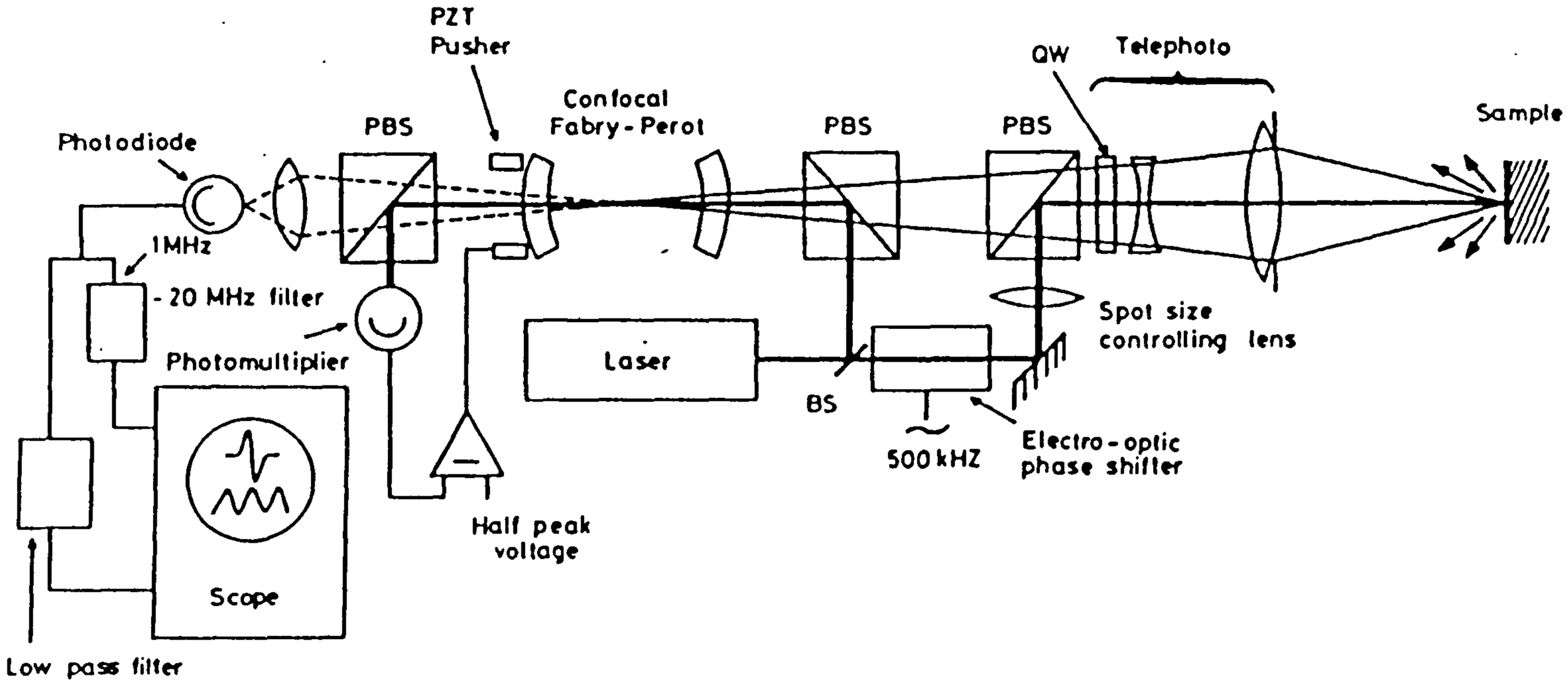

Fig. 3.6 Fabry-Perot interferometer [after Telschow et. al., 1990].

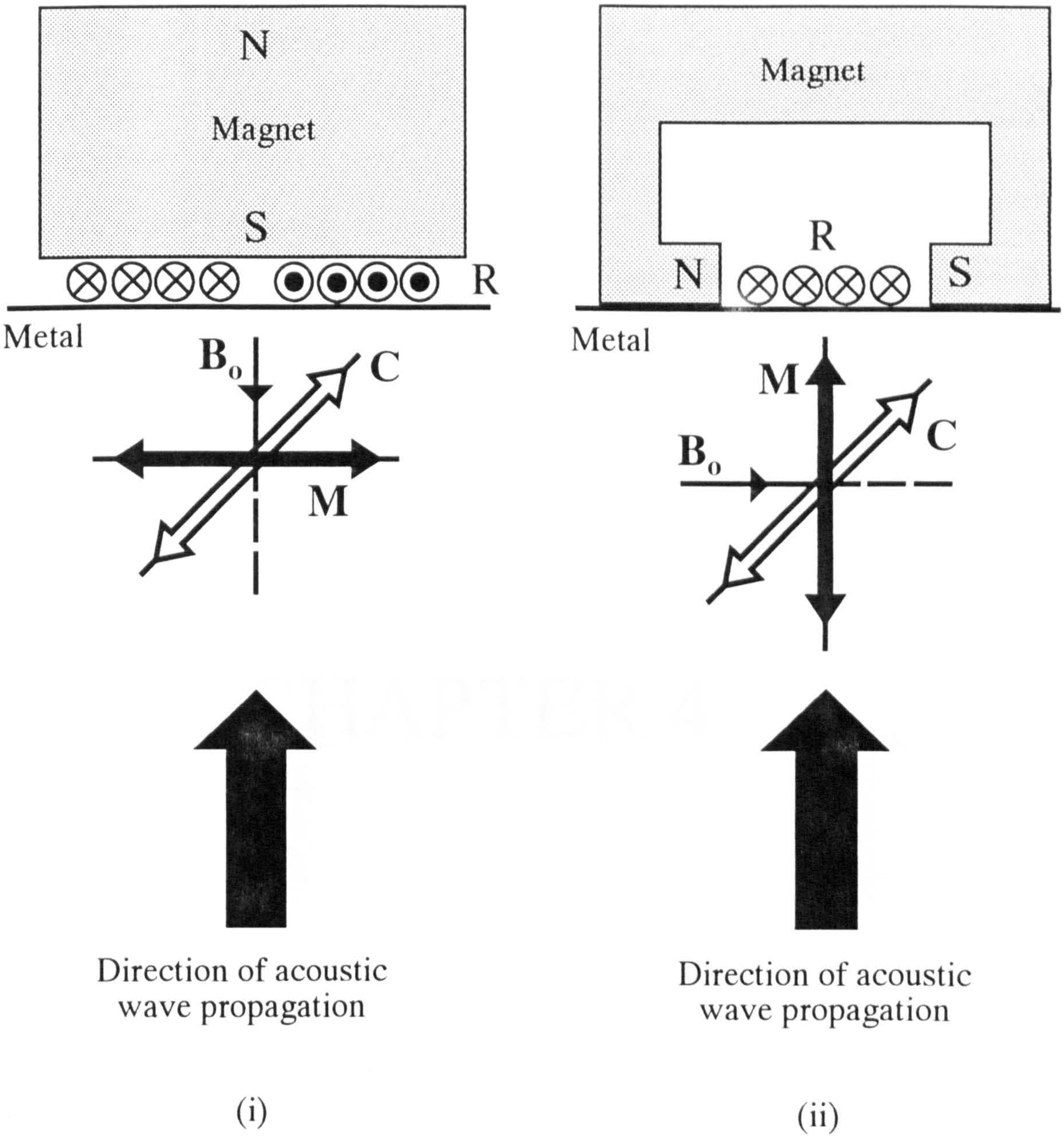

Fig. 3.7 Directional dependence of EMAT to i) shear and ii) longitudinal waves. B is the magnetic field, C the induced current in the sample following the motion M of the surface and R is the receiving coil.

CHAPTER 4

CHAPTER 4

MONITORING OF PARTIALLY MOLTEN ALUMINIUM-SILICON ALLOYS

4.0 Introduction

Aluminium alloys have been used to produce a variety of products, ranging from storage tanks to more advanced aircraft components. The alloy is light and has good corrosion resistance. The main alloying elements used in aluminium alloys are silicon, magnesium, copper and zinc. An aluminium-silicon alloy has excellent casting fluidity and so can be sand and die cast into intricate shapes. Even though sufficient quality can be produced using the commercial aluminium alloy, industrialists have started to use thixoforgeable alloys because of the advantages already mentioned in section 1.1.2. However, the alloy has to be carefully monitored during heating, in particular around the eutectic temperature so that a correct solid/liquid fraction is obtained before it is forced into the die for thixoforging. The thixotropic material for the present study was supplied by Lucas Industries Ltd. who were initially interested in having a quality control system for higher temperature materials, such as copper alloys and tool steel, but finally decided to use the system for lower temperature aluminium alloys in the manufacturing of automotive and aircraft components.

As mentioned in chapter 1, a non-contacting ultrasound system can be a suitable system for the monitoring of the degree of partially molten thixotropic material. However, at elevated temperature, the effect of thermal expansion makes it difficult to determine the actual path length travelled by the acoustic waves with sufficient accuracy. Hence, it would be better to measure a parameter that is

independent of the sample dimensions. For the present thesis, the ratio of the longitudinal wave to the shear wave transit time has been assessed as a means of monitoring the volume of liquid/solid fraction in the material. With the combination of a wide bandwidth (0.5 to 20 MHz) Nd:YAG pulsed laser and a wide bandwidth (1 to 10 MHz) spiral coil shear EMAT as the ultrasound generator and detector respectively, both the longitudinal and shear wave signals were obtained simultaneously at a particular temperature. This was achieved by pulsing a sufficiently high optical power density onto the sample surface to create a strong plasma source. A surface constraint was used to enhance longitudinal generation with thermoelastic and weak plasma sources. Acoustic wave measurements were also extended to the fully molten state.

4.1 Test Samples

Thixotropic materials were the main samples used in the study. However, since these specially produced materials were difficult to obtain and comparatively expensive, non-thixotropic materials were used for trial work. Two thixoforgeable aluminium alloys were used in the experiments, firstly a binary aluminium alloy with 4.86 weight per cent silicon content (Al 4.86 % Si alloy) and secondly a commercial LM25 alloy. The Al 4.86 % Si alloy also contains other elements such as copper, manganese, titanium, zinc, nickel, iron, chromium and magnesium that are present in very small quantities (less than 0.02 %). The analysis was carried out using a quantometer that provide an accuracy of $\pm$ 0.05 per cent for the silicon content. In the case of the LM25 alloy, an Inductively Coupled Plasma Spectrometry (ICPS) analysis result shows that silicon is the major alloying element with 6.66 weight per cent,

followed by magnesium (0.63 %), iron (0.30 %), manganese (0.11 %), titanium (0.10 %) and other elements, such as, copper, zinc, nickel, chromium, zirconium, lead and tin, that are present in less than 0.01 per cent.

The Al 4.86 % Si alloy was produced by the SIMA process at the School of Materials, University of Sheffield. To produce the alloy, a cast billet of 73 mm in diameter previously produced by the continuous casting process was extruded in a 31 mm extrusion die with an extrusion ratio of approximately 6.0 and speed 5 mms^{-1}. In the case of the LM25 samples, the alloy was produced by the Osprey spraying process, which has been described generally in chapter 1. The two non-thixotropic Al-Si alloys used in the study were standard commercial alloys. An energy dispersive X-ray analysis (EDAX) carried out on the two alloys showed that the 32 mm and 60 mm bar samples contain approximately 1.2 and 9.5 atomic per cent of silicon respectively. The analysis also showed that the 32 mm bar contains approximately 1.0 per cent iron and 0.4 per cent manganese.

For the experiments, the Al 4.86 % Si alloy and Al 9.5 % Si alloy samples were disc shaped with dimensions of approximately 30 mm in diameter and 12 mm thick. For the LM25 alloy and Al 1.2 % Si alloy, samples were approximately 40 mm diameter and 14 mm thick.

4.2 Description of the Furnace System

A schematic diagram of the furnace system is shown in figure 4.1. The 270 mm length standard split electric furnace with internal cylindrical bore of 60 mm was used to heat the sample. The upper half of the furnace is hinged so that it could be lifted up to enable easier sample handling during setting up. The electric furnace is

capable of being heated to a maximum control temperature of 1200 °C. Two chromel-alumel (Ni/Cr-Ni/Al) K-type thermocouples were used in the experiment. The control thermocouple that was inserted into one of the two thermowells present in the furnace was connected to the Eurotherm temperature controller used to regulate the furnace heating units. The other thermocouple, that is the measuring thermocouple, was connected to the Digitron digital temperature meter giving the absolute sample temperature reading. The accuracy of the Digitron meter was calibrated using the digital voltmeter that was referenced to the melting point of ice, yielding an absolute accuracy of $\pm$ 3 °C. The furnace support structure was designed and constructed to allow the furnace to be finely adjusted vertically and horizontally for easier laser-EMAT alignment. The support was also designed with three large adjustable studs for adjusting the furnace height with respect to the laser beam when the experiment was carried out with the furnace in the vertical position.

4.3 Water-cooled EMAT

A schematic diagram of the water-cooled EMAT used for the measurements is shown in Figure 4.2. Two different shear EMATs were used for the experiment. The first EMAT was constructed using two 20 x 10 x 5 mm rectangular neodymium-iron-boron (Nd-Fe-B) permanent magnets stacked parallel to each other with similar magnetic poles facing the printed circuit board (PCB) and the mild steel backing material. The PCB has an approximately 15 mm outside diameter, 15 turns photoetched flat spiral coil on one of its faces. The permanent magnets provide a normal field perpendicular to the coil. The magnetic field strength was measured using the Hall effect flux probe and found to be around 0.3 Tesla. The mild steel backing

material was attached below the magnet to reduce the effect of the self-demagnetizing factor and to increase the normal field. Electrical connections to a PCB spiral coil were made in the gap between the two magnets which were housed in a water cooled brass case that provided the electromagnetic shielding and mechanical strength. The water was introduced into the EMAT through a copper tube and was directed around part of the brass casing and out of the EMAT through another copper tube. The electrical connections and the copper tubes were surrounded by a stainless steel holder onto which a BNC connector was attached as shown in the figure. A 0.3 mm thick mica sheet was placed over the coil, not only to protect the coil from mechanical wear but also help to insulate the EMAT from the hot sample. This arrangement of a field normal to the sample surface and a flat spiral receiver coil gives sensitivity to radial motion in the plane of the sample surface and is suited to the detection of the axisymmetric ultrasonic waves generated by a laser source on epicentre.

The second EMAT was constructed using a cylindrical shaped Nd-Fe-B permanent magnet of 20 mm diameter and 7 mm thick to provide the normal field. The magnetic field strength was also measured to be around 0.3 Tesla. In this case, electrical connections to the PCB were made via a small hole drilled in the magnet, and the EMAT coil was protected from mechanical wear and the hot sample by a 0.5 mm thick alumina disc. An earth pin was attached so that the EMAT would be in contact with the sample holder during the measurement, helping to improve the signal to noise ratio.

The laser can be regarded as a point source but in the relatively thin samples used in this work, the dimensions of the EMAT are important, and will affect the effective path length travelled by the acoustic waves (fig. 4.3). The output from the

EMAT results from a convolution of the acoustic field over the active area of the transducer, this is particularly important in the case of the first arrivals, where the wavefront is highly curved. As the acoustic waves bounce within the sample, the subsequent wavefronts tend rapidly to become effective plane waves. As such, measurements carried out on multiple echoes give more accurate results than those using broader first arrivals, however the first arrivals can still be used provided the effective path length of the waves is determined from calibration experiments of the longitudinal and shear wave velocities at room temperature.

4.4 Experimental set-up

A schematic diagram of the experimental set-up to generate and detect acoustic waves in metals at elevated temperature is shown in figure 4.4. The ultrasound was generated by a Lumonics HY 400 Q-switched Nd:YAG laser capable of producing 400 mJ laser pulses with a 10 ns pulse duration. Detection was achieved by a water-cooled spiral coil shear EMAT. A He-Ne laser was initially used to align the EMAT with the laser beam so that measurement could be made on epicentre and at the centre of the sample. A transparent glass slide of 1.0 mm thickness was positioned in front of the Nd:YAG laser at about 45 degrees with respect to the laser beam axis splitting the beam into two. A few per cent of the beam was reflected and detected by a photodiode which in turn triggered the LeCroy 9400A digital oscilloscope, and the remaining light was transmitted through the slide and reached the sample surface. The parallel sided sample was held in a stainless steel holder mounted on two parallel stainless steel tubes lying horizontally across the furnace to reduce heat losses. The holder had a 10 mm hole on the generation side for laser

access. Initially the sample surface at the detection side was unsupported. With this simple design it was found that the metal tends to flow out of the sample holder at high liquid fractions, therefore a 0.5 mm thick alumina disc was attached to the sample holder on the detection side. This not only prevented the molten metal from flowing out of the sample holder but also reduced the effect of sample cooling by the detector. However with an alumina disc on the detection side, the lift-off distance is increased by an additional 0.5 mm and hence reduces the EMAT's sensitivity by approximately 30 per cent. The EMAT was only introduced into the furnace during the taking of a measurement and pulled out again after the waveform had been recorded in the oscilloscope. The stainless steel holder was made to be a close fit to the teflon bush bearing in order to reduce EMAT play and to maintain the EMAT and laser beam alignment as accurately as possible on epicentre.

A further addition to the sample holder was a silica window constraining the sample on the generation side. The window prevented the molten metal from flowing out of the laser beam access hole of the sample holder, in addition to the alumina disc on the detection side. A schematic diagram of the sample set-up or an ultrasonic cell is shown in figure 4.5. The silica window also constrained the sample surface so that a normal force was also present in addition to the force parallel to the sample surface. The window tended to bond to the molten metals and crack on cooling. A mica sheet and an alumina disc, both 0.5 mm thick were also used to support and constrain the sample surface at the generation side, but were found to be less successful. A small molten metal expansion hole was later drilled at the top of the sample holder to enable the molten metal to flow through it and hence reduce the possibility of the alumina disc breaking. The sample temperature was measured using a Ni/Cr-Ni/Al

thermocouple inserted through the bottom surface of the sample holder with its tip in contact with the sample surface. The sample was heated in a standard split electric furnace described in section 4.2. Throughout the study a wideband pre-amplifier having an approximately 55 dB gain and maximum sensitivity at 5 MHz was used to amplify the detected waveform, unless otherwise stated, before it was displayed in the oscilloscope. The waveform was then stored on the personal computer for subsequent analysis. Screened leads were used, connecting the EMAT to the oscilloscope via the pre-amplifier, to help to remove the stray field and improve the signal to noise ratio. Two sets of experiments were carried out, firstly without the silica window, and then with a silica window constraining the sample surface at the generation side. Without the silica window, a 50 mm diameter, 320 mm focal length biconvex lens was used to partially focus the incident laser pulse onto the sample surface, producing a weak plasma. However, with the silica window, a lower laser power density could be used for generation, hence no lens was used.

Experiments were also tried with the set-up in the vertical position as shown in figure 4.6. The sample was supported by a sample holder having a 3 mm hole on the generation side for laser access. The small hole helps to reduce the possibility of the metal flowing down under gravity once the sample starts melting. It was hoped that the detection side would remain flat and no alumina disc would be required. A 1000 mm focal length biconvex lens placed on the sliding bench was used to partially focus the laser beam onto the 45 degree prism which then deflected the beam vertically upwards onto the sample surface. Unfortunately, this arrangement was no better than the horizontal technique. The main problem was in maintaining the alignment of the generating laser spot and the EMAT, as thermal expansion of the furnace and its

supports caused deviation of the laser beam. In addition, even though the laser access hole was made as small as possible, the partially molten metal could still flow through the hole under gravity, increasing the acoustic path length and affecting the directivity of acoustic wave propagation, hence making the analysis difficult and causing errors in the measurements.

4.5 Experimental Technique

In the experiment the sample was initially heated at a ramp rate of 10 °C per minute until the sample temperature approximately reached 500 °C. The sample was then heated at 5 °C per minute until the experiment completed. As mentioned in the preceding section, experiments were carried out with and without a silica window supporting the sample surface at the generation side. When the sample surface was unsupported, it was only possible to take measurements up to low liquid fractions. The surface constraint enabled the measurements to be extended to the fully molten state. In the former case, a plasma source was used to generate the acoustic waves. The 320 mm focal length biconvex lens was initially adjusted to partially focus the incident laser pulse to the required power density so that the longitudinal and shear wave signals could be detected simultaneously. This enabled the required transit time ratio to be determined for the particular temperature, and used to monitor the percentage of solid/liquid fraction. When employing the surface constraint, the experiment was conducted in the thermoelastic regime. It was expected that at elevated temperature, due to thermal expansion, the window would be forced against the sample surface resulting in a strong normal force under thermoelastic conditions. However it is also possible to detect a longitudinal wave signal in addition to the shear

wave even at room temperature if the sample is clamped strongly enough to the silica window to alter the stress boundary condition at the sample surface or by using a plasma source. But in order that the high incident power laser density should not damage the window surface, the thermoelastic source was preferred.

The water flow rate of the EMAT was regulated to be just sufficient to protect the detector from radiant heat (EMAT temperature less than 100 °C) . In order to maintain the properties of the magnet and to avoid excessive sample cooling by the detector, the water-cooled EMAT was only introduced into the furnace to capture the ultrasonic waves and pulled out again when the waveform had been recorded. The captured waveform was smoothed to enable accurate measurement of the transit times. The transit times were measured from the absolute maximum of the arrival either positive or negative depending on its polarity. Wherever possible the transit times were measured using multiple shear and longitudinal wave echoes as this is more accurate than simply measuring the first arrivals. This particularly applies to the shear pulse at higher temperatures because of its low amplitude and relatively broad nature. The effect of the geometry of the EMAT on the effective path length travelled by the acoustic waves was eliminated by determining its value at room temperature. The calibration velocities used to estimate effective path lengths were measured using a conventional piezoelectric transducer for the longitudinal wave, and by using the spiral coil EMAT to generate and detect shear waves, as can be seen in figure 4.7.

4.6 Results and Discussion

4.6.1 Al 4.86 % Si Alloy

Figure 4.8 (a and b) show respectively the measured variation of longitudinal (L) and shear (S) wave velocities in the Al 4.86 % Si alloy heated to the partially molten state. In both cases, the velocities show the normal decrease expected for metals as a function of increasing temperature except for the unusual behaviour in the shear wave velocities between 350-400 °C. Within this region the shear velocity appears to increase slightly before it decreases gradually again with increase in temperature. According to the Al-Si binary phase diagram (fig. 4.9) there should not be any phase transition taking place over this temperature range. This was confirmed by Differential Scanning Calorimetry (DSC) thermal analysis (conducted at Lucas Laboratory in Solihull (see fig. 4.10)) where there is no indication of any transition occuring between 350 to 400 °C, but two endothermic peaks are observed in the semi-solid state, at about 591 °C and 626 °C, which are expected for this alloy. Figure 4.8 (c) shows the expanded shear wave pulse obtained between 325 °C and 430 °C where the longitudinal side wall reflected signal is suspected to be superimposed with and distorted the shear wave pulse, resulting in the kink observed in fig. 4.8 (b). At these temperatures the shear wave velocity error was measured to be $\pm$ 14 ms^{-1}, which is about the size of the symbol used. The longitudinal to shear wave transit time ratio error was calculated to be $\pm$ 0.002.

From the calculations made by applying Snell's law and considering the worst case, that is the L-L side wall reflection signal being detected at the outside edge of the EMAT's coil (see fig. 4.11), it was found that at 360 °C the calculated L-L signal

arrival time of 4.205 μs is very close to that of the experimental shear wave pulse value of 4.222 μs. Therefore it is suspected that the L-L signal, would be superimposed with and distort the shape of the shear wave pulse and cause the errors in the shear wave transit time measurements observed between 350-400 °C. An investigation was also carried out using the Nd:YAG laser as the ultrasound generator and a modified stabilised interferometer as the detector (point source and point detector) to confirm the above phenomena. With this system, it was hoped that the shear pulse and the L-L signal would be distinctly resolved. A detailed description of the experiment and the results obtained will be presented in chapter 6.

Figure 4.8 also shows that the onset of partial melting, determined from the point of intersection between the tangent drawn at the point of greatest slope during the melting stage and the extrapolated base line in the solid state, is clearly indicated at 570 ± 3 °C. The value is slightly lower than 577 °C the eutectic temperature for the Al-Si binary alloy as indicated in the phase diagram (fig. 4.9). This may be due to impurities that are present in small quantities. Our experimental value is also lower than that obtained by the DSC analysis of 577 °C (fig. 4.10). At 577 °C, according to the phase diagram the sample should be 40 % liquid. Immediately above this temperature only the longitudinal wave could be detected as the shear wave signal was greatly attenuated. As the temperature was increased further, measurement could not be made as the partially molten alloy tended to flow out of the sample holder, pile up at the sample base, and stick to the face of the EMAT. Hence, the experiment could only be carried out up to relatively low liquid fractions.

Figure 4.12 shows the typical waveforms obtained at room temperature, 300 °C and at 500 °C for the Al 4.86 % Si alloy, when both ends of the sample surface

were unsupported. The longitudinal and shear wave first arrival pulses denoted by L and S and their subsequent echoes denoted by 3L, 5L, 7L and 9L and 3S respectively, could be clearly observed at room temperature and at 300 °C. Mode converted signals due to the reflection at the boundaries denoted by 2LS, and 2SL were also detected. At room temperature, the laser power density was altered to give a weaker longitudinal and stronger shear wave amplitude. The reason being, as the sample is heated the characteristic of the source changes, less laser energy is needed to melt and ablate the sample surface at the point of incidence, therefore with constant power density applied the degree of ablation increases with temperature. As a consequence the normal stress component increases giving rise to progressively stronger longitudinal waves but weaker shear waves. Hence, at higher temperatures the power density was reduced by either defocusing the laser beam reaching the sample surface or by placing a neutral density filter in between the laser source and the sample to absorb part of the laser energy. By this means a clearly identifiable shear wave was maintained in addition to the reduced amplitude longitudinal wave signals (see fig. 4.12, at 300 °C and 500 °C). Figure 4.13 shows the waveforms at 570 °C and 575 °C. At 570 °C, the onset of partial melting the longitudinal wave and shear wave signals and the mode converted pulse (2LS and 2SL) are clearly observed, however, at 575 °C the shear wave signal is very weak, and changes its polarity from negative to positive which may be indicative of a very strong ablation source [Dewhurst et. al., 1988].

Figure 4.14 shows the measured variation of the longitudinal and shear wave velocities when a silica window and an alumina disc were used to support the sample surface, and the alloy heated to the fully molten state. The longitudinal velocity could

be measured up to the fully molten state and the shear velocity curve shows similar profile to that shown in figure 4.9, where the unusual behaviour between 350 and 400 °C was still observed. The acoustic wave signals could be detected up to a higher percentage of liquid in the semi-solid phase before the signal disappeared. The longitudinal wave could be detected at a higher temperature of 581 °C and the shear wave could be detected up to 579 °C. Above these temperatures the acoustic wave signals disappear, which might be caused by the formations of solid particles in the liquid matrix, with grain sizes much smaller than the wavelength of the ultrasonic waves, resulting in a strong attenuation of the epicentral signal, possibly caused by either a dominant Rayleigh scattering or due to increased liquid path lengths between the particles. The other possible reason for the disappearance of the shear wave signal was the great reduction in the alloy viscosity in the semi-solid state which is therefore unable to withstand the shear stress. However, the longitudinal wave signal could be detected again at 622 °C. Rayleigh scattering attenuation is proportional to the mean grain volume [Bhatia, 1967], it is suspected that before the alloy becomes fully molten, the gradual decrease in solid particles sizes causing less scattering to occur, hence enables the acoustic wave signal to be detected again. When the sample had become fully molten at around 628 °C which corresponds to DSC endotherm, a strong longitudinal pulse and its subsequent echoes could be detected. In the molten state, the longitudinal wave velocity decreases only slightly as the temperature increases.

Figure 4.15 shows the waveforms detected at room temperature and at 571 °C. At room temperature, both the longitudinal and shear wave signals could be detected simultaneously, indicating that the sample surface was well bonded to the silica window and sufficient to create forces normal to the sample surface even with a

thermoelastic source. At 571 °C both bulk waves could still be detected. Figure 4.16 shows the waveforms detected immediately before (at 622 °C) and after (at 628 °C) the sample becomes fully molten. At 622 °C a longitudinal pulse followed by three consecutive small peaks were detected. The first peak detected is thought to come directly from the surface of the damaged silica window where acoustic waves generation could occur and propagate through the sample. The second and third peaks are thought to come from internal reflections within the silica window as shown in figure 4.17. Figure 4.18 shows the waveform where the alloy is clearly in the fully molten state (680 °C). Strong and sharp longitudinal signals were observed. Al 4.86 % Si alloy has a broad melting range of about 60 °C (see fig. 4.10), therefore there is a slow transformation from all solid to all liquid phase. The longitudinal wave velocity was measured at room temperature using the PZT transducer and found to be 6552 $\pm$ 22 ms^{-1} , higher than the value published by Kaye and Laby, [1986] for pure aluminium. In the liquid, the longitudinal wave velocity appears to be reduced by about 20 % from the velocity in the solid which is slightly higher than that reported by Parker et. al., [1985] for pure aluminium.

Figure 4.19 and figure 4.20 show the variation of the transit time ratio (T_L/T_S) of the longitudinal wave to the shear wave for temperatures above 450 °C when the alloy was heated to the partially and fully molten state, respectively. The T_L/T_s ratio curve shows similar behaviour to the velocity measurements, decreasing more rapidly above the solidus. Figure 4.19 shows that the onset of partial melting for Al 4.86 % Si alloy occurs at a ratio of around 0.438 but figure 4.20 shows a slightly higher value of 0.450. It is expected that the ratio should be characteristic of a particular material and is temperature dependent, since it is independent of the sample dimensions, and

depends only on the percentage of solid and liquid present. Hence the ratio may be a suitable parameter for monitoring the percentage of solid and liquid present.

When an alumina disc was used to support the sample surface both on the generation and detection side, only the shear wave signal could be detected since only 15 per cent (measured using the Field Master Meter) of the initial laser energy reached the sample surface. The acoustic waves were generated in the thermoelastic regime. At higher temperature, the longitudinal wave signal only appeared at two instances, that is at 333 °C and 345 °C but disappeared again as the temperature increased. The graph of the shear wave velocity as a function of temperature for this arrangement is shown in figure 4.21. The profile of the graph is similar to that of the results discussed earlier.

When a mica sheet of 0.5 mm thick was used to support the sample surface at the detection side, generation was carried out in the ablation regime. Both the longitudinal and shear wave signals could be detected continuously up to the partially molten state but it was difficult to determine the transit time accurately because of the broad and confusing features at higher temperatures. The shear wave velocity of the alloy measured at room temperature using the shear EMAT as both generator and detector of acoustic waves is 3225 ± 7 ms^{-1}.

4.6.2 LM25 Alloy

Figure 4.22 and 4.23 show the acoustic wave velocity measurements as a function of temperature on the LM25 alloy, with and without the silica window supporting the sample surface at the generation side, respectively. Both figures show

that the onset of partial melting occurs at around 550 °C, a much lower temperature than that of Al 4.86 % Si alloy which might be due to the effect of the presence of 0.63 per cent magnesium content. The value is also lower than that obtained by the DSC analysis which indicates a value of around 567 °C (see fig. 4.24). Again better results were obtained when the sample surface was supported. Longitudinal wave signals could be detected in the fully molten state and the shear wave signals could be detected up to 558 °C, that is in the partially molten state (fig. 4.22). A rapid decrease in the longitudinal wave velocities from the all solid to the all liquid phase indicates that LM25 alloy has a very narrow melting range. The figure also indicates a reduction of about 20 % in the longitudinal velocity from the solid to the liquid state. Figure 4.25 shows the waveforms obtained at room temperature, at the onset of partial melting (550 °C), and at a temperature corresponding to a higher percentage of liquid fraction (562 °C). Similar to the Al 4.86 % Si alloy, strong and sharp longitudinal and shear wave signals and their subsequent echoes could be detected at room temperature which again indicates that the silica window was constraining the surface. At 550 °C both the bulk waves could still be clearly identified but at 562 °C both the detected longitudinal and shear wave signals are weak which is evidence of very high attenuation and scattering of the high frequency components [Dewhurst et. al.,1988]. The shear wave signal changes its polarity from a positive to a negative which is again indicative of increasing plasma formation. Figure 4.26 shows the waveform obtained in the fully molten state, a strong longitudinal wave first arrival is observed but the subsequent echo was not detected which again indicates a very high attenuation possibly due to scattering by gas bubbles in the liquid. Figure 4.27 shows

the longitudinal to shear wave transit time ratio as a function of temperature, the onset of partial melting is clearly indicated to occur at 0.439.

In the second case when the sample surface was unsupported (fig. 4.23), both the longitudinal and shear wave signal measurements could only be made up to few degrees above the onset temperature (550 °C). The longitudinal wave could be measured up to 557 °C and the shear wave up to 552 °C. There was a substantial reduction in the longitudinal wave velocities in the semi-solid state, which is lower by more than 50 % to the velocity in the solid. It is thought that the anomalously low velocities observed are due to the exsolution of the inert gas trapped in the alloy during manufacture. Gas pores could be observed at the centre and other parts of the heated sample surface after it was cooled and polished.

Figure 4.28 shows the waveforms at room and higher temperatures, a pre-amplifier with maximum gain of approximately 46 dB at 1 MHz was used for the measurements. At room temperature the pulses are comparatively broader than that of the Al 4.86 % Si alloy sample and the echoes are not clearly identifiable indicating a sample with comparatively higher attenuation and scattering. Again there was a reduction in the shear pulse amplitude with increasing temperatures as for the reasons that have been explained for Al 4.86 % Si alloy. There was a change in polarity from a positive to negative shear wave pulse after 546 °C which again might be evidence of a very strong ablation. Figure 4.29 shows the waveforms obtained at and above the onset temperature. At 550 °C a strong longitudinal pulse is observed but only a much weaker and broader shear pulse was detected. Higher than this temperature, that is in the partially molten state, only a weaker and broader longitudinal wave pulse was detected as evidence of a very high attenuation. The longitudinal pulse becomes

progressively reduced in amplitude and broader with increasing temperature, and shows substantial increase in the transit time. There are three factors that might contribute to this phenomenon. Firstly the possibility of entrapped inert gases in the alloy and secondly, as the liquid fraction in the alloy increases, the metal tends to flow out of the laser access hole. As a consequence, the sample surface at the generation side bulged and continued increasing in size with temperature, thus increasing the acoustic path length of the longitudinal wave normal to the sample surface. The final reason was due to the slight increase (approximately 0.2 mm) in thickness at the bottom of the sample at the detection side increasing the lift-off distance between the EMAT face and sample surface which hence reduces the detection sensitivity.

The variation in the transit time ratio (T_L/T_S) for temperatures at and above 450 °C is shown in figure 4.30. Initially, the ratio decreases as expected but later above 540 °C and nearer to the onset temperature, the ratio increases until the signals disappear. It is thought that the changes in the polarity of the shear wave mentioned earlier at temperatures above 546 °C causes inaccuracies in the shear transit time measurement and hence the ratio. The calibrated longitudinal and shear wave velocity of the alloy at room temperature was measured to be 6528 ± 24 ms^{-1} and 3244 ± 8 ms^{-1} respectively. The longitudinal wave velocity was measured using the PZT transducer and the shear wave velocity was measured using the shear sensitive EMAT.

4.6.3 Al 1.2 % Si Alloy

Figure 4.31 shows the bulk wave velocities measured for the Al 1.2 % Si alloy as a function of temperature when the alloy was heated up to the fully molten state. At

room temperature, the calibrated longitudinal and shear wave velocity was measured to be 6452 $\pm$ 17 ms^{-1} and 3196 $\pm$ 5 ms^{-1} respectively. Both the longitudinal and shear wave velocities drop gradually up to around 550 °C where a discontinuity is observed. The discontinuity may be due to the phase transformation from the Al + Si solid solution to the Al solid solution (see fig. 4.9). At 600 °C, the onset of melting, the longitudinal wave velocity reduces steeply in the partially molten state until it reaches 650 °C after which it should be totally liquid and starts to flatten. The longitudinal wave velocity appears to drop by about 20 % of the solid velocity before it is fully molten. The shear wave arrival could not be clearly identified above 606 °C just after the sample started melting, although the longitudinal wave and its subsequent echoes could be clearly detected (see fig. 4.32) throughout the two phase state. This may be related to the non-thixoforgeable properties of the alloy which contains dendritic structured particles instead of spheroidal particles in the semi-solid state (refer fig. 1(b&c), and fig. 2 in appendix). It is thought that dendritic particles would attenuate much lesser of the ultrasound wave energy compared to the spheroidal particles enabling the longitudinal wave signals to be detected throughout the two phase state. It is stated by Ahuja and Hendee, [1978] that the shape and orientation of the particles in the acoustic field would influence sound scattering significantly. In a paper written by Blue and McLeroy, [1986] it is mentioned that the attenuation in suspension depends upon the shape of the particles. They found that the measured absorption coefficients for disk-like and needle-shape particles are less than those for equivalent spheres. The different liquid gaps between dendritic and spheroidal particles might also be a contributer to different attenuation levels. Approaching the liquidus temperature, the longitudinal wave signals become stronger and sharp indicating

further reduction in the degree of attenuation. The alloy has a melting range of about 50 °C. Figure 4.33 shows the typical waveform of the alloy in the fully molten state. Strong and sharp longitudinal wave signals could be clearly detected.

4.6.4 Al 9.5 % Si alloy

The variation of the longitudinal and shear wave velocities as a function of temperature of the alloy are shown in figure 4.34. As usual in both cases the velocities decrease gradually with increasing temperatures. However near the eutectic temperature, the longitudinal wave velocity apparently increases slightly up to 600 °C before it reduces again sharply as the percentage of liquid fraction increases. In the case of the shear wave velocity, the slope flattens near the eutectic temperature, no measurements were possible after the onset of partial melting. In this experiment, measurements were only made up to the partially molten state using an unconstrained sample. The calibrated longitudinal and shear wave velocity of the alloy at room temperature was measured to be 6365 ± 19 ms^{-1} and 3229 ± 5 ms^{-1} respectively.

4.7 Conclusions

A combination of a pulsed Nd:YAG laser and a water-cooled shear EMAT has been used to respectively generate and detect acoustic wave signals, both in thixotropic and non-thixotropic aluminium alloys at temperatures up to 700 °C. The system has demonstrated the capability of detecting both the longitudinal and shear wave signals simultaneously for a particular temperature, when ultrasound was generated in the ablation regime for the unsupported sample, and in the thermoelastic

regime for the supported sample. In most cases both bulk waves could be detected from room temperature up to the onset of partial melting. However when the sample surface was supported at both ends measurements could be made to as high as 50 to 60 per cent fraction liquid in the semi-solid state, a condition that is suitable for thixoforging. It has also been demonstrated that the longitudinal to shear transit time ratio could be used to monitor the degree of partial melting as it is independent of the sample dimensions and depends only on the temperature and percentage of solid and liquid present in the sample. In conclusion, this chapter has demonstrated that the Nd:YAG pulsed laser- shear EMAT system when combined with a proper designed ultrasound cell enables acoustic wave measurements to be made to a very high liquid fraction in the semi-solid state, and into the fully molten state. Advantages of the system are that it is non-contact and insensitive to the sample surface conditions.

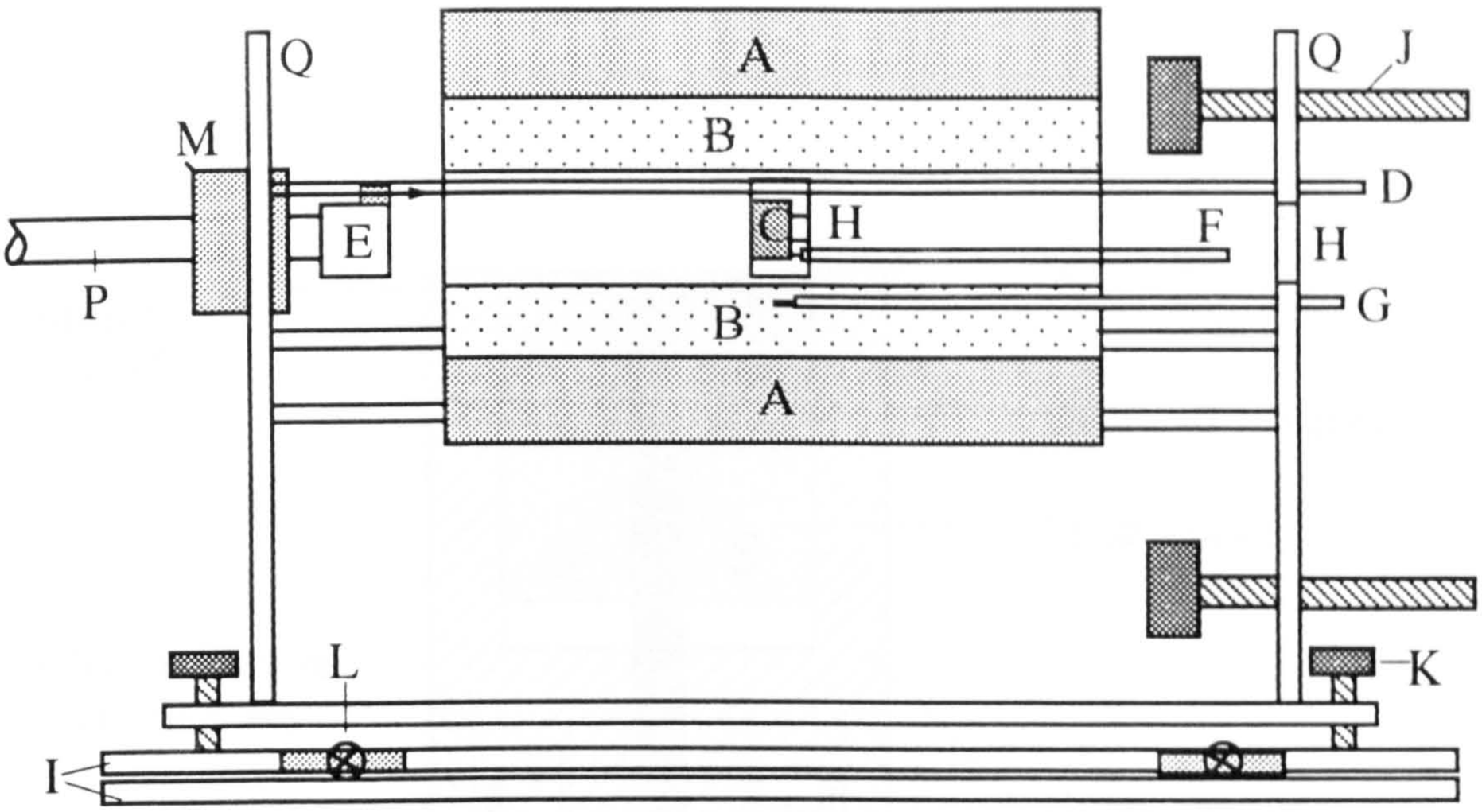

SIDE VIEW

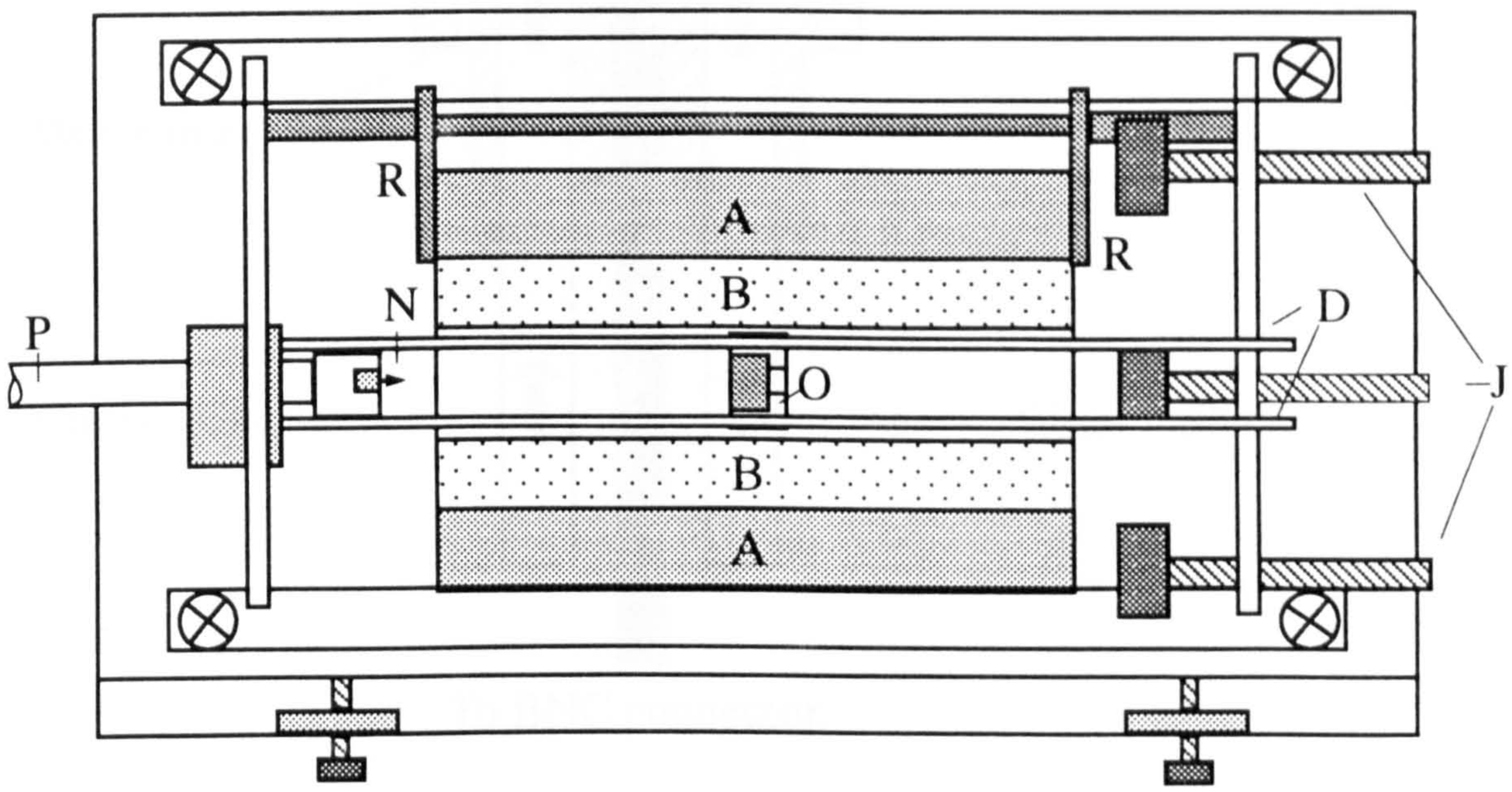

TOP VIEW

A Electric furnace outer layer
B Furnace heating element
C Sample
D Stainless steel tube
E Water-cooled EMAT
F Measuring thermocouple
G Control thermocouple
H Laser access holes
I Base plates
J Horizontal set-up height adjustment stud
K Vertical set-up height adjustment stud
L Adjustable stud (horizontal adjustment)
M Teflon bush bearing
N EMAT earth pin
O Sample holder
P EMAT stainless steel tube holder
Q Furnace support plates
R Hinges

Figure 4.1 Schematic diagram of the furnace system

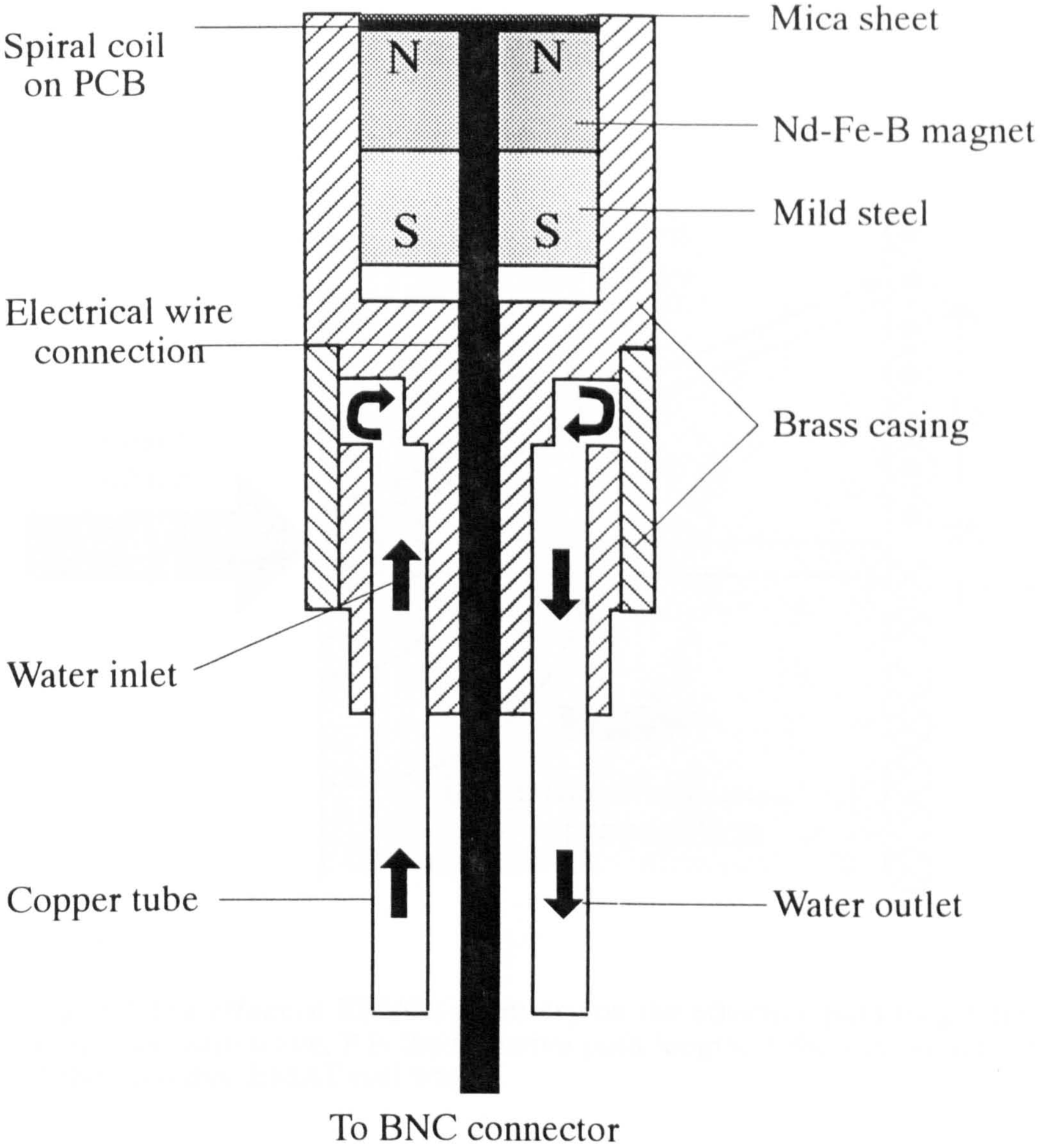

Fig. 4.2 Schematic diagram of the water-cooled spiral coil EMAT

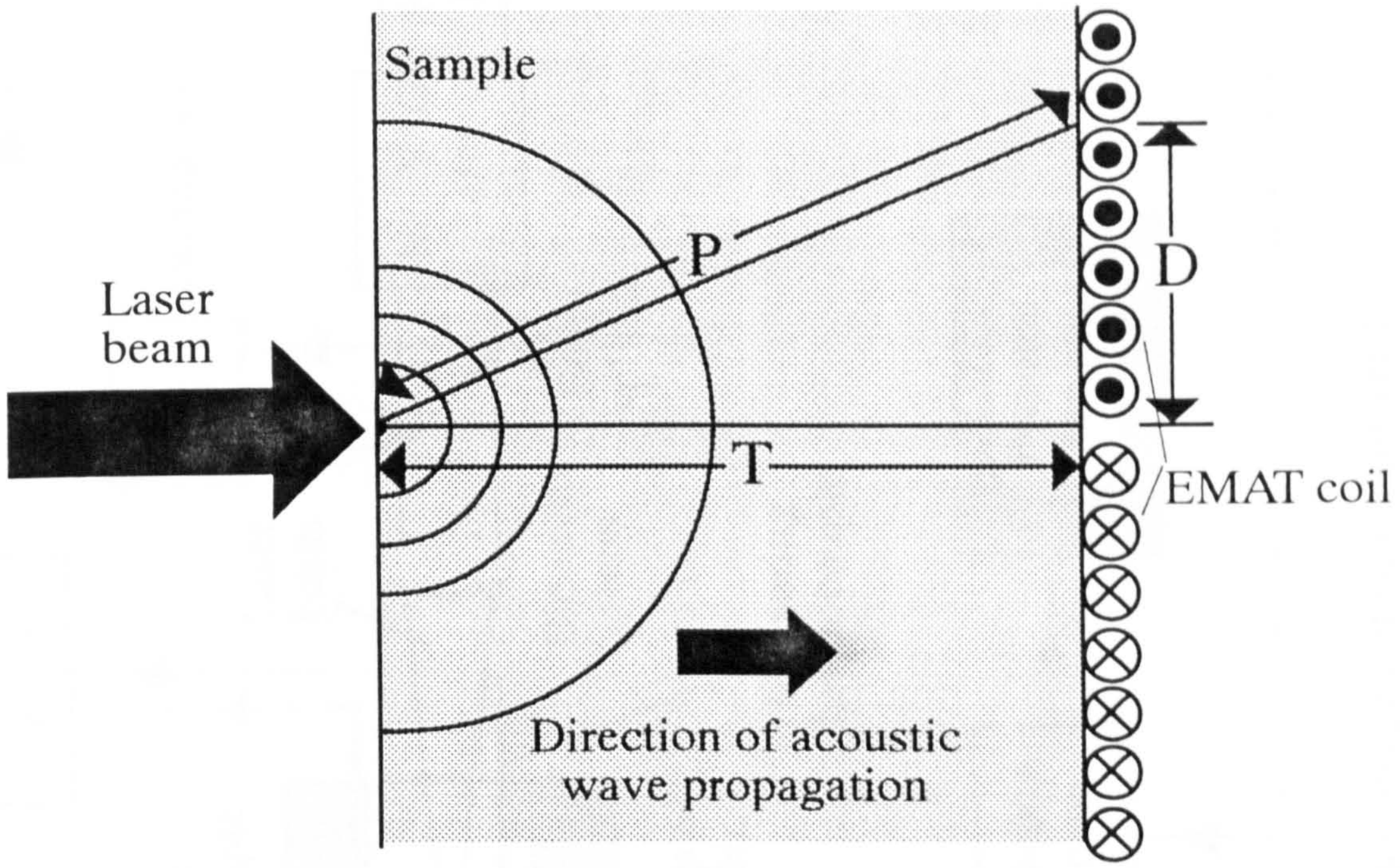

Fig. 4.3 The effect of EMATs geometry on the effective path length travelled by the acoustic wave, P is the effective path length, T the sample thickness and D the effective EMAT coil width.

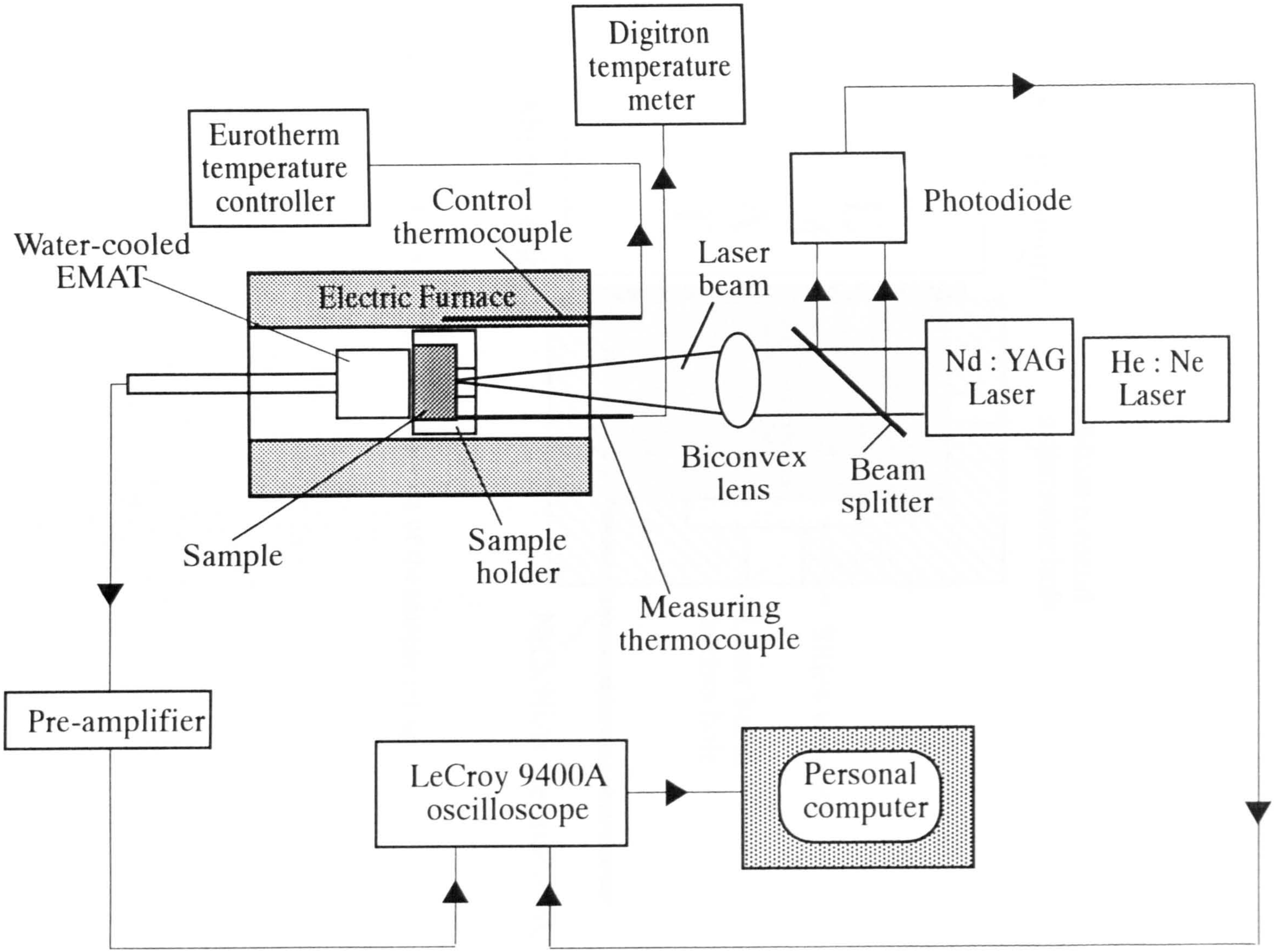

Fig. 4.4 Schematic diagram of the experimental set-up.

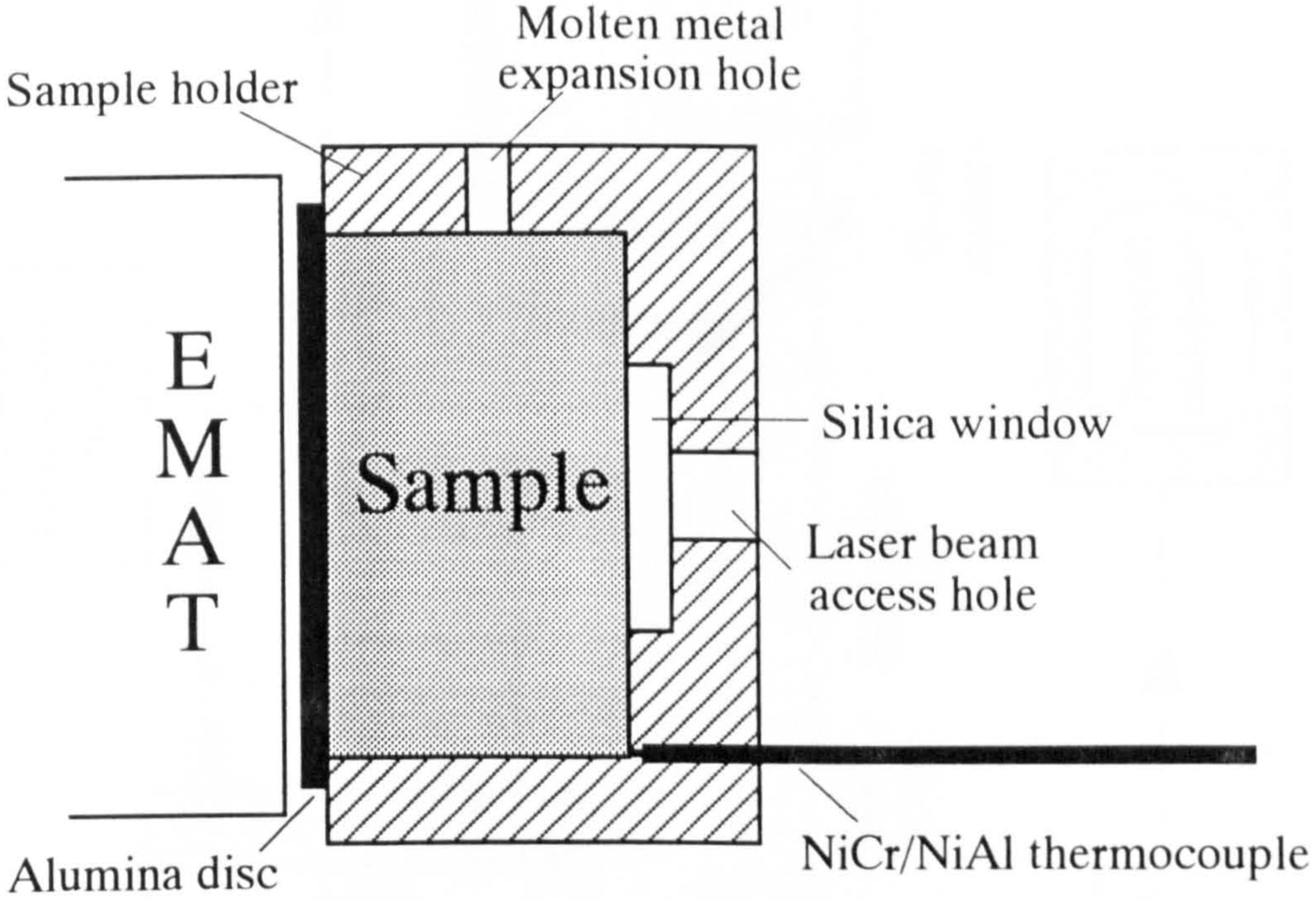

Fig. 4.5 Schematic diagram of the sample set-up.

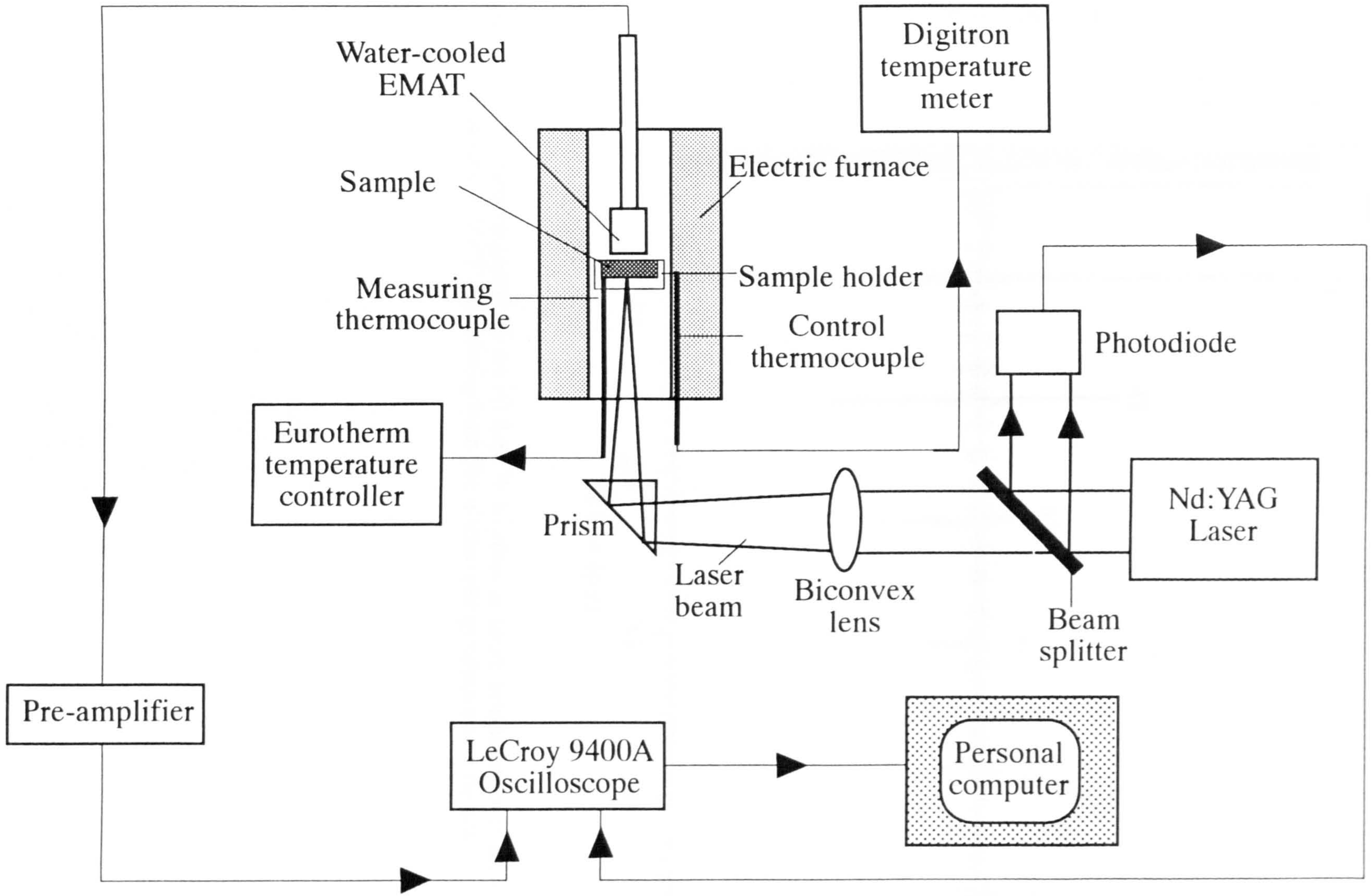

Fig. 4.6 Schematic diagram of the experimental set-up with the furnace in the vertical position.

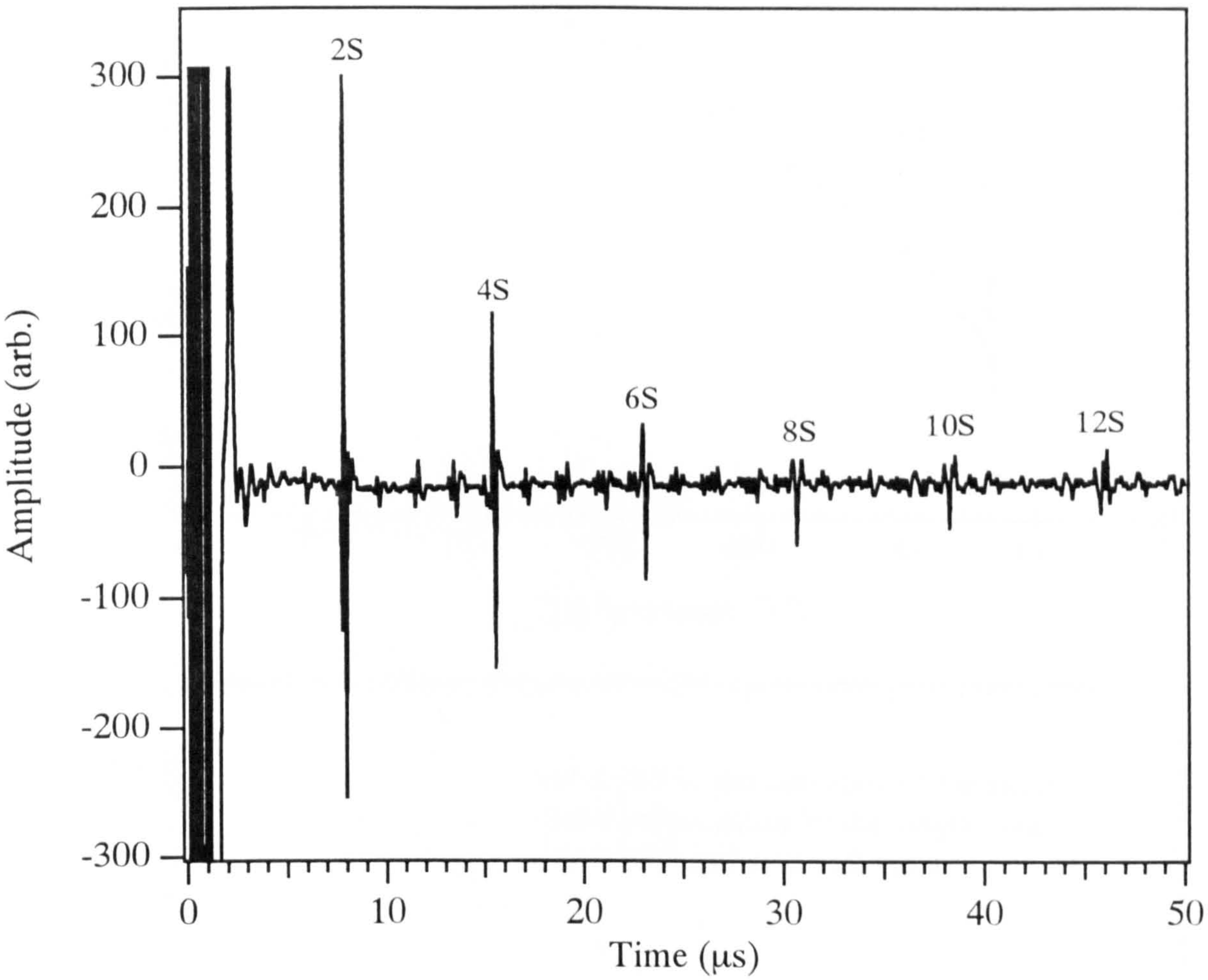

Fig. 4.7 Waveform obtained on the Al 4.86 % Si alloy at room temperature from a shear sensitive EMAT that acts as both the ultrasound generator and detector.

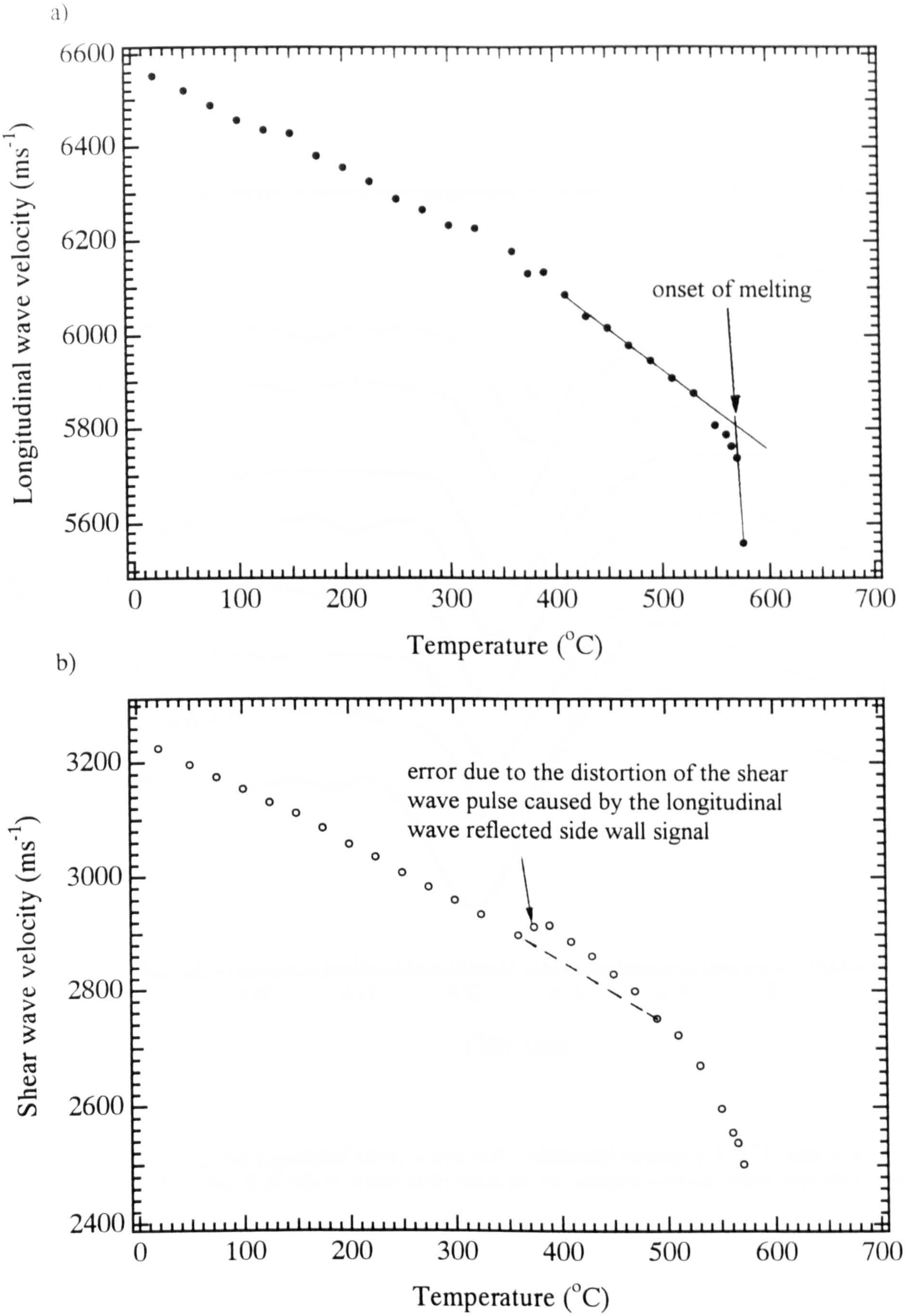

Fig. 4.8 Variation of a) longitudinal and b) shear wave velocity as a function of temperature in Al 4.86 % Si alloy when both ends of the sample surface were unsupported.

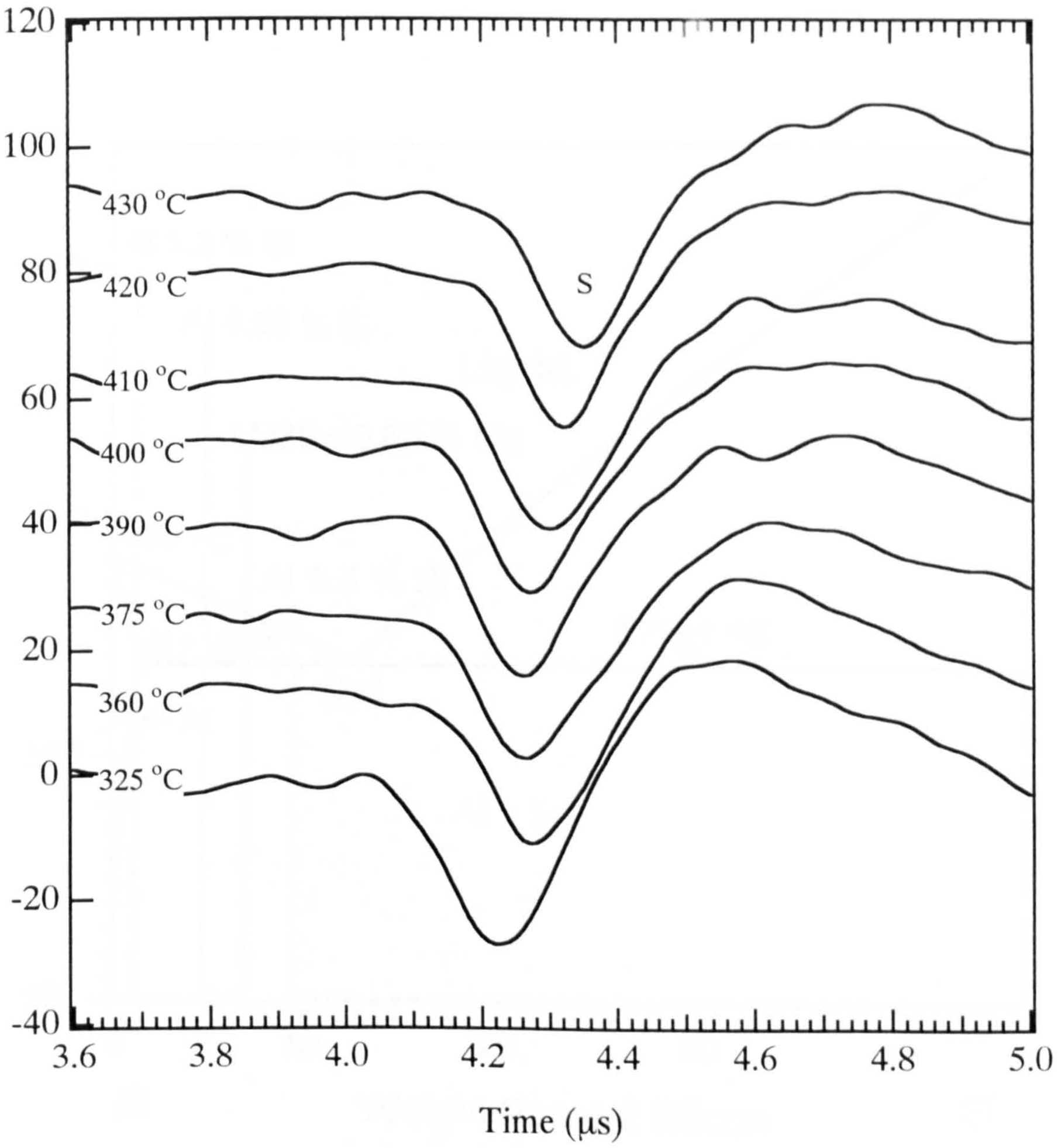

Fig. 4.8(c) Showing the expanded shear wave pulse obtained between 325 °C and 430 °C on Al 4.86 % Si alloy when both ends of the sample surface were unsupported.

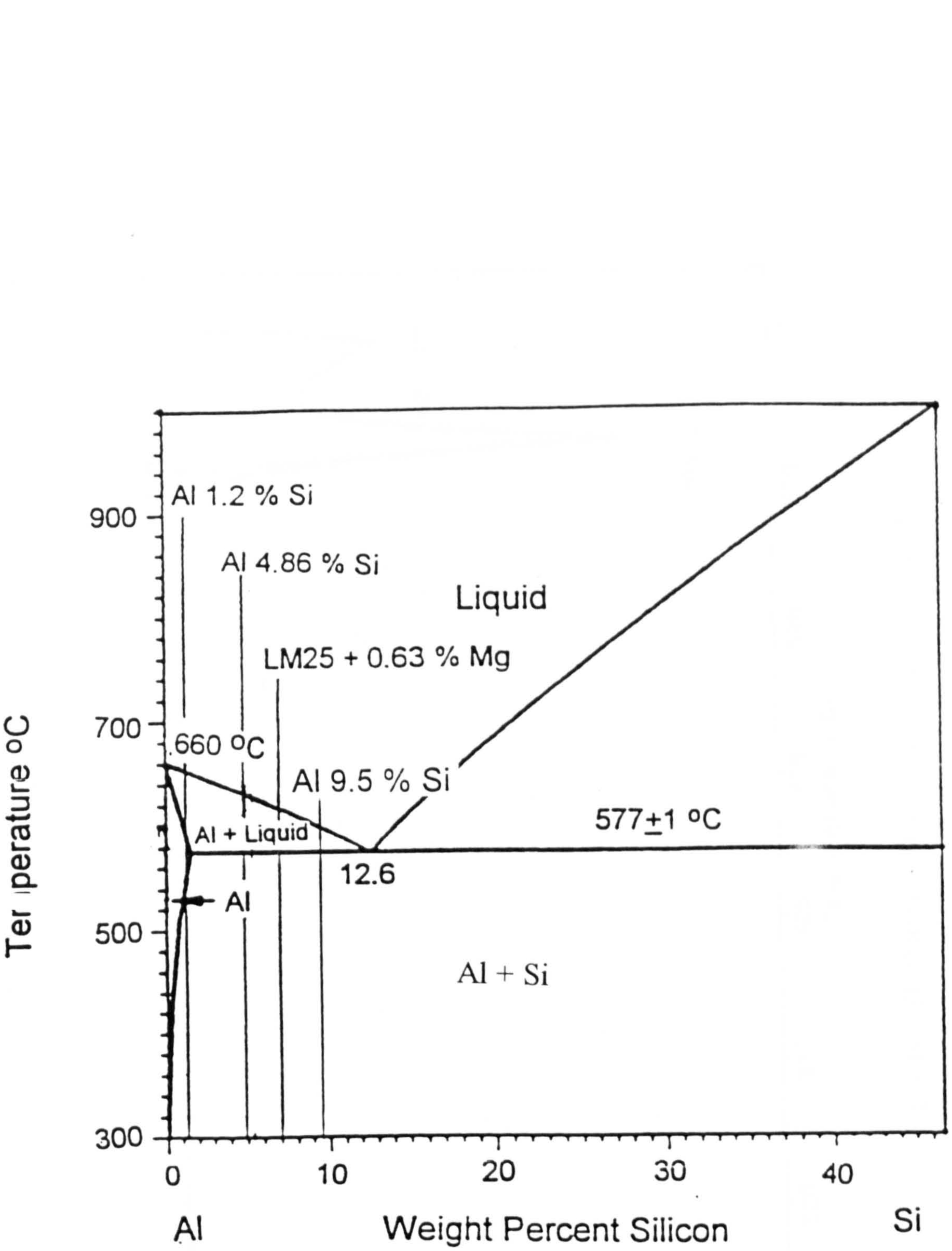

Fig. 4.9 The aluminium-silicon phase diagram.

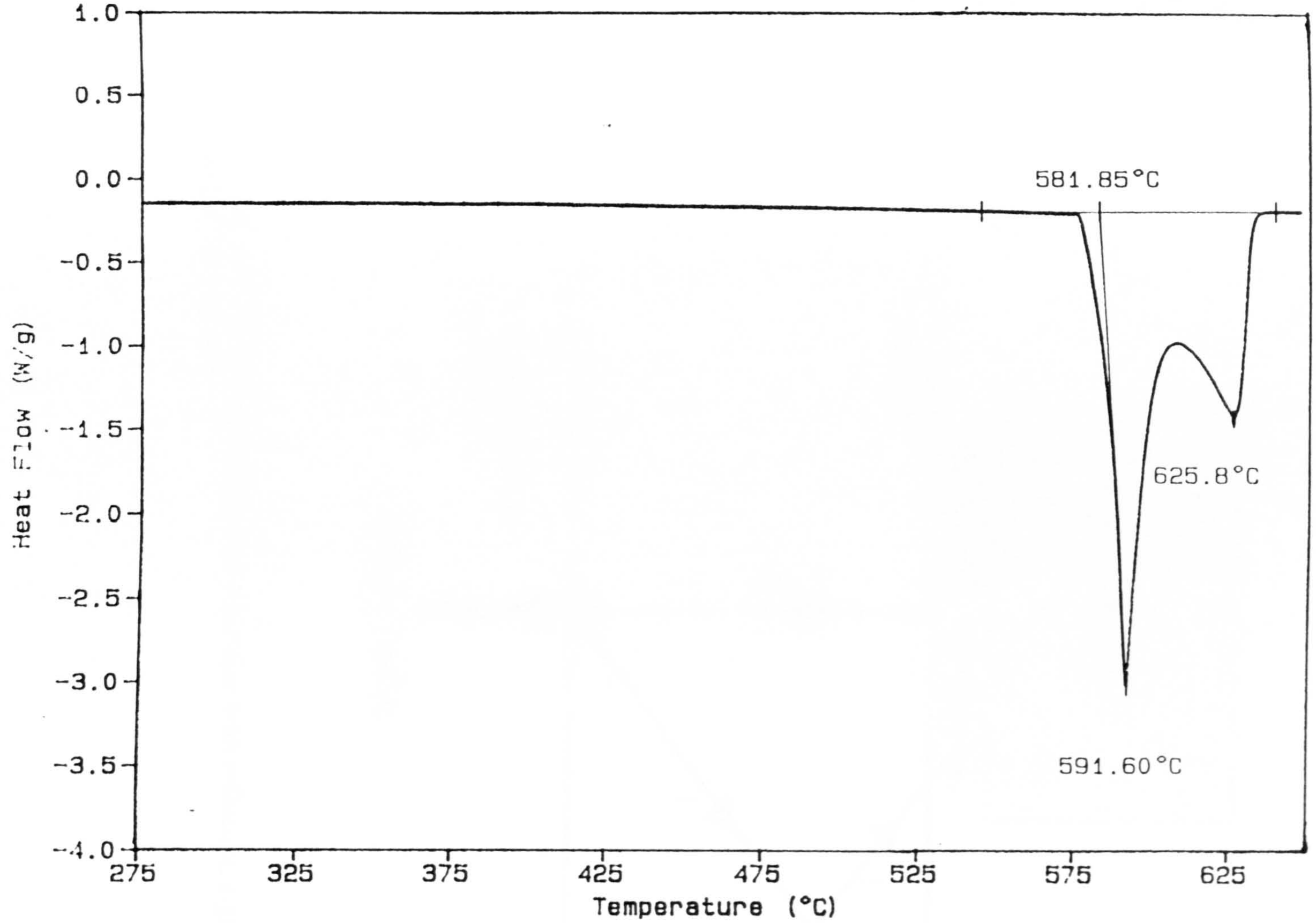

Fig. 4.10 DSC thermal analysis result on Al 4.86 % Si alloy.

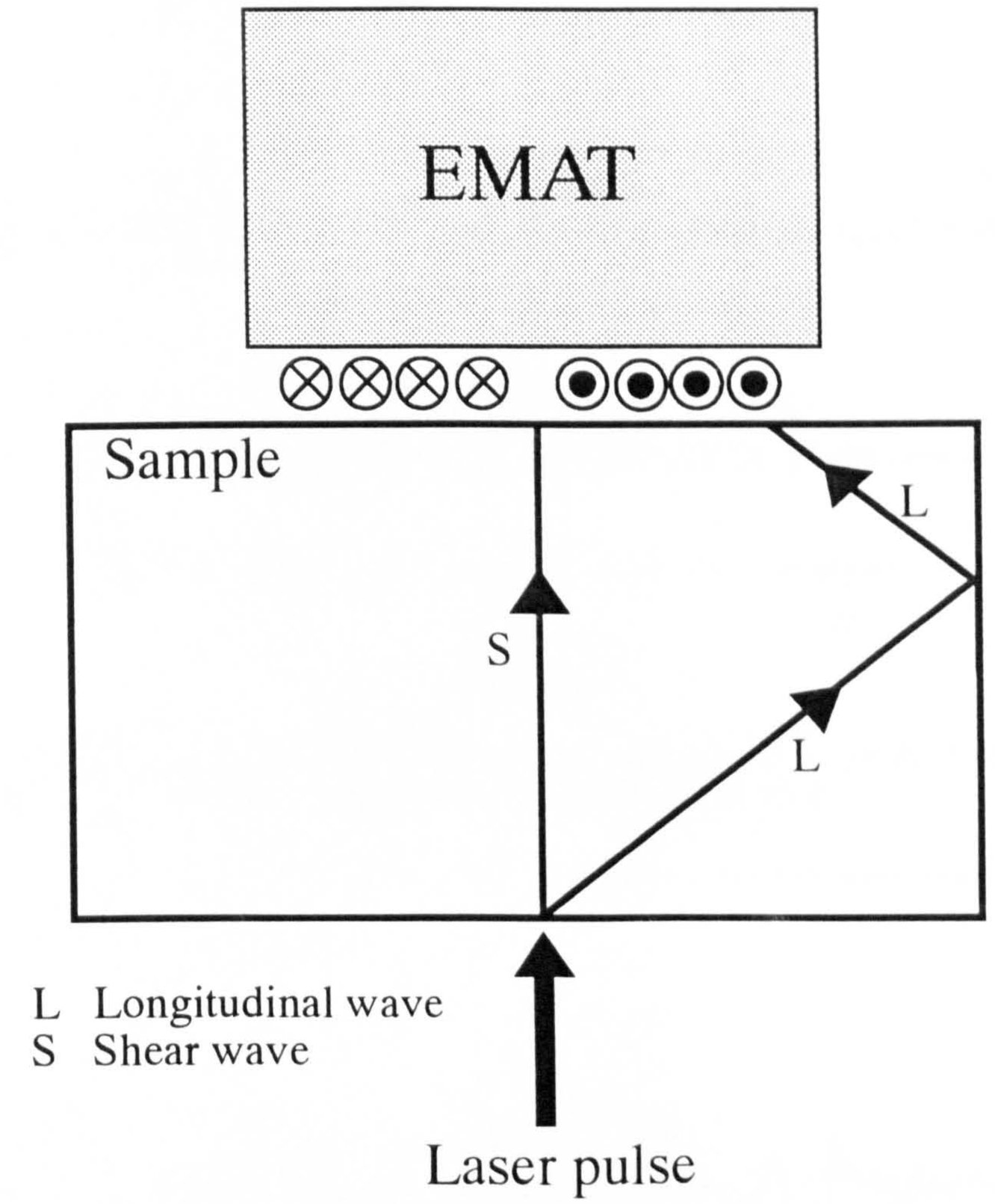

Fig. 4.11 The detection of the longitudinal wave side wall reflection signal at the outer edge of the EMATs coil.

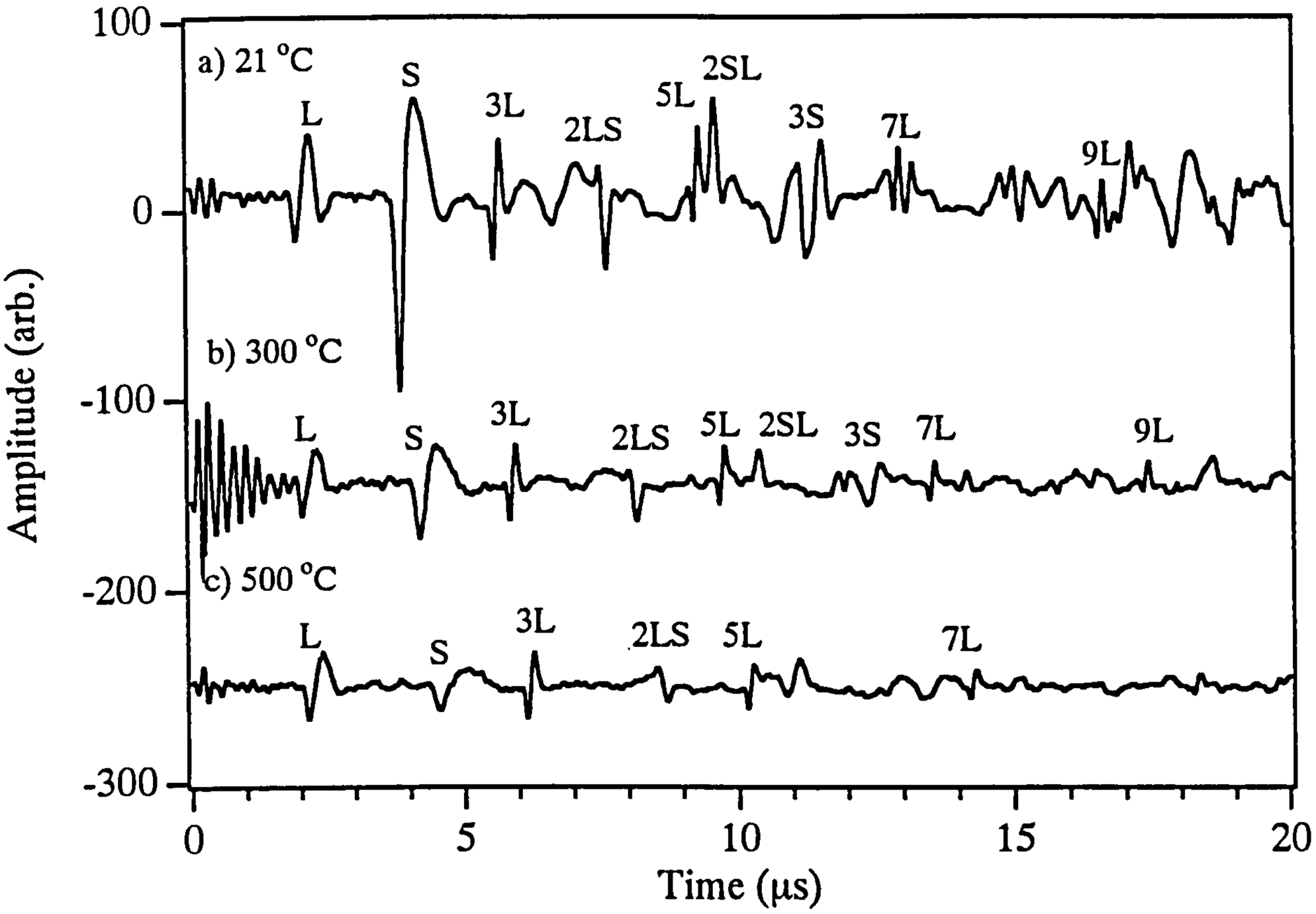

Fig. 4.12 Waveforms obtained at a) 21 °C b) 300 °C and c) 500 °C on Al 4.86 % Si alloy when both ends of the sample surface were unsupported.

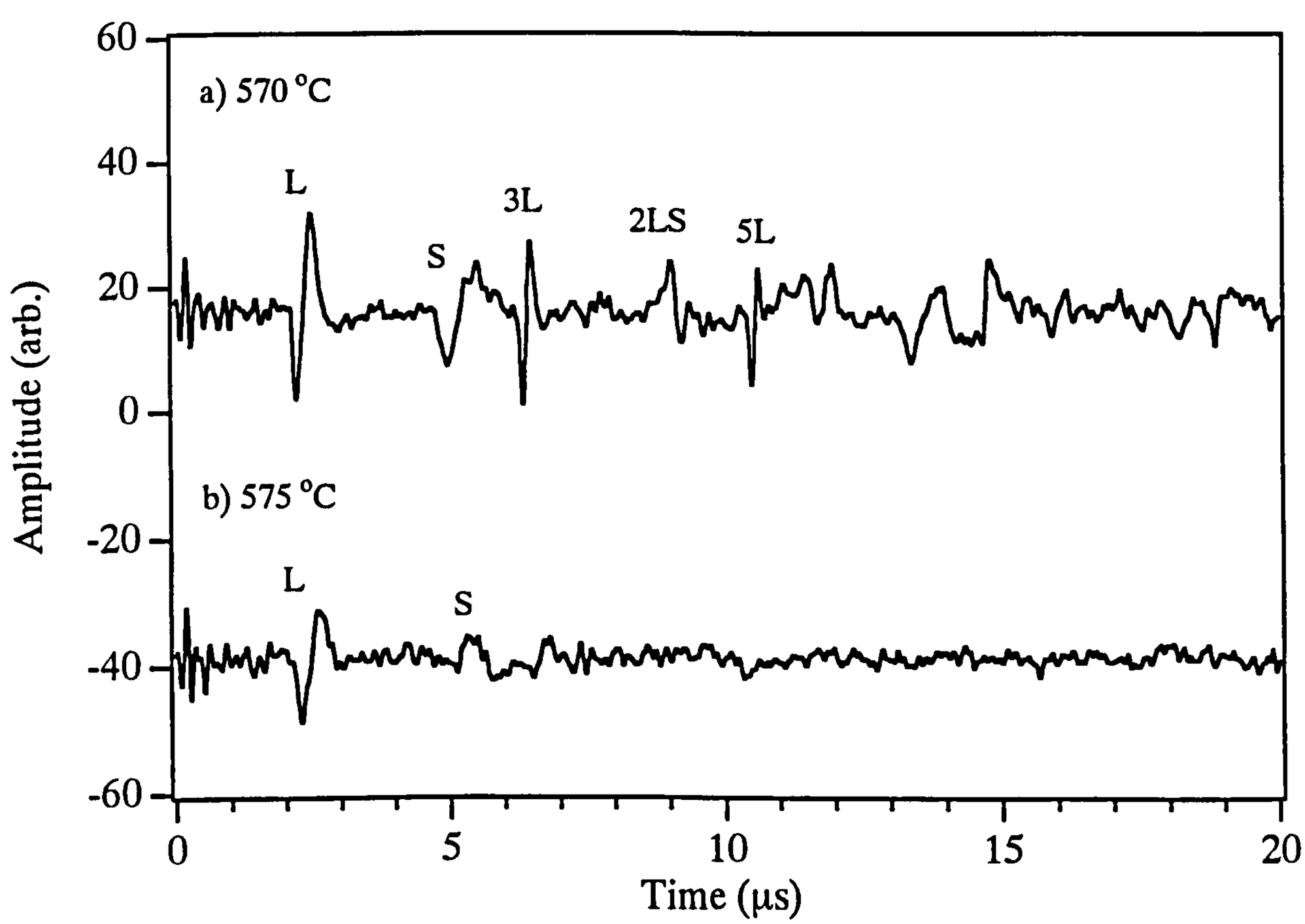

Fig. 4.13 Waveforms obtained a) at the onset of melting and b) in the partially molten state on Al 4.86 % Si alloy when both ends of the sample surface were unsupported.

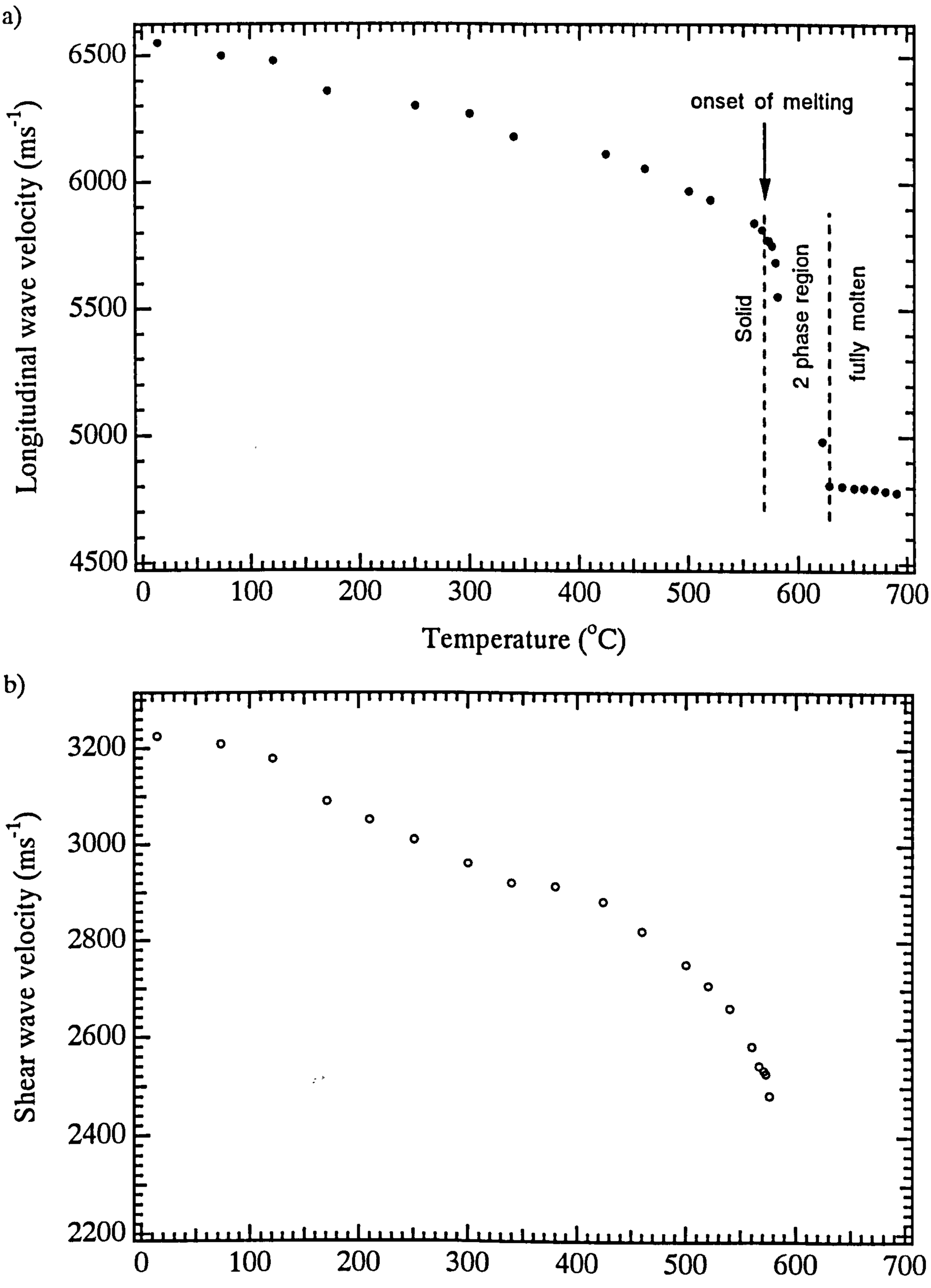

Fig. 4.14 Variation of a) longitudinal and b) shear wave velocity in Al 4.86 % Si alloy as a function of temperature when both ends of the sample surface were supported.

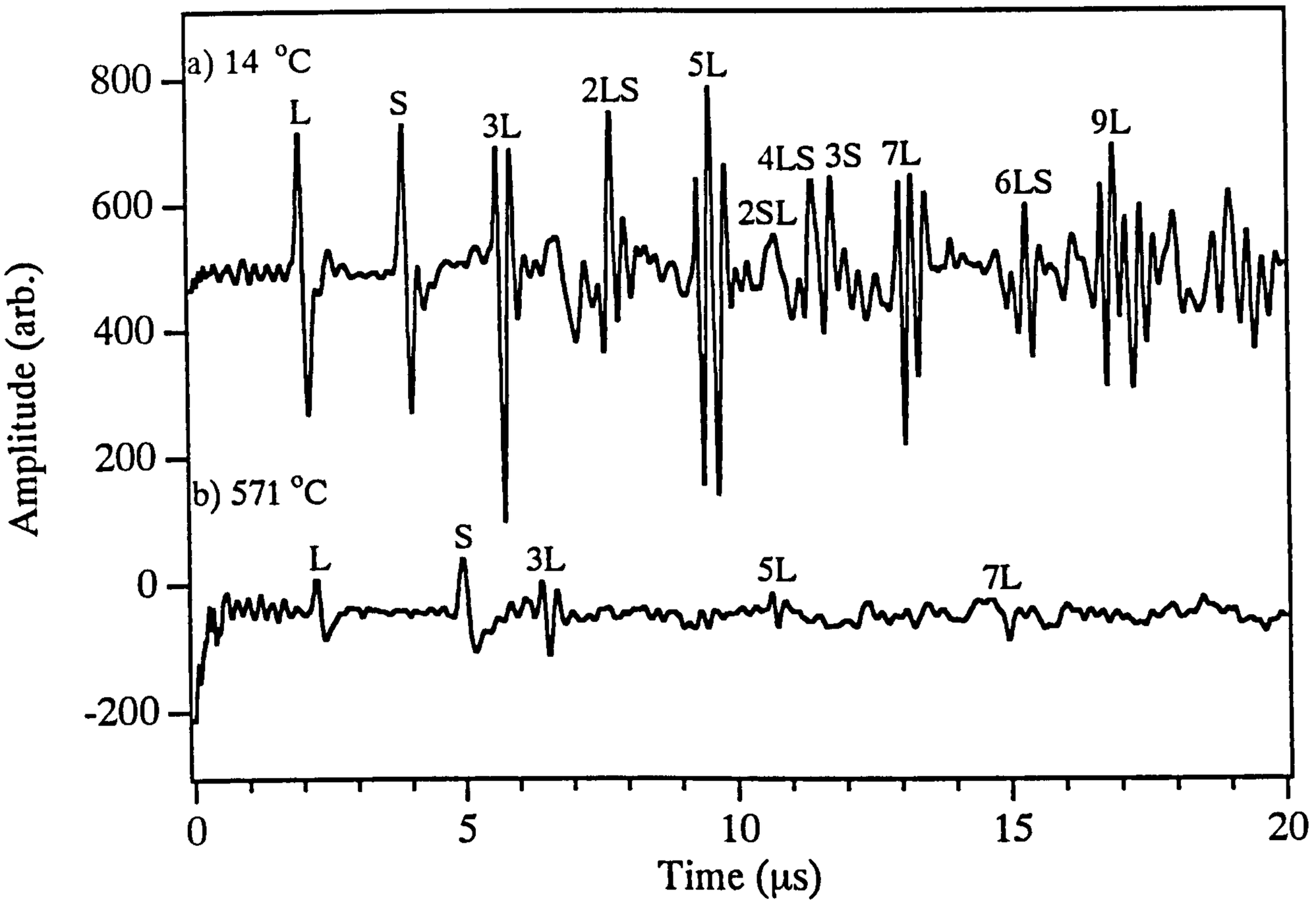

Fig. 4.15 Waveforms obtained at a) room temperature and b) the onset of melting on Al 4.86% Si alloy when both ends of the sample surface were supported.

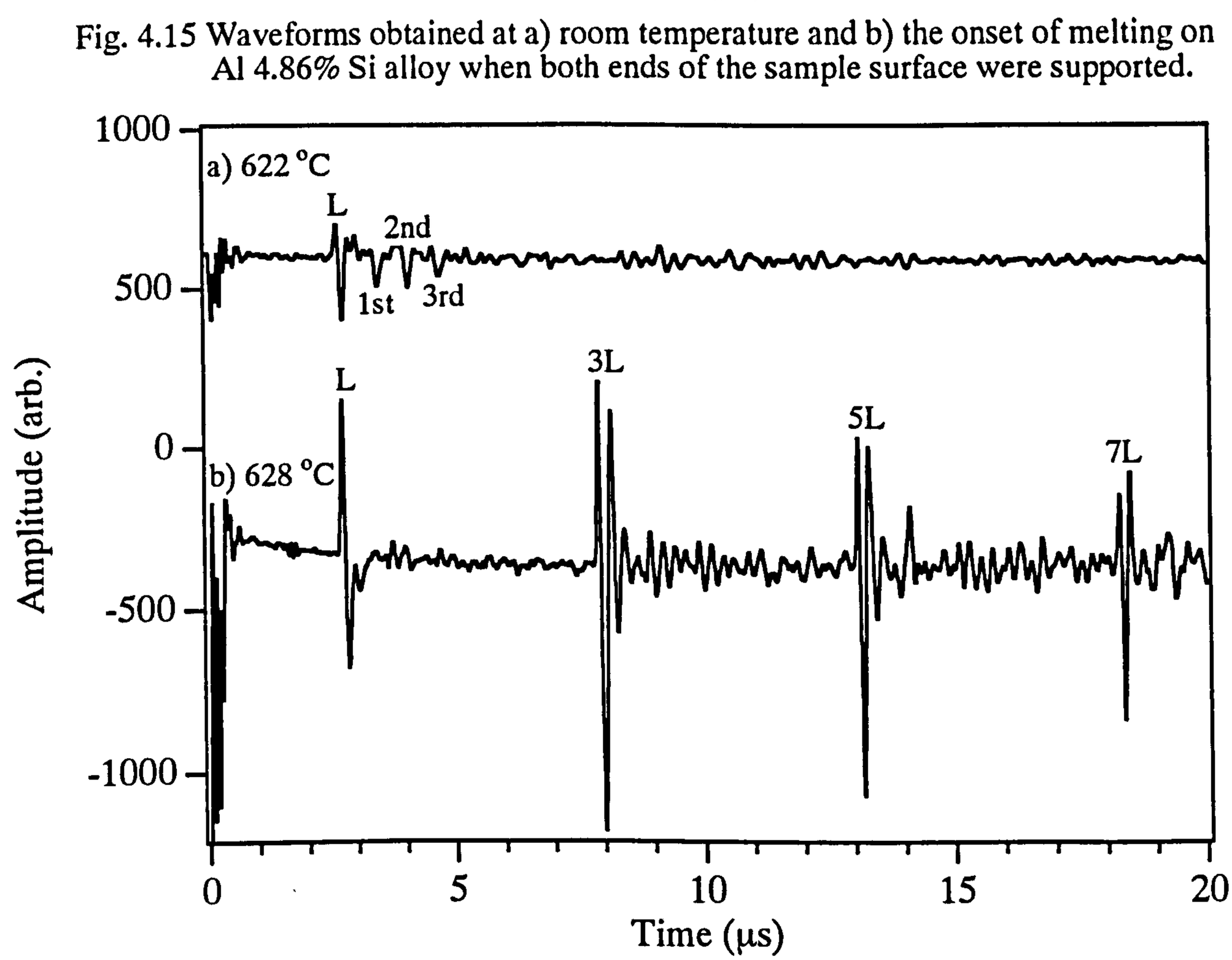

Fig. 4.16 Waveforms obtained at a) immediately before and b) immediately after the Al 4.86% Si alloy becomes fully molten.

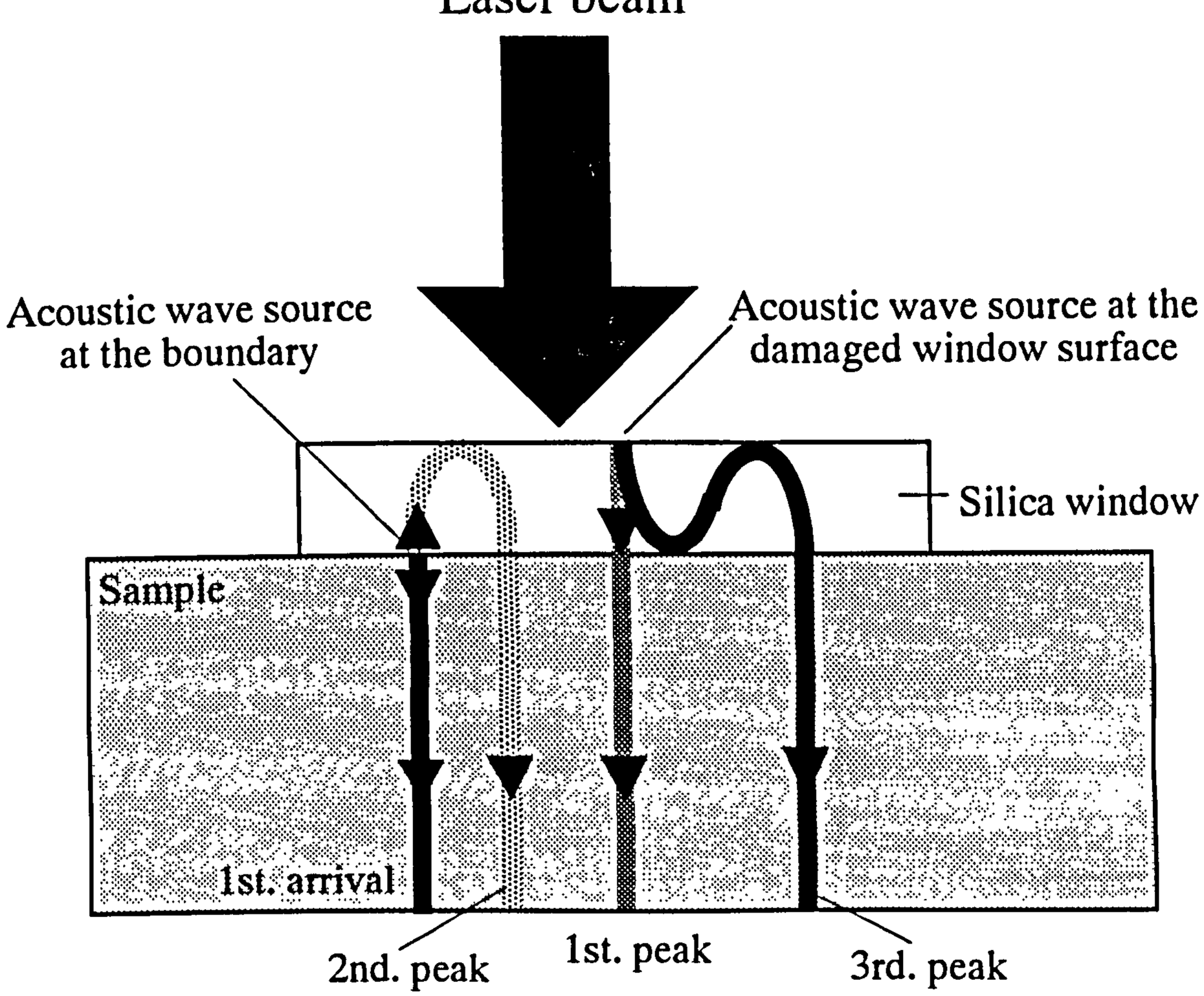

Fig. 4.17 Diagram showing the occurrence of acoustic wave propagation from the damaged surface of the silica window and internal reflections within the window.

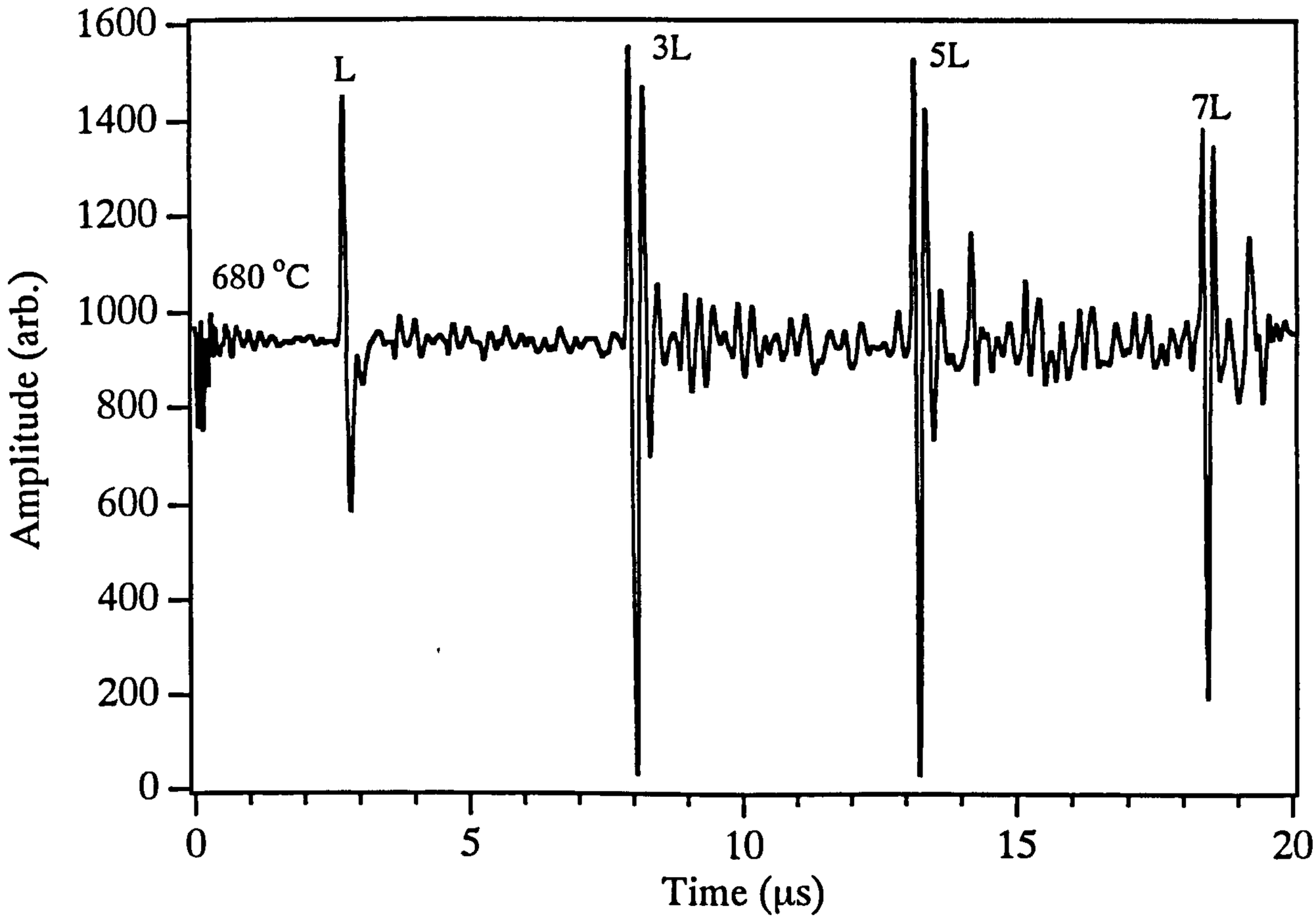

Fig. 4.18 Waveforms obtained in the fully molten state on Al 4.86 % Si alloy.

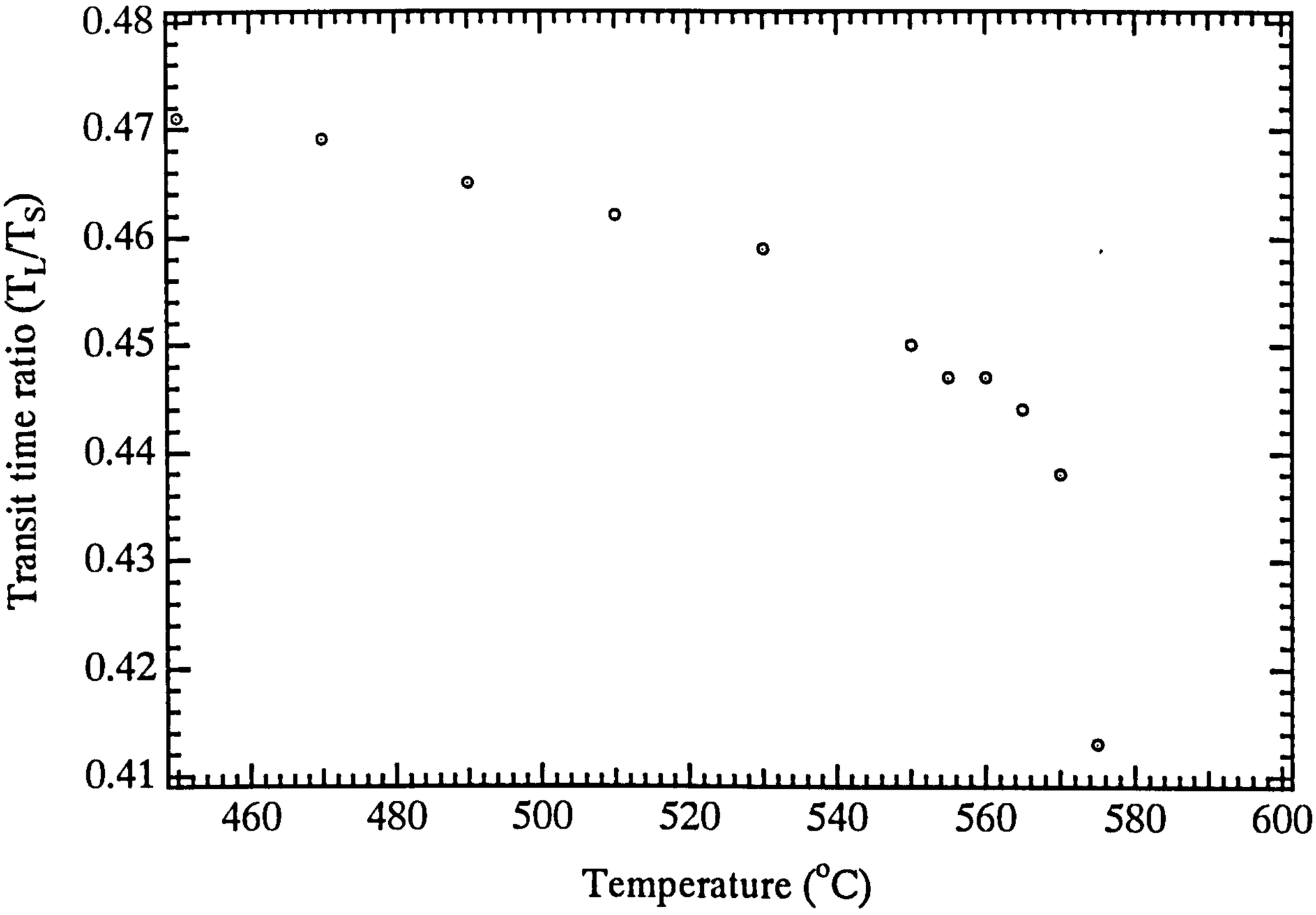

Fig. 4.19 Variation of the longitudinal to shear wave transit time ratio as a function of temperature when the Al 4.86 % Si alloy was heated to the partially molten state.

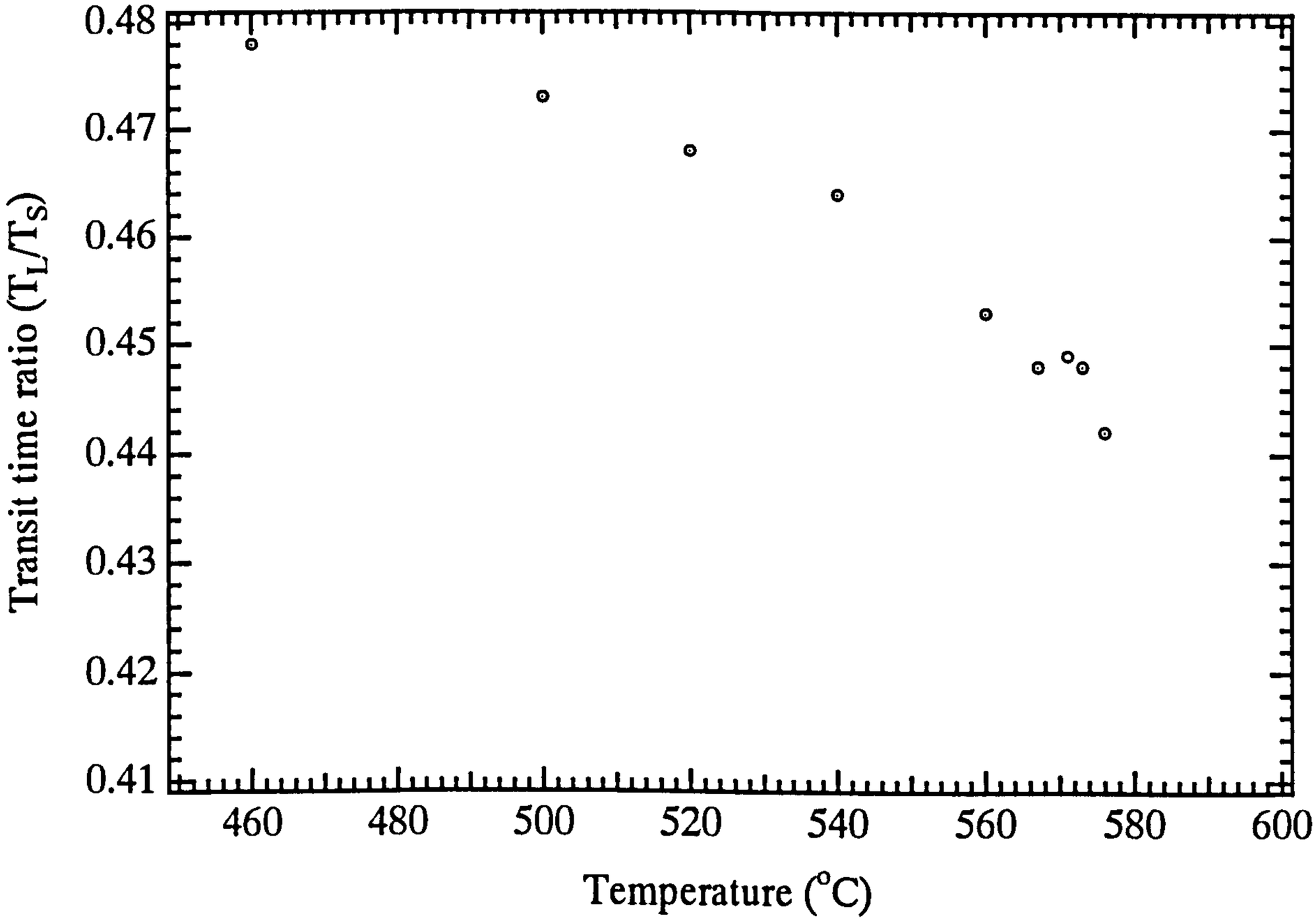

Fig. 4.20 Variation of the longitudinal to shear wave transit time ratio as a function of temperature when the Al 4.86 % Si alloy was heated up to the fully molten state.

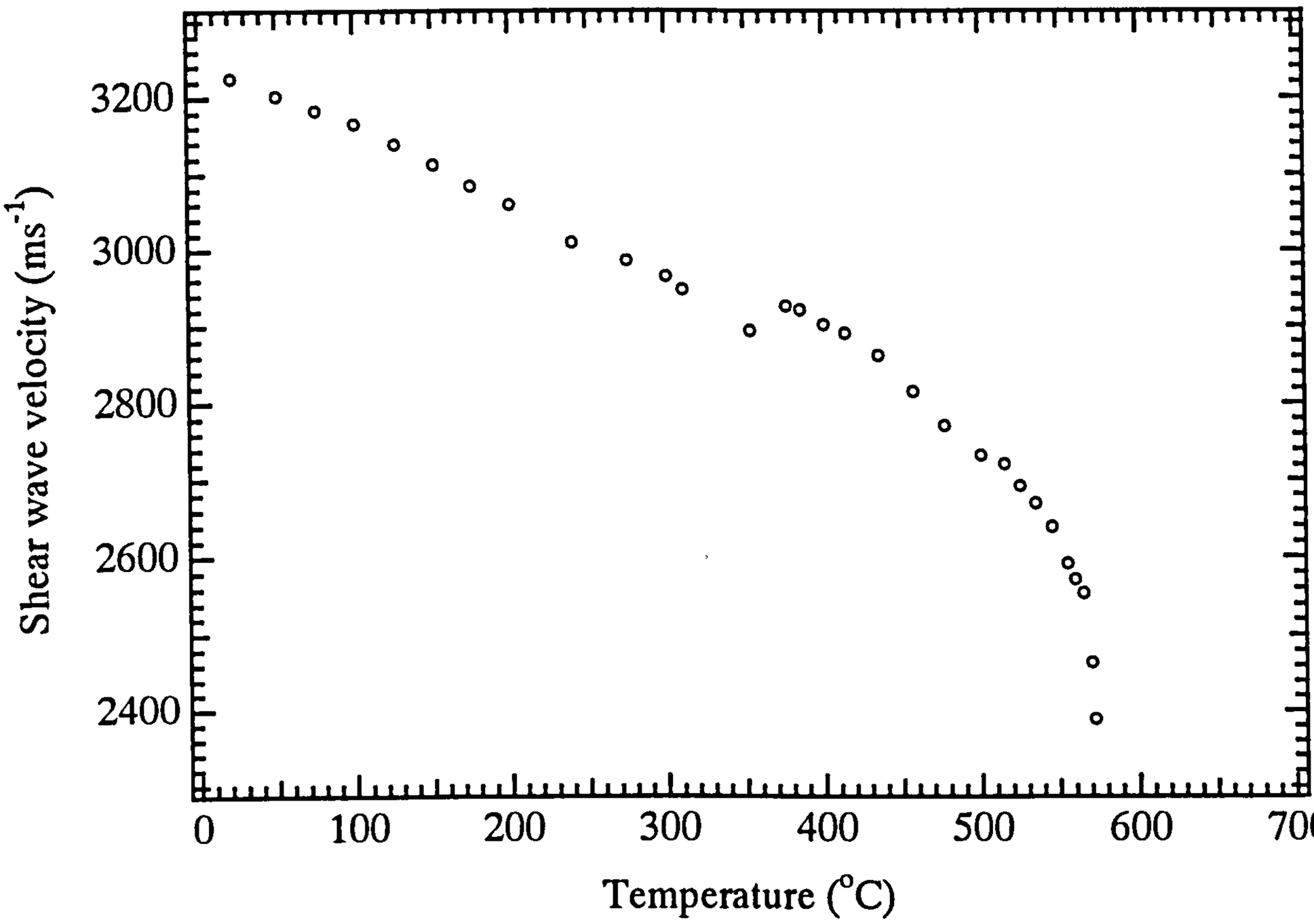

Fig. 4.21 Variation of shear wave velocity as a function of temperature in Al 4.86 % Si alloy when the sample surface on the generation side was supported by an alumina disc.

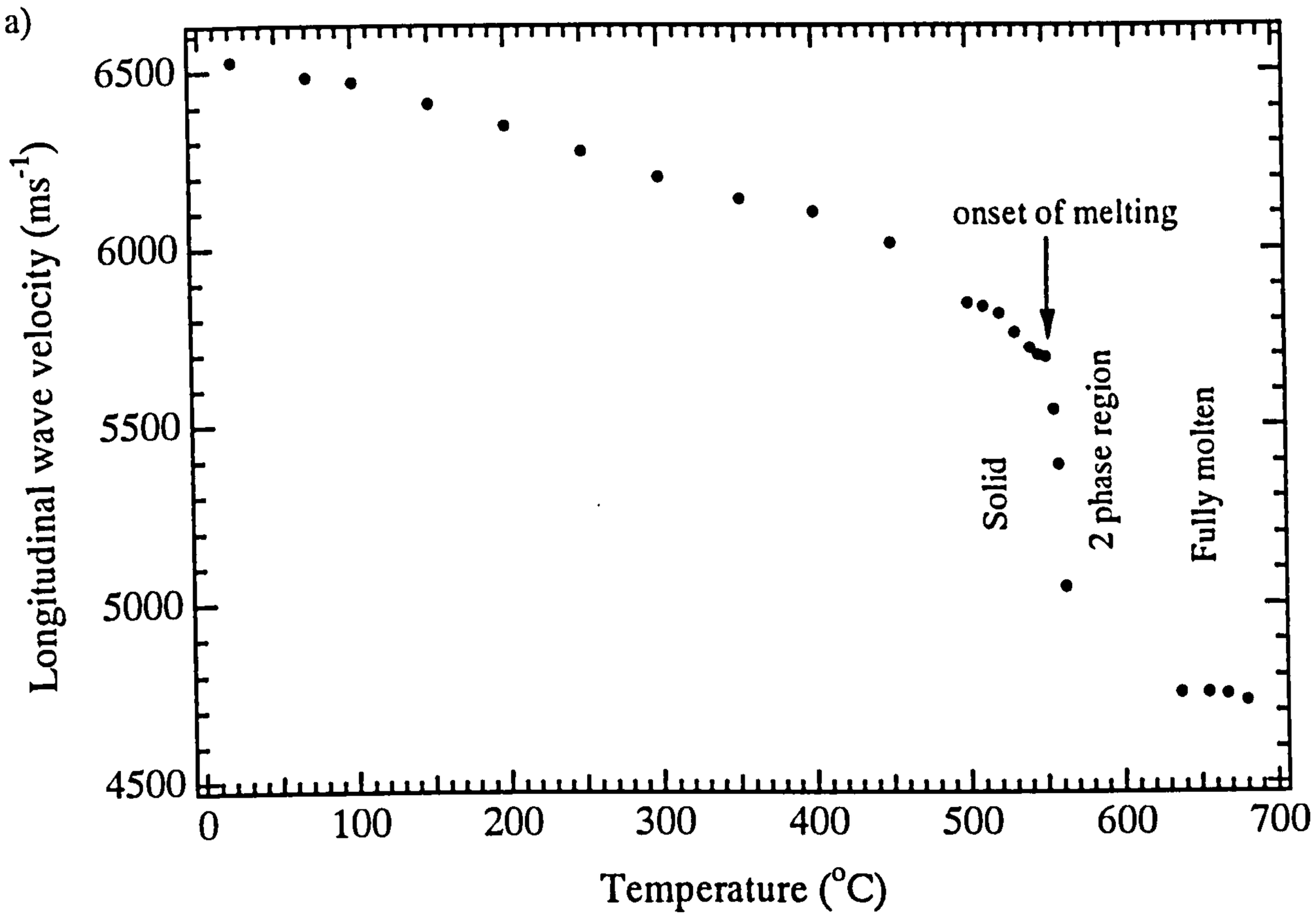

Fig. 4.22 Variation of a) longitudinal and b) shear wave velocity as a function of temperature in LM25 aluminium alloy when both ends of the sample surface were supported.

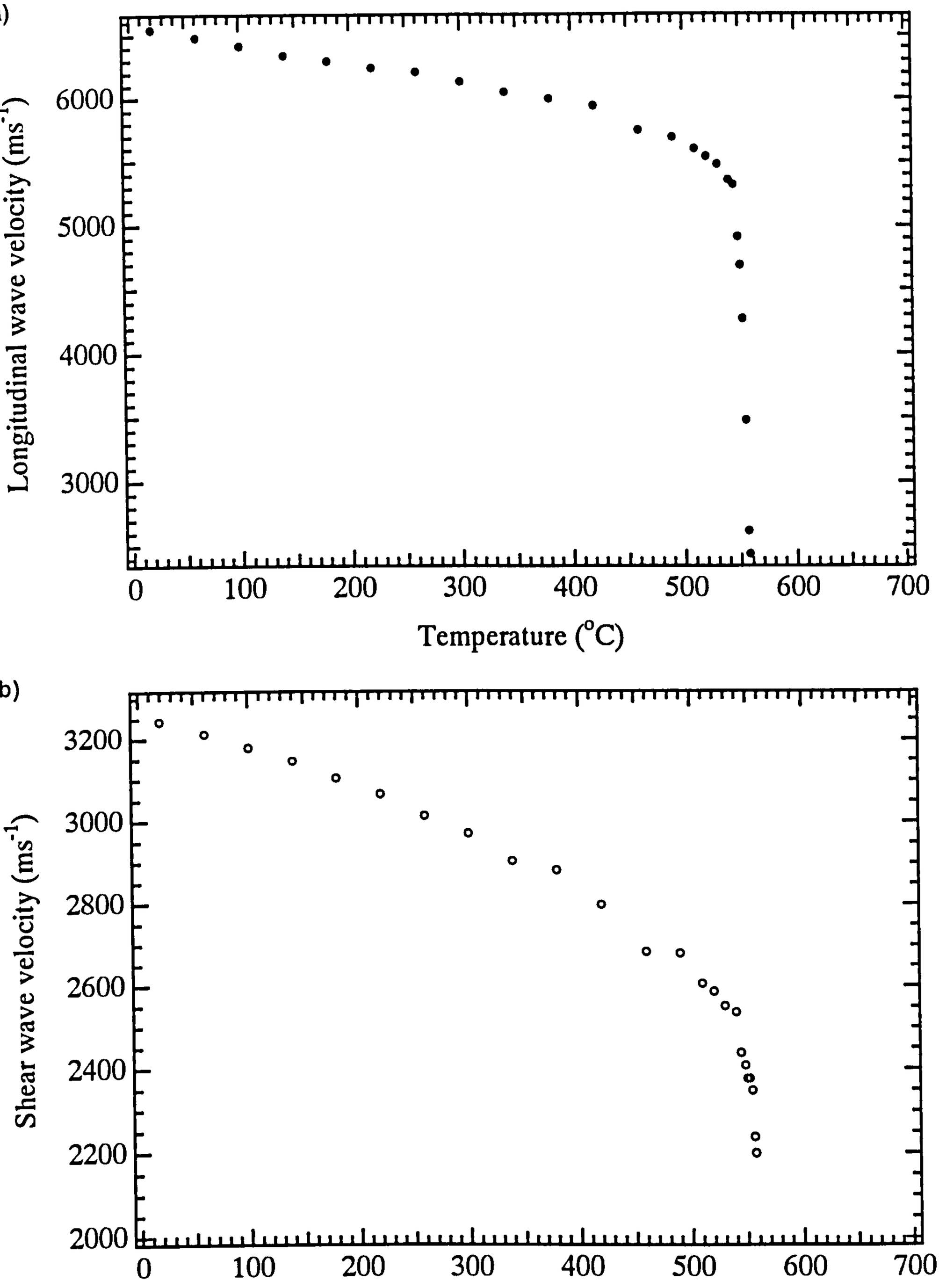

Fig. 4.23 Variation of a) longitudinal and b) shear wave velocity as a function of temperature in LM25 aluminium alloy when the sample surface on the generation side was unsupported.

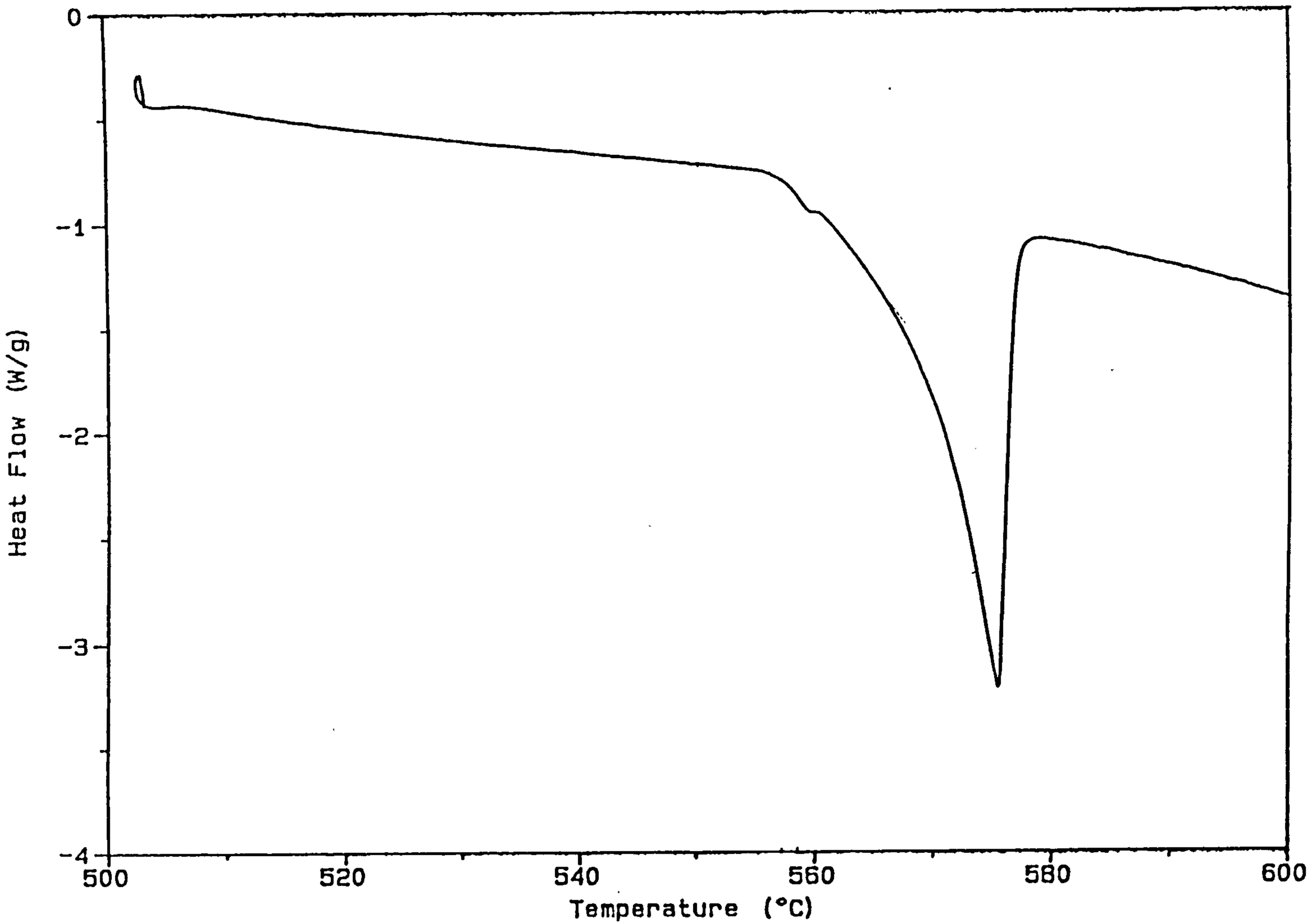

Fig. 4.24 DSC thermal analysis result on LM25 aluminium alloy.

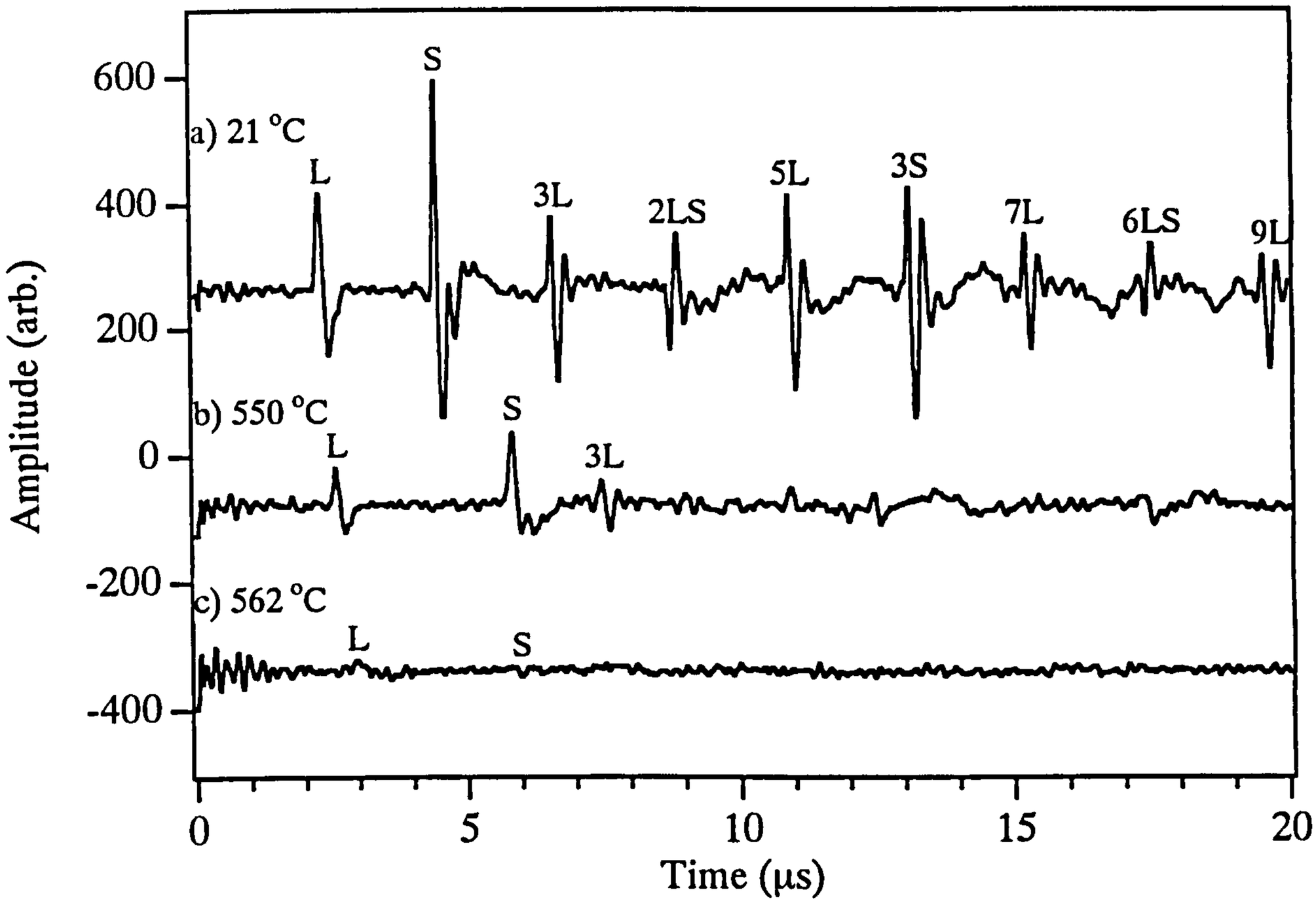

Fig. 4.25 Waveforms obtained a) at room temperature b) at the onset of melting and c) in the partially molten state on LM25 aluminium alloy.

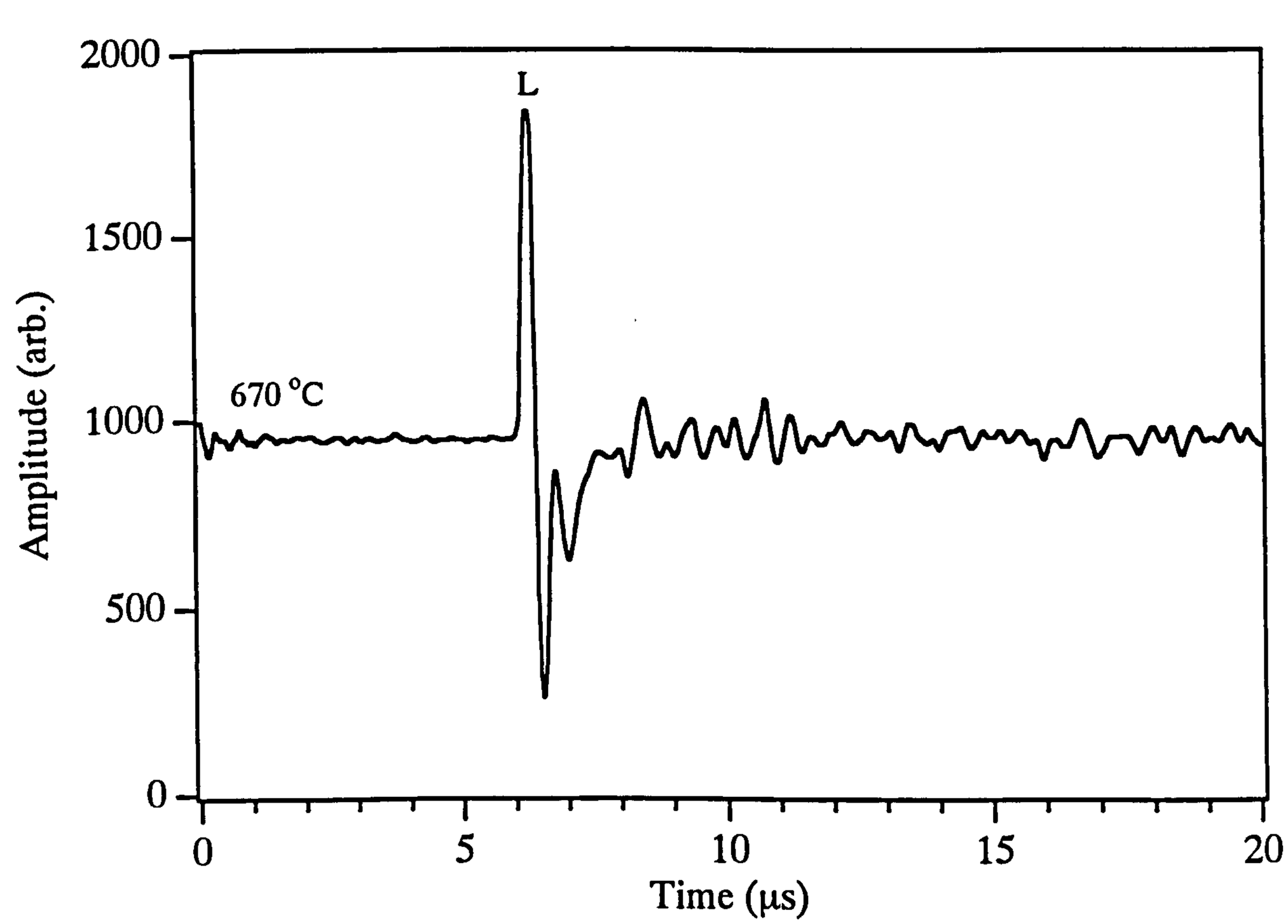

Fig. 4.26 Waveform obtained in the fully molten state on LM25 aluminium alloy.

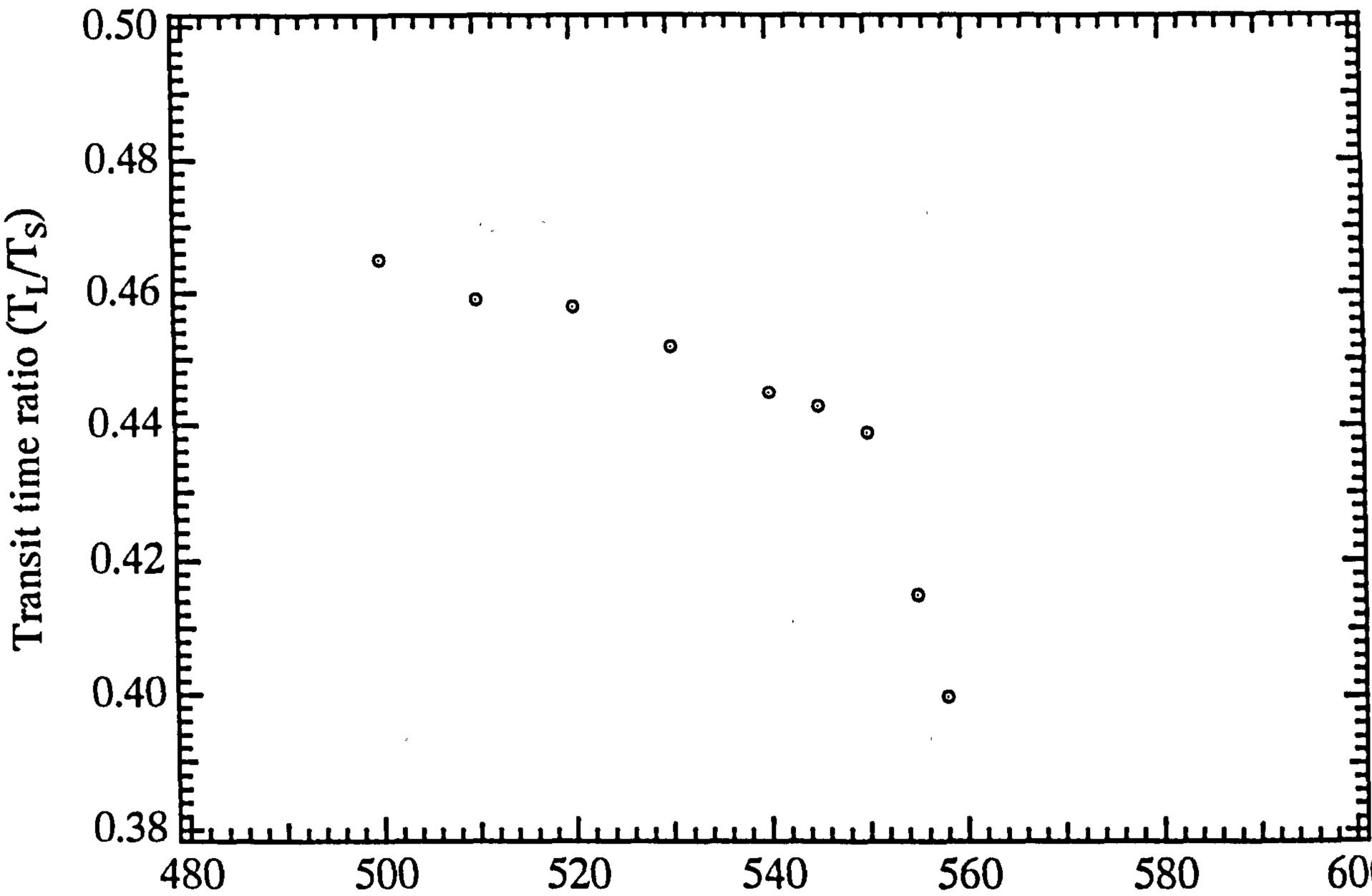

Fig. 4.27 Variation of the longitudinal to shear wave transit time ratio as a function of temperature in LM25 aluminium alloy when both ends of the sample surface were supported.

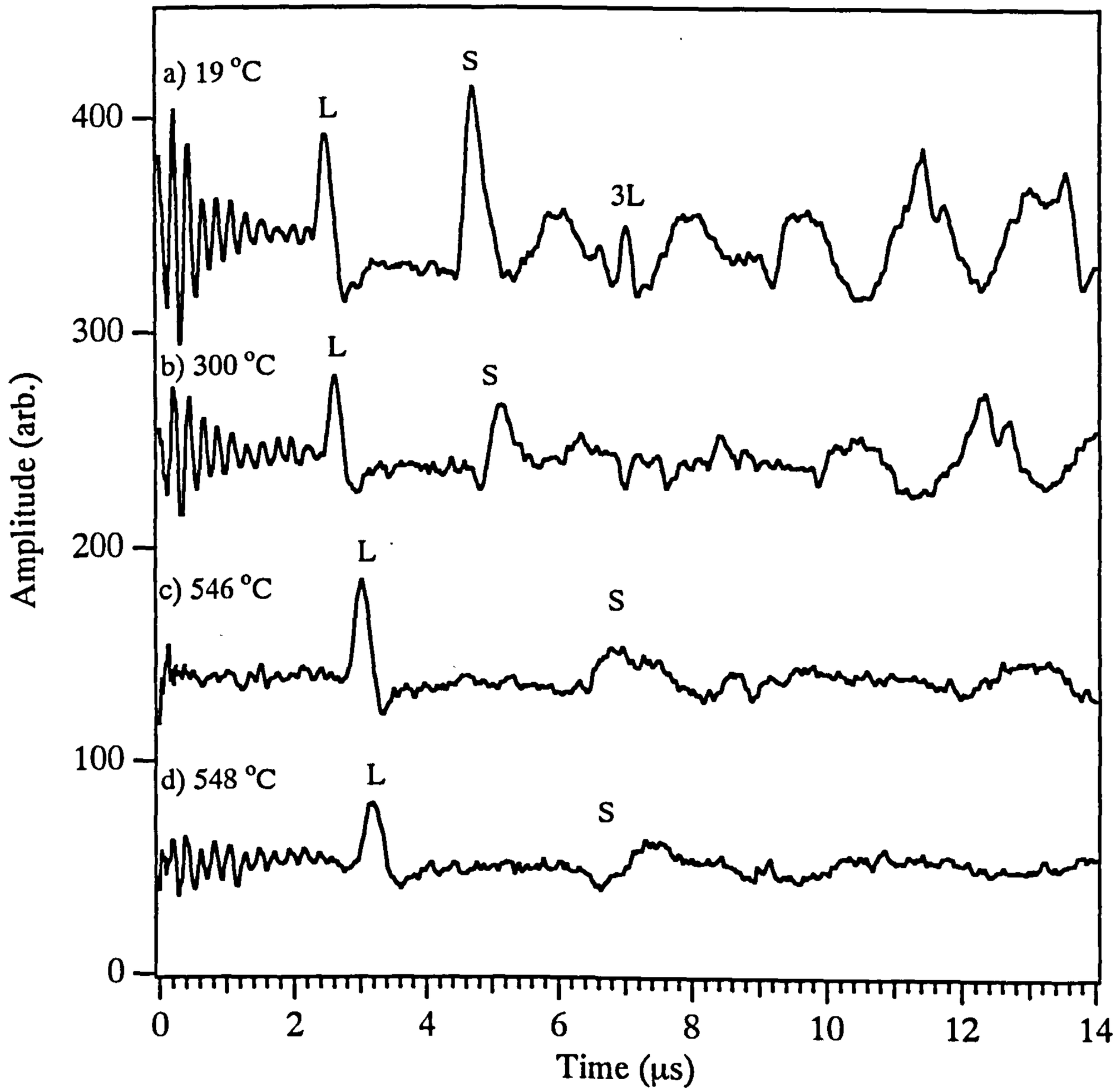

Fig. 4.28 Waveforms obtained at room and higher temperatures in LM25 aluminium alloy.

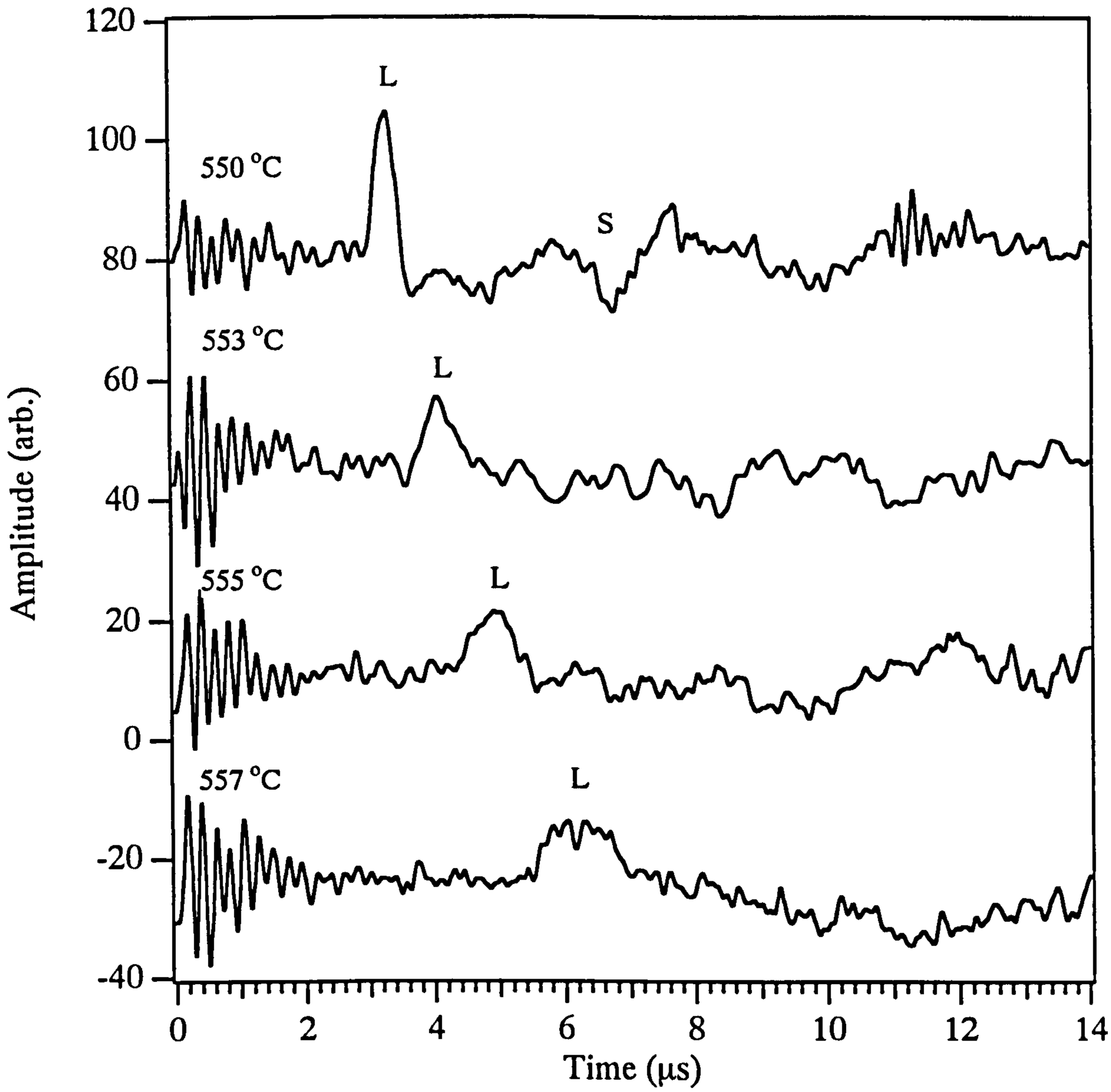

Fig. 4.29 Waveforms showing the substantial increase in the longitudinal wave first arrival transit time with increase in liquid fractions on the LM25 aluminium alloy. The sample surface on the generation side was unsupported.

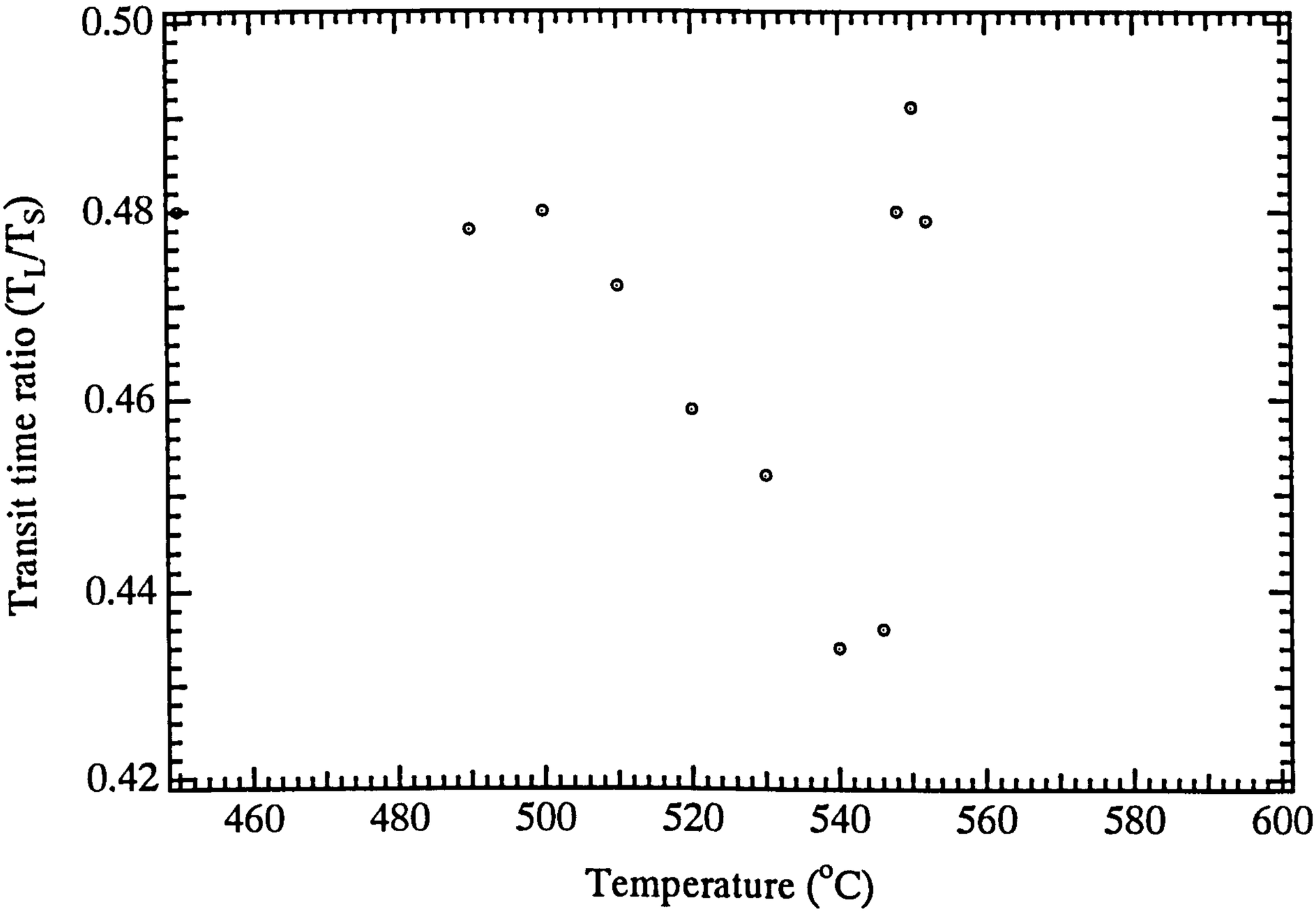

Fig. 4.30 Variation of the longitudinal to shear wave transit time ratio as a function of temperature in LM25 aluminium alloy when the sample surface on the generation side was unsupported.

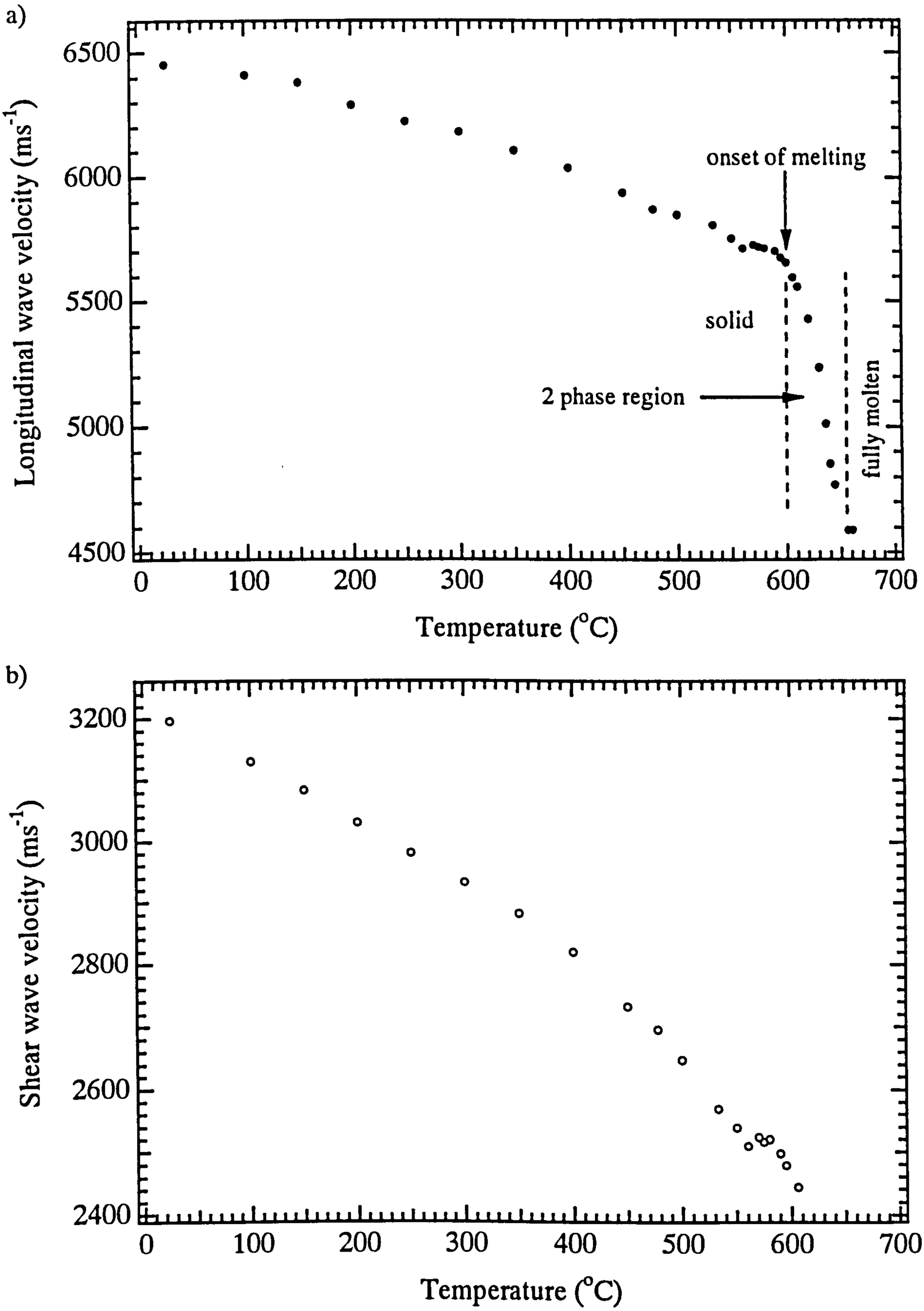

Fig. 4.31 Variation of a) longitudinal and b) shear wave velocity as a function of temperature in Al 1.2 % Si alloy.

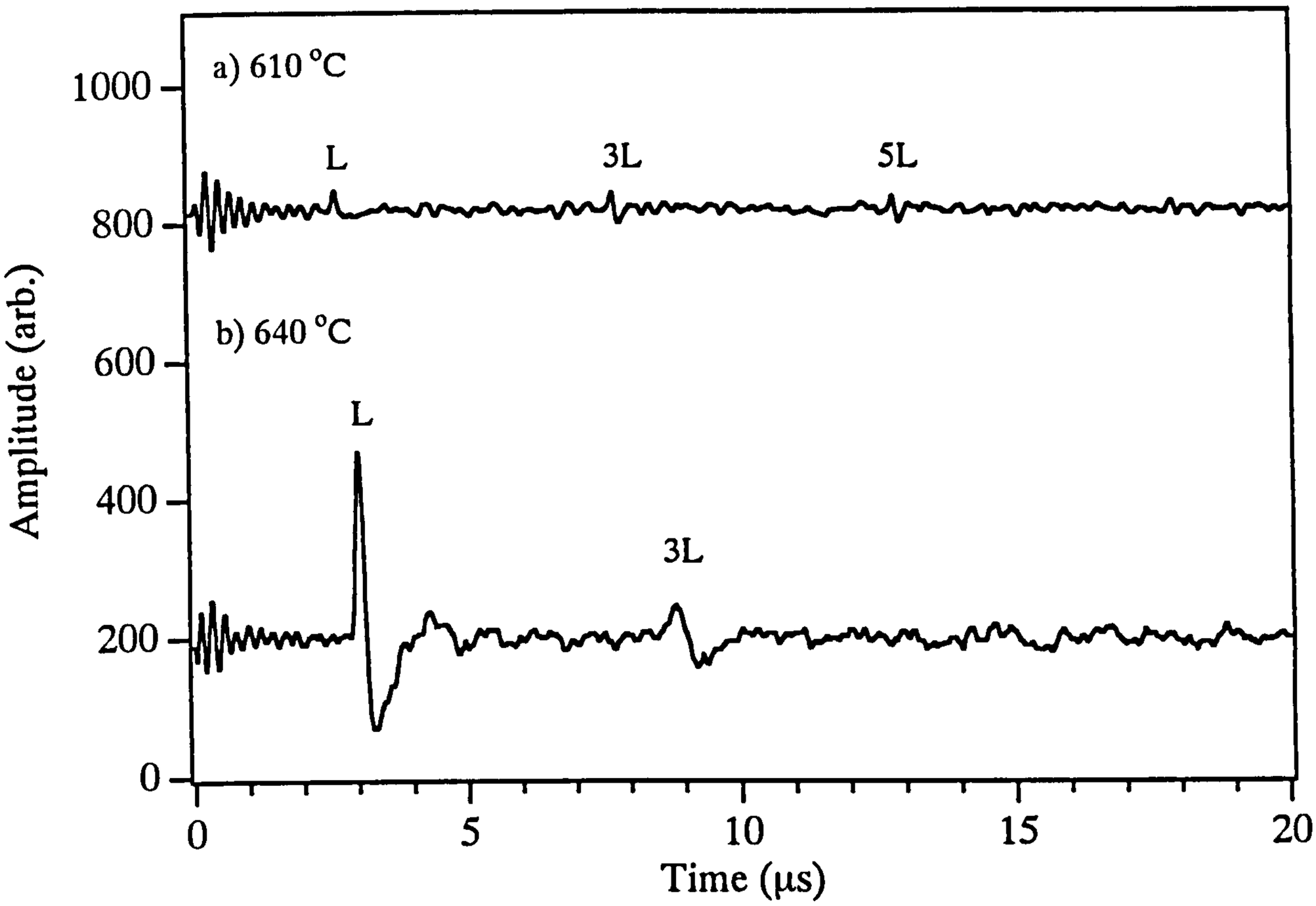

Fig. 4.32 Waveforms obtained in the partially molten state on Al 1.2 % Si alloy.

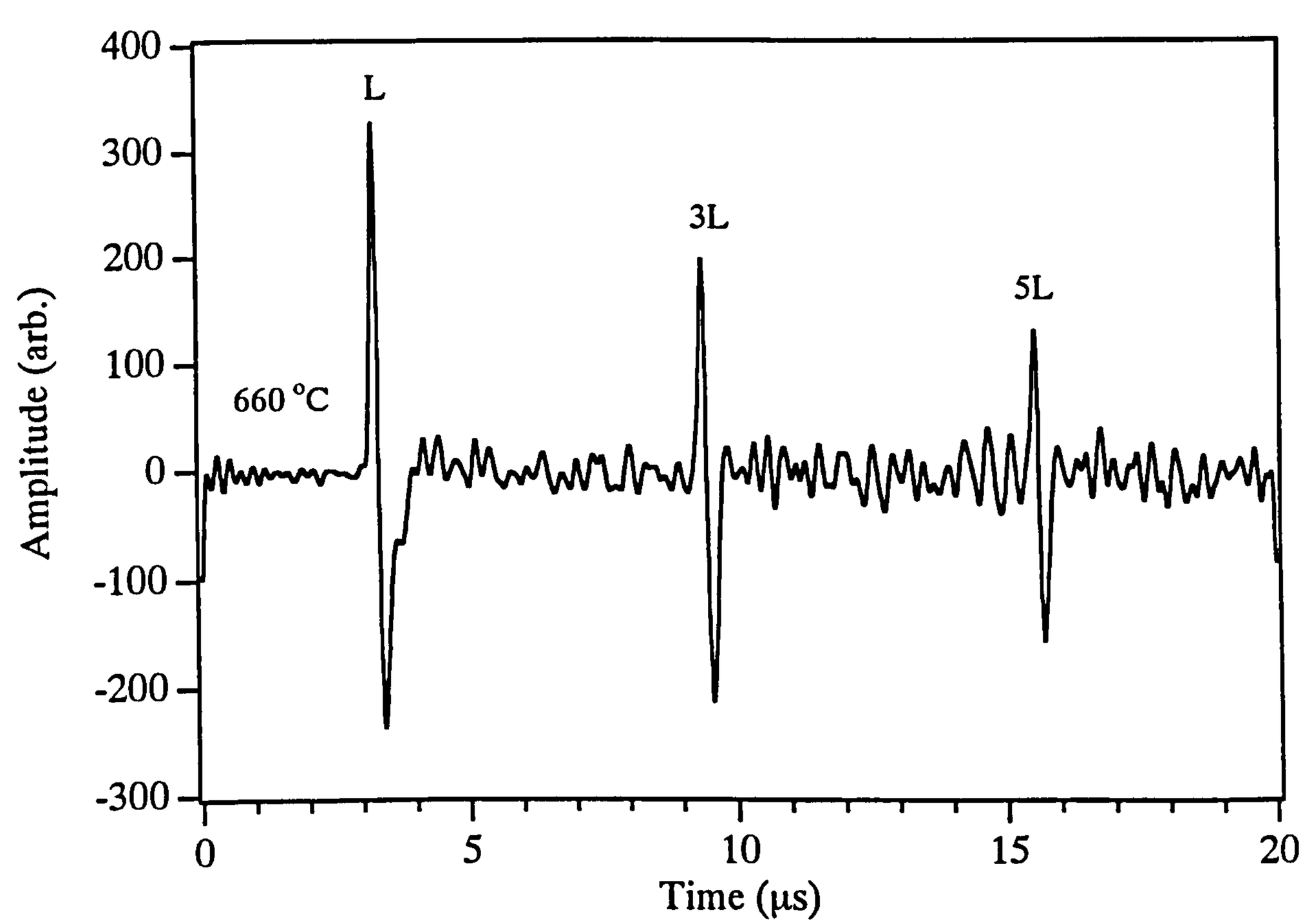

Fig. 4.33 Waveform obtained in the fully molten state on Al 1.2 % Si alloy.

CHAPTER 5

CHAPTER 5

MONITORING OF PARTIALLY MOLTEN HIGH TEMPERATURE MATERIALS

5.0 Introduction

High melting temperature materials with high strength such as copper alloys and tool steels are being widely used in the manufacturing of electrical connectors and cutting tools respectively. As reported by Edwards et. al., [1992], the thixoforgeable materials mentioned above have great potential applications, and Lucas is interested in the development of a control system capable of monitoring those thixoforgeable materials before forging.

This chapter presents the measurements made on a thixoforgeable copper-tin alloy and on M2 tool steel. However due to the difficulty in obtaining the M2 tool steel and due to its high price, a preliminary experiment was conducted on a commercial mild steel up to a sample temperature of 925 °C. The aim was to determine the capability of the laser-EMAT system in making acoustic wave measurements on ferromagnetic material at elevated temperature. According to the iron-carbon phase diagram (fig. 5.1) a steel with 0.865 % carbon should start to melt at approximately 1400 °C, but a much lower temperature was reported by Cau and Robert, [1992]. They reported that a thixoforgeable M2 tool steel with 0.92 % carbon should have liquid fractions of 0.6 and 0.3 at temperatures of 1325 °C and 1280 °C respectively. This is due to the presence of the other alloying elements.

In view of these temperatures the existing electric furnace system could not be used since the maximum temperature obtainable was 1100 °C. However to avoid wasting unnecessary time and cost in designing and constructing a new experimental set-up for measurements above 1300 °C, a trial experiment was conducted on the M2 tool steel using the set-up described in chapter 4. The purpose was to determine the extent to which the laser-EMAT system is capable of detecting the acoustic wave signals in high temperature steel. Once this had been demonstrated successfully, further experiments were then carried out in an induction (R.F) furnace where the M2 tool steel sample was heated into the partially molten state

5.1 Test Samples

Two types of thixotropic material were used for the study, a copper alloy with 10.2 per cent tin (Cu 10.2 % Sn alloy) and the M2 tool steel. The Cu-Sn alloy was produced at the School of Materials, University of Sheffield by the SIMA process described for Al 4.86 % Si alloy . However, the extrusion speed was much faster, at 85 mms^{-1}. The microstructure is therefore much finer. The chemical composition of the alloy was measured using X-ray fluorescence spectroscopy (XRF) with an accuracy of $\pm$ 0.1 atomic per cent. No detectable impurities were present. According to the binary copper-tin phase diagram the Cu 10.2 % Sn alloy should have a wide liquidus/solidus range of about 200 °C (see fig. 5.2). In the case of M2 tool steel, the material was also produced by the SIMA process, where the conventional cast billet was heavily deformed to produce the thixotropic properties in the semi-solid state but the method of inducing the strain was not revealed by its producer, Barworth Flockton Ltd at Sheffield. The composition of the M2 tool steel is:- carbon (0.856 %),

silicon (0.18 %), manganese (0.25 %), chromium (4.23 %), molybdenum (4.97 %), tungsten (6.45 %), vanadium (2.03 %), cobalt (0.20 %), sulphur (0.025 %), phosphorus (0.028 %), nickel (0.17 %), with iron making up the balance. In addition a commercial mild steel of unknown composition was taken from the Physics Department store.

The sample dimensions used in the study varied depending on the shape and size of the raw materials supplied. For Cu 10.2 % Sn alloy the sample was a disc shape with dimensions of approximately 30 mm in diameter and 12 mm in thickness. Two different sample shapes and sizes were prepared for the M2 tool steel, the dimensions of the sample heated in the standard split electric furnace were approximately 60 mm diameter and 13.4 mm thick, and the one heated in the induction furnace was a cylindrical shape with dimensions approximately 60 x 60 mm. The mild steel sample was rectangular in shape with dimensions approximately 60 mm in length, 40 mm wide and 12.6 mm thick.

5.2 Experimental Set-up

5.2.1 Standard Split Furnace

The experimental set-up for measurements on a Cu 10.2 % Sn alloy, M2 tool steel (when heated up to 1100 °C) and mild steel was similar to that arranged for the aluminium alloys described in chapter 4. In the case of the mild steel and tool steel the only difference was the method of holding the sample inside the furnace. The mild steel was clamped to the sample holder whereas the tool steel sample was held directly by two parallel stainless steel tubes. The type-K thermocouple was inserted into an approximately 2 mm deep drilled hole in the generation side. Since in the study

the samples were heated to much higher temperatures than necessary for the aluminium alloys a fire-brick, approximately 12 mm thick, was placed between the furnace and the detector, when measurements were not made. This was to protect the EMAT from radiant heat and also to reduce heat loses from the furnace.

5.2.2 R.F Induction Furnace

A schematic diagram of the experimental set-up for the M2 tool steel when heated to the partially molten state is shown in figure 5.3. A through transmission arrangement was used with the EMAT detector vertically aligned with the laser beam. The sample was enclosed in a 100 mm internal diameter and 500 mm length transparent silica tube. One end of the sample was turned by lathe to approximately 48.5 mm diameter so that it would recess into a vertical position on a 49 mm internal diameter alumina tube that sits on the brass end base. Both ends of the silica tube were fitted with an aluminium ring and vertically supported by brass end plates with a water-cooled copper coil brazed to each of them. Two holes were drilled through the brass base and the aluminium end plate at the generation side, one hole at the centre for laser access and the other hole about 40 mm from the centre, for the type K thermocouple. The brass end base at the detection side was fixed to an aluminium end plate fitted with a stainless steel bush bearing for guiding and to enable smooth sliding of the EMAT when taking the measurement. A trigger button was used to automatically fire the laser the instant the EMAT was in the measuring position. A water cooled R.F heating coil fitted over the silica tube at the position where the sample was placed. Basically, the coil and the sample act respectively as the primary and secondary of a transformer. The number of coil turns was pre-determined so that

the impedance of the coil would match that of the sample enabling the current to couple to the sample and heat it. Nitrogen gas was introduced into the silica tube to reduce the rate of sample surface oxidation. An alternating current with frequency of around 300 KHz was applied to the copper coil which encircled the sample, producing a magnetic field which in turn induced a current flow in the sample, heating and melting it.

A 45 degree prism was placed below the silica tube to reflect the laser beam vertically upwards onto the sample base. A 500 mm focal length biconvex lens was used to focus the laser beam onto the sample surface so that a strong longitudinal wave would be generated which in turn could be detected by the EMAT.

5.3 Experimental Procedure

The experimental procedure adopted for measurements on the Cu 10.2 % Sn alloy and mild steel was basically similar to that described in chapter 4. In the case of the Cu-Sn alloy two experimental procedures were applied. In both cases a Lumonics HY 400 Nd:YAG laser capable of producing 200 mJ, 10 ns pulse acted as the ultrasound generator and a water-cooled spiral coil EMAT as the detector. In the first procedure, the sample surface on the generation side was unsupported and the ultrasound was generated in the weak ablation regime in order to obtain both the longitudinal and shear wave signals simultaneously. The degree of ablation was adjusted using a 320 mm biconvex lens so that bulk waves could be detected with reasonable amplitude allowing accurate transit time measurements. In the second procedure, the experiment was conducted in the thermoelastic regime. A silica window was used to prevent the molten metal from flowing out of the sample holder

and to constrain the sample surface at higher temperatures. A 0.5 mm thick alumina disc was used to support the sample surface on the detection side in both the above procedures. As explained in chapter 4 the purpose was to reduce the effect of sample cooling by the water-cooled EMAT, and to prevent the molten metal from flowing out of the sample holder, hence preventing the molten metal from sticking to the EMAT surface. For the mild steel, the sample was clamped to the sample holder and the ultrasound generated in the plasma regime. The sample was heated up to 925 °C, a few degrees above the ferritic to austenitic phase transition temperature.

The measurement on the M2 tool steel were carried out using two different experimental arrangements. In the trial experiment the tool steel was heated in an electric furnace where measurements could only be made up to 1100 °C. These were complemented by measurements in the R.F furnace, which were only taken above the Curie temperature. There are basically two reasons why we limited the R.F furnace work in this way. Firstly, we already had acoustic wave results on the M2 tool steel up to 1100 °C from the trial experiment mentioned above, and secondly, we wished to avoid the need to hold the sample rigidly in position in the R.F furnace when the EMAT is brought close to the sample. Below the Curie temperature the sample is ferromagnetic and therefore tends to be attracted to the EMAT when taking measurements. Above the Curie temperature the tool steel becomes paramagnetic, and hence is not attracted to the EMAT. The sample was heated up to a maximum temperature of around 1300 °C in the R.F furnace where it should be in the semi-solid state. In both cases acoustic wave generation was achieved by the ablation mechanism.

5.4 Results and Discussion

5.4.1 Cu 10.2 % Sn alloy

The calibrated longitudinal and shear wave velocities at room temperature were measured to be 4615 $\pm$ 5 ms^{-1} and 2130 $\pm$ 26 ms^{-1} respectively. Figure 5.4 shows the measured variation of both bulk wave velocities as a function of temperature when the sample surface on the generation side was unsupported. In this case acoustic wave measurements could only be made a few degrees into the partially molten state. As expected the figure shows a decrease in both the longitudinal and shear wave velocities with increasing temperature. The longitudinal wave velocity could be determined up to 832 °C immediately after the onset of melting at around 830 °C according to the Cu-Sn phase diagram. The signal disappeared when the fraction of liquid starts to increase. The situation is worse in the case of the shear wave where the signal could only be identified up to 706 °C, even though the laser power density was reduced to decrease the degree of ablation. Figure 5.5 shows the typical waveform obtained on the Cu 10.2 % Sn alloy at room temperature. The amplitude of the longitudinal and shear wave signals is very low (< 20 mV). This may be caused by both the higher density and the coarse grain structure of the alloy (refer fig. 3 in appendix), which result respectively in reduced EMAT sensitivity [Dobbs, 1973], and loss in the acoustic wave energy due to attenuation by scattering.

Similar to the Al-Si alloys, better results were obtained when both ends of the sample surfaces were supported. The longitudinal and shear wave velocities could be determined at a much higher temperatures as shown in figure 5.6. The longitudinal wave velocity could be determined after the onset of melting and continues to

decrease rapidly until it reaches 862 °C, above which no signal could be detected. However at 1027 °C, where the alloy should be fully molten according to the phase diagram (fig. 5.2), the longitudinal wave signal reappears but the longitudinal wave velocity appears to increase at the higher temperatures in the molten state instead of decreasing as expected for pure metals [Parker et. al., 1985]. In the velocity calculations it is assumed that the shape and thickness of the sample is maintained, hence the beam path length is constant. However when the metal becomes fully molten there may be some loss of material flowing out of the sample holder which causes the effective path length to be reduced hence decreasing the travel time to reach the detector. The shear wave velocity could be determined up to 820 °C but the shear wave feature disappeared at the onset of melting.

Since the experiment was conducted in the thermoelastic regime, only a shear wave signal was detected at room temperature as shown in figure 5.7. As the temperature increases, the longitudinal wave pulse starts to appear (at 200 °C) but the feature is very weak. At 326 °C the longitudinal wave signal becomes stronger and its subsequent echoes could be detected indicating that the silica window has begun to be strongly bonded to, and constrain the sample surface, resulting in a strong normal force in addition to the stresses parallel to the sample surface due to thermal expansion. The mode converted signals were also detected. Figure 5.8 shows the waveforms at 830 °C and 862 °C. At 830 °C the alloy has just started melting, and at 862 °C it is in the two phase state with about 20 % liquid according to the phase diagram. In the two phase state the high ultrasonic attenuation caused by scattering, results in weak signals. Figure 5.9 shows the waveforms obtained at 1027 °C and 1085 °C in the fully molten state. At 1027 °C the alloy just started melting and at 1085

°C the alloy had been in the molten state for quite sometime, only the longitudinal wave pulse could be detected. At 1085 °C even though the direct longitudinal wave pulse signal is reasonably strong (approximately 34 mV) no echo is detected providing evidence of the very high ultrasonic attenuation possibly due to exsolved gases.

5.4.2 Mild Steel

The calibrated longitudinal and shear wave velocities of mild steel measured at room temperature are 5922 $\pm$ 7 ms^{-1} and 3211 $\pm$ 10 ms^{-1} respectively. Figure 5.10 shows the temperature dependence of the longitudinal and shear wave velocities in mild steel. Similar results were obtained by Papadakis et. al., [1972], Wadley et. al., [1986], and McKie, [1987] using different ultrasonic measuring systems. It is observed that up to 600 °C both graphs show a gradual decrease in the velocities with increasing temperature. Between 600 °C and approximately 723 °C the eutectoid temperature, there is a slight increase in the gradient indicating a slightly greater rate of fall in the velocities. After this stage the longitudinal wave velocity decreases more gradually again while the shear wave velocity apparently increases non-uniformly. The latter is probably due to the reduced accuracy of the transit time measurements because of the weak and broad features detected (see fig. 5.13).

Figures 5.11 shows the waveform obtained at room temperature. Both the longitudinal and shear waves signals and their subsequent echoes could be detected. Figure 5.12 shows the waveforms obtained immediately below (750 °C), around (760 °C) and immediately above (775 °C) the Curie temperature. At 750 °C both the longitudinal and shear waves signal could still be clearly detected. At 760 °C close to the Curie temperature, the acoustic wave signals reduce in amplitude and there is a

change in the longitudinal wave signal polarity from a negative to a positive initial peak. At 775 °C an enhancement of the longitudinal wave signal is observed but the shear wave signal is greatly reduced. Similar phenomena had been observed by Whittington, [1978], and Lee and Ahn, [1992] using the EMAT-EMAT system. Figure 5.13 shows the waveforms at a much higher temperatures up into the γ-austenitic phase region (see fig. 5.1). Clear longitudinal wave signals could still be observed but their amplitudes had reduced greatly compared to that obtained at 775 °C. The shear wave signal features are weak and broad making accurate transit time measurements difficult.

5.4.3 M2 Tool Steel

Figure 5.14 shows the variation of the longitudinal and shear wave velocities with increasing temperature on the M2 tool steel. The longitudinal velocity in the approximately 61.5 mm thick sample appears to be slightly higher than that obtained from the approximately 14 mm thick sample. This might be caused by the misalignment of the laser beam and the EMAT due to thermal expansion which affected the effective path length travelled by the acoustic wave. The behaviour for the M2 tool steel is similar to that of the mild steel where there is a gradual decrease in the velocities up to 600 ° C, and followed by an increase in the rate of fall up to the Curie temperature. Above the Curie temperature the longitudinal wave velocity decreases gradually again up to 1100 °C. However, there is a discontinuity observed at around 900 °C on the 14 mm sample but not on the thicker sample. This is possibly because only few measurements were taken on the thicker sample. The calibrated

longitudinal and shear wave velocity were measured to be 6065 ± 8 ms^{-1} and 3359 ± 10 ms^{-1} respectively at room temperature.

Figure 5.15 shows typical waveforms obtained on the approximately 14 mm thick M2 tool steel at room temperature. The longitudinal and shear wave pulse and their subsequent echoes could be readily detected. Figure 5.16 shows the expanded waveforms obtained at 752 °C, 762 °C (close to the Curie temperature) and at 772 °C. In a similar manner to the mild steel there is a change in the polarity of the longitudinal wave signal, but in this case from a positive to a negative initial peak on passing through the Curie temperature (752 °C). The broadening observed in the peaks of the longitudinal wave pulse at 772 °C could be due to saturating the pre-amplifier. At 1100 °C, both the longitudinal and shear wave pulse and their subsequent echoes could still be clearly detected (fig. 5.17).

Figure 5.18 shows the waveform obtained on the 61.5 mm thick M2 tool steel at room temperature. Sharp longitudinal and shear wave signals could be clearly detected. Other features were also detected between the shear wave first arrival and the longitudinal wave echo which might comes from the side wall reflection. Figure 5.19 shows the waveforms obtained at 980 °C and 1140 °C in the austenitic phase region when the sample was heated in an induction furnace in a nitrogen controlled atmosphere. At 980 °C the longitudinal wave pulse and its subsequent echo could still be detected, however at 1140 °C only the longitudinal wave pulse was detected and no measurement could be made after this temperature.

Figure 5.20 shows the temperature dependence of the measured longitudinal and shear waves amplitude. The laser power density was kept constant throughout the experiment, and the signal amplitude was measured from the extreme positive and

negative polarity of the pulse. The longitudinal wave signal increases gradually up to 500 °C. Between 500 °C and 750 °C it maintains a steady value, and at 752 °C the amplitude suddenly drops rapidly before a brief recovery to its earlier value followed by a rapid drop until at 860 °C it remains almost constant again. The shear wave signal amplitude follows a totally different trend, at room temperature the amplitude is slightly higher than the longitudinal wave because the laser power density was initially adjusted to be in a very weak ablation regime. The amplitude remains almost constant up to 250 °C. A broad peak is observed at 300 °C and above 500 °C the shear wave signal amplitude increases gradually up to a maximum value at 752 °C. The amplitude suddenly reduces rapidly until it reaches 780 °C after which it remains almost constant up to 1100 °C.

5.4.4 Discussion on Mild Steel and M2 Tool Steel

5.4.4.1 Factors Affecting the Velocity-Temperature Profile

The longitudinal and shear wave velocities for both the mild and tool steel show similar profiles as a function of temperature (fig. 5.10 and fig. 5.14) . Below the Curie temperature the curve could be separated into three regions, between the room temperature and 600 °C, between 600 °C and the eutectoid temperature, and between the eutectoid temperature and the Curie temperature. In the case of ferromagnetic material, at room temperature additional forces due to the magnetic order contribute to its rigidity. As the temperature of the material increases the magnetic order is disturbed and is destroyed at the Curie temperature by thermal agitation [McKie, 1987]. Therefore in the first region the gradual drop in the velocities could be due to

the increase in normal elastic strain and the additional strain associated with a stress-induced magnetic domain reorientation. In the second region the slightly faster rate of fall in the velocities may be due to the approaching Curie temperature. In the third region, in addition to the loss in ferromagnetism, the rapid drop in the velocities could also be caused by the dissolution of the carbide phase [Papadakis, et. al., 1972, and Wadley et. al., 1986] and loss of the magnetostriction effect. In order to explain the first phenomenon, it would be better first to refer to the iron-carbon phase diagram (figure 5.1) where it is clearly shown that at ambient temperature both the hypoeutectoid mild steel and the hypereutectoid tool steel consist of a mixed microstructure of an α-ferrite phase and a carbide known as cementite (Fe_3C) (refer fig. 4 in appendix). Therefore the measured velocity in the two ferromagnetic steels could be regarded as the average of the velocities of its constituents. Above the eutectoid temperature the carbide phase is unstable and rapidly dissolves. Since in this case the acoustic wave velocity in the carbide is greater than that of the α-ferrite the average velocity of the mild steel is considerably reduced. The second phenomenon is related to a change in Young's modulus caused by magnetostriction and is known as the ΔE effect. Referring to figure 5.21 taken from Bozorth, [1951] , at I/I_s (the ratio of magnetism to saturation magnetism) of 0.14, for I and I_s equal to 0.3 (for the Nd-Fe-B magnet) and 2.12 Tesla (in mild steel) respectively, the change in elasticity ($\Delta E/E$) caused by the EMATs magnetisation at room temperature on annealed iron (since there is no curve for mild steel) is estimated to be less than 0.01 per cent. Therefore the magnetostriction effect would not expected to significantly affect the results.

At elevated temperature as the sample approaches the Curie temperature (768 °C for pure iron) a transition from a ferromagnetic to a paramagnetic mild steel begins,

and the transition is completed once the Curie temperature is reached. The transformation of the body-centered cubic (BCC) lattice α-ferrite to the face-centered cubic (FCC) lattice γ-austenite phase that occurs in this region could also affect the velocity but since the velocity in the γ-austenite is faster than the α-ferrite transformation then the α to γ phase transformation would tend to increase the velocity [Hub, 1962]. After this stage, the sample becomes wholly paramagnetic and the effect of magnetostriction disappears. In the case of the tool steel the discontinuities observed around 900 °C could be as a result of the complete ferritic to austenitic phase transformation where there is a volume increase associated with this transformation.

5.4.4.2 Factors Affecting the Acoustic Wave Signals Amplitude

The variations in the longitudinal and shear wave signal amplitude with increasing temperature in the mild and tool steel may possibly be as a result of the combined effects from the inherent attenuation of acoustic waves in the material, and the efficiency of generation and detection. The first effect is related to the characteristic of the material [Tripathi and Verma, 1973], and the decrease in the longitudinal and shear wave velocities [Bhatia, 1967, and Darbari et. al., 1968]. The characteristic of the material is shown by Tripathi and Verma, [1973] in their study of ultrasonic attenuation as a function of temperature in a 1 % carbon steel at 5 MHz. They found that there is a broad peak at around 215 °C indicating a slight increase in attenuation which then remains almost constant up to the eutectoid temperature (723 °C), however, the slope changes abruptly twice, between 750 °C and 900 °C, and from

900 °C to 985 °C. It was thought that the broad peak at 215 °C may be related to the Curie temperature of the ferromagnetic cementite phase. Martius and Bratina, [1961] suggested that the oscillations of the magnetic moments in the domain walls may give rise to the magnetic attenuation in the carbon steels. Between 750 °C to 900 °C the abrupt rise in attenuation is thought to be due to the gradual transformation of the unstable ferrite into the austenite phase with the dissolution of the cementite phase in it. The other possibility that was not mentioned by Tripathi and Verma is the transition from a ferromagnetic to a paramagnetic mild steel that should occurs at the Curie temperature of around 760 °C. Above 900 °C the rapid increase in attenuation is thought to be caused by the complete transformation of the austenitic phase and the increase in the grain size as the temperature is further increased. The reduction in the longitudinal and shear wave velocities is related to the weakening of the interatomic forces due to thermal expansion as the temperature rises causing a decrease in the elastic constants. Thermal expansion also causes an increase in the sample volume and hence a decrease in the density of the material. Since the acoustic wave velocity is dependent on both the elastic constants and density of the material, and most materials exhibit a decrease in velocity with increasing temperature, the reduction in interatomic forces is the dominant effect. It has been demonstrated by many authors [Papadakis et. al., 1972, Dewhurst et. al., 1988, and Mak and Gauthier, 1993] and the results obtained in this thesis confirm that in general, the longitudinal and shear wave velocities decrease with increasing sample temperature. The relationship between attenuation and velocity is given by Bhatia, [1967] by equations (2.18) and (2.19) of chapter two in this thesis. The expression shows that the longitudinal (α_l) and shear (α_s) attenuation coefficients are greatly dependent on and are inversely proportional to

the acoustic wave velocities. Therefore with the decrease in both of the bulk wave velocities at elevated temperature, the attenuation coefficients are expected to increase and hence increase the signal amplitude decay rate.

The generation efficiency is related to the strength of the laser source [McKie, 1987], and the sample surface condition [Davies, et. al., 1992]. The former depends on the degree of ablation generated by the pulsed laser. As the temperature of the sample increases less energy is required to ablate the sample surface at the point of incidence. If the initial laser power density that was sufficient to cause only a weak ablation with a significant thermoelastic component is kept constant, the degree of ablation would then increase with increasing sample temperature. As a result of this the longitudinal and the shear wave signals are expected to increase and decrease respectively as a function of temperature. A change in polarity of the shear wave may also occur as the ablative component becomes dominant over the thermoelastic component. The latter is affected by the presence of scale on the surface of the sample. In this case the M2 tool steel sample was heated in air allowing the sample surface to oxidise and form dark coloured scale (magnetite) at higher temperatures. This scale layer having a lower reflectivity than the clean steel would result in an increase in the amount of laser energy being absorbed by the sample, and hence increase the ultrasound energy generated into the material.

The EMATs detection efficiency is affected by the presence of magnetite on the sample surface [Parkinson and Wilson, 1977, and Edwards and Palmer, 1990], and the characteristic of both the mild and tool steels. Magnetite is ferromagnetic below a Curie temperature (T_C) of 585 °C [Callister, 1991] and it is therefore likely that magnetostriction in the magnetite scale layer on the sample surface will enhance the

EMAT detection sensitivity below T_C. Above T_C, the magnetite becomes paramagnetic and hence its effect on the detection sensitivity disappears.

At room temperature up to the Curie temperature the mild and tool steel are ferromagnetic, therefore the acoustic wave signal detected by the EMAT may be as a result of the combined effect of the Lorentz force and magnetostriction mechanisms. In the case of mild steel, at 760 °C, the reduction in the acoustic wave signal amplitude and the change in the longitudinal wave signal polarity could both be related to the complete ferromagnetic to paramagnetic phase transformation. The ferromagnetic to paramagnetic phase transition results in the loss of the mild steel magnetic properties and hence the disappearance in the magnetostriction effect. The acoustic wave signal was therefore only detected by the Lorentz force mechanism resulting in the reduction of the signal amplitude. The change in the longitudinal wave pulse polarity has been reported by Edwards and Palmer, [1990] through comparisons of waveforms obtained from an aluminium alloy, a mild steel and a stainless steel at room temperature using a Nd:YAG laser as the ultrasound source and a normal motion sensitive EMAT as the detector. They observed that the longitudinal wave polarity on the waveforms obtained from a non-magnetic aluminium alloy and stainless steel is opposite to that of the magnetic mild steel. A similar phenomenon is observed in the tool steel at 762 °C (fig. 5.16) but the polarity is opposite to that of the mild steel, instead of from a negative to a positive initial peak it is vice versa. The reverse in polarity could be due to the different EMAT being used for the measurement on the two materials. The measurement on the mild steel was taken using the EMAT with two rectangular permanent magnets stacked parallel to each other, and the measurement on the tool steel was made using the EMAT with a

cylindrical magnet. It is possible that the polarity of permanent magnets used in the two EMATs was different giving a corresponding inversion in the induced voltage signals.

Just above the Curie temperature, at 775 °C in the mild steel (fig. 5.12) and at 772 °C in the case of tool steel (fig. 5.16), the enhancement in the longitudinal wave signals could be caused by the EMAT cooling a thin skin of the material back into the ferromagnetic phase causing a concentration and redistribution of the EMATs magnetic field giving enhanced sensitivity to longitudinal wave and/or is possibly due to volume magnetostriction. Normally volume magnetostriction only occurs at very high fields in steels close to the saturation magnetisation (M_s), however near the Curie temperature M_s is below the level of field which can be obtained from an EMAT and volume magnetostriction is a possible mechanism.

Well above the Curie temperature when both the bulk and the detection surface of the material are paramagnetic the detected acoustic wave signals are relatively weak (fig. 5.13) compared with that in the ferromagnetic phase (fig. 5.12) because detection is only achieved by the Lorentz force mechanism. At 925 °C (fig. 5.13) the weaker acoustic wave signals detected in the mild steel could be caused by the coarse γ-austenitic phase that causes the increase in the attenuation due to scattering, in particular the Rayleigh scattering. It is estimated that with the ultrasound frequency between 0.5 to 20 MHz generated by the pulsed laser, and the longitudinal wave velocity value of 4720 ms^{-1} (taken from fig. 5.10), the corresponding acoustic wavelength is calculated to be 4.72 mm and 240 μm respectively. Therefore for attenuation due to Rayleigh scattering to occur the average austenitic grains size must be much smaller than 2 mm diameter. In the M2 tool steel the acoustic wave signals

could still be detected above 1100 °C even though it is expected that above this temperature the austenitic grain structures should become coarser (refer fig. 5 in appendix) and Rayleigh scattering more extensive.

5.5 Conclusions

This chapter has demonstrated the capability of the laser-EMAT system for making acoustic wave measurements on thixotropic and non-thixotropic materials with higher melting points. In the case of the thixotropic Cu 10.2 % Sn alloy, measurements could be made up to approximately 20 % liquid fraction in the semi-solid state, and up to 1085 °C in the fully molten state. In the case of the commercial mild steel and the thixotropic M2 tool steel the laser-EMAT system has demonstrated that the ferromagnetic to paramagnetic transition temperature could possibly be detected, indicated by the sudden drop in the signal amplitude and the change in the polarity of the longitudinal wave pulse. Finally, measurements on the approximately 61.5 mm thick M2 tool steel sample using the R.F furnace has further demonstrated the capability of the Nd:YAG pulsed laser and the spiral coil permanent magnet EMAT to generate and detect ultrasound respectively, in a thick and highly attenuating sample of similar size to those used for commercial thixoforging to a temperature as high as 1140 °C.

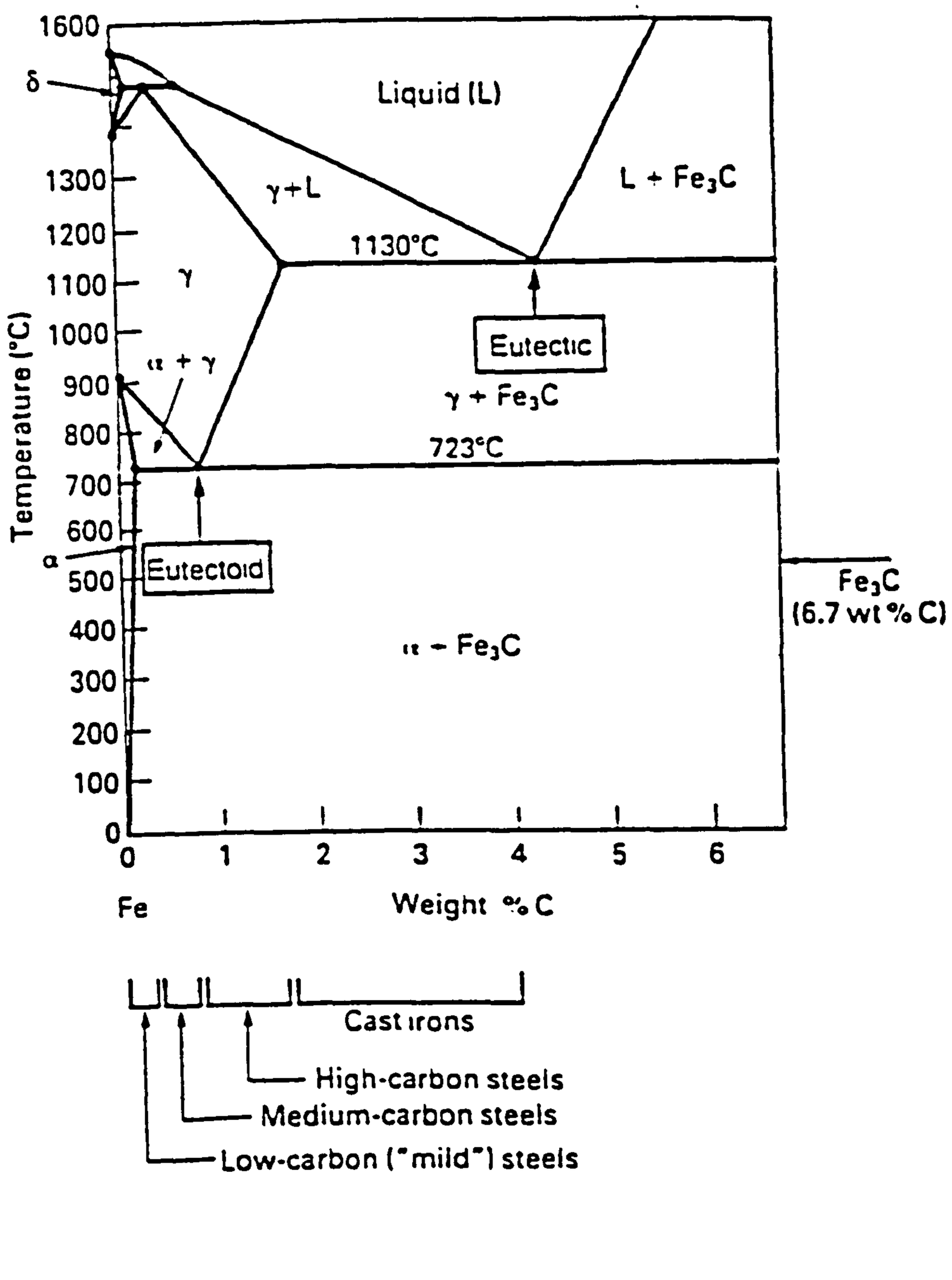

Fig. 5.1 The iron-carbon phase diagram.

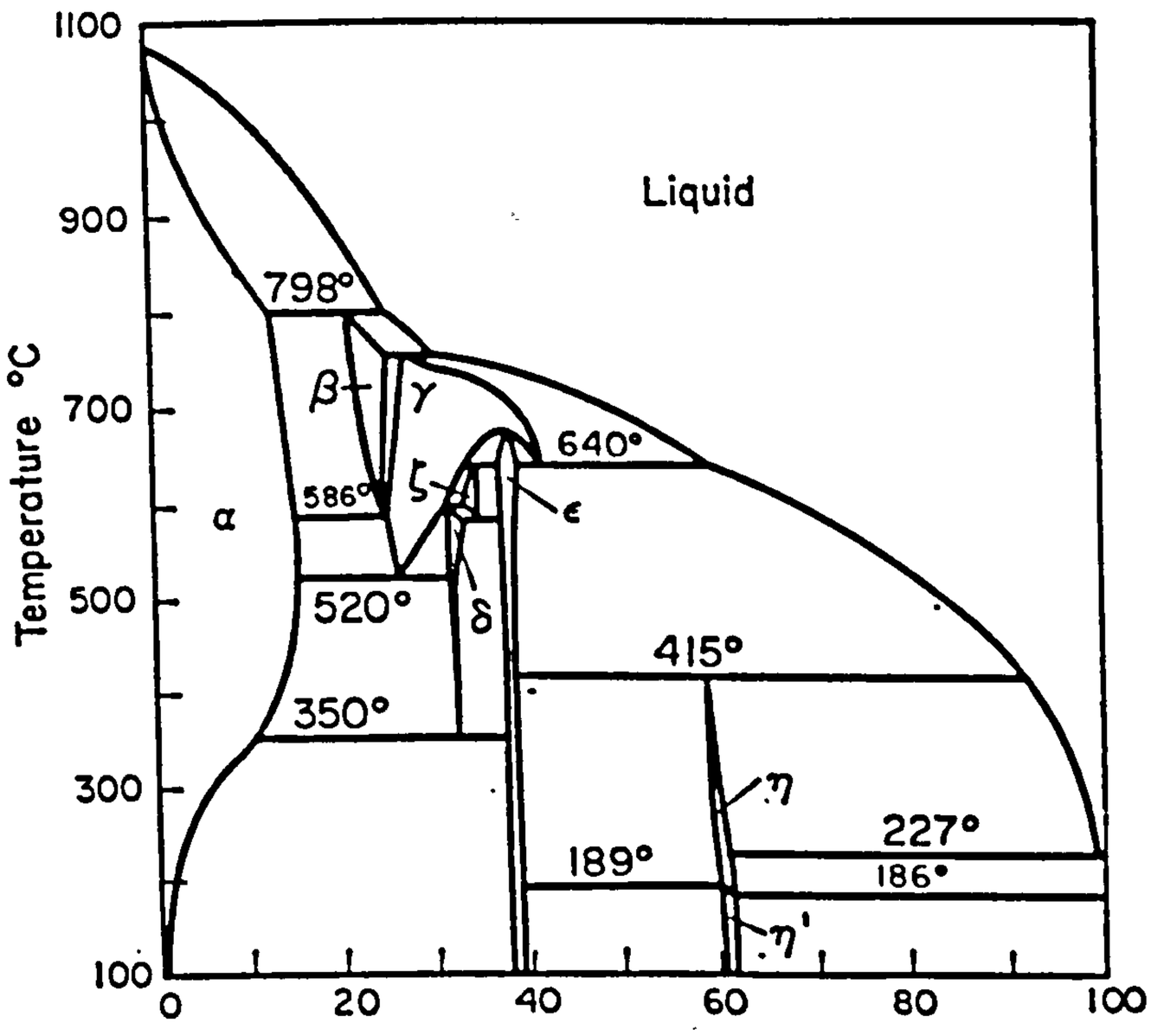

Fig. 5.2 The copper-tin phase diagram.

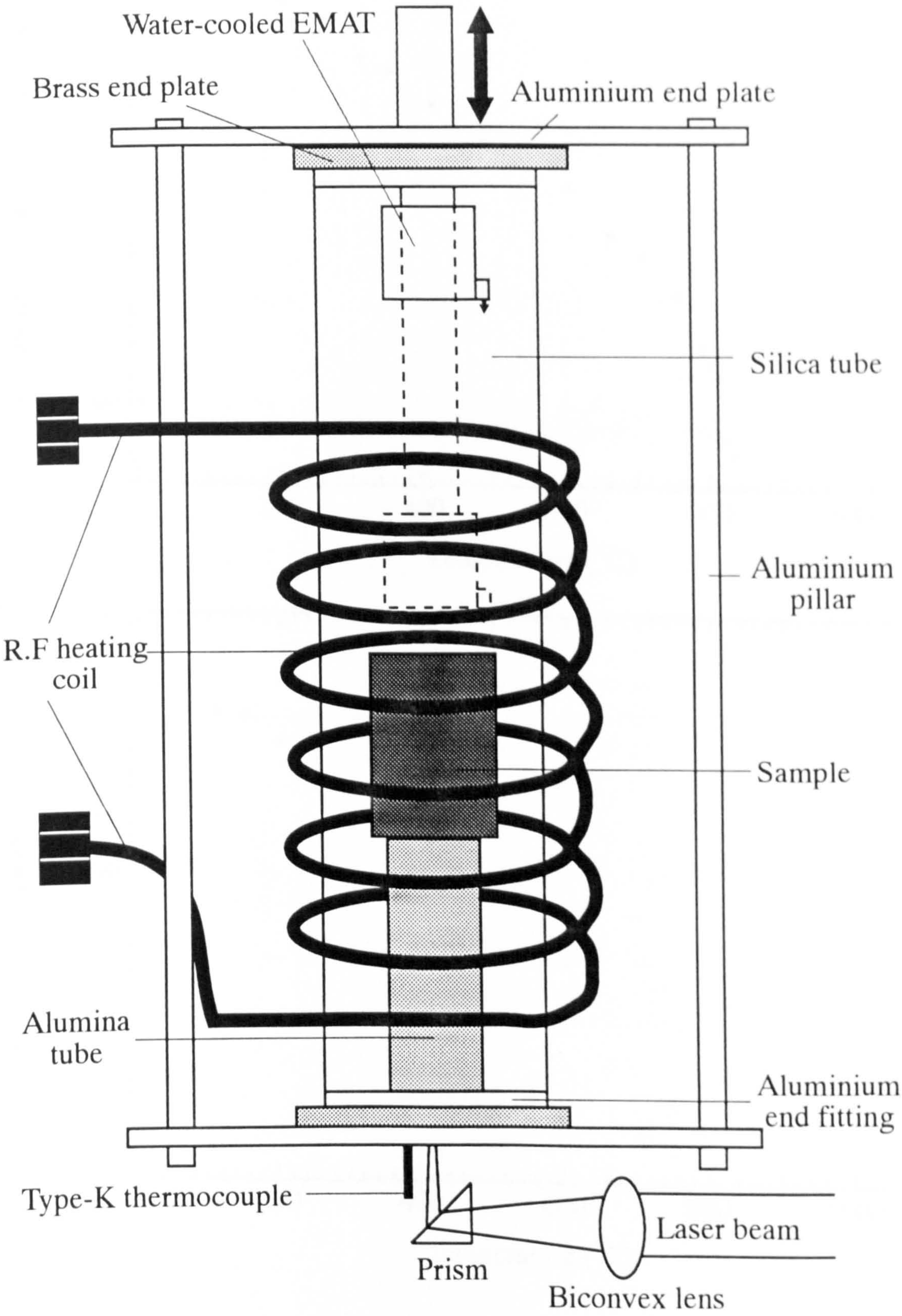

Fig. 5.3 Experimental arrangement for the M2 tool steel heated in an induction furnace.

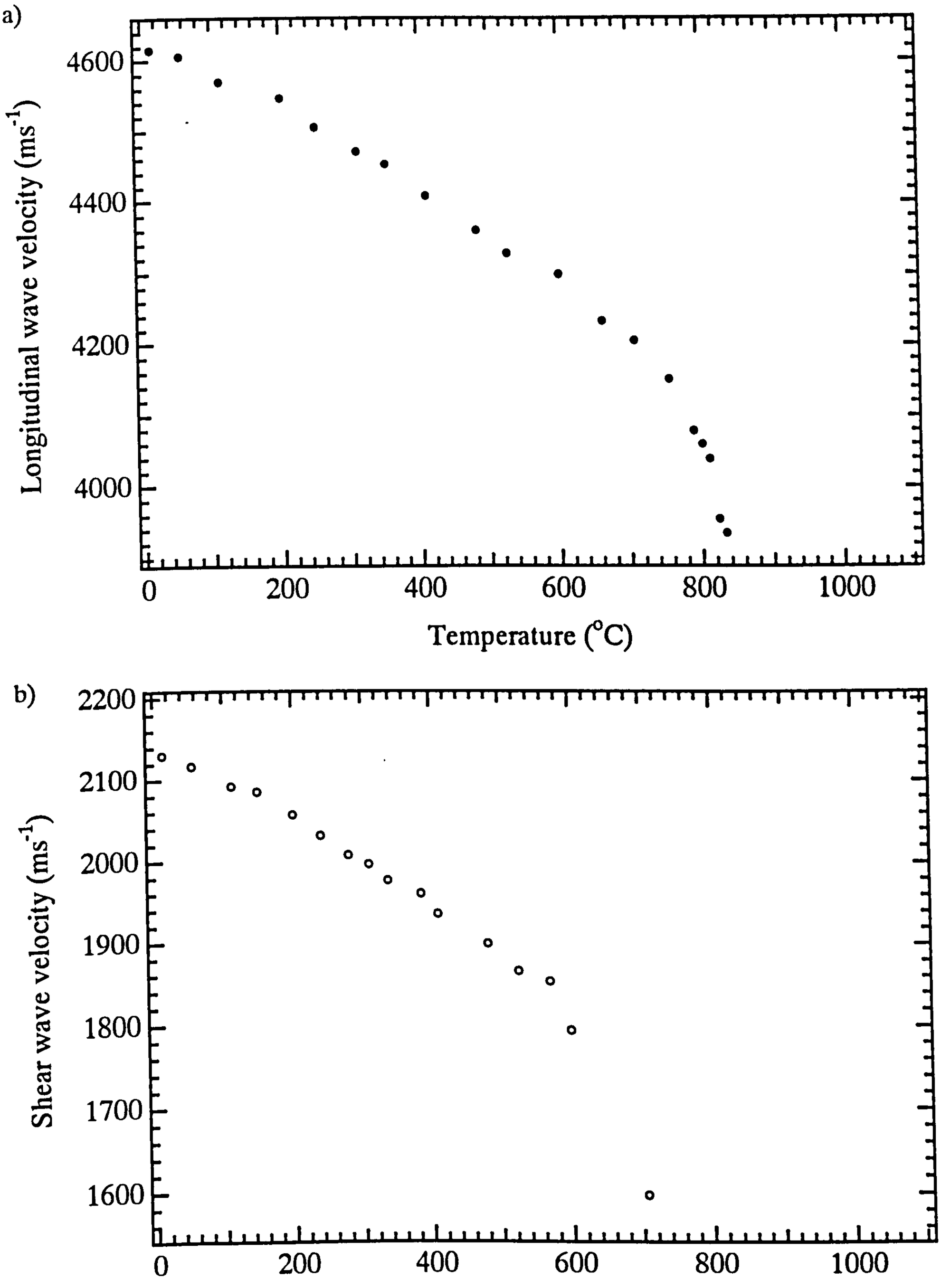

Fig. 5.4 Variation of a) longitudinal and b) shear wave velocity as a function of temperature in Cu 10.2 % Sn alloy when the sample surface on the generation side was unsupported.

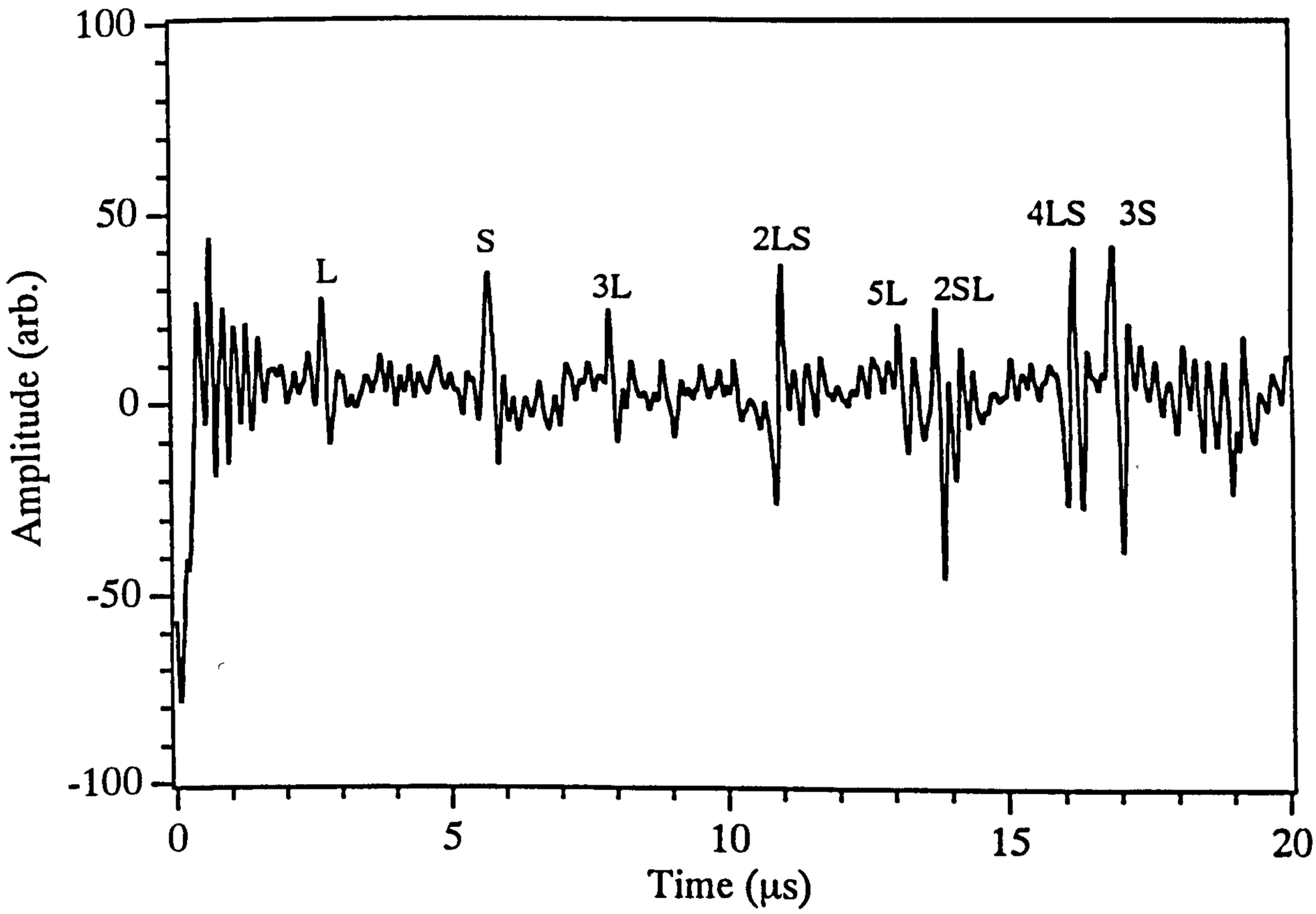

Fig. 5.5 Room temperature waveform on Cu 10.2 % Sn alloy when the sample surface on the generation side was unsupported.

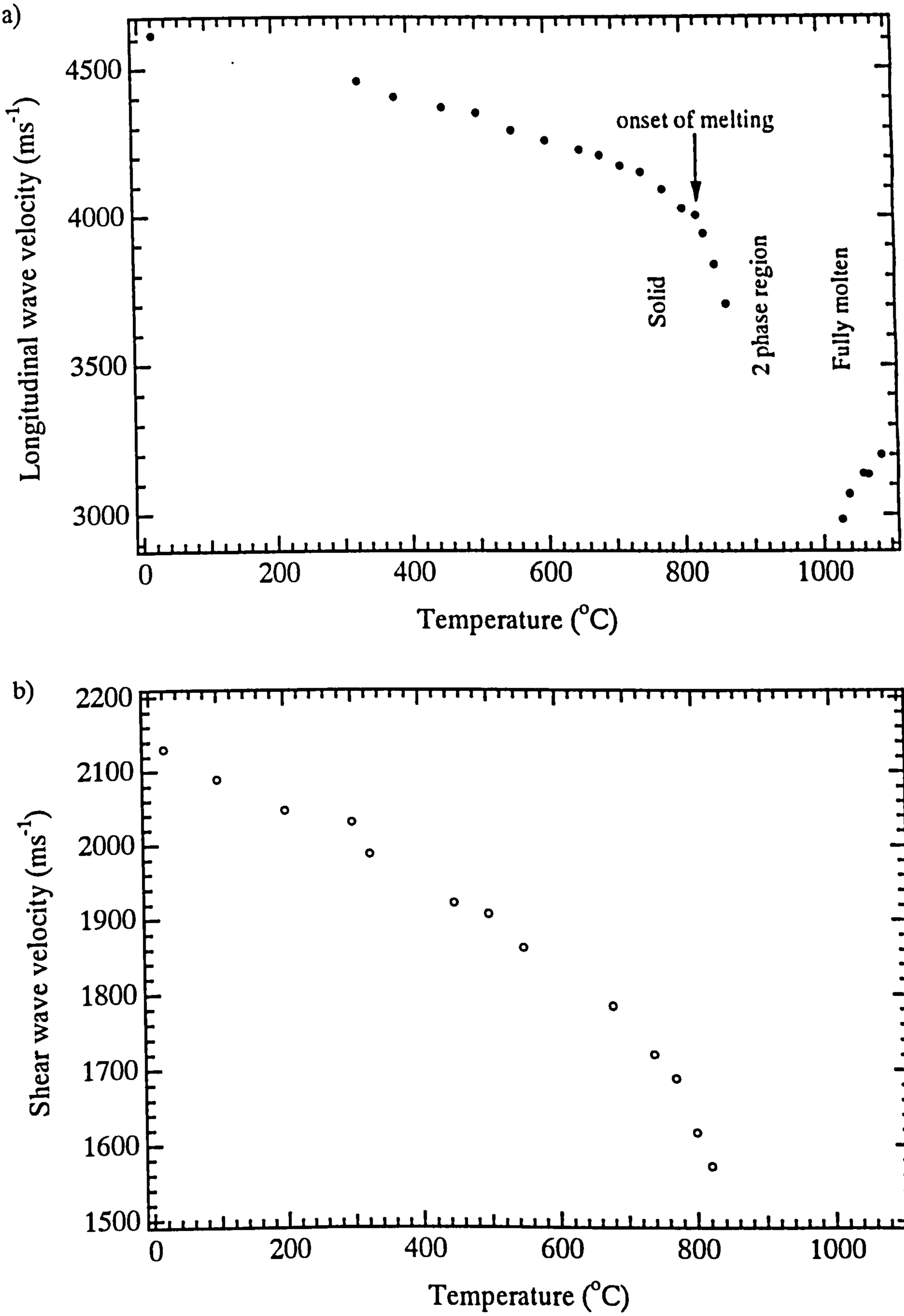

Fig. 5.6 Variation of a) longitudinal and b) shear wave velocity as a function of temperature in Cu 10.2 % Sn alloy when both ends of the sample surface were supported.

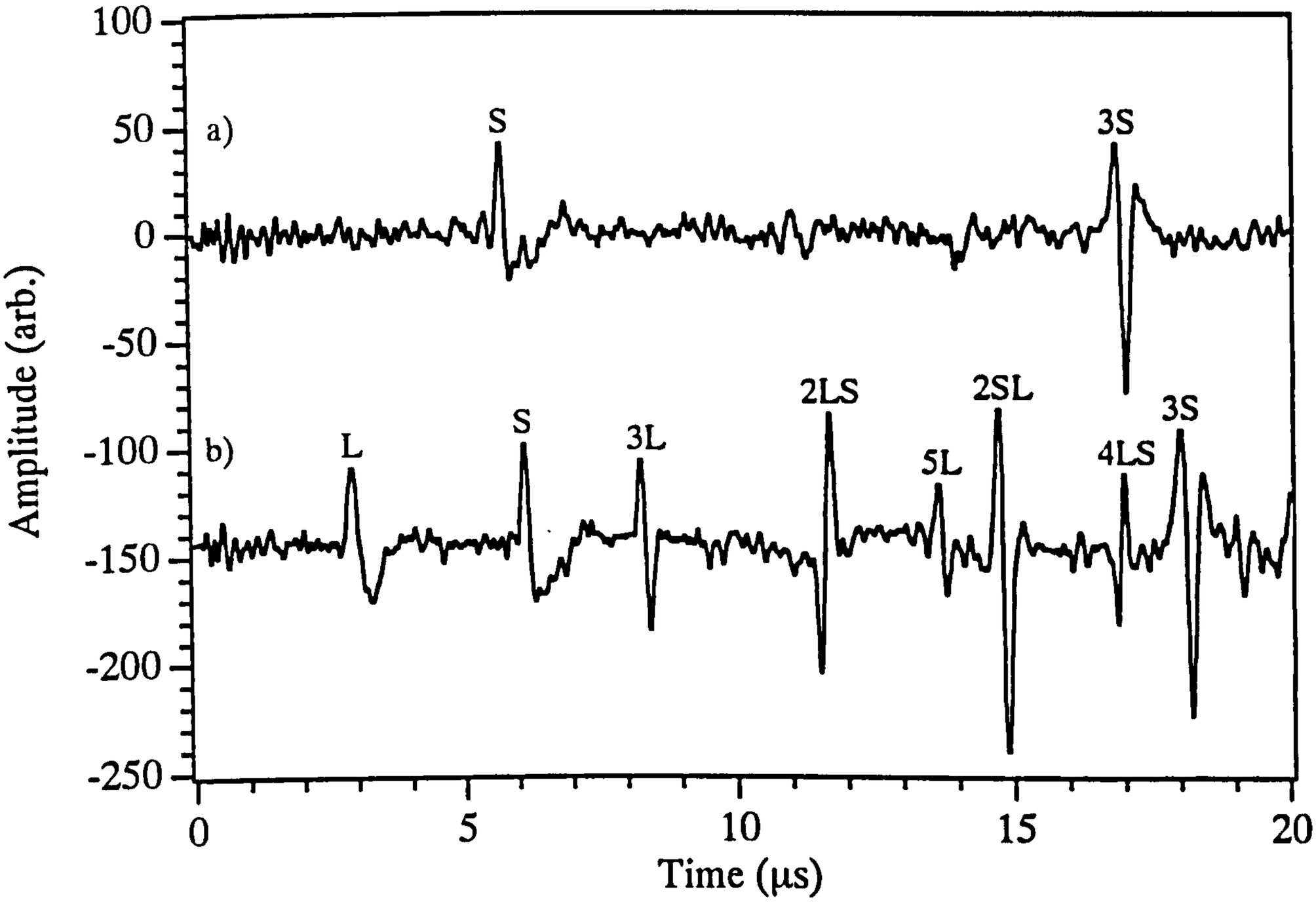

Fig. 5.7 Waveforms obtained at a) room temperature and b) 326 °C on Cu 10.2 % Sn alloy when both ends of the sample surface were supported.

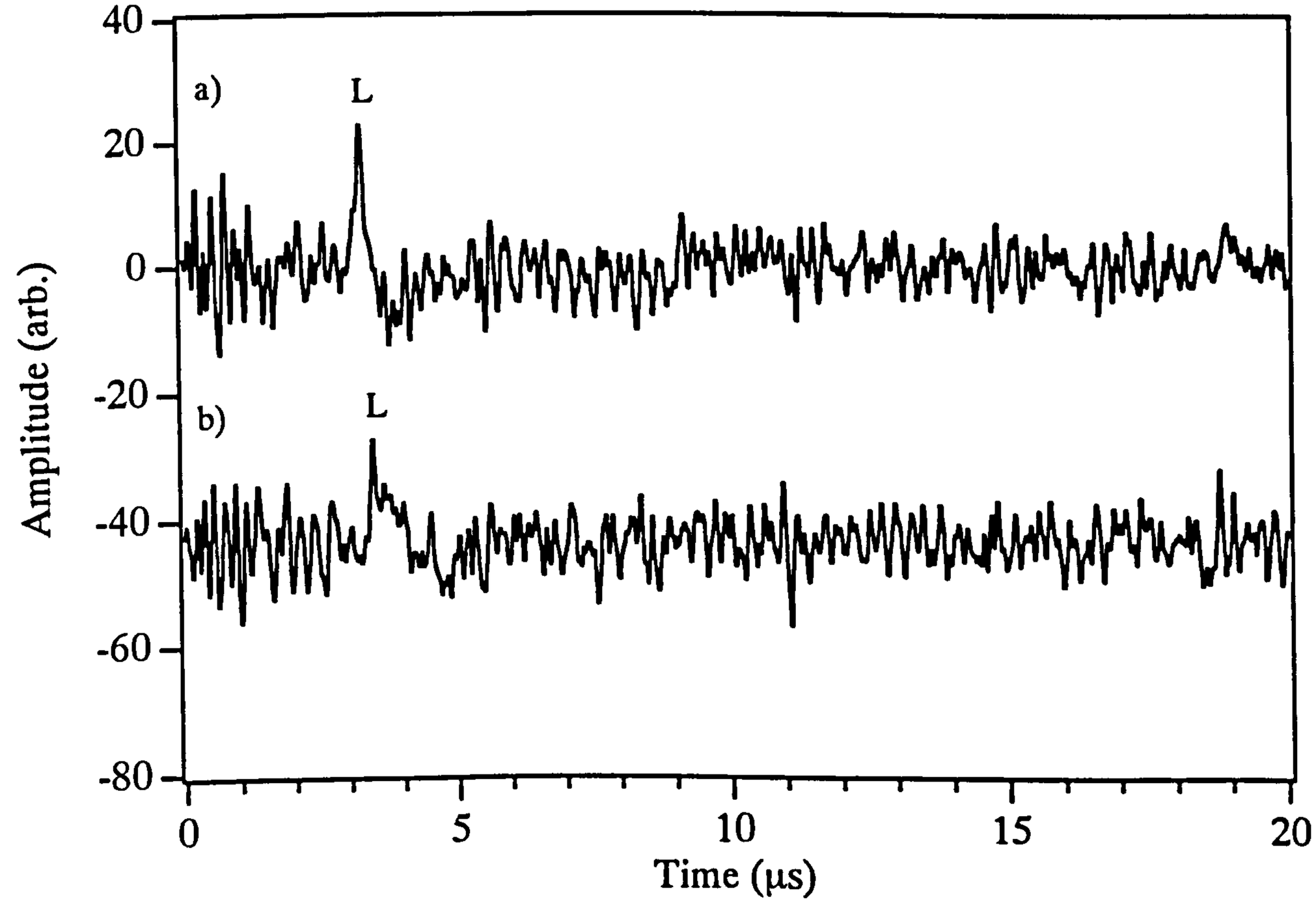

Fig. 5.8 Waveforms obtained at a) 830 °C and b) 862 °C on Cu 10.2 % Sn alloy when both ends of the sample surface were supported.

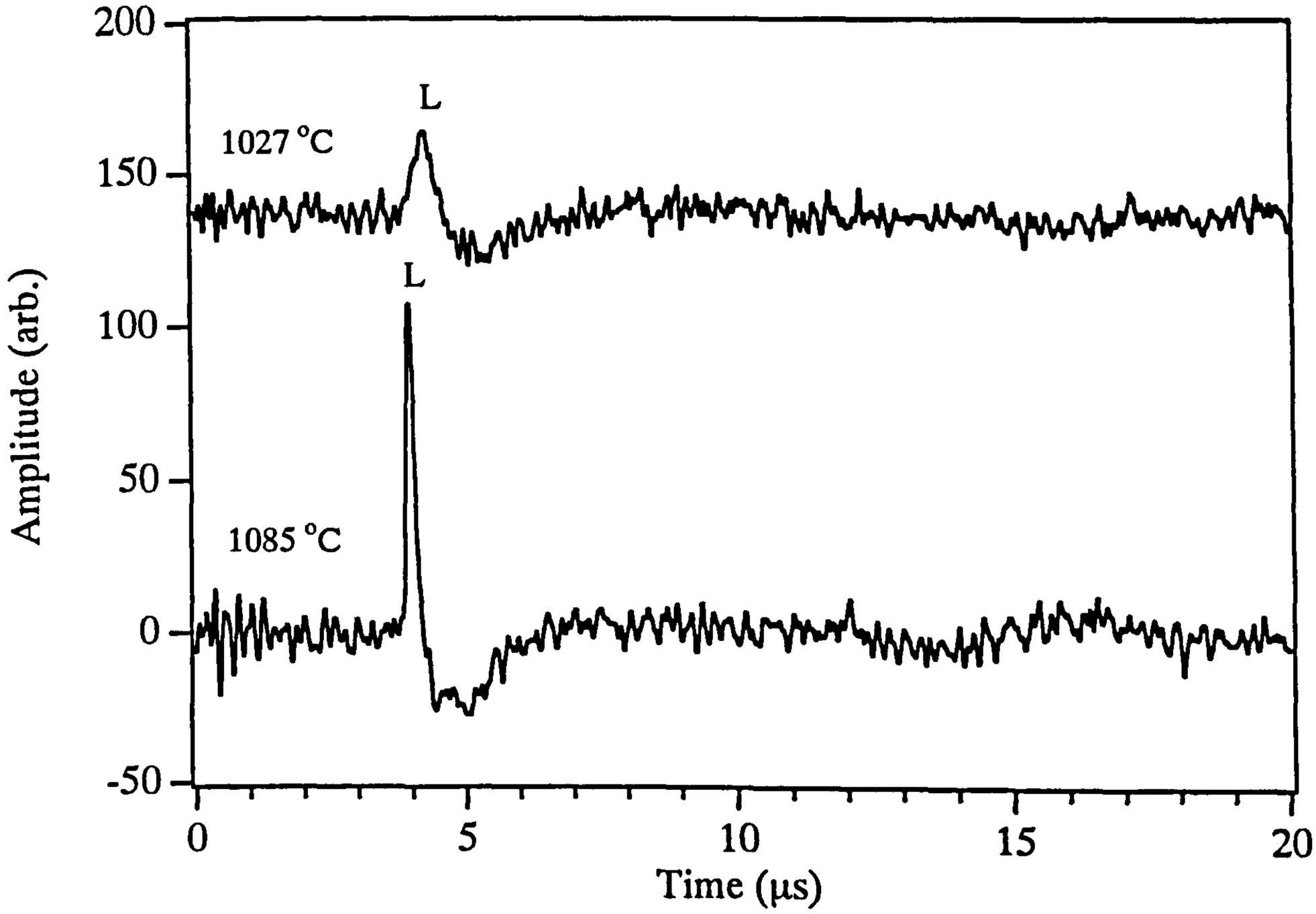

Fig. 5.9 Waveforms obtained on the Cu 10.2 % Sn alloy in the fully molten state.

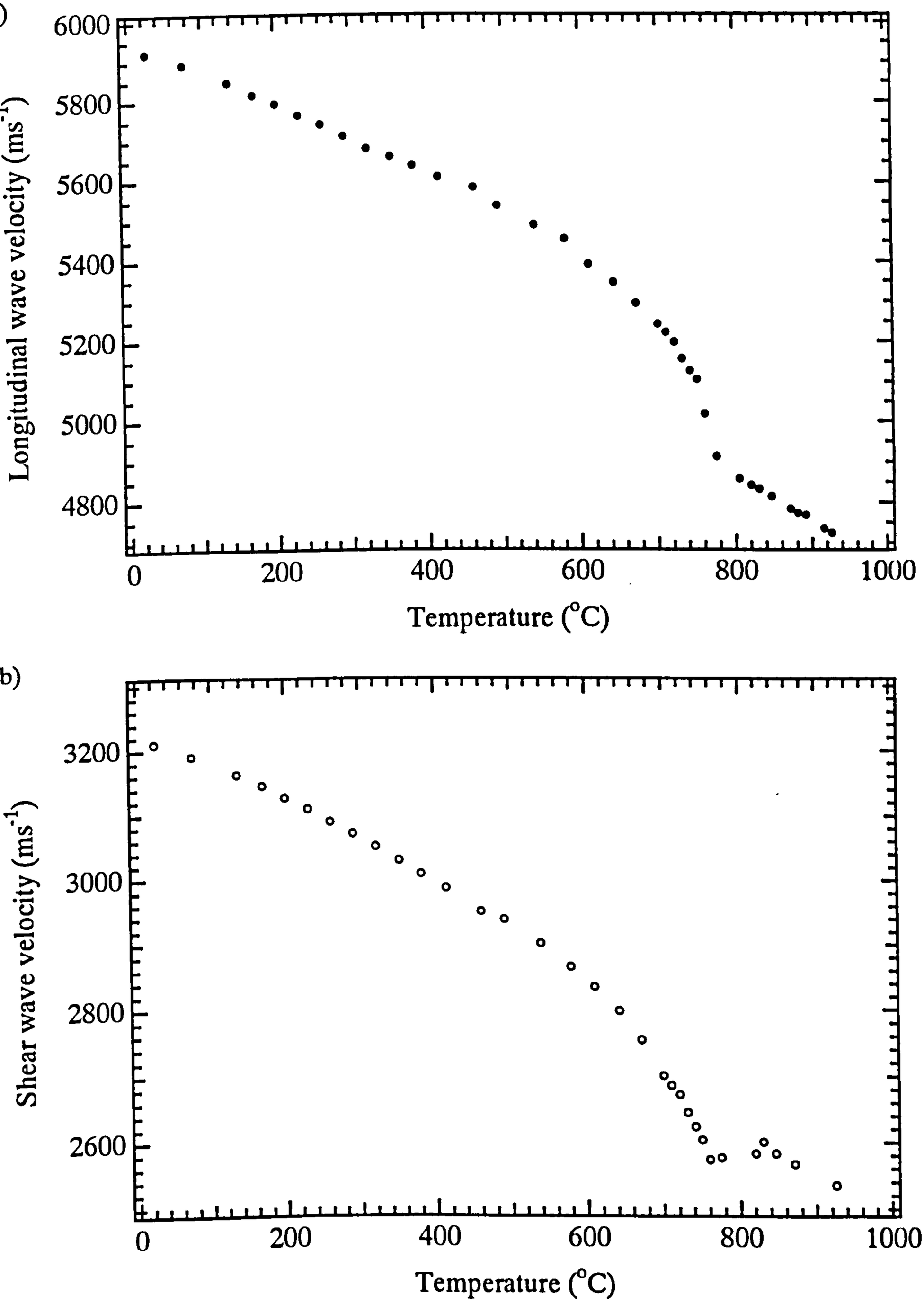

Fig. 5.10 Variation of a) longitudinal and b) shear wave velocity as a function of temperature in mild steel.

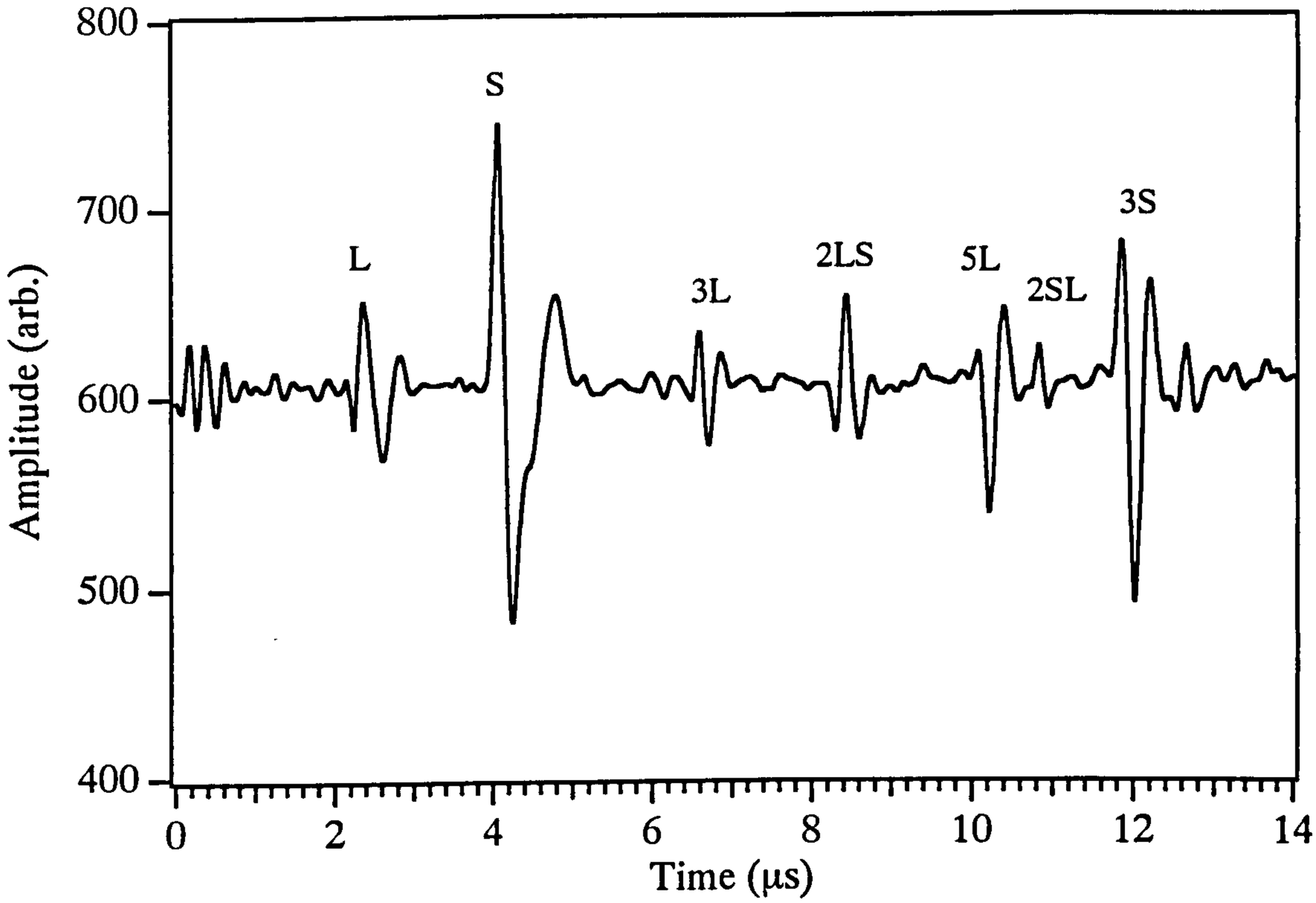

Fig. 5.11 Waveform obtained on the mild steel at room temperature.

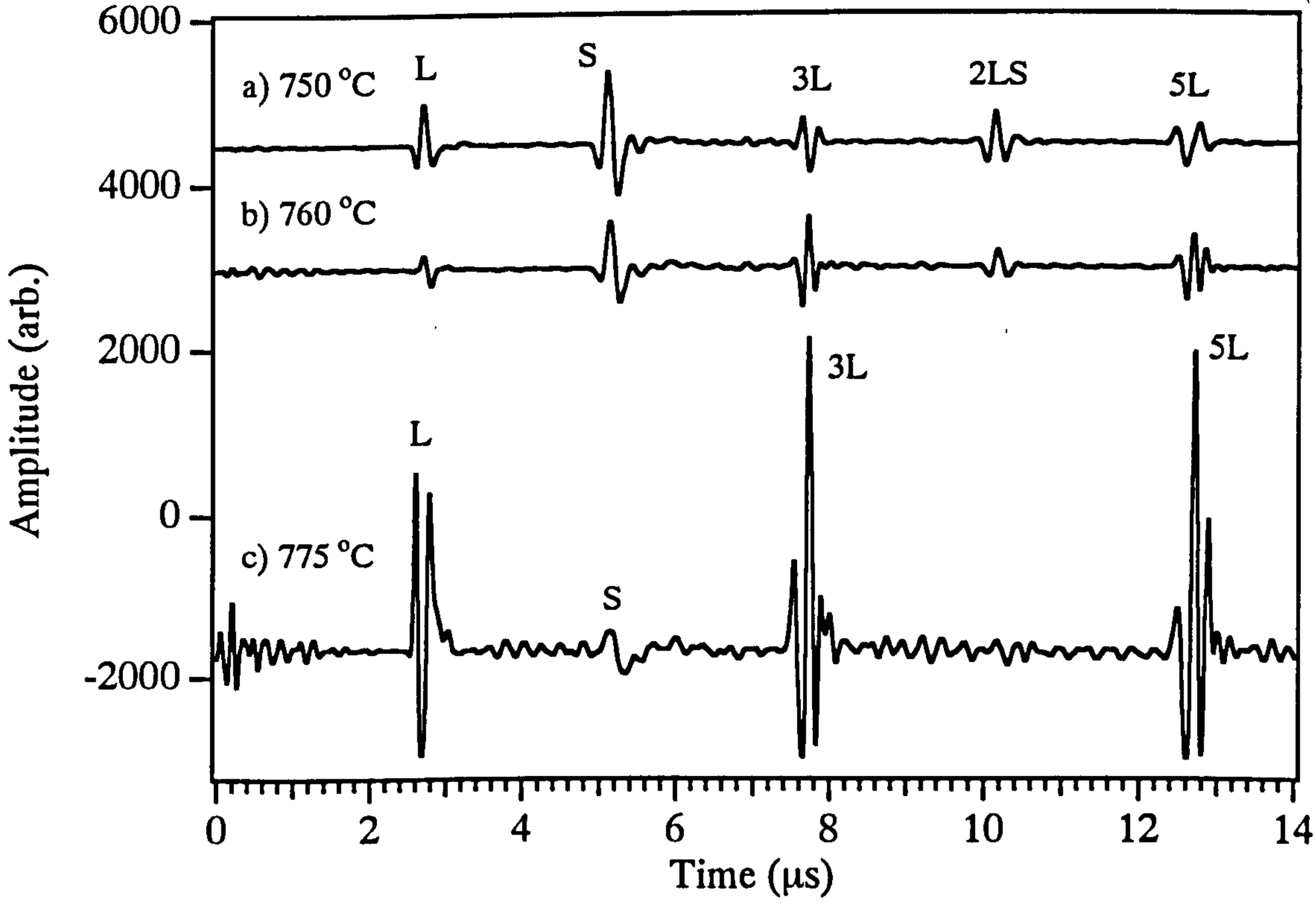

Fig. 5.12 Waveforms obtained on the mild steel at a) immediately below b) around and c) above the Curie temperature.

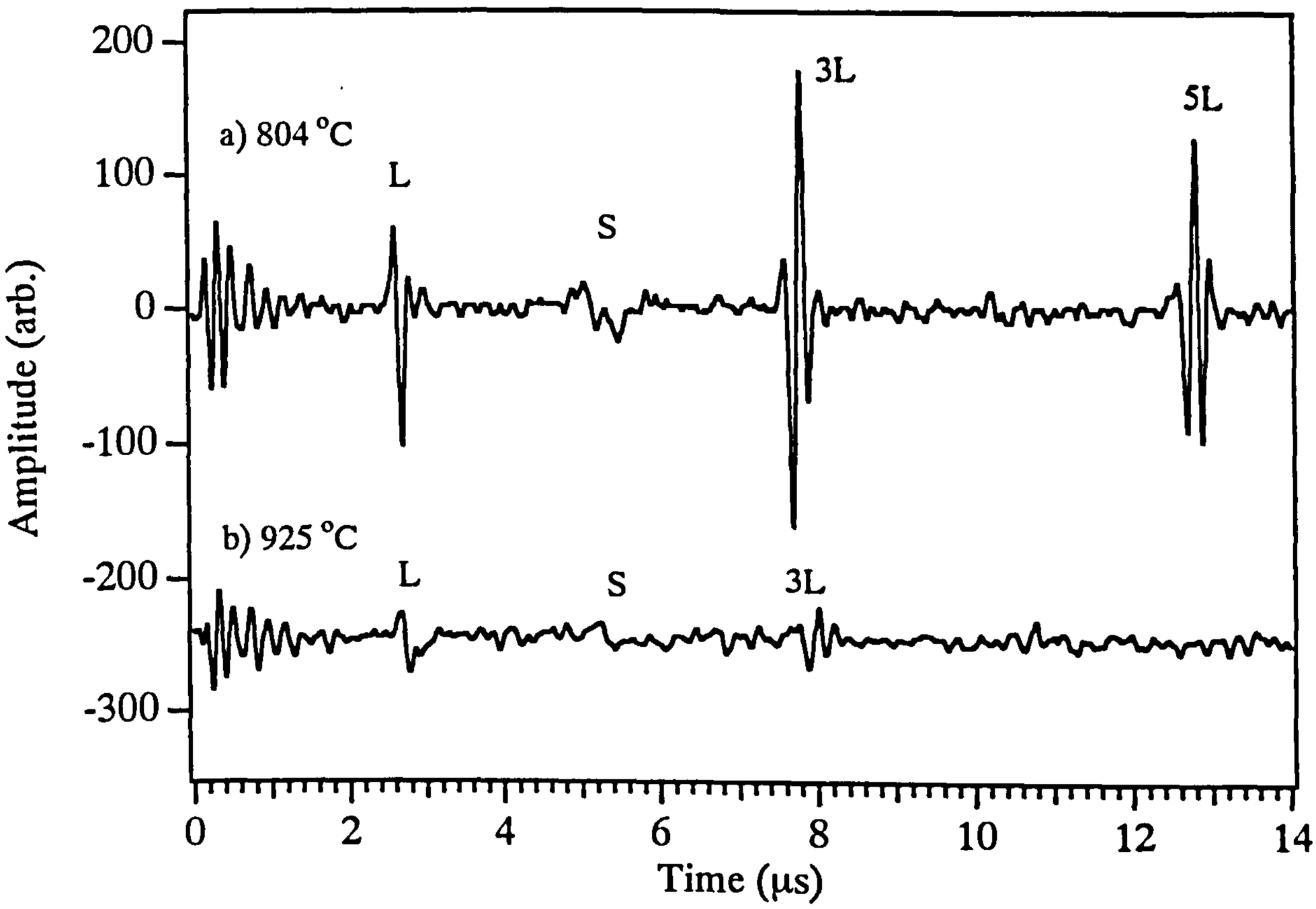

Fig. 5.13 Waveforms obtained on the mild steel at a much higher temperatures.

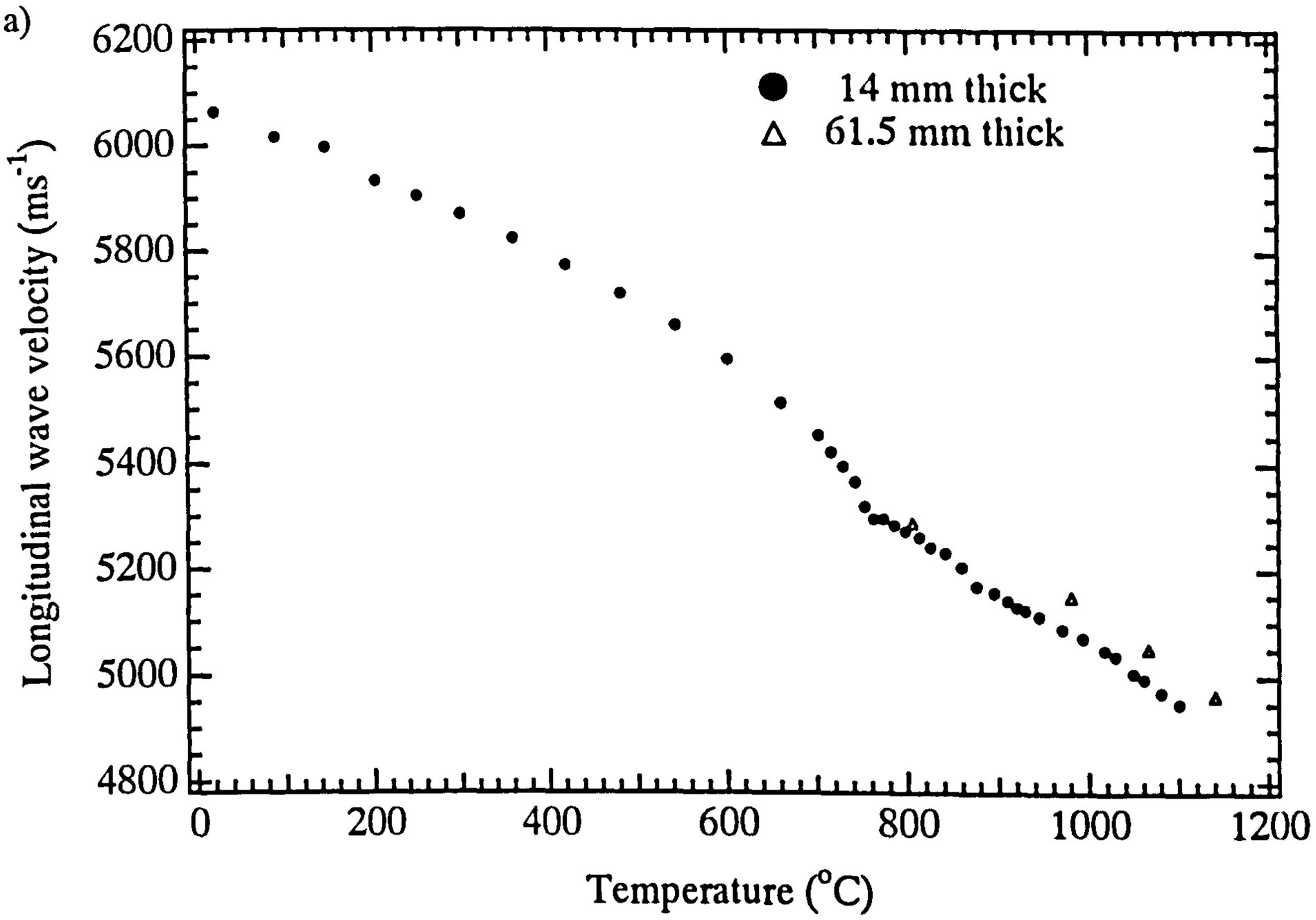

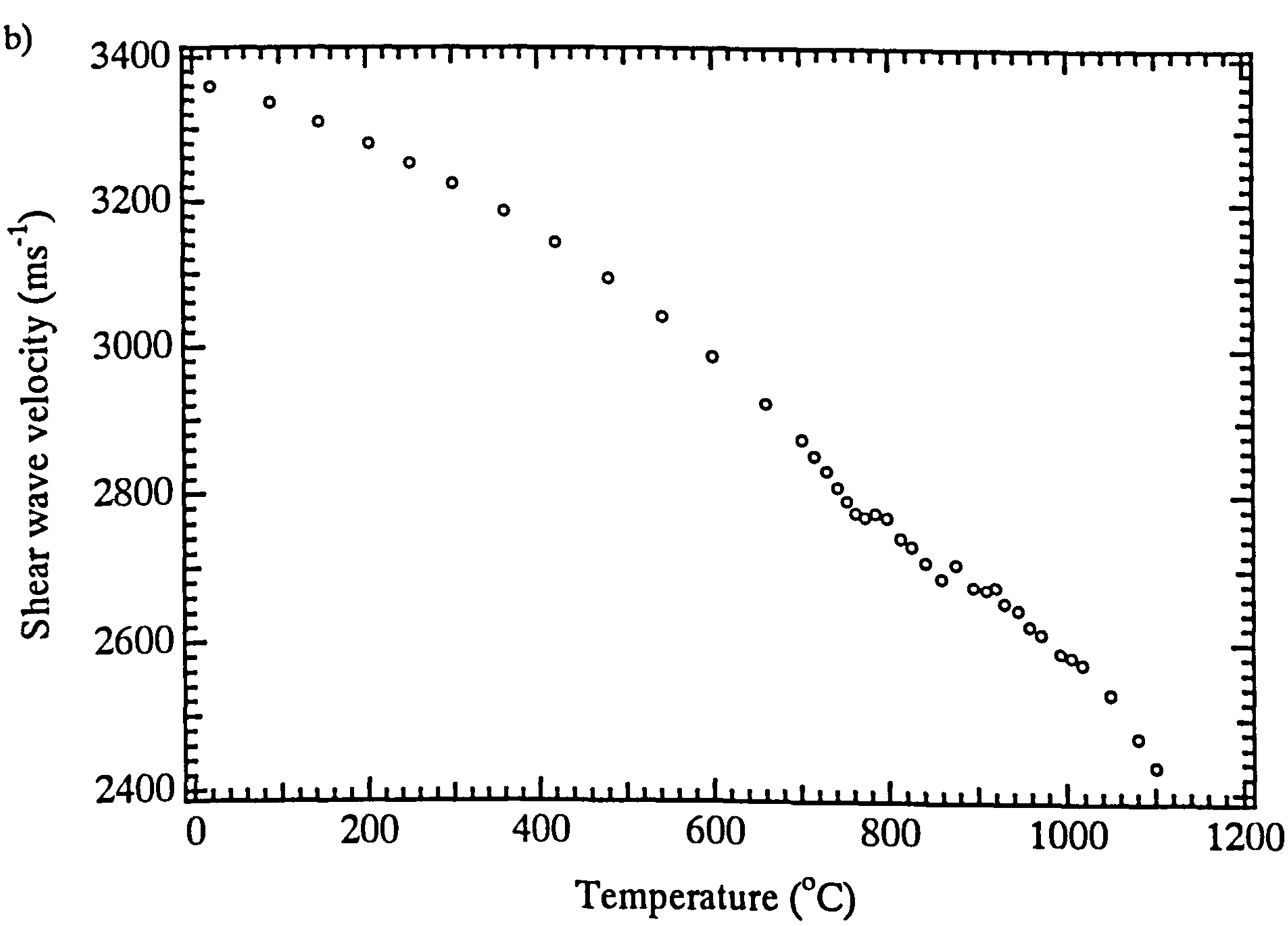

Fig. 5.14 Variation of a) longitudinal and b) shear wave velocity as a function of temperature in M2 tool steel.

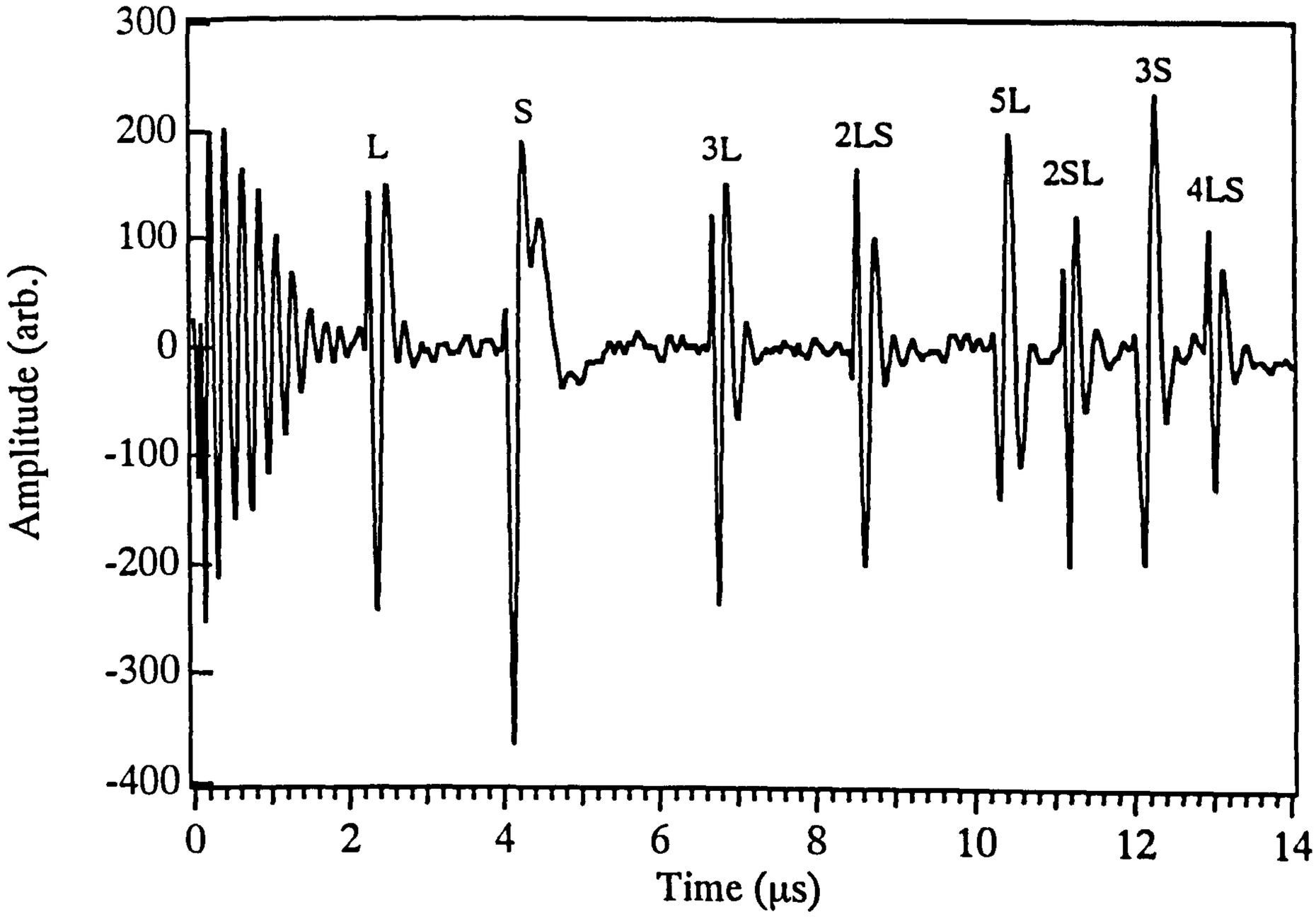

Fig. 5.15 Waveform obtained on the approximately 14 mm thick M2 tool steel at room temperature.

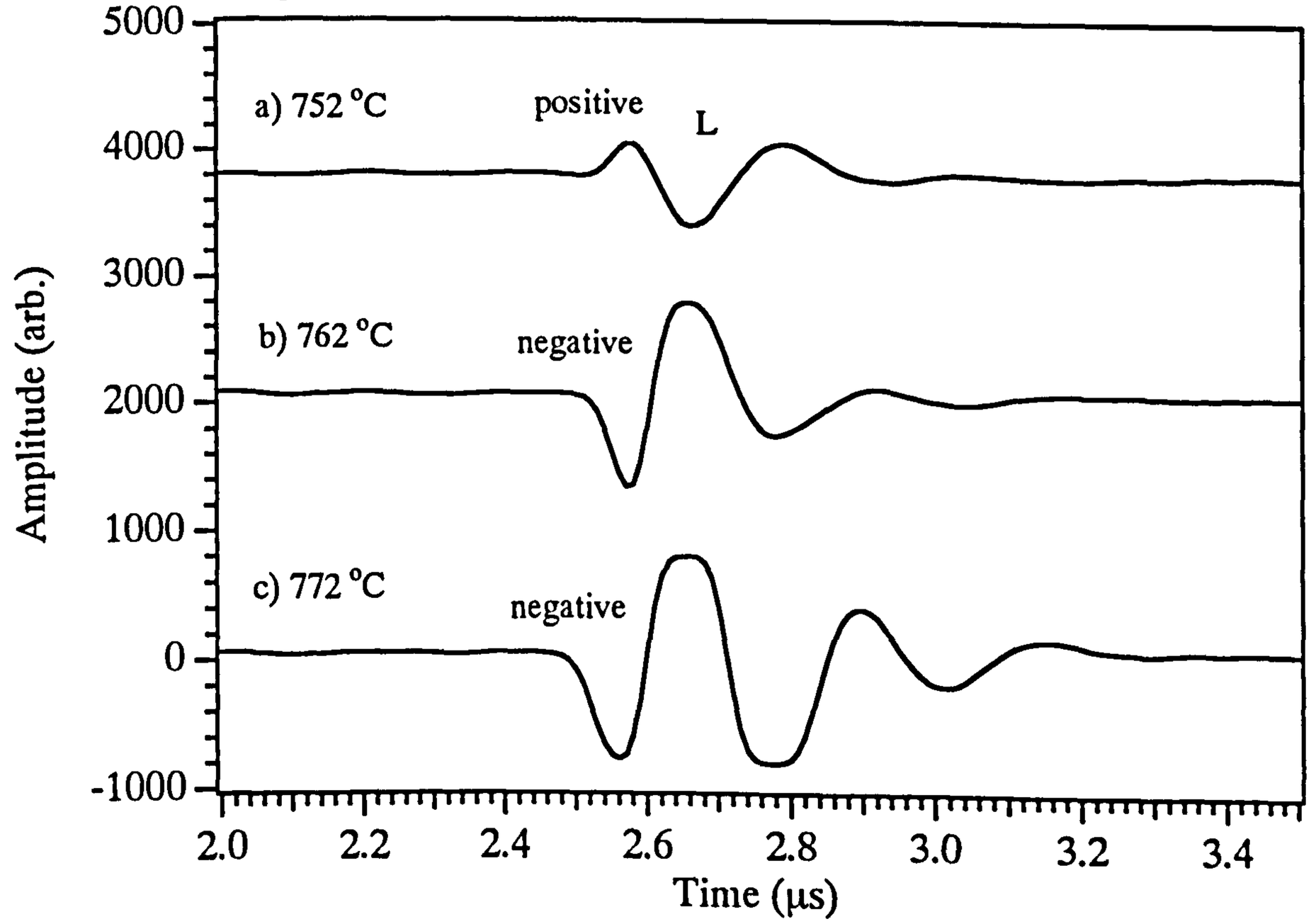

Fig. 5.16 Expanded waveforms on the M2 tool steel obtained at a) immediately below b) around and c) immediately after the Curie temperature.

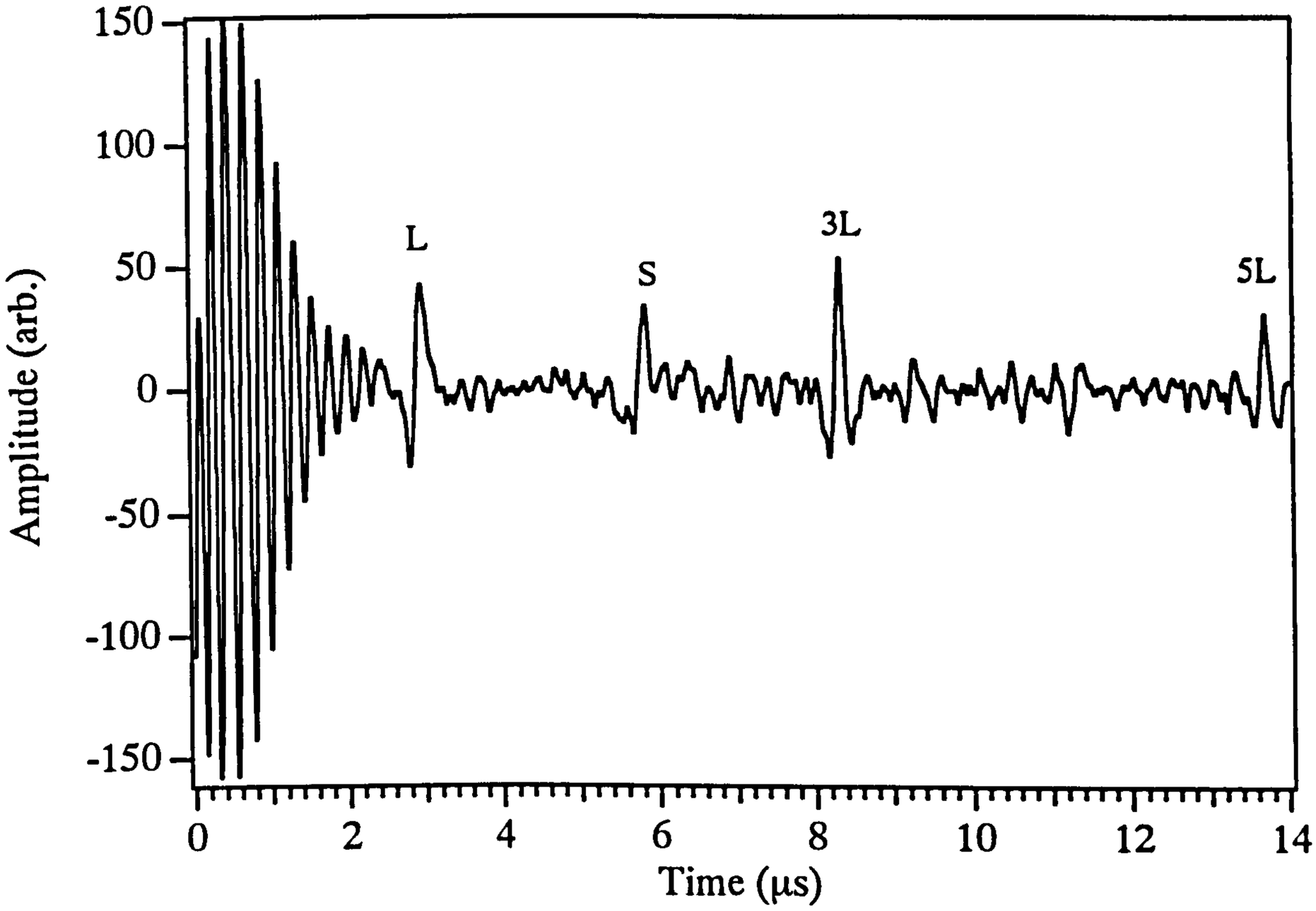

Fig. 5.17 Waveform obtained on the approximately 14 mm thick M2 tool steel at 1100 °C.

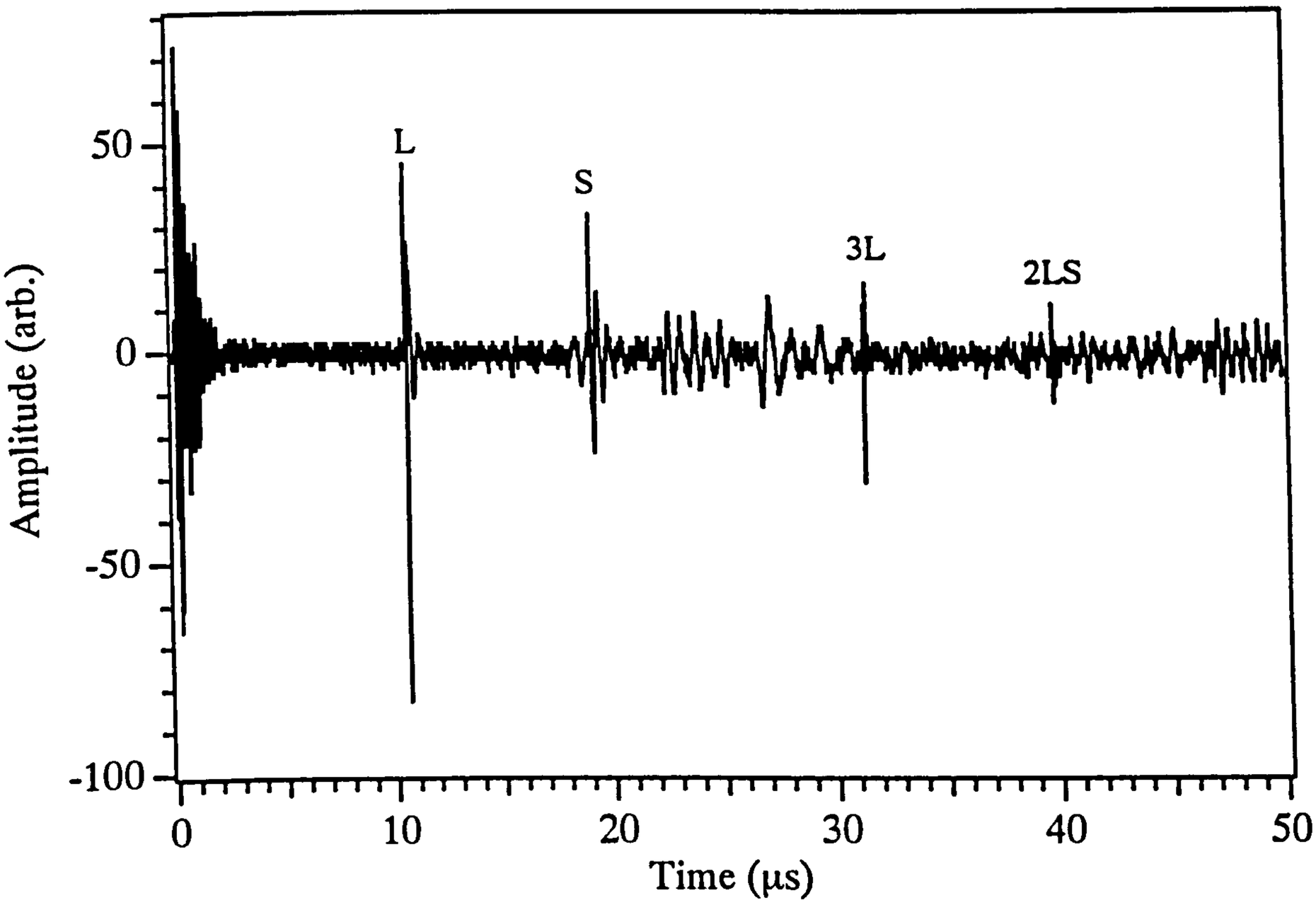

Fig. 5.18 Waveform obtained on the 61.5 mm thick M2 tool steel at room temperature.

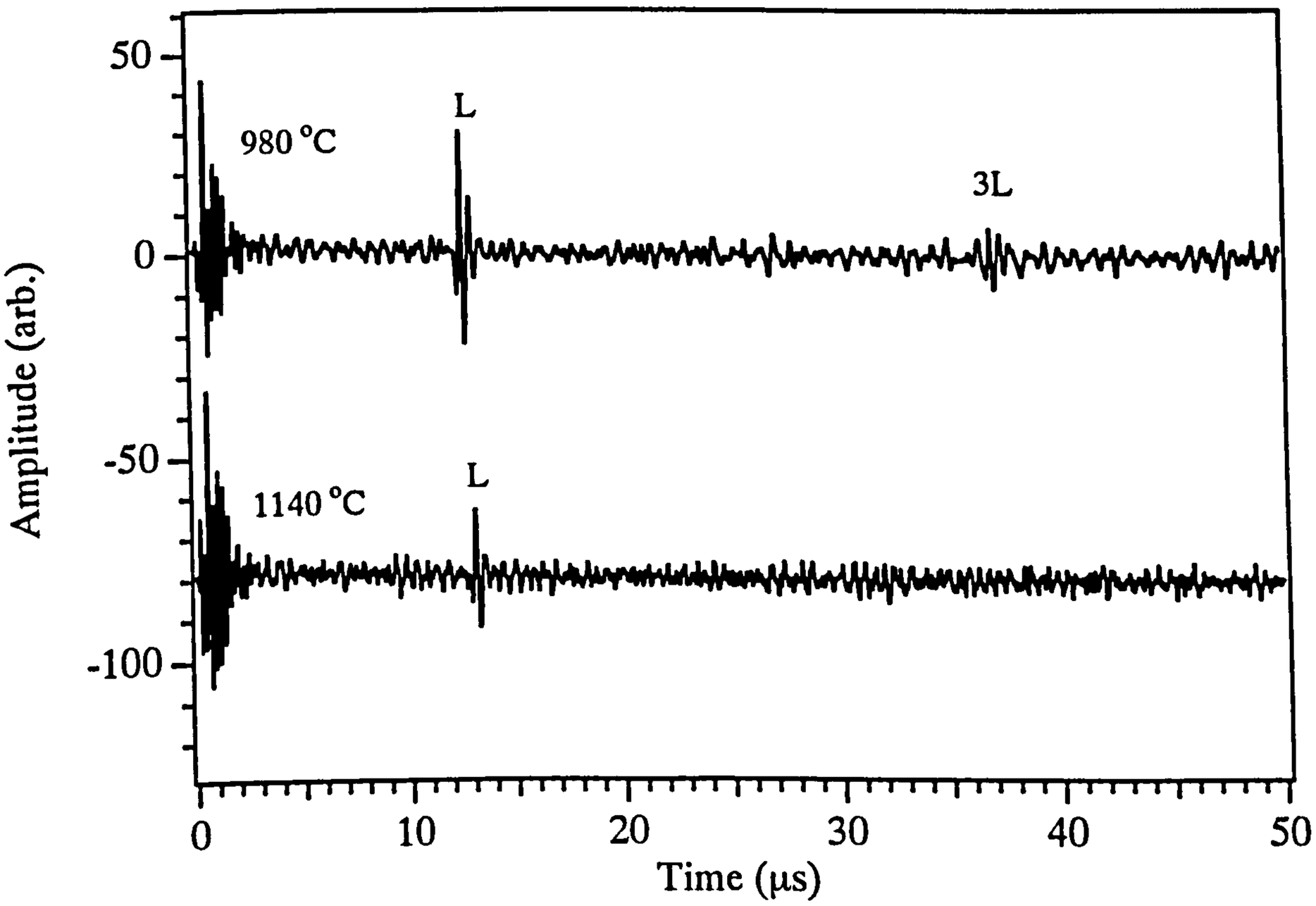

Fig. 5.19 Waveforms obtained on the 61.5 mm thick M2 tool steel at higher temperatures in the austenitic phase region.

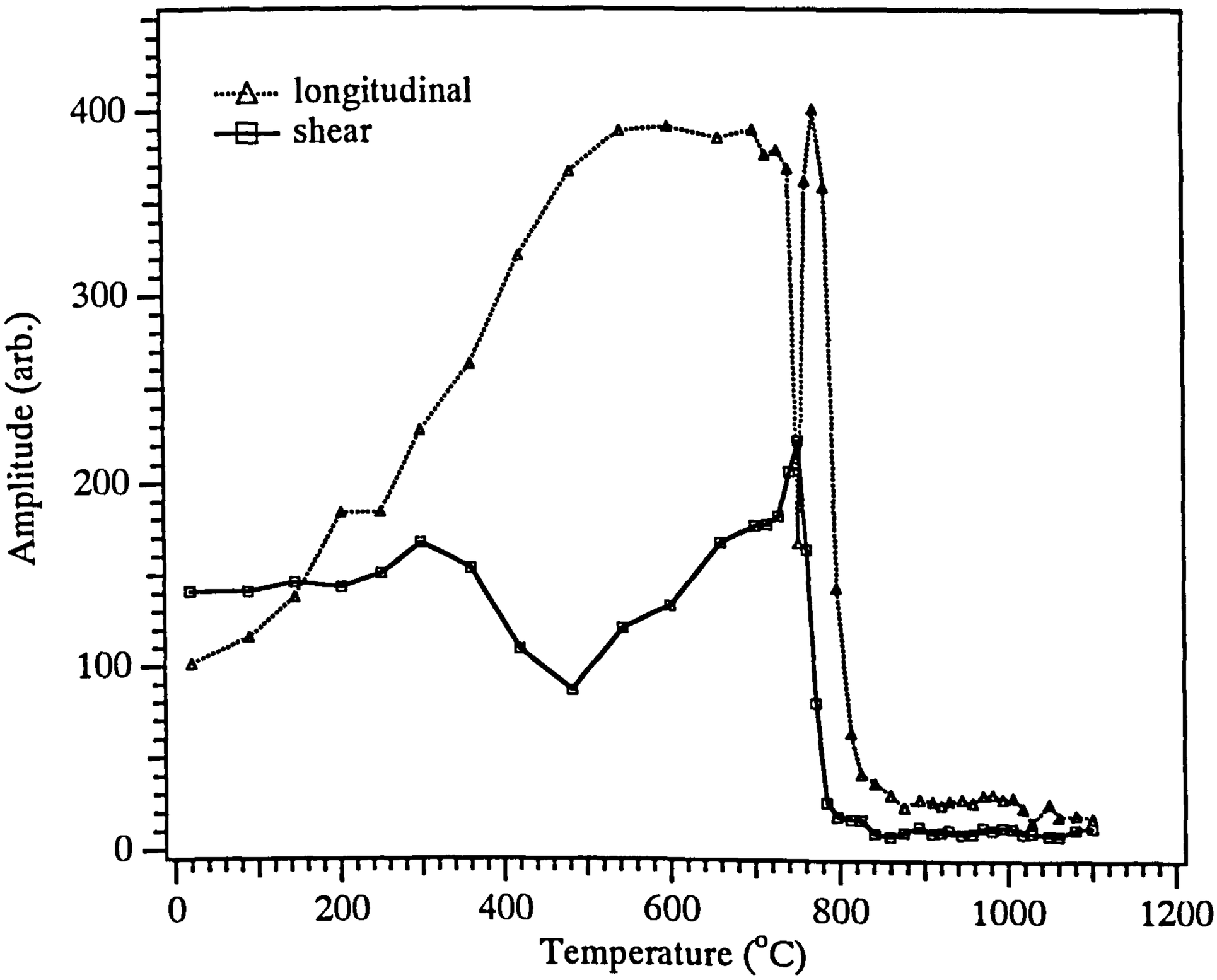

Fig. 5.20 Variation of acoustic waves signal amplitude with increasing temperature in M2 tool steel.

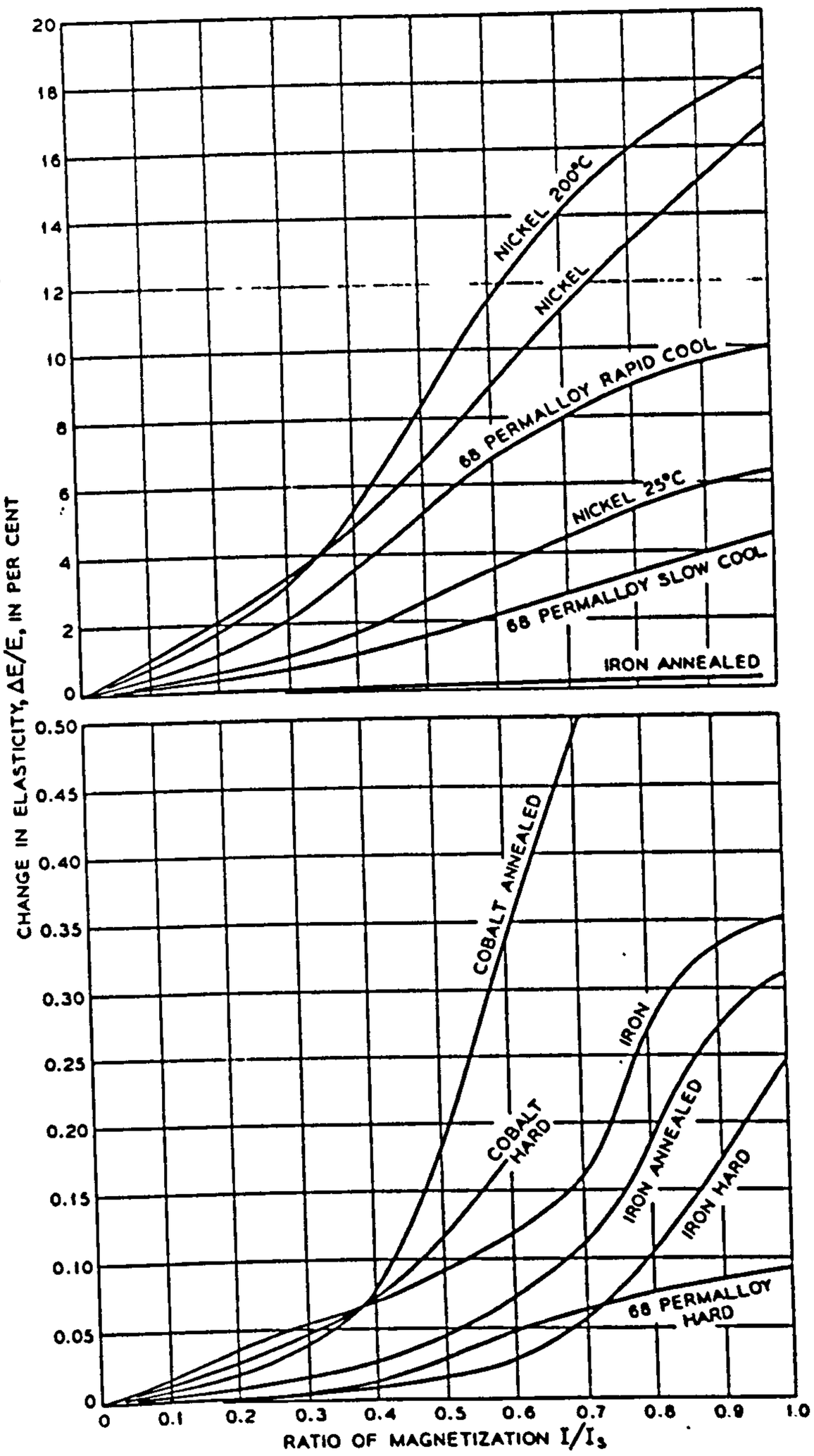

Fig. 5.21 Change in elasticity for a number of materials, as a function of ratio of magnetism to saturation magnetism I/Is (after Bozorth, 1951).

CHAPTER 6

CHAPTER 6

AN INVESTIGATION OF ERRORS CAUSED BY FINITE DETECTOR SIZE AND LASER EFFICIENCY

6.0 Introduction

This chapter describes investigations into the efficiency of the chosen laser-EMAT system and analyses systematic errors. The cooling effect of the EMAT on the samples is measured. To this end a range of different lasers have been used as ultrasonic generators together with various ultrasonic detectors. Section 6.1 examines the cause of the unusual behaviour of the shear velocity as a function of temperature observed between 350 and 400 °C in Al 4.86 % Si alloy. In this temperature range the velocity should be decreasing as the temperature increases instead of increasing. Section 6.2 describes an experiment carried out to determine the effect of the water-cooled EMAT detector on the temperature of the sample and therefore the acoustic wave transit time measurement. In order to carry out this measurement the existing experimental technique described in chapter 4 had to be upgraded. The experiment was designed in such a way that acoustic wave measurements could be made only after the EMAT was allowed to cool the sample for a certain pre-set time. A device that can automatically trigger the laser the moment the EMAT detector is at the measuring position (minimum lift-off distance) or at various delays of up to 8 seconds was designed. Finally, section 6.3 describes an experiment to compare the efficiency of pulsed Nd:YAG and CO_2 lasers as ultrasound generators at elevated

temperatures. Comparisons were made on low melting point aluminium alloy and high melting point M2 tool steel.

6.1 Experiment to Determine the Cause of the Unusual Behaviour of the Shear Wave Velocity Profile Between 350 and 400 °C in Al 4.86 % Si Alloy.

The etched coil of the shear EMAT used for the measurement in chapter 4 has a diameter of approximately 15 mm. The spatial resolution is therefore poor compared to a smaller coil EMAT or a "point" detector. With the EMAT it would be difficult to distinguish between the direct shear wave pulse and the L-L side wall reflected signal which may well be superimposed on and therefore distort the shear wave arrival between 350-400 °C in the Al 4.86 % Si alloy (fig.6.1). It was hoped that with the use of a "point" detector of approximately 1 mm diameter the two features could be distinctly resolved, allowing the shear wave transit time to be measured more accurately.

A schematic diagram of the experimental arrangement is shown in figure 6.2. A pulsed Q-switched Nd:YAG laser described in chapter 4 and a stabilised Michelson interferometer were used as the ultrasound generator and detector respectively. A continuous wave (cw) frequency doubled Nd:YAG laser (Adlas 300) with wavelength of 0.53 μm and 90 mW power was used to provide green light for the interferometer [Bushell et. al., 1992]. The system is very sensitive to the low frequency, large amplitude background vibrations and hence needs to be stabilised before carrying out an experiment. This was achieved by feeding back the low frequency signal to a vibrating reference mirror using the compensating stabiliser and monitoring the response on the LeCroy 9400A digital oscilloscope.

An Al 4.86 % Si alloy sample, approximately 12 mm thick and 30 mm in diameter, was mounted in the stainless steel holder that was supported by two stainless steel tubes lying horizontally in a split electric furnace. The sample was unsupported on either side, and the two Nd:YAG laser beams were initially aligned so that measurements could be made on epicentre. Subsequent adjustments were made to the furnace to ensure that the interferometer beam was always normal to the parallel sided sample and the measurements were always on epicentre despite any movement of the sample surface due to thermal expansion. The sample surface at the detection side was mirror polished so that maximum light would be reflected back to the detector enabling maximum detection sensitivity. To achieve a plasma source, a 320 mm focal length lens was used at the generation side partially focusing the laser beam. Since the intention of the experiment was to study the cause of the unusual behaviour that occurs between 350 and 400 °C, the sample was only heated to a sample temperature of 530 °C. At lower temperatures the waveforms were obtained using single shots however above 370 °C in order to improve the signal to noise ratio, the signals were averaged several times.

Figure 6.3(a) shows the typical displacement waveform obtained on the alloy at room temperature. A longitudinal wave L and its echo 3L, and a shear wave S are clearly observed. A broad feature, possibly the L-L side wall reflected signal was also detected immediately after the shear wave signal. Other features were also observed after the 3L peak which might come from side wall mode converted signals. The feature directly following the S arrival could also be clearly observed on the velocity waveform (fig. 6.3(b)) obtained by differentiating the displacement waveform. The differentiated waveform should correspond to that detected by an EMAT since they

are velocity sensitive devices. The transit time of the broad feature was measured to be approximately 4.44 μs after the triggering of the laser pulse, slower by 0.61 μs than the shear wave signal.

It should be noted that with the plasma source used here, the directivity pattern of the longitudinal wave is almost spherical in shape with maximum intensity normal to the sample surface. Since the diameter of the sample is relatively small, reflection and mode conversion of the wave could easily occur at the side wall of the sample and arrive at the detector. The most distinct L-L wave should come from that generated at the centre of the sample, propagate to the middle of the side wall and reflect direct to the detection spot. From the calculations made, the distinct L-L wave should arrive 4.94 μs after the laser was fired if the detection laser was perfectly aligned at the centre of the sample (see fig. 6.1(a)), much slower than the measured value of 4.44 μs (from the waveform shown in fig. 6.3(a)). A possible reason for this error is that the Nd:YAG laser might have not impinged at the centre of the sample because there may have been a misalignment of the He:Ne laser that was used for the initial alignment of the Nd:YAG laser. As a consequence, the path length travelled by the L-L wave would be shorter and hence reducing the travel time. If we assume that the Nd:YAG beam is offset by 2 mm from the centre of the sample and the interferometer beam is offset by 1.5 mm on the same side of the sample as the Nd:YAG laser (see fig. 6.4), then the travelled time of the L-L wave is calculated to be 4.44 μs. In order to ensure that the error was due to misalignment, the room temperature measurement was repeated using a lens to reduce the detection spot to approximately 100 μm and the laser carefully aligned. In this case the measurement was made with the sample outside the furnace. The detected waveform obtained after

optimising the alignment of the sample and the two Nd:YAG beams is shown in fig. 6.3(c). The waveform was averaged 50 times. Similar to fig. 6.3(a) a clear feature could be detected between the S pulse and the 3L peak. The transit time of the feature was measured to be approximately 4.98 μs which is quite close to the calculated value of the L-L peak of 4.94 μs. Hence we can conclude that the feature observed between the S pulse and the 3L peak is the L-L side wall reflected signal. It is essential to note that in the case of the laser-EMAT system used for the thesis, the slight misalignment of 1 to 2 mm between the pulsed Nd:YAG laser beam and the EMAT detector is not critical for the measurement because the EMAT's coil width is approximately 8 mm which is reasonably large (see fig. 6.1), and the output from the EMAT is resulting from the convolution of the acoustic field over the active area of the transducer.

We observed that, as the temperature increased, the feature progressively merged with and distorted the shear wave pulse (see figure 6.5). Between 465 °C and 530 °C as shown in figure 6.6 the feature disappears, it is suspected that at these temperatures the feature is superimposed on the shear wave pulse. When the transit time is measured from the shear wave signal (distorted or not) and the calculated velocity plotted against temperature, an almost identical curve to that obtained by the laser-EMAT system was observed. This is shown in figure 6.7.

We have therefore demonstrated that the L-L side wall reflected signal detected between the shear wave pulse and the 3L peak progressively merges with the shear wave pulse as temperature increases. This distorts the shear wave pulse shape causing the unusual behaviour of the shear wave velocity between 350 and 400 °C.

6.2 Temperature Gradient Measurement

As the sample was heated near to the melting temperature, the flow rate of the cooling water supplied to the EMAT was increased to maintain the EMAT below 100 °C. The EMAT temperature was normally checked by finger contact with its front surface from time to time as the temperature increases. It is possible that with the increase in flow rate, the water-cooled EMAT will have a greater cooling effect on the sample, creating a temperature gradient across the sample thickness and causing errors in the measurement of the temperature dependence of the acoustic wave velocities. Therefore, an experiment was carried out to determine the extent of the effect of sample cooling by the water-cooled EMAT on the acoustic wave transit time measurements using the arrangement shown in figure 6.8.

A laser trigger box (LTB) with a delay timer setting between 0.7 s and 8.0 s was designed for this experiment (see fig. 6.9), enabling the laser to fire only after the EMAT has been in the measuring position at the sample surface for the pre-set time. The LTB was clamped onto the EMATs' stainless steel tube holder with its position adjusted so that the trigger button would start the laser fire sequence at the instant when the EMAT was in contact with the sample surface (fig. 6.9). Laser triggering was achieved when the trigger button was pushed against the adjustable stud fixed to the bush bearing. The sensitivity was checked by observing the amplitude of the detected acoustic wave signals, and maximum signal amplitude should be obtained at minimum lift-off. Minor adjustment of the lift-off was made by turning the stud clockwise or anticlockwise.

The experiment was carried out on a commercial aluminium alloy sample which was approximately 14 mm thick and 40 mm in diameter. Two K-type

Ni/Cr-Ni/Al thermocouples were used to measure the sample surface temperature on opposite sides of the sample. The thermocouple on the detection side was inserted into a 2 mm deep hole and connected to the temperature pre-amplifier, designed to have a sensitivity of approximately 4 mV/°C. The amplified signal then passed through a low pass filter to remove high frequency noise before the temperature cooling/heating curve was recorded on a LeCroy 9310 oscilloscope. The other thermocouple was connected directly to a Digitron temperature meter to provide the sample temperature reading at the generation side. A cable was also connected between the temperature pre-amplifier and the Digitron temperature meter to measure the absolute sample temperature reading at the detection side. The sample was heated in a standard split electric furnace with a ramp rate of 10 °C per minute to the set-point temperature of 550 °C and kept constant to that temperature. However due to heat losses, the sample only reached 500 °C and remained constant at that temperature.

The first temperature gradient measurement was made with a pre-set delay time of approximately 0.7 s. The second and third measurements were made with the delay time set to approximately 8 s, the latter being made to determine whether the cooling caused by the EMAT was detectable on the generation side. Every ultrasonic waveform was recorded in the LeCroy 9400A oscilloscope and transferred to the personal computer for subsequent analysis.

Figure 6.10 and 6.11 show the variation of the sample surface temperature at the detection side as a function of cooling/heating time when the water-cooled EMAT was allowed to be in contact with the sample surface for approximately 0.7 s, and 8 s, respectively before the laser triggers. From figure 6.10 it can be observed that when

the sample surface was cooled for about 0.7 s the surface temperature reduces by about 1 °C. The curve also shows that there was a delay of about 1.8 s between laser triggering and manually pulling the EMAT out of the furnace. During the delay, the curve indicates that the sample surface cooled quite rapidly with a slope of about 3 °C per second. Once the EMAT was pulled out of the furnace the surface temperature increases quite rapidly for about 1.5 s until it reaches approximately 499 °C. It then increases very slowly for another 1 °C until it reaches 500 °C and remains constant at that temperature until the next measurement. Figure 6.9 also shows that the cooling curve has an initial slope of about 3 °C per second which then reduces exponentially until the laser triggers, that is after the EMAT has been in contact to the sample for approximately 8 s. The cooling curve almost flattens when the EMAT was removed from the sample. Figure 6.12 shows the cooling curve of the sample surface obtained from the generation side, and it is clear that there is no observable cooling. This indicates that the cooling effect only reaches a certain depth from the detection surface even after the EMAT has been in contact with the sample surface for about 8 s, much longer than the 1 s typically taken to obtain the waveform.

Figure 6.13(a) shows the waveforms obtained from an aluminium alloy where the sample surface temperatures on the detection side are 499 °C and 491 °C as a result of the EMAT being in position for approximately 0.7 s, and 8 s, respectively. The strong, sharp longitudinal wave signals and weak, broad shear wave signals provide an indication of the high degree of ablation. Mode converted signals due to the boundary conditions at the sample surface were also detected. Figure 6.13(b) shows the expanded waveforms of the longitudinal wave pulse, it is clear that there is hardly any difference in the longitudinal wave transit times in both cases. The

difference was measured to be only 2 ns. Figure 6.13(c) shows the expanded waveforms of the shear wave pulse, a difference of the order of 24 ns in the transit times could be observed, which corresponds to a velocity difference of 12 ms^{-1}. In terms of the longitudinal to shear transit time ratio the difference was found to be only 0.002.

From the experiment, it was observed that the sample cooling due to the water-cooled EMAT only reduces the temperature at the sample surface and does not cool the whole sample since the sample surface temperature reading at the generation side was unaffected. Only slight differences in the acoustic wave's transit times were measured even with a surface temperature difference of 8 °C. Hence, it is concluded that the sample cooling due to the water-cooled EMAT does not have a significant effect on the accuracy of the transit time measurements and the cooling is superficial. In practice, the EMAT is in contact with the sample for less than one second for a typical measurement and the laser could be fired 100 μs after the EMAT contact if necessary.

6.3 Comparison Between Pulsed Nd:YAG and CO_2 Lasers as Ultrasound Generators at Elevated Temperature

The pulsed Nd:YAG laser used in the study has a wavelength of 1.06 μm which is the near infrared region of the electromagnetic spectrum. It is invisible and hazardous to the human eye. An unfocused Nd:YAG beam has a diameter of approximately 5 mm. A pulsed CO_2 laser which is well into the infrared region (wavelength 10.6 μm) is less hazardous compared to the Nd:YAG laser. However,

because of its longer wavelength most of its energy tends to be reflected from a metal surface and the amount absorbed is only sufficient to generate a thermoelastic acoustic source. The CO_2 laser used for the comparison has a square profile beam of approximately 25 x 25 mm.

The amount of incident laser energy reflected by the sample depends on the nature of the sample and the wavelength of the radiation. For most metals, and for electromagnetic radiation in the visible part of the spectrum the reflectivity of a clean sample can be approximately expressed as [Scruby and Drain, 1990] :-

$$R = 1 - 4/(\mu_o \sigma c \delta) \qquad (6.1)$$

where δ is the skin depth which is expressed as $(\pi\sigma\mu_r\mu_o\varpi)^{-1/2}$, μ_o and μ_r are the permeability of free space and relative permeability of the material respectively, σ is the conductivity, c is the velocity of light and ϖ is the angular frequency of the laser light. Typically a metal absorbs 10 to 50 per cent of the Nd:YAG beam depending on the material, and acts as a good mirror to a CO_2 beam absorbing less than 10 % of the energy. The reflectivities of a polished aluminium surface and a polished steel sample are 98.7 % and 90 % respectively at a wavelength of 10.6 μm [Edwards et. al., 1989]. Hence the first three laser mechanisms described in chapter 3, namely, thermoelastic, ablation and the source due to a constrained surface can be used to generate ultrasound with sufficient efficiency using the pulsed Nd:YAG laser, however the ablation source leaves a small (1 μm) damage pit on the sample surface. The size of the damage is too small to be of concern in this study. Studies of the CO_2 laser as an ultrasound generator have been reported by Taylor, [1992]. Since only a small amount of the CO_2 laser energy is absorbed at the sample surface, the air breakdown source

(described in section 3.1.1.4) which is a perfect non-destructive source needs to be used for ultrasonic generator using the CO_2 laser.

The experimental arrangement for the measurements is shown in figure 6.14. The Coherent (Hull) Minibrand Transversely Excited Atmospheric (TEA) CO_2 laser used is capable of producing 2 J laser pulses. The CO_2 laser has approximately one quarter of its energy in a 50 ns spike followed by a lower power tail lasting for 1 to 2 μs. It is the fast spike that is responsible for the ultrasonic generation. Detection was achieved by a water-cooled spiral coil EMAT described in chapter 4. An antireflection biconvex lens was used to focus the laser beam just in front of the sample surface to produce the air breakdown ultrasonic source. In this case the lenses used for the study were either germanium or zinc selenide. The zinc selenide lens with a focal length of 100 mm was used for the experiments on the lower melting point aluminium alloy sample while the germanium lens with a longer focal length of 200 mm was used on the higher melting point M2 tool steel sample. The parallel sided aluminium alloy sample was mounted on two parallel stainless steel tubes lying horizontally across the furnace. In the case of M2 tool steel, the sample was held by an existing specially designed stainless steel holder that was mounted on the parallel stainless steel tubes mentioned earlier. The sample temperature was measured using a Type K Ni/Cr-Ni/Al thermocouple with its tip inserted about 2 mm into the aluminium alloy sample, and in the case of the M2 tool steel sample the thermocouple was just in contact with the sample surface at the generation side. The sample was heated in a 200 mm cylindrical bore electric furnace. An alumina fibre board with approximately 30 mm aperture was placed between the lens and the furnace to protect the lens from radiant heat and also to reduce heat losses. An alumina fibre board was also placed at the end of the furnace

at the detection side to reduce heat losses and to protect the EMAT detector from the radiant heat. As usual the EMAT was momentarily brought into contact with the opposite face of the samples to capture the ultrasonic waves and pulled out of the furnace as soon as the waveform had been recorded on the oscilloscope. The amplified waveform was band pass filtered before being stored on the personal computer for subsequent analysis.

Various ultrasound generation mechanisms in metals have already been extensively investigated for the Nd:YAG laser source. For the aluminium alloy and the M2 tool steel results presented here two geometries were used, firstly with a silica window constraining the sample surface and secondly using the ablation mechanism. Both give good sensitivity to both longitudinal and shear waves over a wide temperature range. The CO_2 results were taken using the air breakdown mechanism giving a strong longitudinal source. The larger source dimensions also give better source directivity.

Figure 6.15 shows the waveforms obtained using the Nd:YAG laser on an approximately 12 mm thick Al 4.86 % Si alloy up to sample temperature of 500 °C. Figure 6.16 shows the corresponding waveforms obtained with the CO_2 laser on a commercial aluminium alloy approximately 20 mm thick over the same temperature range. Both figures show strong and sharp acoustic wave signals detected at room temperature, and a decrease in the signal amplitude with increasing temperatures. In this case comparison was not made on the same Al 4.86 % Si alloy because of two reasons. Firstly, the Al 4.86 % Si alloy supplied was approximately 33 mm in diameter only slightly larger than the dimension of the CO_2 laser beam of 25 mm x 25 mm. Secondly, the sample was heated in the large diameter bore electric furnace, therefore

in order to use the existing set-up available for the furnace, a larger diameter and thicker sample was prepared. Figure 6.17 shows similar waveforms obtained on thixoforgeable M2 tool steel up to 912 °C, anomalously high signals are obtained for both the Nd:YAG and CO_2 lasers at 762 °C, which should be just above the Curie temperature. Similar to that explained in chapter 5 for the mild steel at 775 °C, the enhanced sensitivity to longitudinal wave may be due to the EMAT cooling a thin skin of the material back into the ferromagnetic phase causing a concentration and redistribution of the EMATs magnetic field and/or is possibly due to volume magnetostriction. Also as explained in chapter 5 it is possible for volume magnetostriction to occur if near the Curie temperature the saturation magnetisation (M_s) is below the level of field which can be obtained from an EMAT. At the highest temperature the Nd:YAG waveform has better signal to noise ratio than the CO_2 where the arrivals are almost indiscernible. The metal should be in the austenitic state at this temperature where the ultrasound attenuation due to scattering is very high [Tripathi and Verma, 1973].

In conclusion the pulsed Nd:YAG and CO_2 lasers have similar performance on the low temperature aluminium alloys, but the Nd:YAG laser is more efficient at the higher temperatures. The CO_2 laser should therefore be preferable for industrial applications on low temperature aluminium alloys because the scattered laser beam can be absorbed by only few millimetres thick of plastic, and lesser safety procedure is needed. However for higher temperature materials a pulsed Nd:YAG laser is preferable.

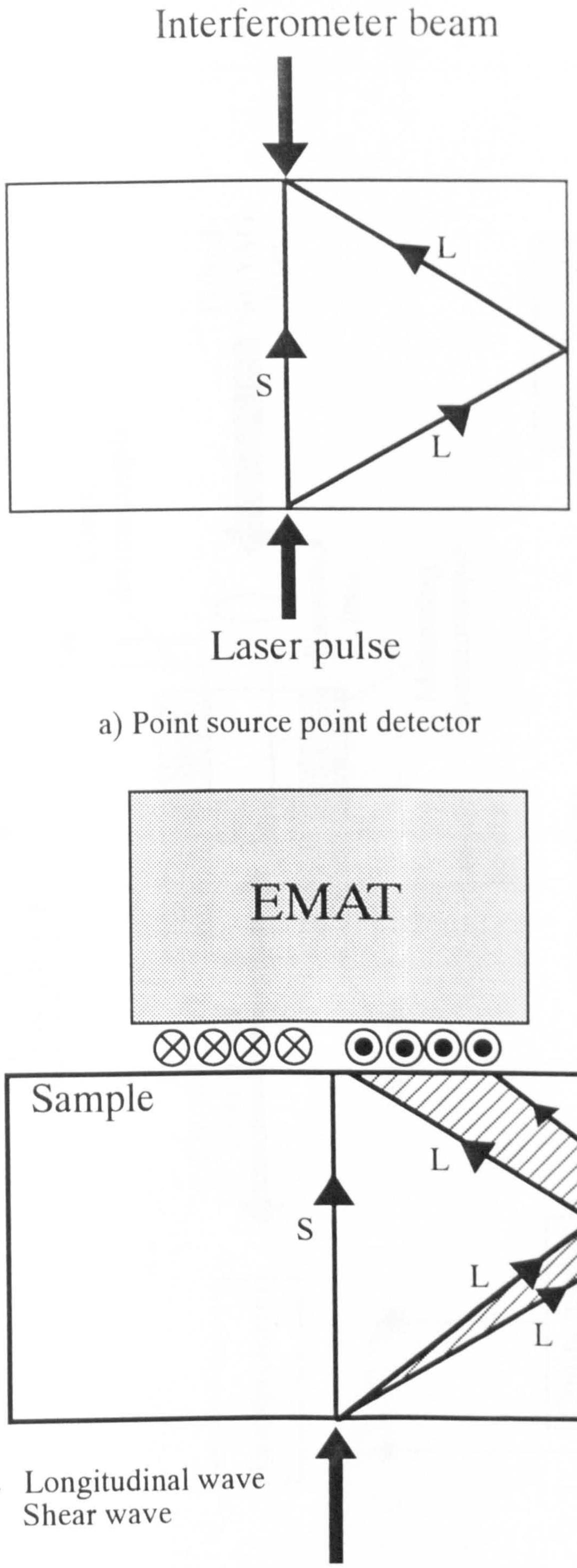

Fig. 6.1 The effect of detector size on the spatial resolution.

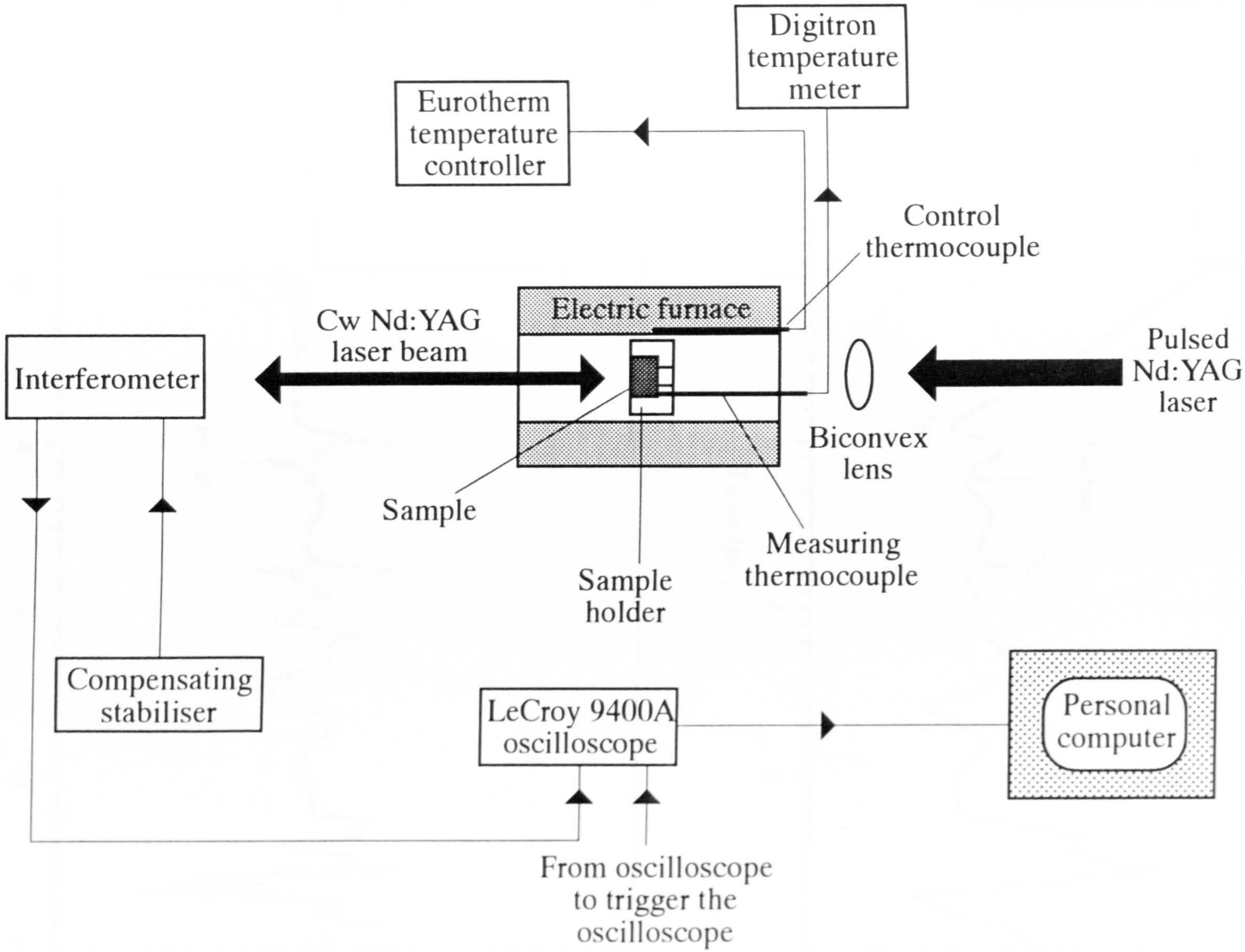

Fig. 6.2 Experimental arrangement for the laser-laser system.

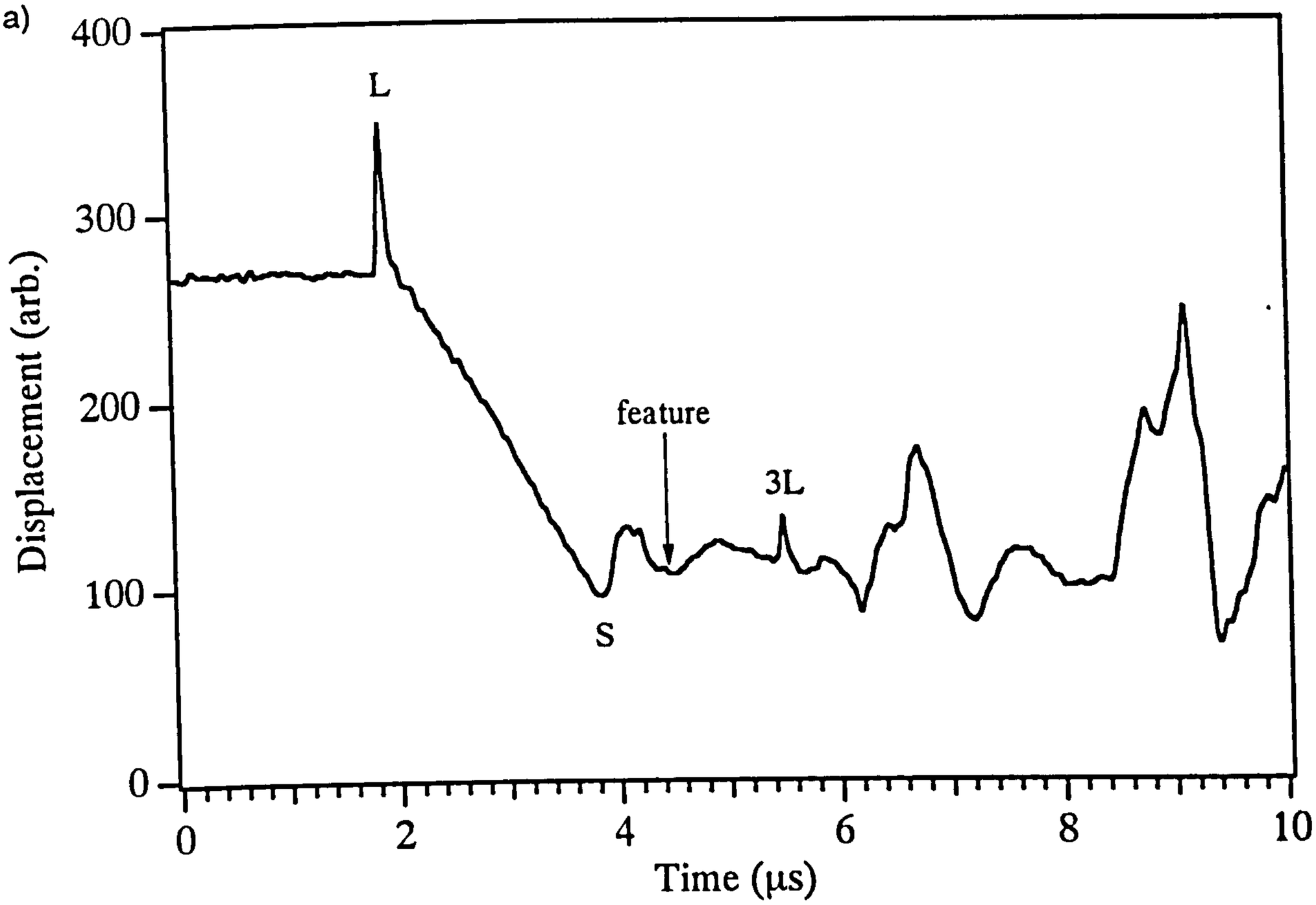

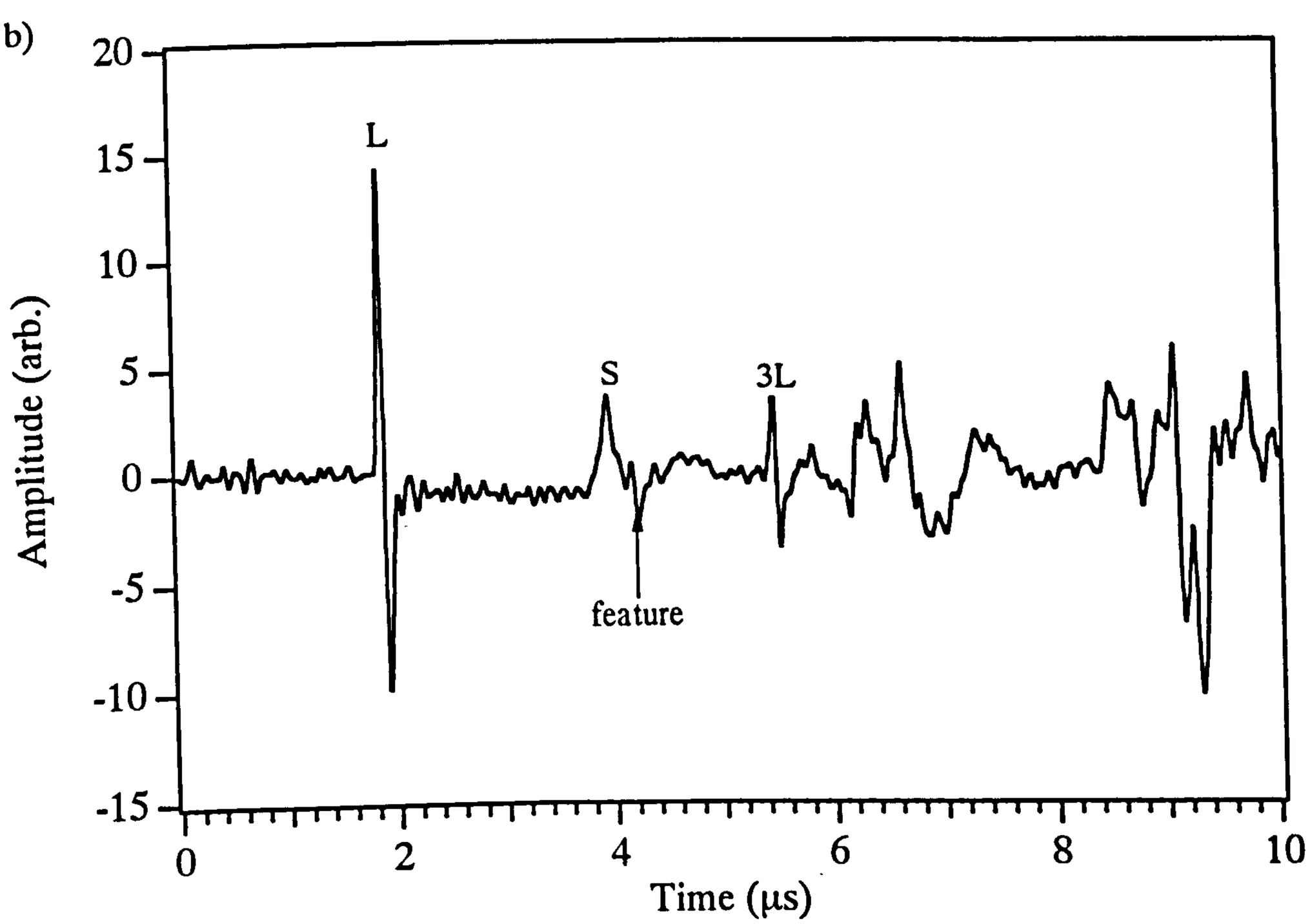

Fig. 6.3 a) Displacement and b) velocity waveform of Al 4.86 % Si alloy at room temperature.

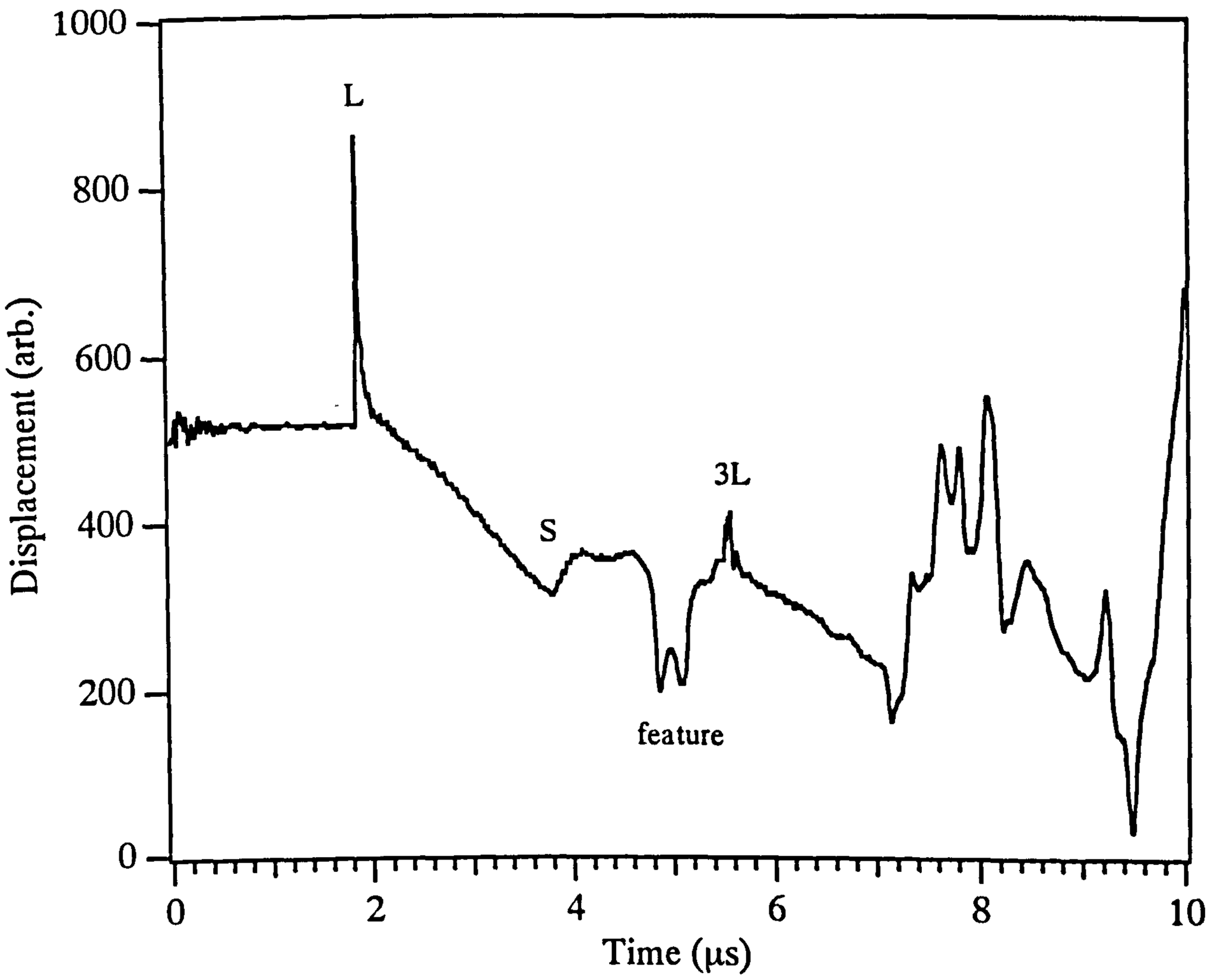

Fig. 6.3(c) Waveform obtained on the Al 4.86 % Si alloy at room temperature with a better interferometer and Nd:YAG beams alignment.

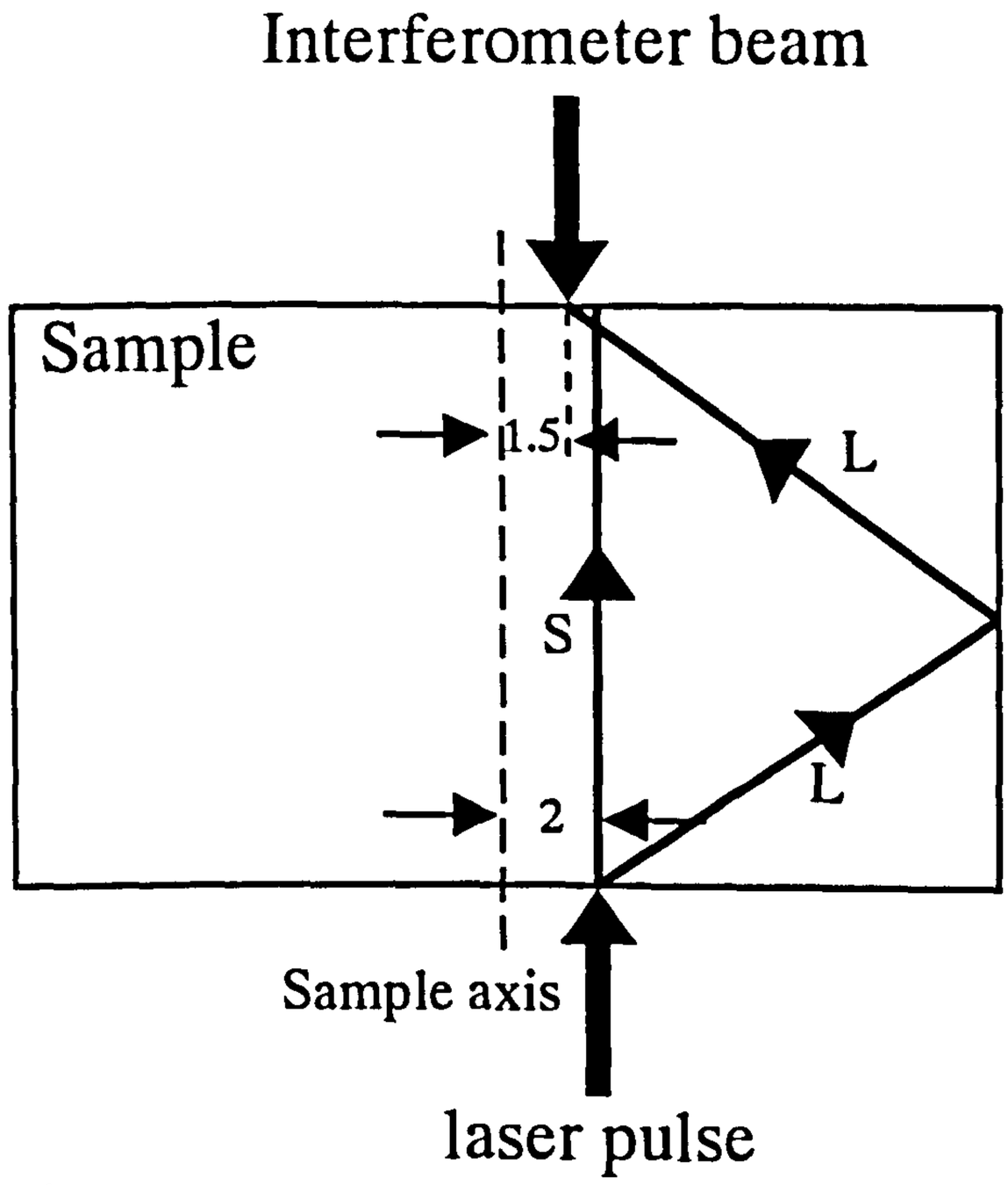

L Longitudinal wave
S Shear wave
Unit of offset: in mm

Fig. 6.4 Showing the misalignment of the two generation and detection Nd:YAG beams from the central axis of the sample.

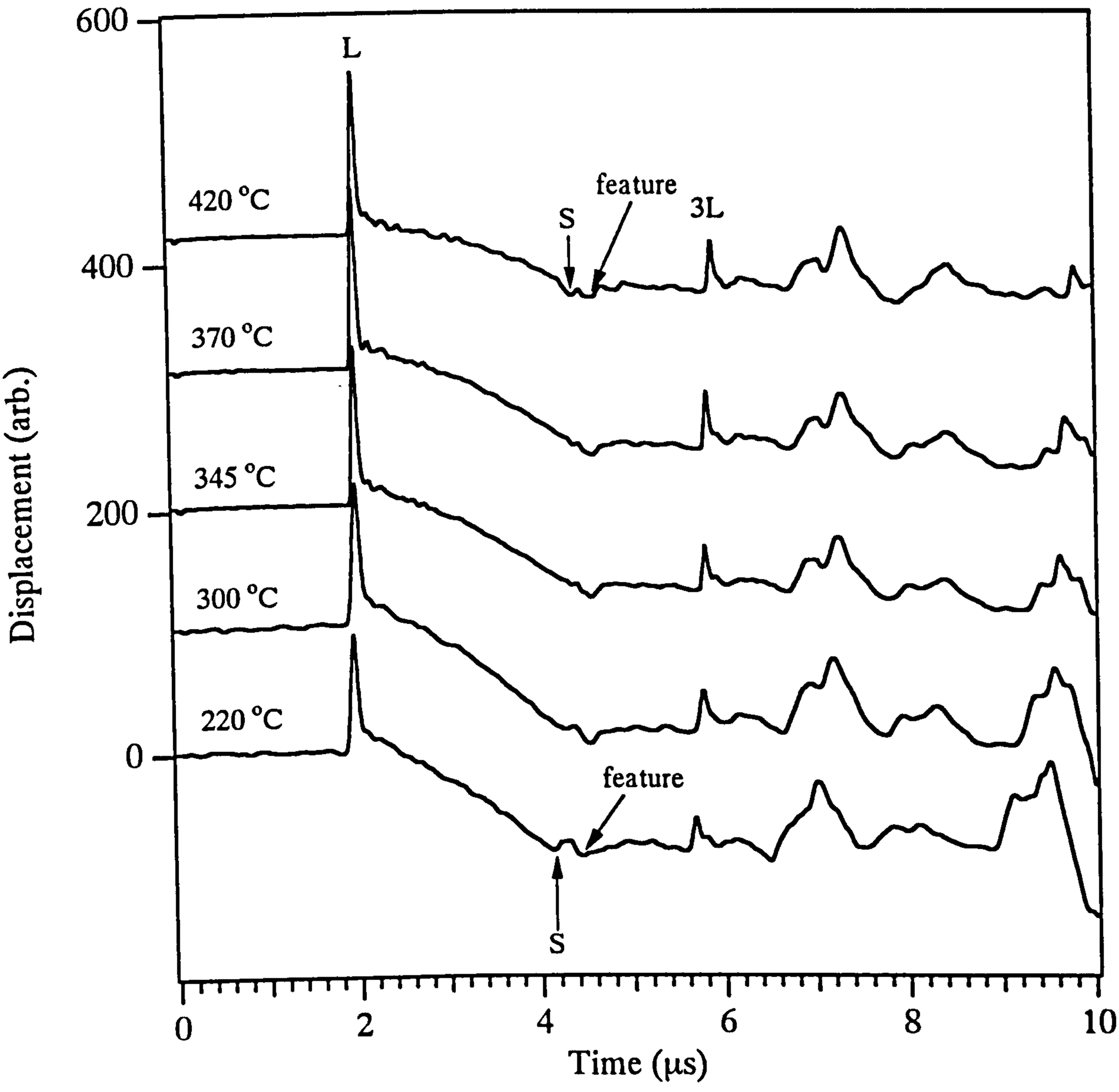

Fig. 6.5 Graph showing the distortion in the shear wave signal shape with progressive increase in temperature.

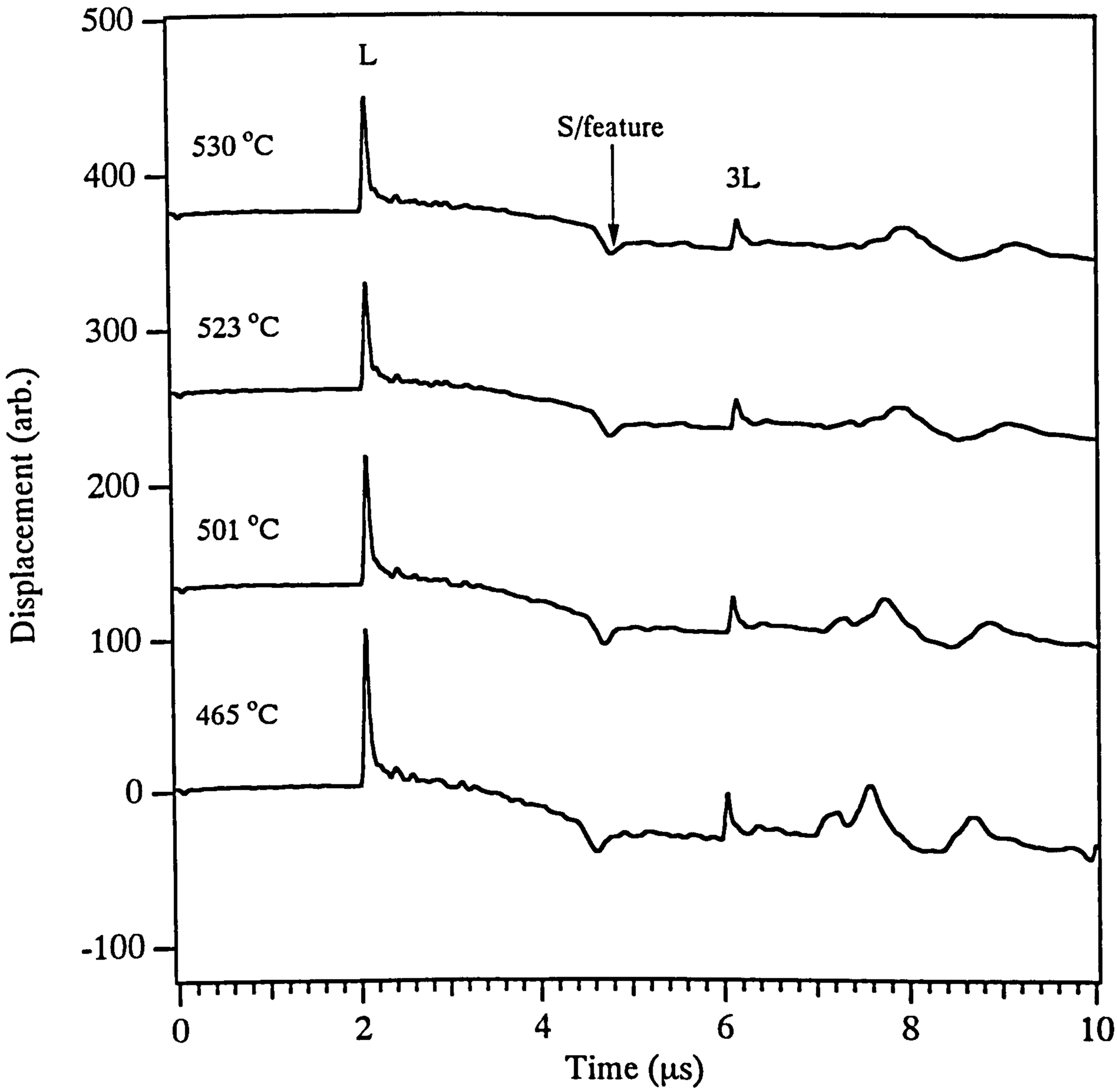

Fig. 6.6 Graph showing the disappearance of the feature at temperatures between 465 °C and 530 °C.

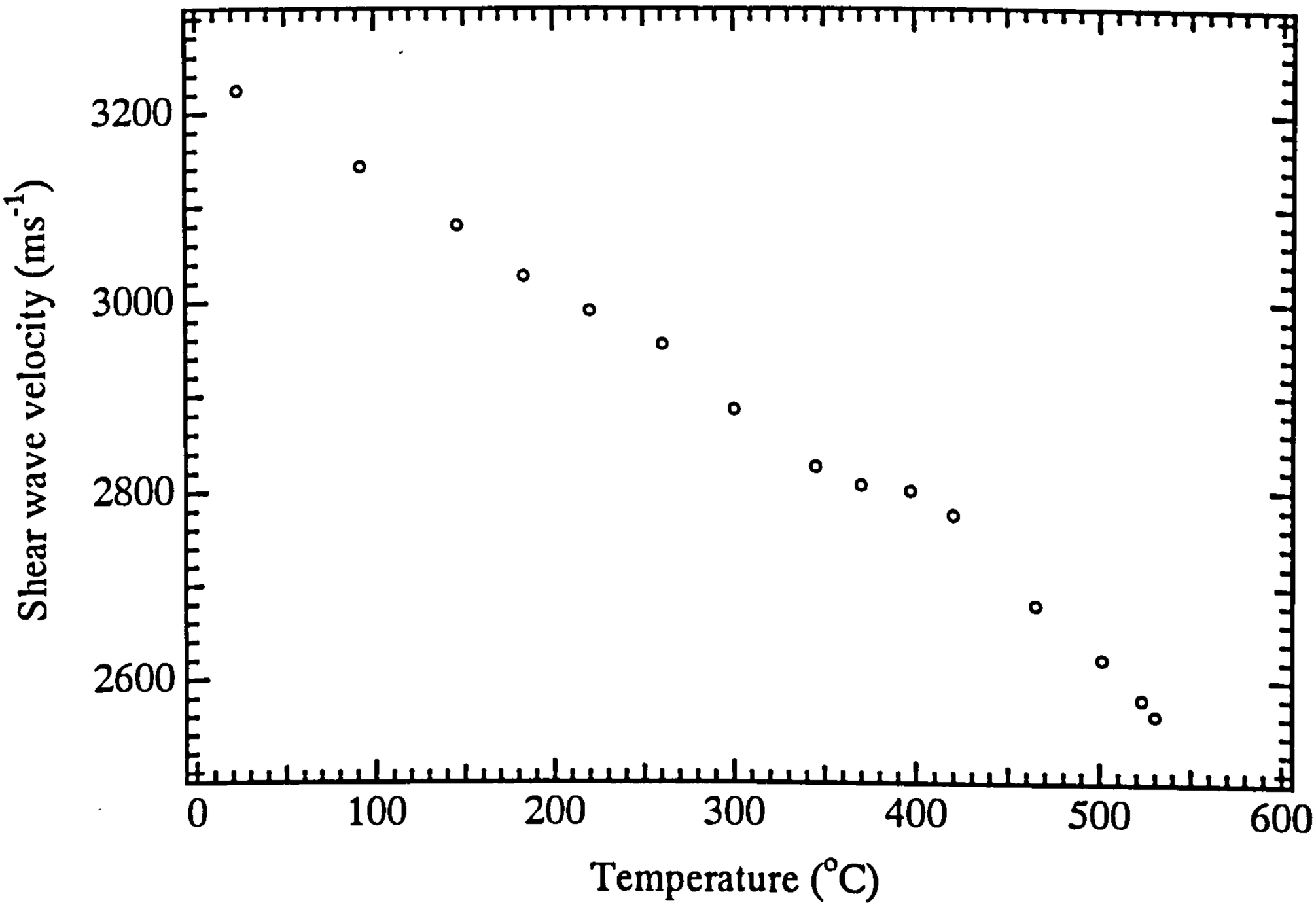

Fig. 6.7 Shear wave velocity variation as a function of temperature in Al 4.86 % Si alloy using Nd:YAG pulsed laser as the ultrasound generator and an interferometer as the detector.

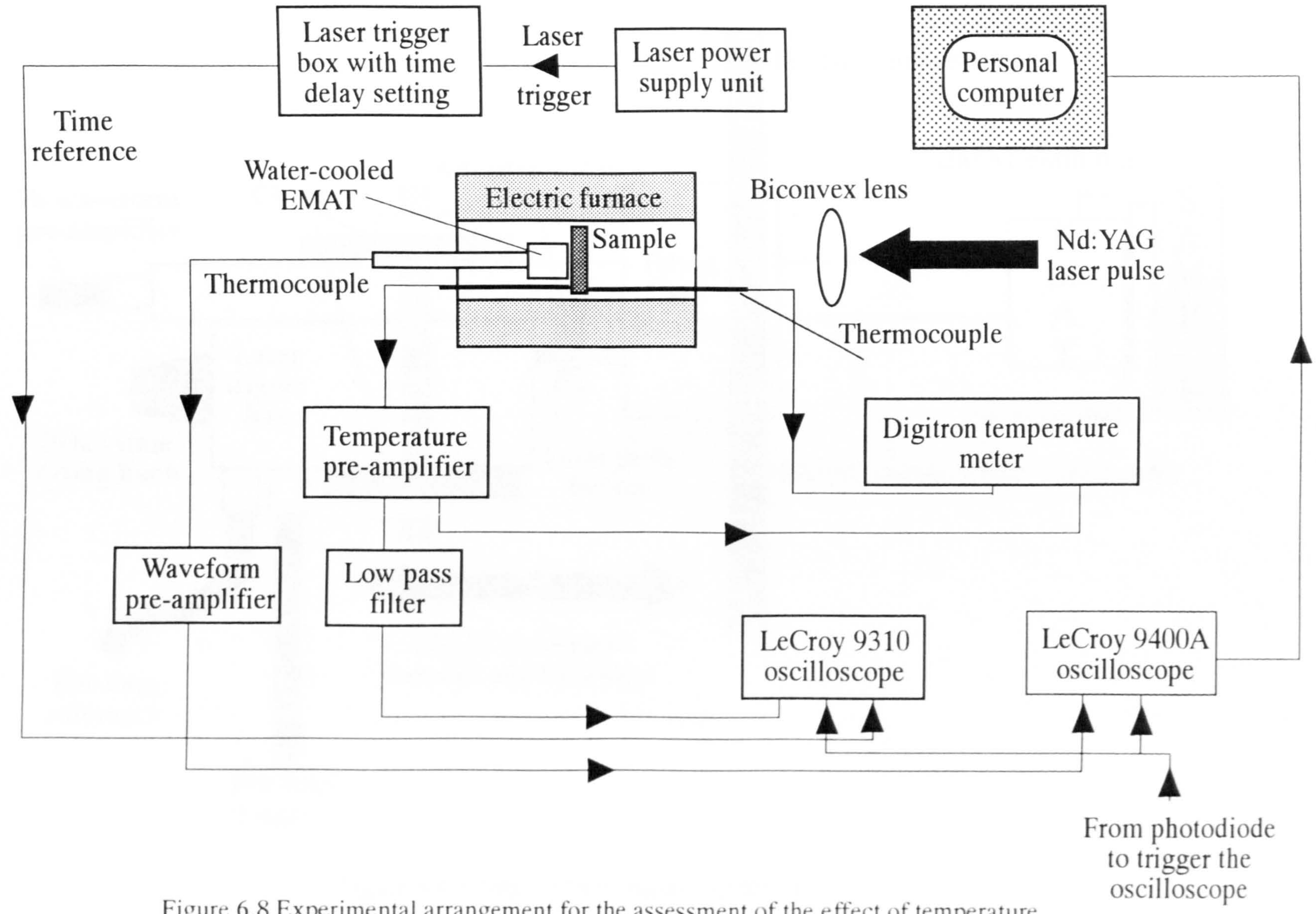

Figure 6.8 Experimental arrangement for the assessment of the effect of temperature gradients

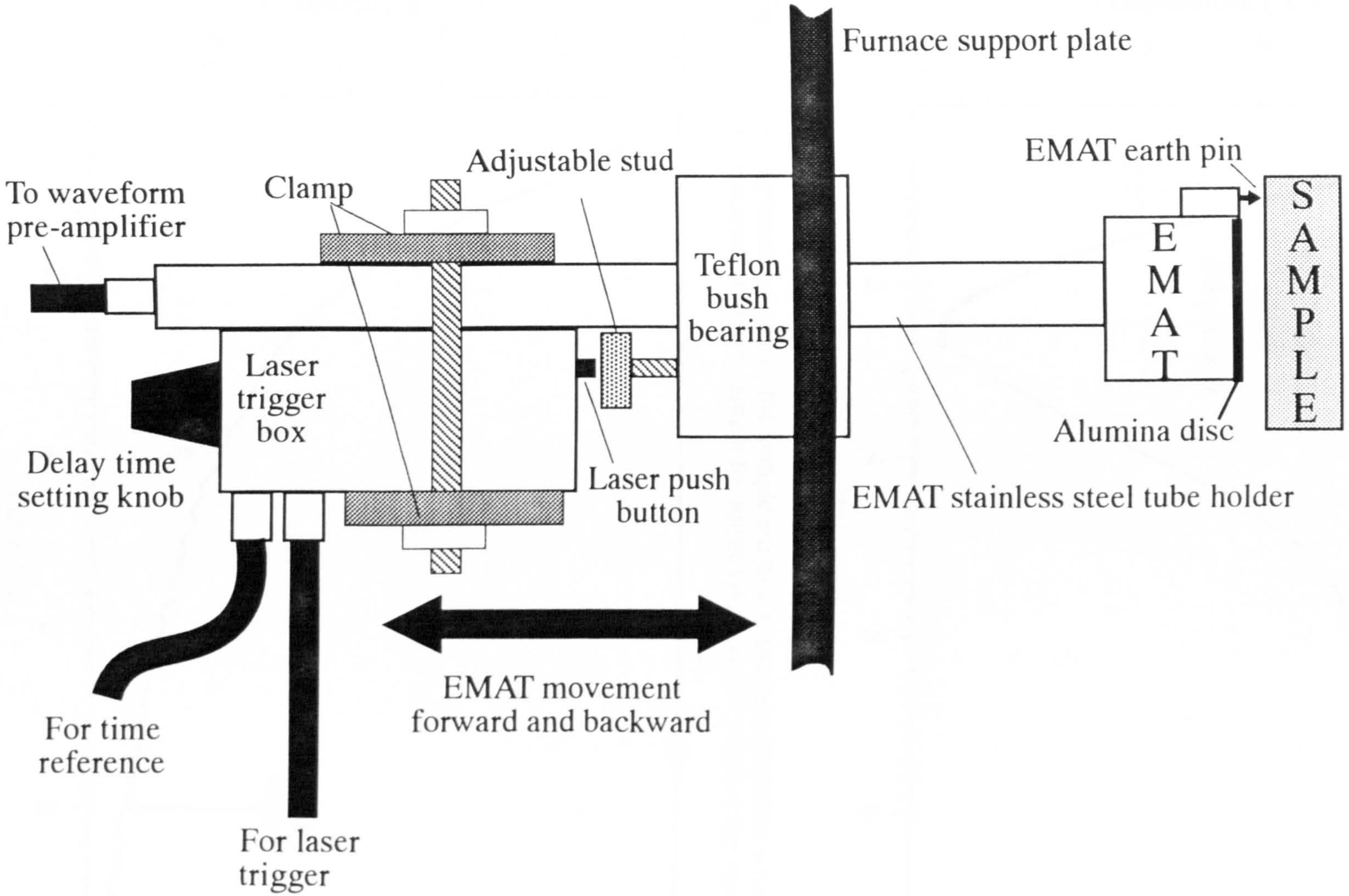

Figure 6.9 Set-up for laser trigger adjustment.

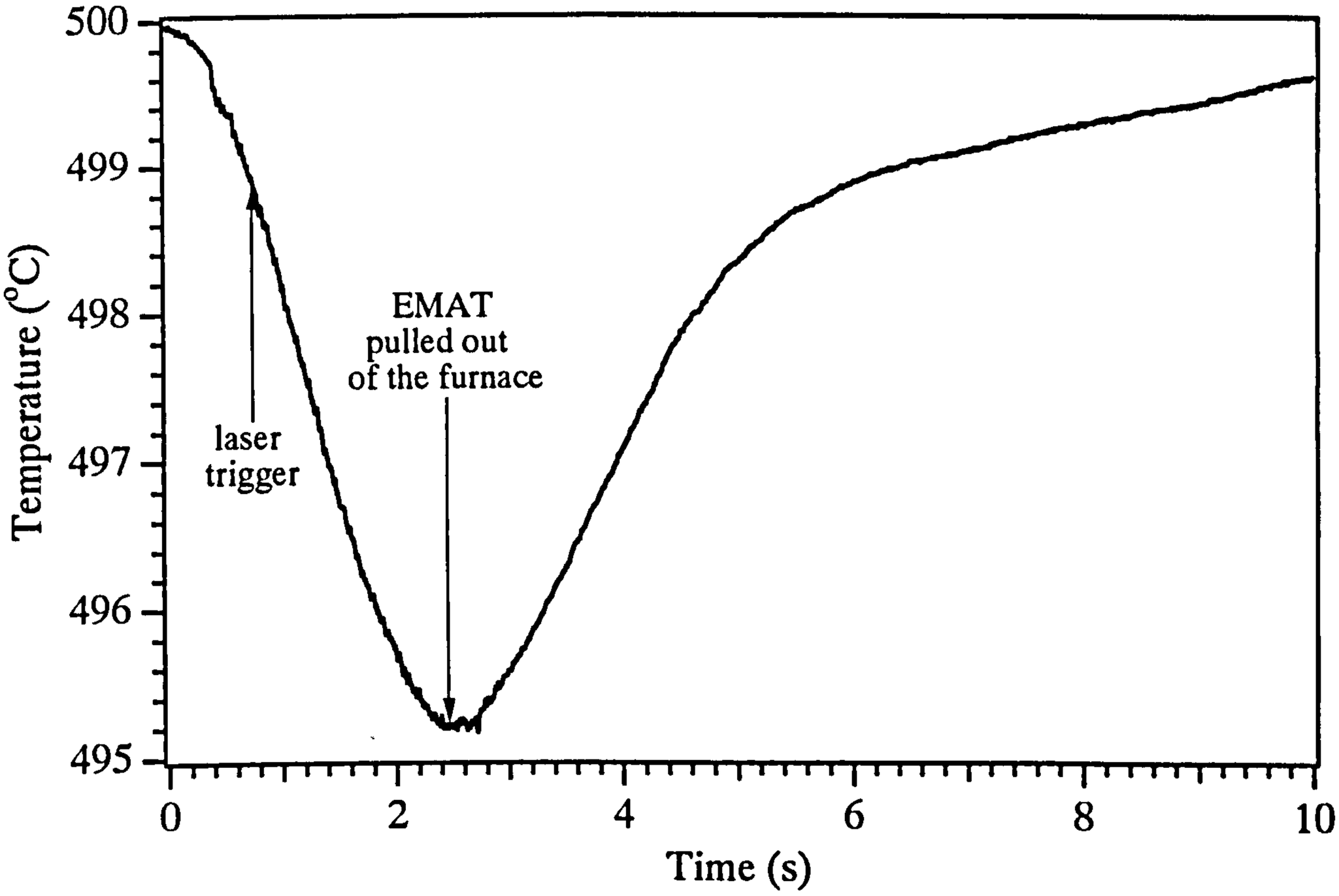

Fig. 6.10 Cooling/heating curve of the sample surface at the detection side when the EMAT was in contact with the sample for approximately 0.7 s before the laser triggers.

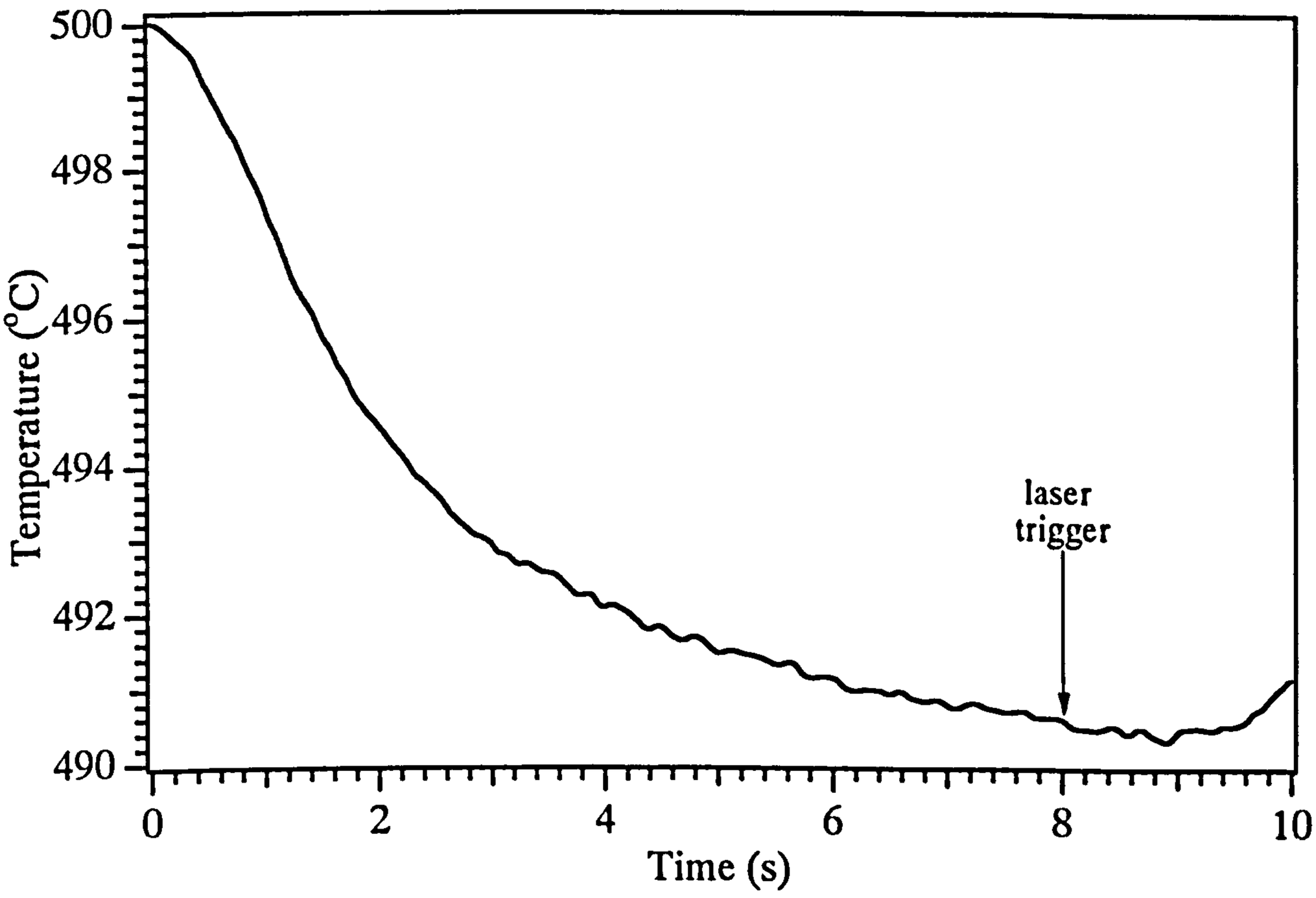

Fig. 6.11 Cooling curve of the sample surface at the detection side when the EMAT was in contact with the sample for approximately 8 s before the laser triggers

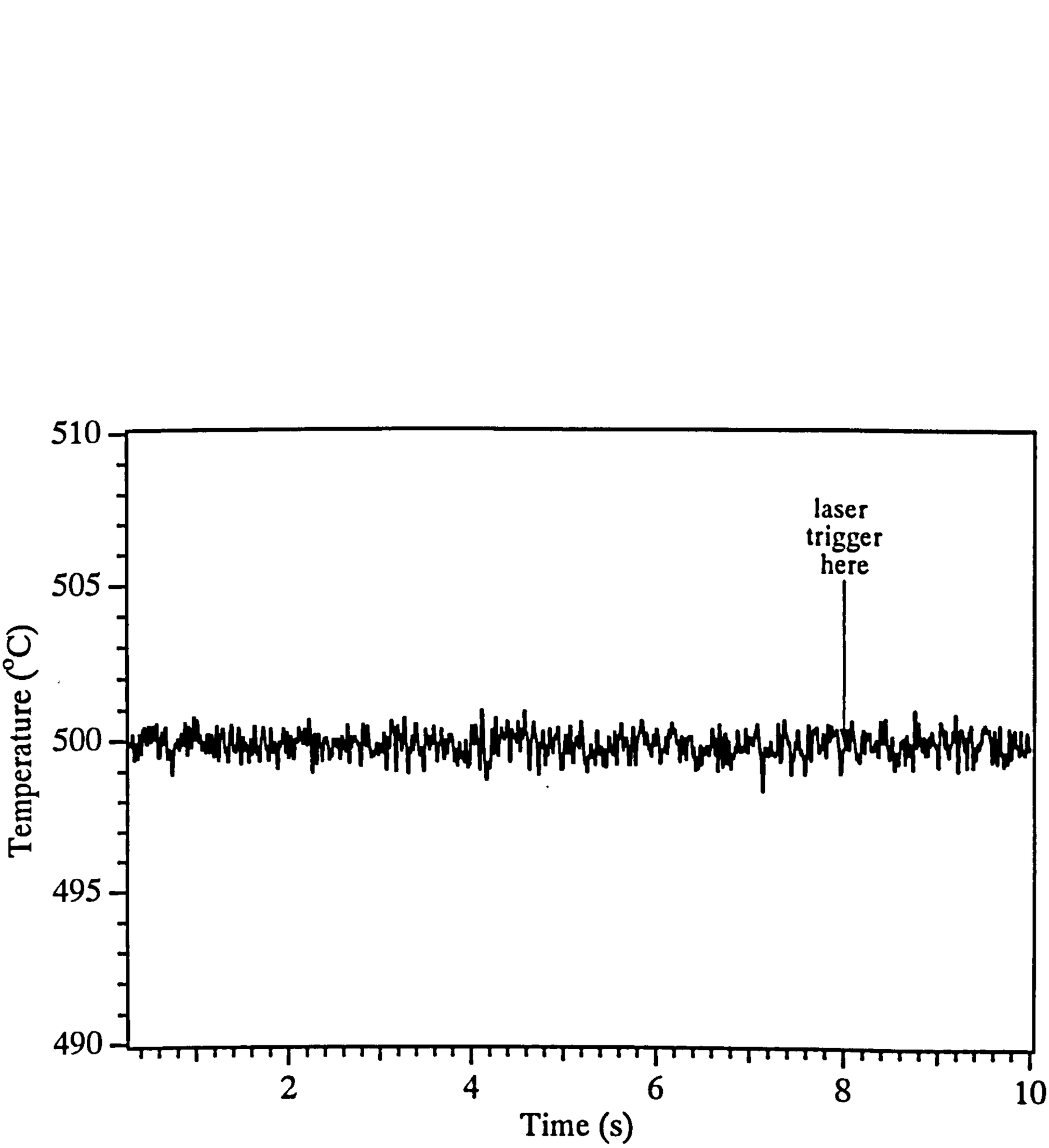

Fig. 6.12 Cooling curve of the sample surface at the generation side after the EMAT has been in contact with the sample for approximately 8 s.

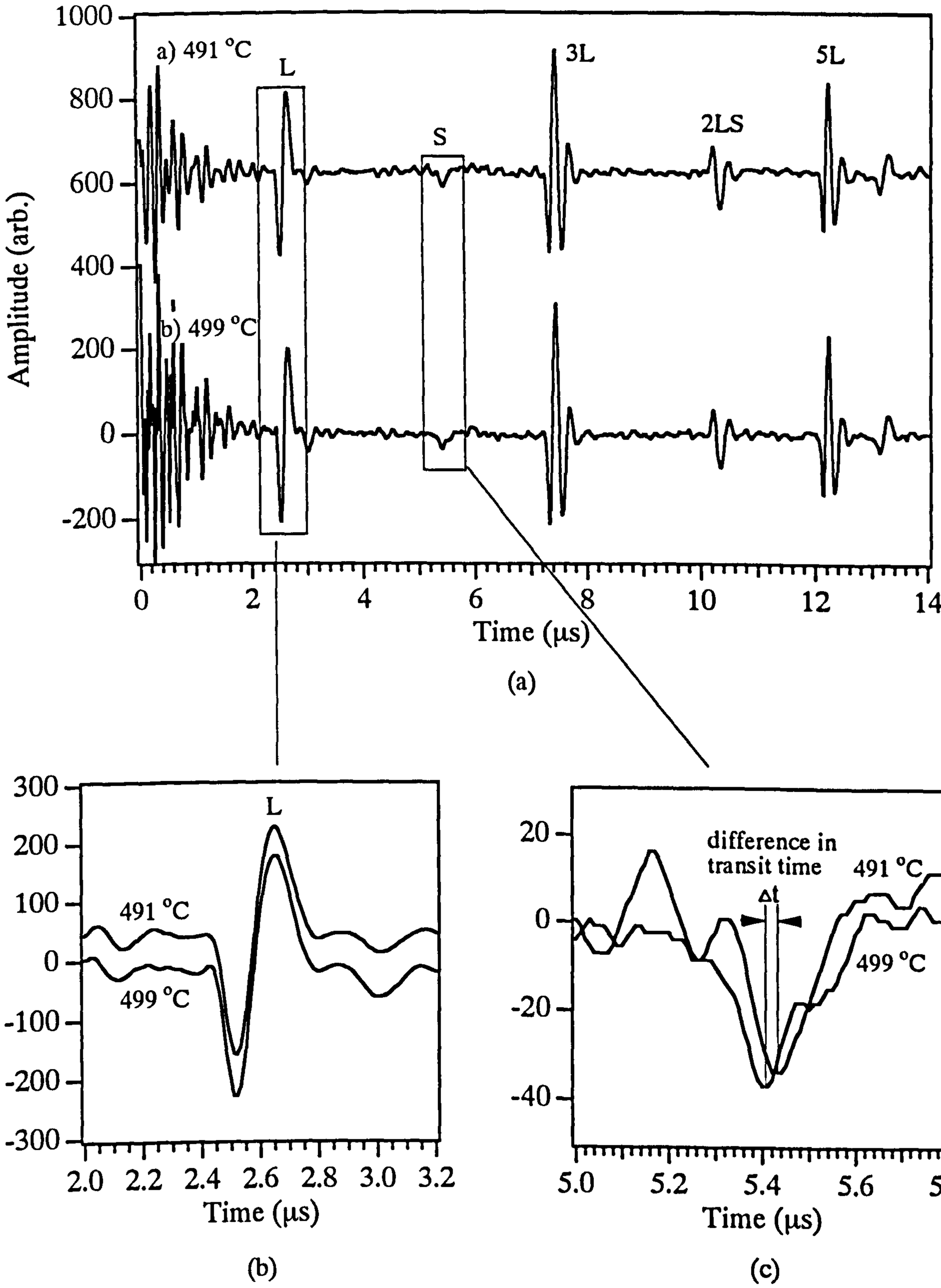

Fig. 6.13 (a) Waveforms obtained from an aluminium alloy at the detection sample surface temperature of 491 and 499 °C, (b) expanded waveforms of the longitudinal wave pulse and (c) expanded waveforms of the shear wave pulse.

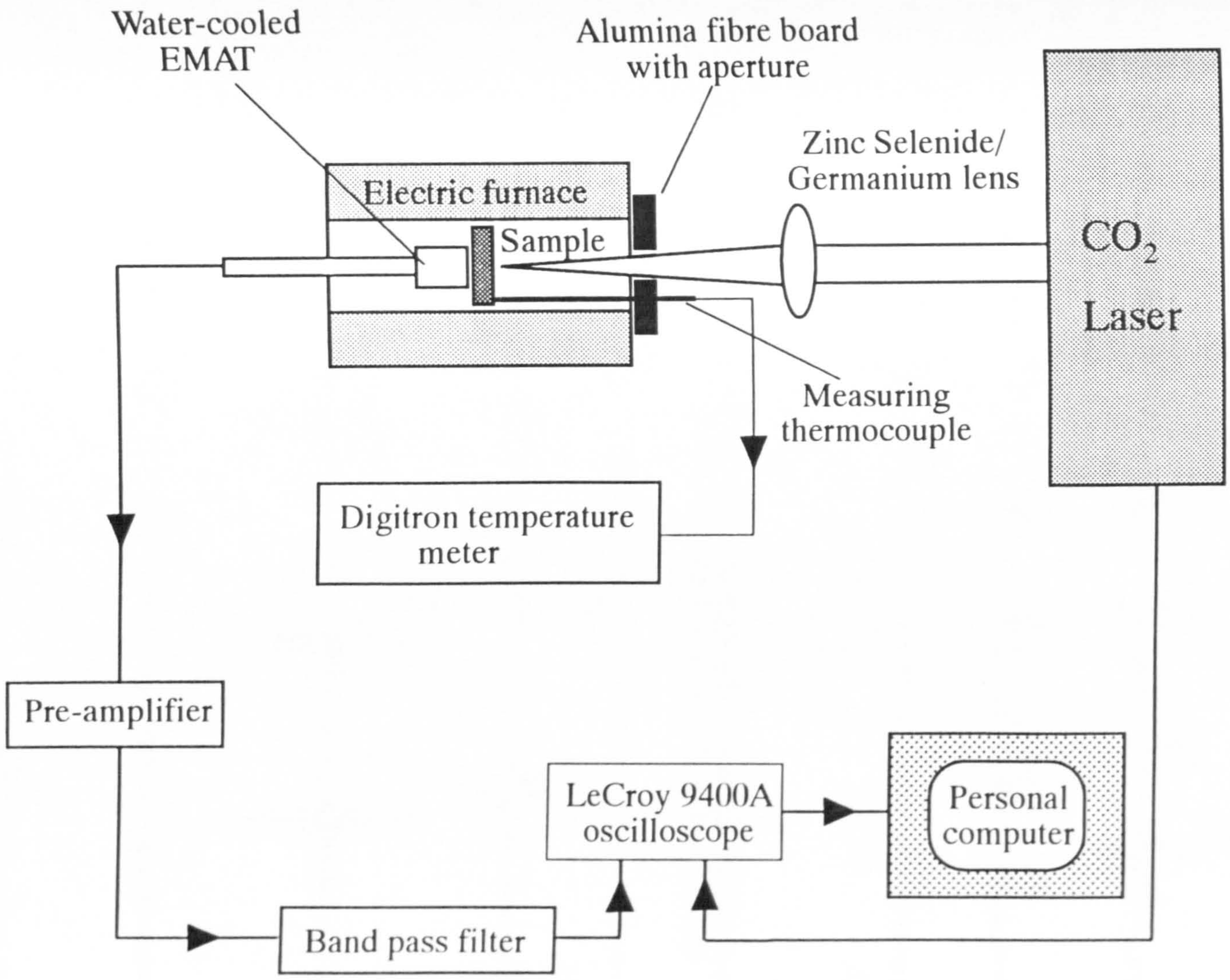

Fig. 6.14 Experimental arrangement for the CO_2-EMAT system.

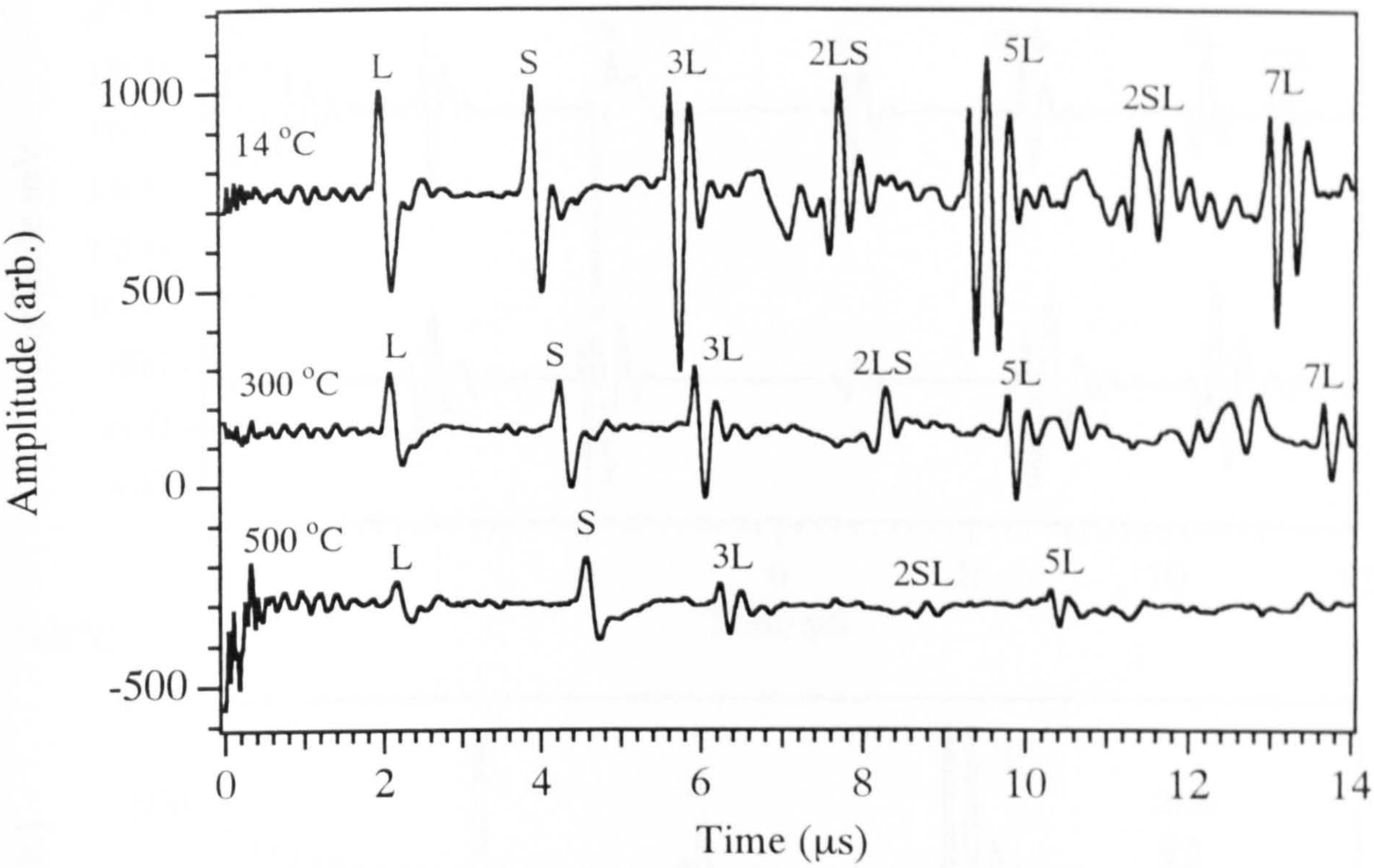

Fig. 6.15 200 mJ Nd:YAG laser with a silica window constraining the approximately 12 mm thick Al 4.86 % Si alloy surface on the generation side.

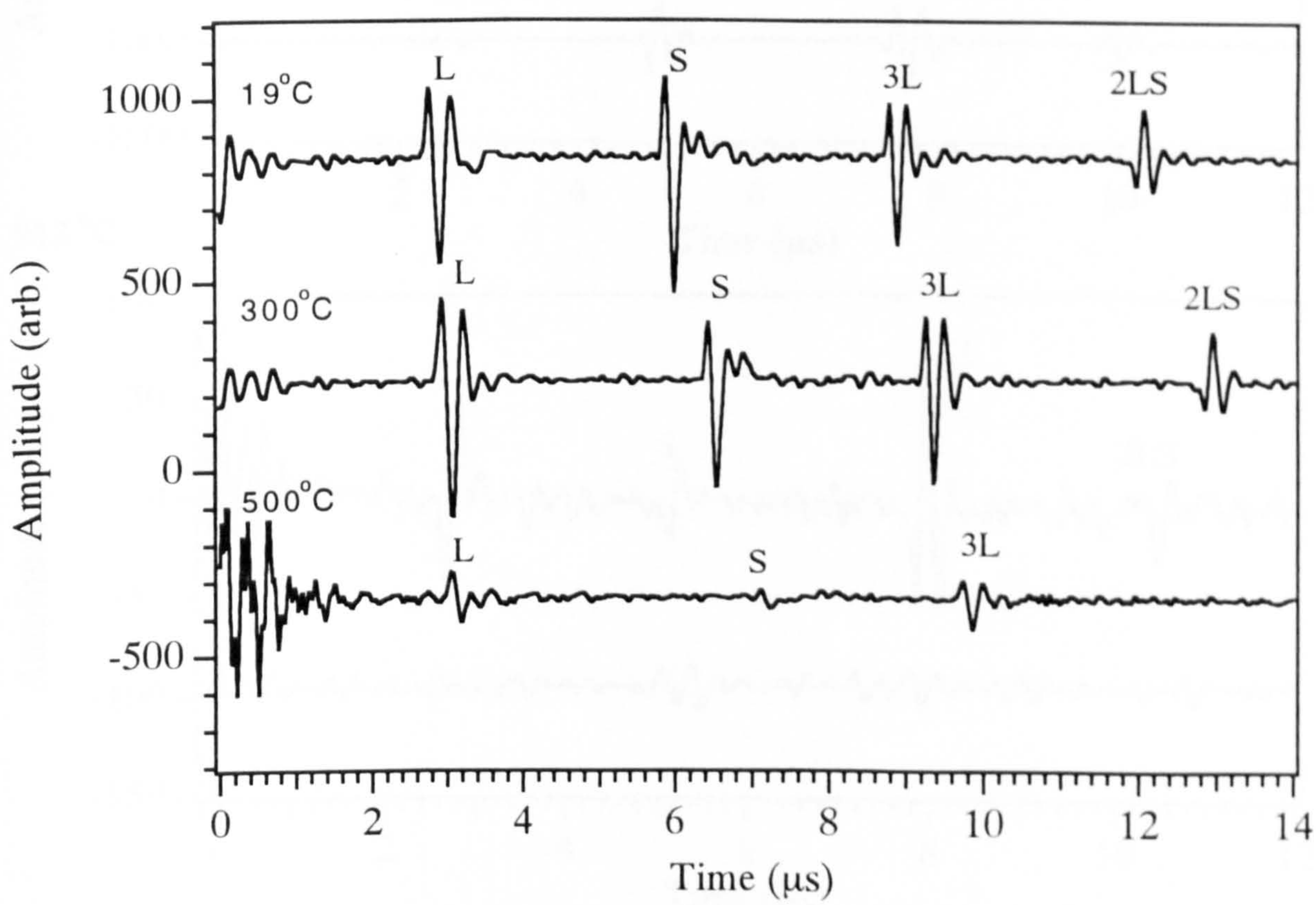

Fig. 6.16 CO_2 laser on approximately 20 mm thick aluminium alloy.

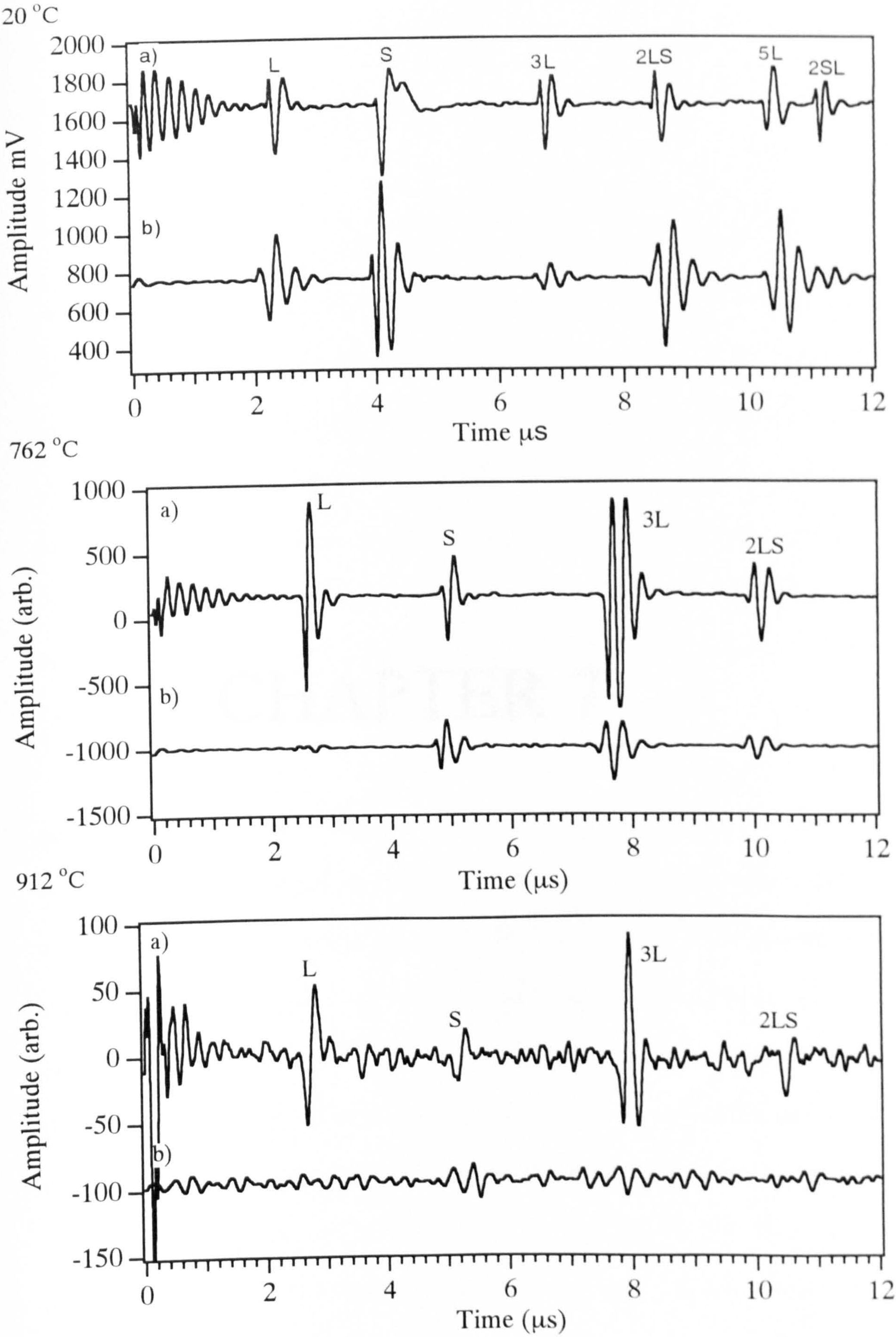

Fig. 6.17 a) Nd:YAG and b) CO_2 waveforms on M2 tool steel.

CHAPTER 7

CHAPTER 7

CONCLUSIONS AND FURTHER WORK

The work reported in this thesis has demonstrated that the laser-EMAT system is capable of making acoustic wave measurements not only in the semi-solid state but also into the fully molten state. The onset of melting had a marked effect on the ultrasonic propagation causing either a sharp drop in both the bulk wave velocities, or a sharp drop in the longitudinal wave velocity coupled with the total disappearance of the shear wave signal. The onset temperature could also be detected by the sudden drop in the ratio of the longitudinal to shear wave transit time. With the laser-EMAT system described in the thesis measurements have been made to sample temperatures as high as 1140 °C.

The ultrasound system comprised a pulsed Nd:YAG laser as the ultrasound generator and a water-cooled spiral coil permanent magnet EMAT as the detector. When either a weak ablation source or thermoelastic source on a constrained surface is used as the generation mechanism, the system enables both the longitudinal and shear waves to be generated and detected simultaneously. An ultrasonic cell was designed to contain and to maintain the geometry of the thixoforgeable alloy during the melting process. The cell consisted of a stainless steel sample holder, an alumina disc supporting the sample surface on the detection side and a transparent silica window supporting the sample surface on the generation side. This enables measurements to be made well into the partially molten state and even into the fully liquid state for the case of longitudinal waves.

Chapter 3 described the various non-contacting ultrasonic systems, either laser-laser, laser-EMAT or EMAT-EMAT that have been used for investigations on different types of commercial materials at elevated temperatures. We believe that the work discussed in this thesis is the first demonstration of a non-contacting ultrasonic system capable of making measurements not only above the solidus temperature but also well above the liquidus temperature.

7.1 Performance of the Laser-EMAT System on Al-Si alloys

The performance of the designed laser-EMAT system on Al-Si alloys is very encouraging. Acoustic wave measurements on the thixoforgeable alloys were made up to a liquid fraction of 50 to 60 % into the semi-solid state, a condition that is suitable for thixoforming. In the case of the commercial Al 1.2 % Si alloy measurements were made throughout the mixed solid/liquid phase. The system has also proved its capability for making measurements in the fully molten state on all the alloys heated above the liquidus temperature. Strong longitudinal pulses and their subsequent echoes could be detected in the liquids of the Al 4.86 % Si alloy and the Al 1.2 % Si alloy, however only the direct longitudinal transit could be detected on the LM25 alloy.

Approaching the onset of melting, problems were encountered similar to those faced by McKie, [1987] and Edwards et. al., [1992] using the laser-laser system. The detected shear wave signals were weak and broad even after the laser power density was reduced to maintain the laser source close to the ablation threshold. Another problem encountered was the change in the shear wave polarity around the onset of

melting. Both the problems mentioned above affected the accuracy of the shear transit time measurements.

7.2 Performance of the Laser-EMAT System on High Melting Temperature Alloys.

The liquidus and solidus temperatures for the Cu 10.2 % Sn alloy occur at much higher temperatures compared to the Al-Si alloys. Results obtained on the thixoforgeable copper alloy has further demonstrated the capability of the laser-EMAT system in making acoustic wave measurements into the semi-solid and the fully molten state even at the higher temperatures. In the case of the steel alloys the laser-EMAT system has demonstrated that it is possible to detect the ferromagnetic to paramagnetic phase transition temperature from the sudden reduction in signal amplitude and the change in polarity of the longitudinal wave pulse (fig. 5.12). Acoustic wave measurements on the M2 tool steel were made up to 1140 °C only, and no ultrasonic signal was detected above this temperature.

It had been mentioned in chapter 5 that the M2 tool steel could not be heated above the solidus temperature using the standard split electric furnace since the heating elements are rated to 1200 °C and the maximum sample temperature achievable is 1100 °C. To overcome this limitation an R.F induction furnace was used for higher temperatures. However in order to prevent the dynamic magnetic field from the heating coil interfering with the magnetic field of the EMAT and hence the detection mechanism, the furnace had to be switched off prior to making the measurement. There was a considerable drop in the sample temperature the moment the EMAT was brought into close contact with the sample surface. Therefore for making measurement around the onset of melting, the sample has to be heated well

into the partially molten state where the lower melting point solid solution surrounding the spheroidal particles has started to melt and leaving the particles floating within the liquid metal. When the furnace was switched off the sample temperature dropped and the alloy started to solidify back into the solid state creating a material with a complex structure which might comprise a coarse austenitic structure and spheroidal structure surrounded by the solidified liquid solution. It is possible that this complex structure caused great attenuation to the acoustic wave energy due to scattering, in particular Rayleigh scattering, resulting in the undetectable acoustic wave signal.

7.3 Suggested Further Work

The laser-EMAT system used has proved capable of making acoustic wave measurements into the semi-solid state of the thixoforgeable Al-Si alloys and the Cu 10.2 % Sn alloy, and it is expected to be suitable for monitoring the softness or estimating the percentage of solid/liquid fractions of thixotropic metal before the forming process. It has been mentioned earlier in chapter one that a thixotropic metal when heated to a certain solid/liquid fraction possesses a low fluid flow behaviour that is useful for thixoforming, in particular for producing engineering components with intricate shapes. The determination of the temperature indicating the correct softness of the metal in the semi-solid state is essential in order to produce high quality engineering components. Therefore, substantial work is still needed, this time in the actual industrial environment, in order to prove the suitability of an ultrasonic technique for monitoring the solid/liquid fractions prior to the thixoforming process. Once this has been proved, the control system has to be further upgraded, such as

automating the system so that the push-pull of the water-cooled EMAT does not have to be manually controlled. Furthermore it will be necessary to regulate the laser power density so that both the longitudinal and the shear wave (if possible) signals are detectable up to the condition suitable for thixoforging.

It appears that in the case of the mild and tool steel there are a few possible factors that may contribute to the rapid decrease in the longitudinal and shear wave velocities and the increase in ultrasonic attenuation, between the eutectoid and the Curie temperature. The factors are the progressive transformation of BCC α-ferrite to FCC γ-austenite phase, the dissolution of the Fe_3C solid solution and the transformation from a ferromagnetic to a paramagnetic phase. However the real factors that dominate the ultrasonic properties are still uncertain and therefore a detailed study is required.

In order to have data on the semi-solid state of the M2 tool steel using the laser-EMAT system, the sample has to be heated in an electric furnace to avoid any interference with the EMAT detector, and to enable measurements to be conducted while the sample is being slowly heated. This method is the best route for a laboratory test. If the present R.F furnace is to be used to duplicate the sample heating method normally implemented in the industry then the existing set-up shown in figure 5.3 has to be upgraded to enable quick ultrasonic measurement to be taken the moment the furnace is switched off. Otherwise, other combinations of non-contacting ultrasonic systems such as the laser-laser system has to be consider. A Fabry-Perot interferometer that is less sensitive to the sample surface condition and the industrial environment can be used as the detector replacing the EMAT. With this system monitoring can be carried out remote from the furnace and the sample, which

therefore eliminates the problem of having to switch off the R.F furnace before taking the measurement. However the suggested system is much more expensive than the laser-EMAT system used in this thesis and would have little relevance to the final industrial application.

A thixoforging system which could use a laser-EMAT system could be designed. An illustration of the suggested thixoforging system is shown in figure 7.1. The slug could be fed onto a ceramic pedestal, resting on a hydraulic or pneumatic ram below the furnace and pushed to the heating position. Once the slug had been heated to the required condition it would be removed from the R.F coil rapidly to a testing position where the laser-EMAT system has been set. If the slug is accepted it would then proceed to the thixoforging mould. If the slug failed the test by either being heated beyond or below the required condition, then for the former the slug has to be rejected and pushed out of the silica tube through the opening window by the actuated plunger, but for the latter the slug could be brought back to the heating position and the subsequent heating parameters adjusted accordingly.

The theoretical graphs plotted in chapter 2 were based on a simple model where the velocities in the solid and liquid phases were represented by the straight line fits from the experimental data. In the semi-solid state the curves were plotted following Atkinson and Kytomaa, [1992] which might be suitable for a fixed temperature and monodispersed particles but not on materials consisting of interconnected particles, and variable solid to liquid fraction ratio as a result of increasing temperature. Therefore it is suggested that a more appropriate model should be developed to predict the behaviour of the longitudinal wave velocity in the two phase region, taking into consideration the variation of particle sizes, the acoustic

waves boundary behaviour at the solid/liquid interface and the interconnection between particles as the sample temperature progressively rises. Such a model would help to relate the acoustic wave measurement to liquid fraction.

7.4 References

CHAPTER 1

[01]. Collot, J., United States Patent, No. 4,510,987, 1985

[02]. Collot, J., 25th Annual Conference of Metallurgist, Toronto, 1986.

[03]. Edwards, C. and Palmer, S.B., "Feasibility Study of Ultrasonic Techniques for Measuring the Degree of Partial Melting of Al-Si Alloys", 1990, (Unpublished).

[04]. Flemings, M.C., Metallurgical Transactions A, **Vol. 22A**, 1991, page 957-981.

[05]. Flemings, M.C., Reik, R.G. and Young, K.P., Material Science Engineering, **Vol. 25**, 1976. page 103-117.

[06]. Gabathuler, J.P., Barras, D., Krahenbuhl, Y. and Weber, J.C., 2nd International Conference Proceeding on Semi-solid Processing of Alloys and Composites, 1992, page 33-46.

[07]. Hutchins, D.A., Hu, J. and Lundgren, K., Materials Evaluation, **Vol. 44**, Sept. 1986, page 1244-1253.

[08]. Kenney, M.P., Courtois, J.A., Evans, R.D., Farrior, G.M., Kyonka, C.P., Koch, A.A. and Young, K.P., ASM Metals Handbook, 9th Edition, **Vol. 15**, 1988, page 327-338

[09]. Kiuchi, M. and Sugiyama, S., 2nd International Conference Proceeding on Semi-solid Processing of Alloys and Composites, 1992, page 47-56.

[10]. Leatham, A., Ogilvy, A., Chesney, P. and J.V. Wood, J.V., Metallic Materials, **Vol. 5**, 1989, page 140-143.

[11]. McLelland, A.R.A., Atkinson, H.V., Kapranos, P. and Kirkwood, D.H., Materials Letters, **Vol. 11**, 1991, page 26-30.

[12]. Monshinin, M., 2nd International Conference Proceeding on Semi-solid Processing of Alloys and Composites, 1992, page 149-158.

[13]. Spencer, D.B., PhD. Thesis, Massachusetts Institute of Technology, Cambridge, MA, 1971.

[14]. Young, K.P., Kyonka, C.P. and Courtois, J.A., United States Patent, No. 4,415,374, 1983.

CHAPTER 2

[01]. Achenbach, J.D., "Wave Propagation in Elastic Solids", (North-Holland Pub. Company, New York), 1980.

[02]. Ahuja, A.S. and Hendee, W.R., Jour. Acoustic Society of America, **Vol. 63**, No. 4, April 1978, page 1074-1080.

[03]. Allegra, J.R. and Hawley, S.A., Jour. Acoustical Society of America, **Vol. 51**, 1972, page 1545-1564.

[04]. Atkinson, C.M. and Kytomaa, H.K., 2nd International Conference on Semi-solid Processing of Alloys and Composites, 1992.

[05]. Bhatia, A.B., "Ultrasonic Absorption", (Clarendon Press, Oxford), 1967.

[06]. Biot, M.A., Jour. Acoustical Society of America, **Vol. 28**, 1956, page 169-191.

[07]. Blitz, J., "Elements of Acoustics", (Butterworths, London), 1964.

[08]. Blue, J.E. and McLeroy, E.G., The Jour. of the Acoustical Society of America, **Vol. 44**, No. 4, 1968, page 1145-1148.

[09]. Cracknell, A.P., "Ultrasonics", (Wyhekam Pub., London), 1980.

[10]. Darbari, G.S., Singh, R.P. and Verma, G.S., Jour. of Applied Physics, **Vol. 39**, No. 5, April 1968, page 2238-2245.

[11]. Ensminger, D., "Ultrasonics-The Low-and High-Intensity Applications", (Marcel Dekker, Inc., New York), 1973.

[12]. Gooberman, G.L., "Ultrasonics Theory and Application", (The English Universities Press Ltd.), London, 1968.

[13]. Hampton, L.D., The Jour. of the Acoustical Society of America, **Vol. 42**, No. 4, 1967, page 882-890.

[14]. Kamioka, H., Japanese Jour. of Applied Physics, **Vol. 22**, No 12, Dec. 1983, page 1805-1809.

[15]. Kamioka, H., Jour. of the Physical Society of Japan, **Vol. 53**, No. 4, 1984, page 1349-1355.

[16]. Kamioka, H. and Sumino, Y., Jour. of the Physical Society of Japan, **Vol. 53**, No. 9, 1984, page 3036-3041.

[17]. Kaye, G.W.C. and Laby, T.H., " Tables of Physical and Mechanical Constants", (Longman, London), 1986.

[18]. Kolsky, H., "Stress Waves in Solids", (Clarendon Press, Oxford), 1953.

[19]. Mason, W.P., "Physical Acoustics and the Properties of Solids", (D. Van Nostrand Company, Inc., New York), 1958.

[20]. Mason, W.P. and McSkimin, H.J., Jour. of Applied Physics, **Vol. 19**, Oct. 1948, page 940-946.

[21]. Papadakis, E.P., The Jour. of the Acoustical Society of America, **Vol. 37**, No. 4, April 1965, page 703-710.

[22]. Shutilov, V.A., "Fundamental Physics of Ultrasound", (Gordon and Breach Science Pub., New York), 1988.

[23]. Silber, F.A. and Ganglbauer, C., Nondestructive Testing, 1970, page 429-432..

[24]. Webber, G.M.B. and Stephens, R.W.B., Physical Acoustics, **Vol. IV**-Part B, 1970, page 53-97.

[01]. Alers, G.A. and Burns, L.R., Materials Evaluations, **Vol. 45**, Oct. 1987, page 1184-1189.

[02]. Andrews, K.A., " Testing at High Temperatures", in "Ultrasonic Testing", (Edited by Szilard, John Wiley & Sons, New York), 1982, page 411-436.

[03]. Aussel J.D. and Monchalin, J.P., Jour. of Applied Physics, 1989, **Vol. 65**, No. 8, page 2918-2922.

[04]. Boyd D.M. and Sperline, P.D., Rev. of Progress in Quantitative Nondestructive Evaluation, **Vol. 8**, 1988, page 1677-1683.

[05]. Billson D.R. and Hutchins, D.A., Rev. of Progress in Quantitative Nondestructive Evaluation, **Vol. 12**, 1993, page 1661-1666.

[06]. Brammer, J.A. and Percival, C.M., Experimental Mechanics, June 1970, page 245-250.

[07]. Calder, C.A., Draney, E.C. and Wilcox, W.W., Jour. of Nuclear Materials, **Vol. 97**, 1981, page 126-136.

[08]. Calder, C.A. and Wilcox, W.W., "Characterisation of Materials for Service at Elevated Temperature", (Edited by G.V. Smith, ASME), 1978, page 169-181.

[09]. Cole, P.T., Ultrasonics, July 1978, page 151-155.

[10]. Cooper, J.A., PhD. Thesis, University of Hull, 1985.

[11]. Darbari, G.S., Singh, R.P. and Verma, G.S., Jour. of Applied Physics, **Vol. 39**, No. 5, April 1968, page 2238-2245.

[12]. Davies, S.J., Edwards, C., Taylor, G.S. and Palmer, S.B., Jour. Physics D: Applied Physics, **Vol. 26**, 1993, page 329-348.

[13]. Dewhurst, R.J., Edwards, C., McKie, A.D.W. and Palmer, S.B., Jour. of Applied Physics, **Vol. 63**, No. 4, Feb. 1988, page 1225-1227.

[14]. Dobbs, E.R., Research Techiques in Nondestructive Testing, **Vol. 2**, 1973, page 419-441.

[15]. Edwards, C., "Contactless Generation and Detection of Ultrasound", Technical Report for Shell Research, Arnhem, 1994.

[16]. Edwards, C., Palmer, S.B. and Hornsby, M.J., 2nd International Conference Proceeding on Semi-solid Processing of Alloys and Composites, 1992, page 22-32.

[17]. Frost, H.M., Physical Acoustic, (Academic Press, London), **Vol. XIV**, 1979, page 179-275.

[18]. Hutchins, D.A. and MacPhail, J.D., Jour. Physics E: Science Instrument, **Vol. 18**, 1985, page 69-73.

[19]. Hutchins, D.A., Hu, J. and Lundgren, K., Materials Evaluation, **Vol. 44**, Sept. 1986, page 1244-1253.

[20]. Kawashima, K., IEEE Trans. on Sonics and Ultrasonics, **Vol. SU-31**, No. 2, March 1984, page 83-94.

[21]. Kubota, J., Sasaki, S., Sato, I., Ito, S., Kadowaki, T., Yamaguchi, H., Fujisawa, K. and Murayama, R., Materials Evaluation, **Vol. 46**, March 1988, page 523-526.

[22]. Lavender, J.D., Jour. of Research, SCRATA, **Vol. 12**, March 1971, page 31-35.

[23]. Lee, S.S. and Ahn, B.Y., Nondestructive Testing and Evaluation, **Vol. 7**, 1992, page 253-261.

[24]. Maxfield, B.W., Kuramoto, A. and Hulbert, J.K., Materials Evaluation, **Vol. 45**, Oct. 1987, page 1165-1183.

[25]. McKie, A.D.W., PhD Thesis, University of Hull, 1987.

[26]. Monchalin, J.P. and Heon, R., Materials Evaluation, **Vol. 44**, Sept 1986, page 1231-1237.

[27].Parkinson G.J. and Wilson, D.M., British Jour. of NDT, July 1977, page 178-184.

[28]. Scruby, C.B., Dewhurst, R.J., Hutchins, D.A. and Palmer, S.B., Research Techniques in Nondestructive Testing, **Vol. 5**, 1982, page 281-327.

[29]. Scruby, C.B. and Drain, L.E., "Laser Ultrasonics and Applications", (Adam Hilger Ltd., Bristol), 1990, page 223-324.

[30]. Taylor, G.S., PhD. Thesis, University of Warwick, 1992.

[31]. Telschow, K.L., Walter, J.B. and Garcia, G.V., Jour. of Applied Physics, Dec. 1990, page 6077-6082.

[32]. Wadley, H.N.G.,. Norton, S.J., Maver, F. and Droney, B., Phil. Trans. Royal Society, London, A 320, 1986, page 341-361.

[33]. Whittington, K.R., British Jour. of NDT, Sept. 1978, page 242-247.

[34]. Wilkinson, L., British Jour. of NDT, Sept. 1964, page 94-100.

CHAPTER 4

[01]. Ahuja, A.S. and Hendee, W.R., Jour. Acoustic Society of America, **Vol. 63**, No. 4, April 1978, page 1074-1080.

[02]. Bhatia, A.B., "Ultrasonic Absorption", (Clarendon Press, Oxford), 1967.

[03]. Blue, J.E. and McLeroy, E.G., The Jour. of the Acoustical Society of America, **Vol. 44**, No. 4, 1968, page 1145-1148.

[04]. Dewhurst, R.J., Edwards, C., McKie, A.D.W. and Palmer, S.B., Jour. of Applied Physics, **Vol. 63**, No. 4, Feb. 1988, page 1225-1227.

[05]. Kaye, G.W.C. and Laby, T.H., " Tables of Physical and Mechanical Constants", (Longman, London), 1986.

[06]. Parker, R.L., Manning, J.R. and Peterson, N.C., Jour. of Applied Physics, **Vol. 58**, No. 11, Dec. 1985, page 4150-4164.

[01]. Bhatia., A.B., "Ultrasonic Absorption", (Clarendon Press, Oxford), 1967.

[02]. Bozorth, R.M., "Ferromagnetics", (D. Van Nostrand Company Inc., Canada), 1951, page 210.

[03]. Callister, W.D., Materials Science and Engineering-An Introduction, (John Wiley & Sons Inc., Canada), 1991, page 689.

[04]. Cau, E.R. and Robert, M.H., 2nd International Conference Proceeding on Semi-solid Processing of Alloys and Composites, 1992, page 1-10.

[05]. Darbari, G.S., Singh, R.P. and Verma, G.S., Jour. of Applied Physics, **Vol. 39**, No. 5, April 1968, page 2238-2245.

[06]. Davies, S.J., Edwards, C., Taylor, G.S. and Palmer, S.B., Jour. Physics D: Applied Physics, **Vol. 26**, 1993, page 329-348.

[07]. Dewhurst, R.J., Edwards, C., McKie, A.D.W. and Palmer, S.B., Jour. of Applied Physics, **Vol. 63**, No. 4, Feb. 1988, page 1225-1227.

[08]. Dobbs, E.R., Research Techiques in Nondestructive Testing, **Vol. 2**, 1973, page 419-441.

[09]. Edwards, C. and Palmer, S.B., IEEE Trans. on Magnetics, **Vol. 26**, No. 5, Sept. 1990, page 2080-2084.

[10]. Edwards, C., Palmer, S.B. and Hornsby, M.J., 2nd International Conference Proceeding on Semi-solid Processing of Alloys and Composites, 1992, page 22-32.

[11]. Hub, D.R., Proceeding 4th International Congress Acoustic, Copenhagen, Aug. 1962, paper J51.

[12]. Lee, S.S. and Ahn, B.Y., Nondestructive Testing and Evaluation, **Vol. 7**, 1992, page 253-261.

[13]. Mak, D.K. and Gauthier, J., Ultrasonics, **Vol. 31**, No. 4, 1993, page 245-249.

[14] Martius, U.M. and Bratina, W.J., Jour. of Applied Physics, **Vol. 32**, No.3, Suppl. 280S-281S, 1961

[15]. McKie, A.D.W., PhD Thesis, University of Hull, 1987.

[16]. Papadakis, E.P., Lynnworth, L.C., Fowler, K.A. and Carnevale, H., The Jour. of the Acoustical Society of America, **Vol. 52**, No. 3 (Part 2), 1972, page 850-857.

[17].Parker, R.L., Manning, J.R. and Peterson, N.C., Jour. of Applied Physics, **Vol. 58**, No. 11, Dec. 1985, page 4150-4164.

[18].Parkinson, G.J. and Wilson, D.M., British Jour. of NDT, July 1977, page 178-184.

[19].Tripathi, R.C. and Verma, G.S., The Jour. of the Acoustical Society of America, **Vol. 53**, No. 5, 1973, page 1344-1345.

[20].Wadley, H.N.G., Norton, S.J., Maver, F. and Droney, B., Phil. Trans. Royal Society, London, A 320, 1986, page 341-361.

[21].Whittington, K.R., British Jour. of NDT, Sept. 1978, page 242-247.

CHAPTER 6

[01]. Bushell, A.C., Edwards, C. and Palmer, S.B., Rev. of Progress in Quantitative Nondestructive Evaluation, **Vol. 11**, 1992, page 569-576.

[02]. Edwards, C., Taylor, G.S. and Palmer, S.B., Jour. Physics D: Applied Physics, **Vol. 22**, 1989, page 1266-1270.

[03]. Scruby, C.B. and Drain, L.E., "Laser Ultrasonics and Applications", (Adam Hilger Ltd., Bristol), 1990, page 223-324.

[04]. Taylor, G.S., PhD. Thesis, University of Warwick, 1992.

[05]. Tripathi, R.C. and Verma, G.S., The Jour. of the Acoustical Society of America, **Vol. 53**, No. 5, 1973, page 1344-1345.

CHAPTER 7

[01]. Atkinson, C.M. and Kytomaa, H.K., 2nd International Conference on Semi-solid Processing of Alloys and Composites, 1992.

[02]. Edwards, C., Palmer, S.B. and Hornsby, M.J., 2nd International Conference Proceeding on Semi-solid Processing of Alloys and Composites, 1992, page 22-32.

[03]. McKie, A.D.W., PhD Thesis, University of Hull, 1987.

APPENDIX

a)

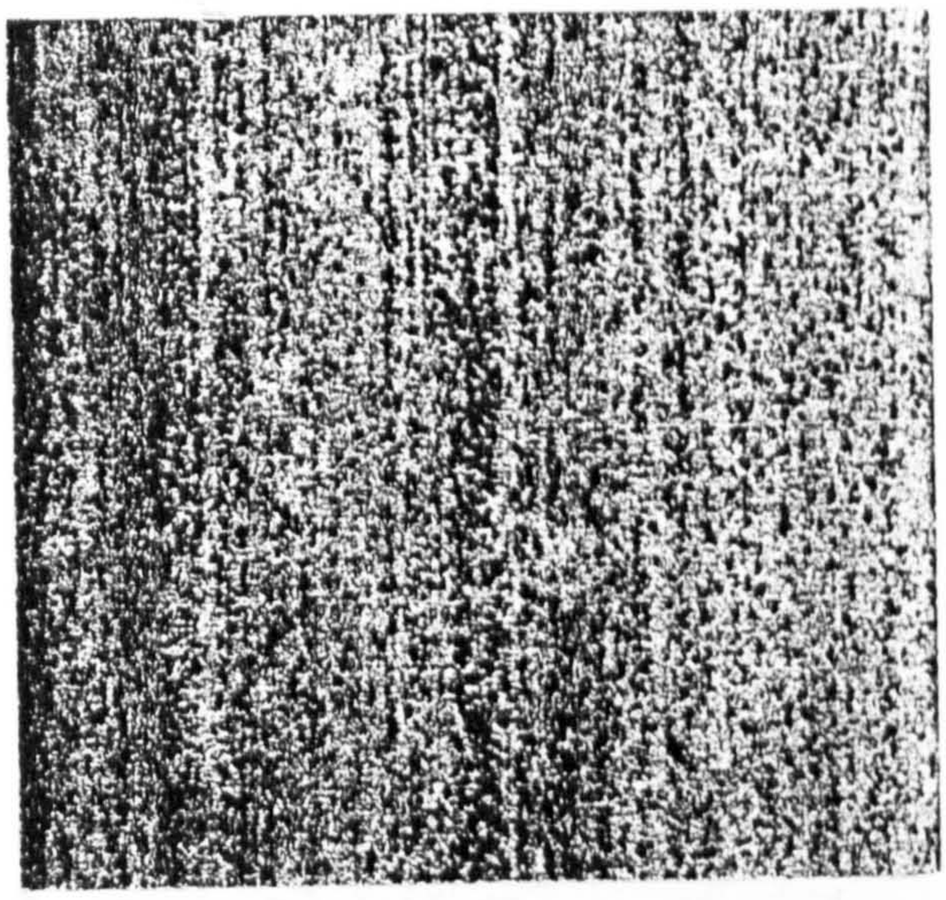

b)

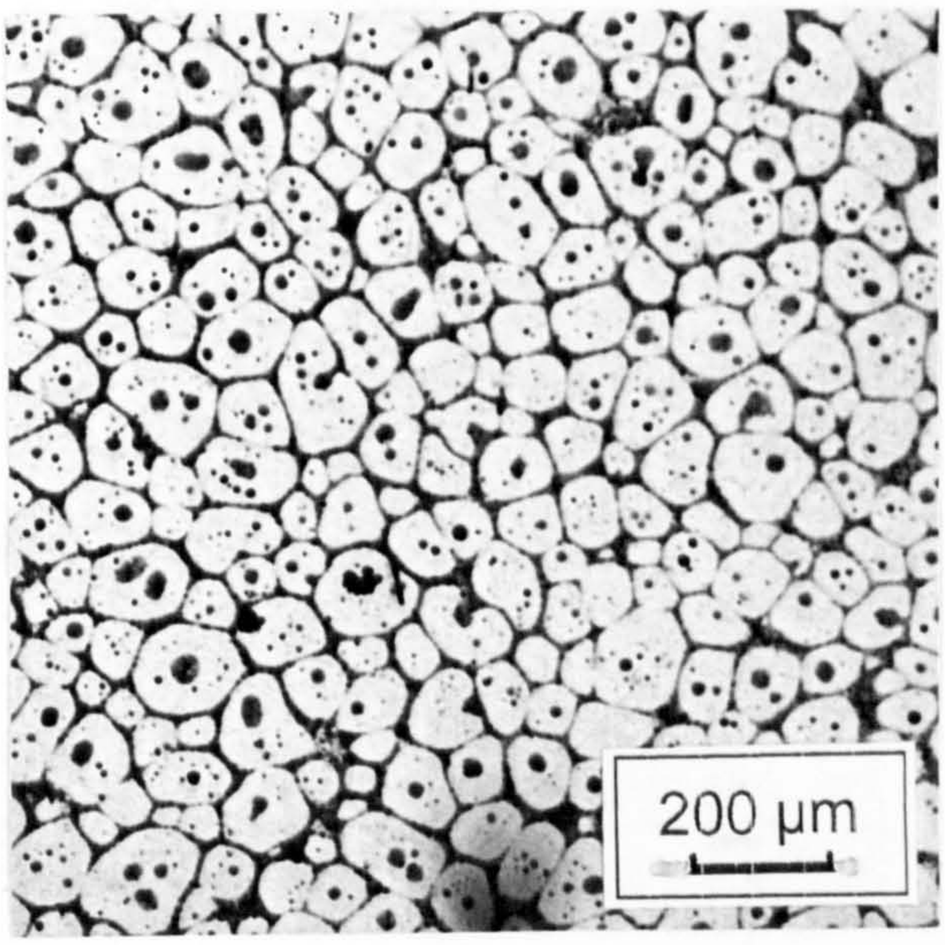

c)

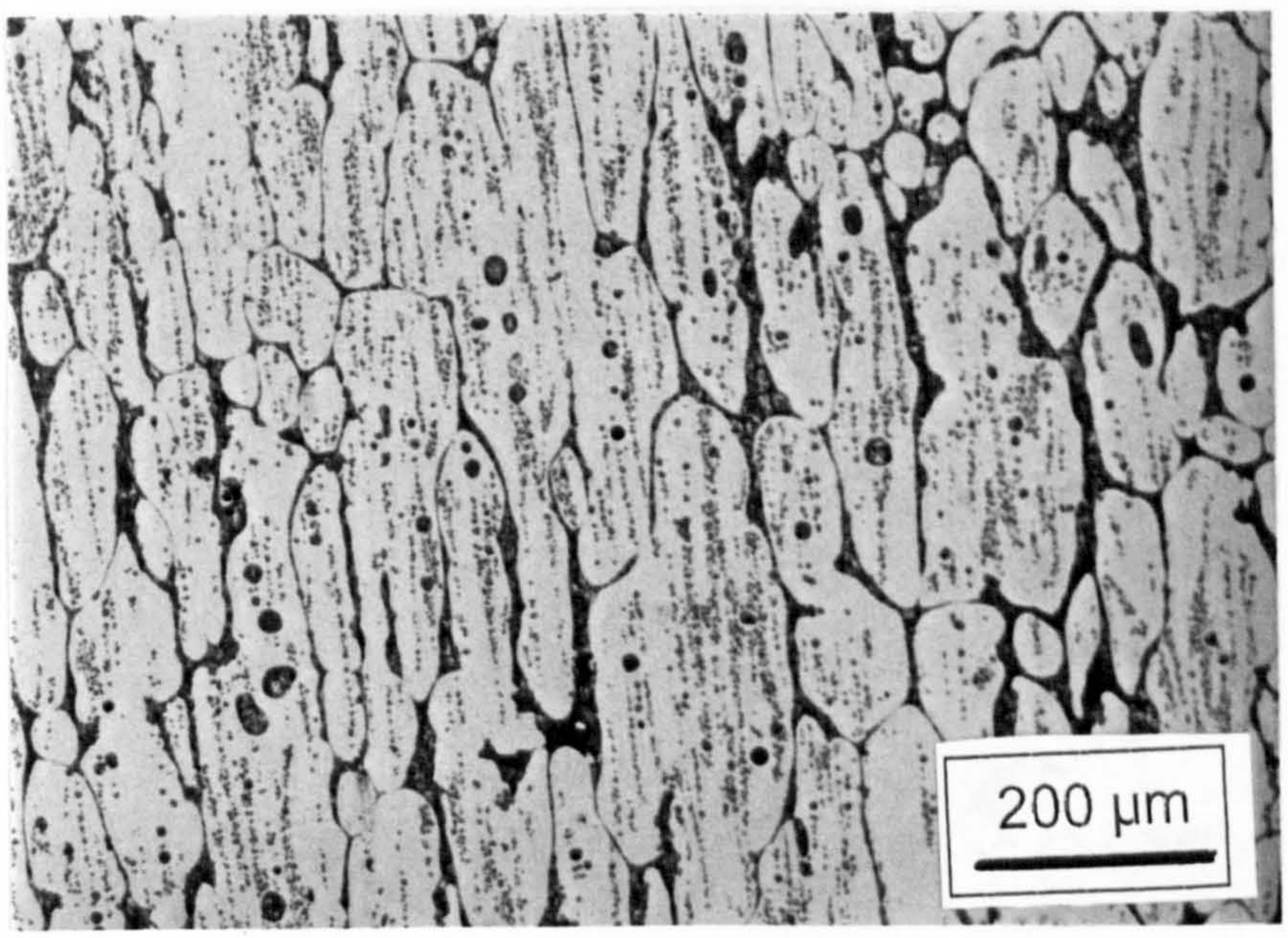

Fig. 1 Microstructures of Al 4.86 % Si alloy a) as extruded , b) & c) after isothermal heating for 10 mins at 590 °C and quenched in brine, perpendicular and parallel to the direction of extrusion respectively. The microstructures show the spheroidised structures necessary for thixoforming.

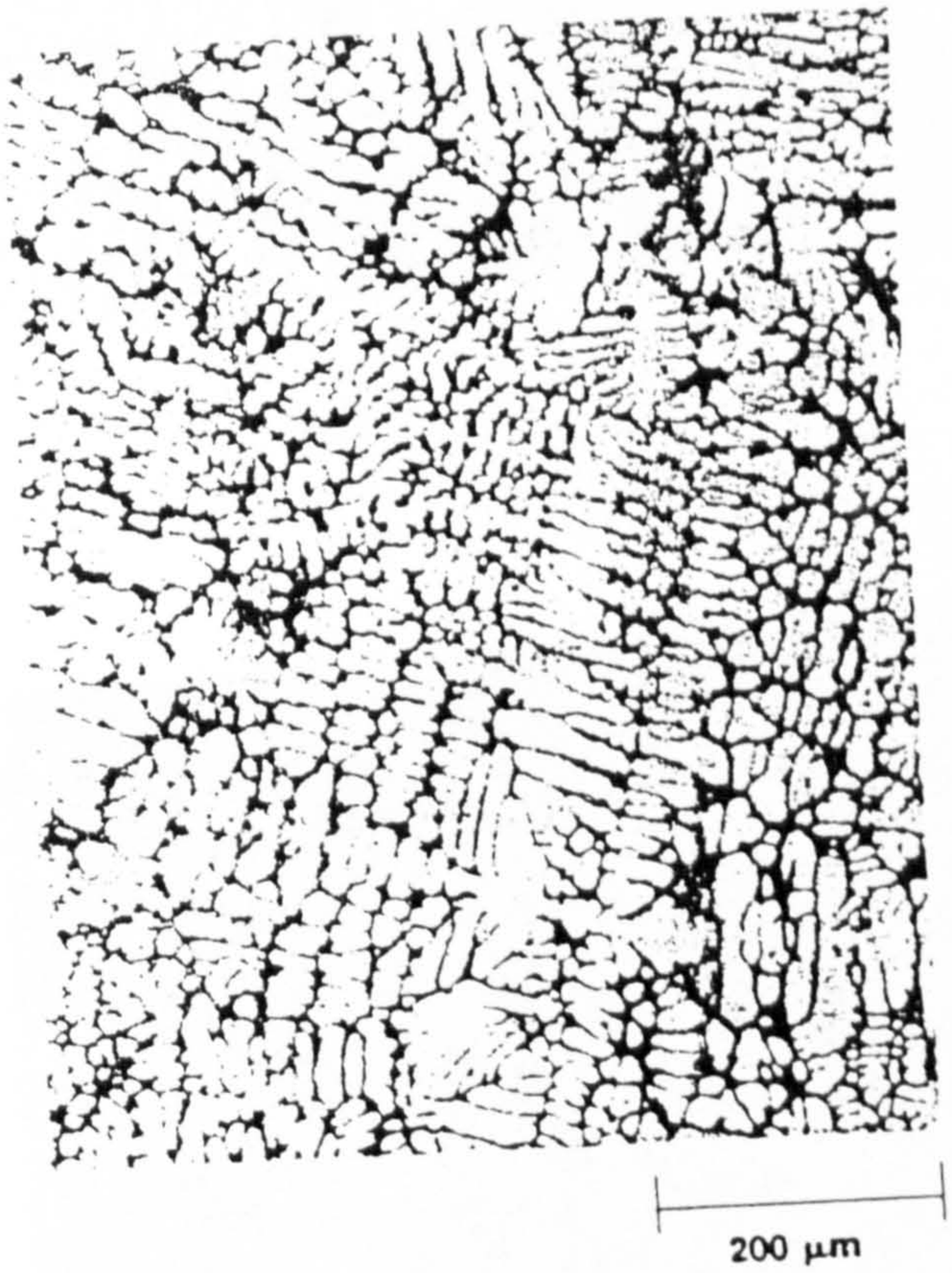

Fig. 2 Microstructures of cast Al-Si alloy showing dendritic structures.

a)

b)

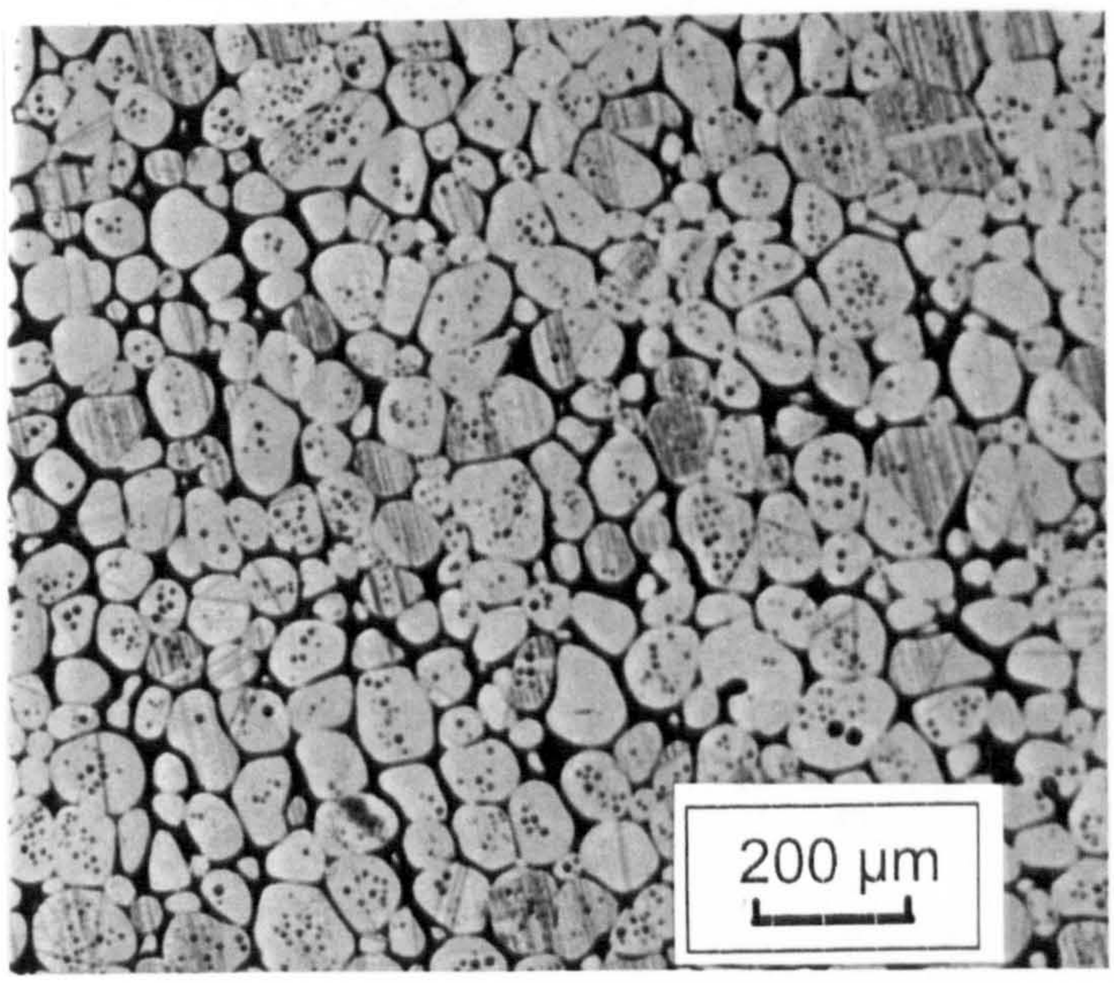

Fig. 3 Microstructures of Cu 10.2 % Sn alloy a) as extruded, and b) isothermally heated to 890 °C for 10 mins and quenched in brine. At 890 °C the spheroidised structures necessary for thixoforming are shown.

Fig. 4 Microstructures of mild steel that was normalised by austenizing at 900 °C for 30 mins and cooling in air. The microstructure consists of ferrite (white) and pearlite (ferrite + cementite) (dark).

a)

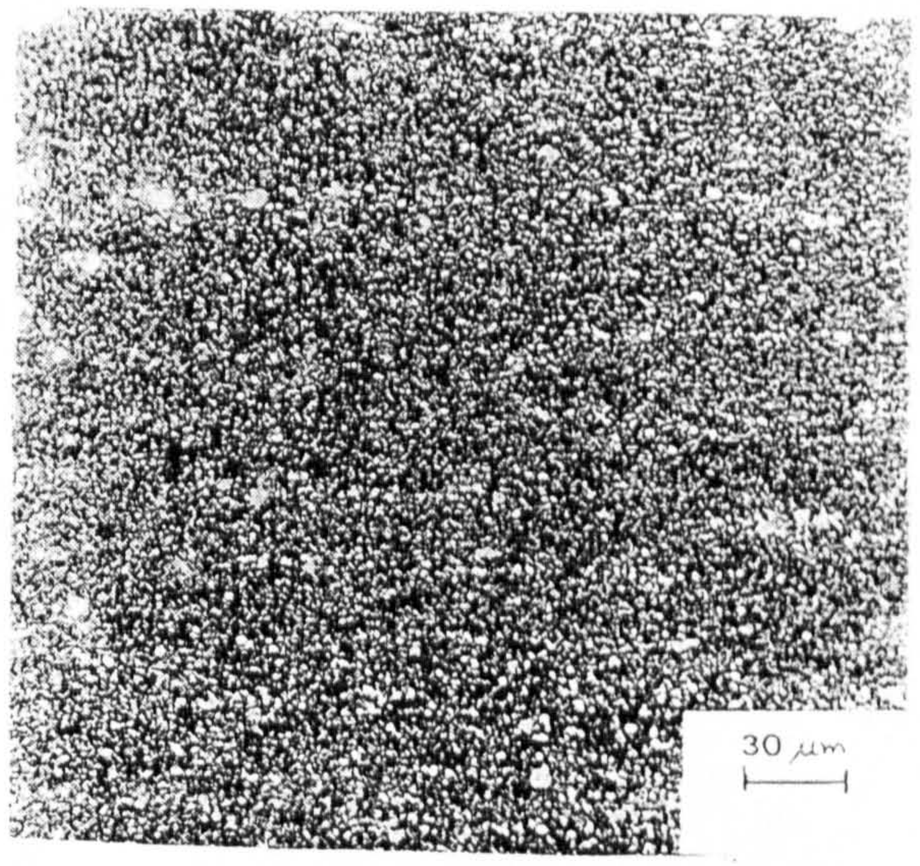

b)

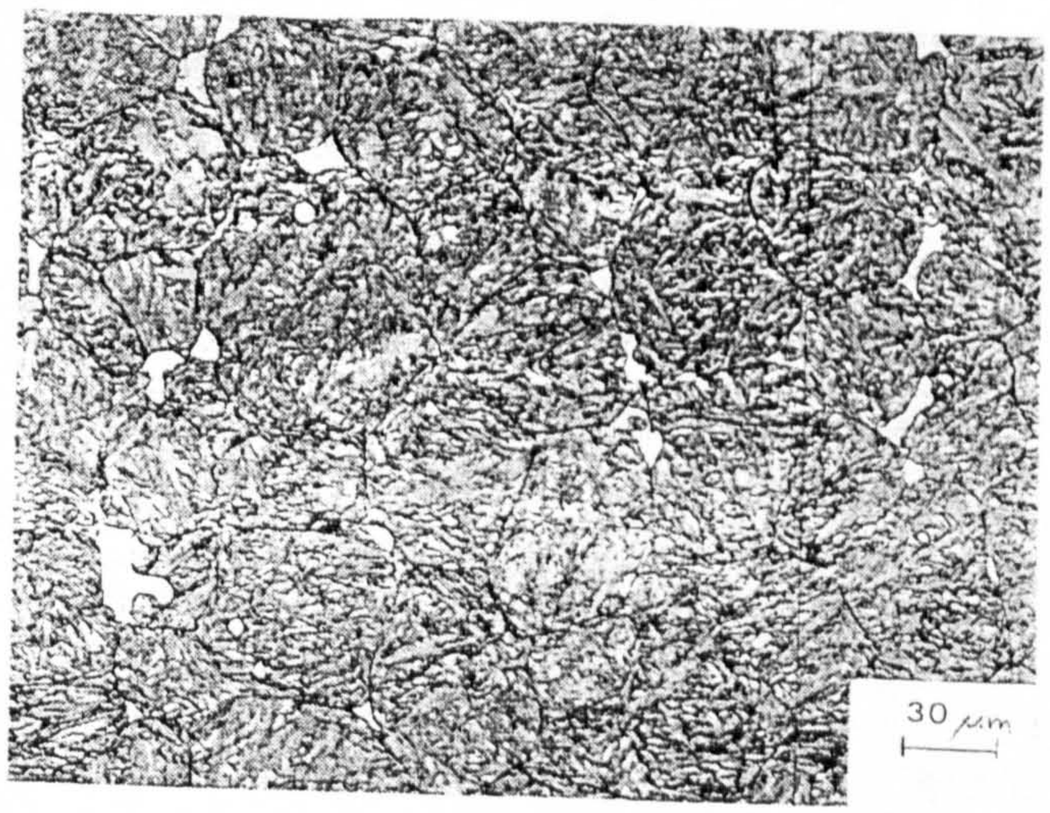

c)

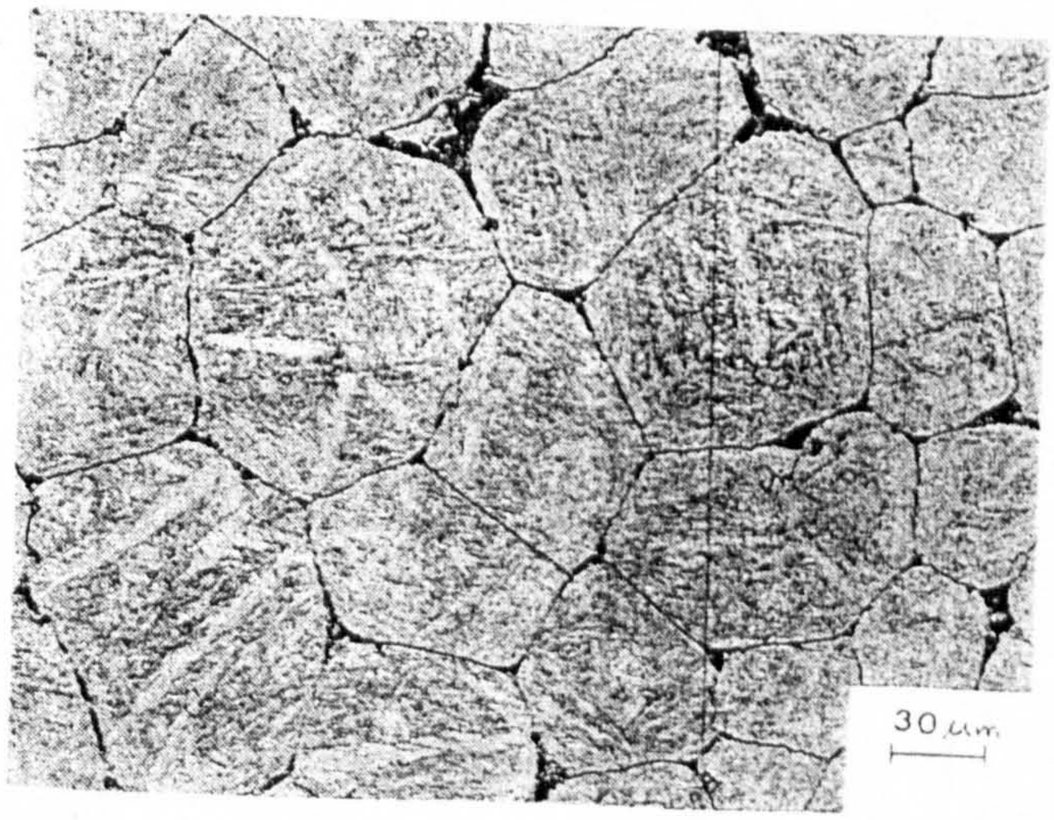

Fig. 5 Microstructures of M2 tool steel a) as extruded b) isothermally heated to 1280 °C for 30 mins, and c) isothermally heated to 1325 °C for 30 mins.

CHAPTER 2

[01]. Achenbach, J.D., "Wave Propagation in Elastic Solids", (North-Holland Pub. Company, New York), 1980.

[02]. Ahuja, A.S. and Hendee, W.R., Jour. Acoustic Society of America, **Vol. 63**, No. 4, April 1978, page 1074-1080.

[03]. Allegra, J.R. and Hawley, S.A., Jour. Acoustical Society of America, **Vol. 51**, 1972, page 1545-1564.

[04]. Atkinson, C.M. and Kytomaa, H.K., 2nd International Conference on Semi-solid Processing of Alloys and Composites, 1992.

[05]. Bhatia, A.B., "Ultrasonic Absorption", (Clarendon Press, Oxford), 1967.

[06]. Biot, M.A., Jour. Acoustical Society of America, **Vol. 28**, 1956, page 169-191.

[07]. Blitz, J., "Elements of Acoustics", (Butterworths, London), 1964.

[08]. Blue, J.E. and McLeroy, E.G., The Jour. of the Acoustical Society of America, **Vol. 44**, No. 4, 1968, page 1145-1148.

[09]. Cracknell, A.P., "Ultrasonics", (Wyhekam Pub., London), 1980.

[10]. Darbari, G.S., Singh, R.P. and Verma, G.S., Jour. of Applied Physics, **Vol. 39**, No. 5, April 1968, page 2238-2245.

[11]. Ensminger, D., "Ultrasonics-The Low-and High-Intensity Applications", (Marcel Dekker, Inc., New York), 1973.

[12]. Gooberman, G.L., "Ultrasonics Theory and Application", (The English Universities Press Ltd.), London, 1968.

[13]. Hampton, L.D., The Jour. of the Acoustical Society of America, **Vol. 42**, No. 4, 1967, page 882-890.